UNIVERSIDAD COMPLUTENSE DE MADRID

FACULTAD DE CIENCIAS FÍSICAS
DEPARTAMENTO DE FÍSICA ATÓMICA, MOLECULAR Y NUCLEAR

TESIS DOCTORAL

Ultra fast timing study of exotic nuclei around ^{78}Ni: the β decay chain of ^{81}Zn

Estudio de coincidencias ultrarrápidas en núcleos exóticos alrededor del ^{78}Ni: la cadena de desintegración β del ^{81}Zn

MEMORIA PARA OPTAR AL GRADO DE DOCTOR

PRESENTADA POR

Vadym Paziy

DIRECTOR

Luis Mario Fraile Prieto

Madrid, 2017

UNIVERSIDAD
COMPLUTENSE
MADRID

Facultad de Ciencias Físicas

Departamento de Física Atómica, Molecular y Nuclear

Dissertation for the Degree of Doctor of Philosophy in Physics

ULTRA FAST TIMING STUDY OF EXOTIC NUCLEI AROUND ^{78}Ni: THE β DECAY CHAIN OF ^{81}Zn

ESTUDIO DE COINCIDENCIAS ULTRARRÁPIDAS EN NÚCLEOS EXÓTICOS ALREDEDOR DEL ^{78}Ni: LA CADENA DE DESINTEGRACIÓN β DEL ^{81}Zn

---

Vadym Paziy

Supervisor
Dr. Luis Mario Fraile Prieto

April 2016

Посвящаю моим родителям

Людмиле и Александру, и моим научным руководителям

Луису и Генриху

Contents

Summary

The evolution of single-particle states in neutron-rich nuclei provides a key information on their nuclear structure and is an important ingredient for the development of nuclear models that can be applied to predict the structure at the borderline of nuclear map. The role of neutron excitations across shell gaps and the evolution proton-neutron interaction can be studied in these exotic nuclei. In particular, magic nuclei are key players for the mapping of the single-particle degrees of freedom around closed cores. A special region of interest is found around the doubly-magic $^{78}_{28}Ni_{50}$. In addition, gross properties of these nuclei play a role in the astrophysical rapid neutron capture process. Nuclei in the vicinity of ^{78}Ni have motivated recent experimental and theoretical studies, aimed at the understanding of the nuclear structure in this region with a large neutron excess.

In this thesis we investigate the nuclear structure of ^{81,80}Ga, ^{81}Ge and ^{81}As, populated in the β decay chain of ^{81}Zn, which was produced at ISOLDE, CERN in the framework of a systematic fast-timing investigation of neutron-rich nuclei populated in the decay of Zn. The selectivity and efficiency of the production of Zn ion beams had been previously optimized in order to guarantee the most pure beam of $^{77-82}$Zn nuclei. The estimated yield of ^{81}Zn was 600 ions/μC giving an average activity of β particles during the experiment of about 10000 counts per second. The experimental setup included two HPGe detectors, two $LaBr_3$(Ce) detectors and a NE111A plastic scintillator for β particle detection. Coincidences with the β detector were used for γ-ray background suppression, and γ-γ coincidences between the HPGe detectors to determine the level schemes. For half-life measurements the combination of $LaBr_3$(Ce) scintillator crystals and Time-to-Amplitude Converters was employed. The signals from the detectors were processed by a digital data acquisition (DAQ) system composed by four Pixie-4 Digital Gamma Finder cards, specially designed for γ-ray spectroscopy which was used for decay level schemes and the Advanced Time Delayed ("fast-timing") $\beta\gamma\gamma$(t) method employed to measure the excited level lifetimes. From the structural point of view, the isotopes under study are relatively simple systems with a few particles and/or holes outside the doubly-magic core, and thus can be treated rather successfully within the nuclear shell model.

The semi-magic $^{81}_{50}Ga_{31}$ is the most interesting case. It has only 3 valence protons outside of ^{78}Ni core with the lowest proton orbits being $p_{3/2}$ and $f_{5/2}$. The $M1$ transition between these states should be l-forbidden and therefore significantly slow (tens of picoseconds). After data analysis we have significantly expanded the level scheme with 47 new levels and 70 transitions in the energy range up to 6.5 MeV. The 290(4)-ms half-life of ^{81}Zn measured in this work is in good agreement with the previous studies [Pad10, Xu14]. The direct β feeding to the ^{81}Ga ground state measured in our experiment is compatible with zero, and much lower than proposed previously by Padgett *et al.* [Pad10], thus compatible with both $5/2^+$ and $1/2^+$ assignments for the ^{81}Zn ground state. We do not

observe β nor γ population to the $9/2^+$ state seen in other $N = 50$ isotones. The level scheme of ^{80}Ga populated in the β-delayed neutron emission from ^{81}Zn was built for the first time, containing 11 γ transitions that de-excite 9 energy levels. The P_n branching was measured to be 23(4)%. For the first time we have measured the half-life of the first excited state in ^{81}Ga to be $T_{1/2} = 60(10)$ ps, which indicates a l-forbidden $M1$ transition of 351 keV between $\pi p_{3/2}$ to the $\pi f_{5/2}$ configuration. For the second excited state a half-life of 23(16) ps was found. This allows to propose a $\pi(f_{5/2})^3$ *cluster* configuration built on the ^{78}Ni core, and a $3/2^-$ spin-parity assignment for this state.

The level scheme of ^{81}Ge populated from the β decay of ^{81}Ga includes 15 new γ transitions and 11 new energy levels, giving in total 111 transitions depopulating 47 energy levels. Fast-timing measurements have allowed to measure three precise half-lives of the 711-, 896- and 1723-keV states in ^{80}Ge, yielding 3.48(8) ns, 257(13) and 31(7) ps respectively. Systematic considerations in the $A = 81$ region combined with the $E1$ multipolarity of 216-keV transition confirms the assignment of the pair of intruders of $1/2^+$ and $5/2^+$ at 679 and 711 keV respectively. Additionally, the low $B(E2)$ value of 711-keV γ-ray determined with its half-life of 711-keV state indicates weak collectivity, and thus confirms the single-particle configuration of $5/2^+$ intruder.

The energy levels of ^{81}As were simultaneously populated in the β decay of both long-lived $1/2^+$ isomer and the $9/2^+$ ground state of ^{81}Ge. In total, 5 energy levels 12 not previously observed γ transitions were placed in the decay scheme $1/2^+$ and 7 energy levels with and 12 new γ transitions were assigned tot he decay scheme of $9/2^+$ ground state of ^{81}Ge. We do observe the $9/2^+$ state at 2625 keV, but no de-exciting transition to $5/2^-$ level was detected and no conclusion can be made on $\pi g_{9/2} \rightarrow \pi f_{5/2}$ proton excitation energy investigation. For the first time, five half-lives of the low-lying 93-, 290-, 336-, 738- and 1129-keV states in ^{81}As were measured, yielding 113(9)-, 53(13)-, 170(5)-, $\leq$30- and 33(10)-ps values. Our results are consistent with the $9/2^-$ spin of 1129-keV level, the $7/2^-$ spin of 738-keV level and the $5/2^-$ spin of 336-keV level. The new half-lives of the 93- and 290-keV states provide strong arguments for spin-parity assignments of $1/2^-$ and $3/2^-$. We confirm the $E2$ behaviour for 792- and 738-keV line, and the mixed $M1 + E2$ nature for 336- and 197-keV transitions. From our measurements a pure or almost pure $M1$ character of the 93-keV transition connecting the first-excited state to the ground state is deduced. This points towards a dominating single-proton configuration for the 93-keV state.

In conclusion, the results obtained in this thesis provide new information about structure of three nuclei around the doubly-magic ^{78}Ni: ^{81}Ga, ^{81}Ge and ^{81}As. Our half-life measurements of the excited states give rise to clarify the nuclear structure of exotic nuclei far away from the stability line. The new properties of ^{81}Ga (and ^{80}Ga) were summarized in an article submitted to *Physical Review C* journal, while the results on ^{81}Ge and ^{81}As are under preparation to be submitted. Our comprehensive measurement of the ^{81}Zn β-decay to ^{81}Ga is the closest approach to date to the spectroscopy of the β-decay of ^{79}Ni to ^{79}Cu, which has only one proton above the ^{78}Ni core. It can be a future challenge for fast timing experiments.

Resumen en castellano

El estudio de la evolución de los estados de particula independiente en núcleos ricos en neutrones, además de proporcionar valiosa información sobre la estructura nuclear, es de gran importancia para el desarrollo de modelos nucleares teóricos que predicen con exactitud la estructura nuclear en núcleos elejados del valle de estabilidad. El estudio de estos núcleos permite también determinar el papel que desempeñan las excitaciones de neutrones a lo largo de las diferentes capas nucleares junto con la evolución de las interacciones que se producen entre los protones. Son de especial interés las especies situadas en regiones cercanas a los nucleos doblemente mágicos, como el $^{78}_{28}\mathrm{Ni}_{50}$, ya que presentan el escenario perfecto para determinar los grados de libertad de las partículas independientes en las capas cerradas. Asimismo, ciertas propiedades de estos núcleos juegan un papel importante en las procesos de nucleosíntesis como el proceso r (captura rápida de neutrones). Debido a estos hechos, estos núcleos han sido durante las últimas décadas la razón de amplios estudios, tanto experimentales como teóricos, cuyo objetivo era entender las modificaciones en estrucutra nuclear en la región con gran exceso neutrónico.

Esta tesis describe el estudio de los núcleos de ^{81,80}Ga, ^{81}Ge y ^{81}As, poblados en la cadena de desintegración β del ^{81}Zn. El núcleo padre, ^{81}Zn, fue producido en ISOLDE, CERN aprovechando la gran pureza de los haces radiactivos de Zn, cuya selectividad y eficiencia habian sido optimizadas con anterioridad. El montaje experimental consta de dos detectores de HPGe, dos detectores de centelleo ultrarrápidos de $LaBr_3$(Ce) y un centelleador plástico (NE111A) que actúa como el detector β. Los esquemas de niveles se construyían basándose en las coincidencias γ-γ entre los HPGe aprovechando su buena resolución energética, mientras que las medidas de vidas medias se hicieron con el uso del centelleador plástico y los detectores de $LaBr_3$(Ce), junto con los TACs (Time-to-Amplitude converters). El método de coincidencias ultrarrápidas o "fast-timing" $\beta\gamma\gamma$(t)' fue utilizado para determinar las vidas medias de los estados excitados. Las señales de cada detector fueron procesadas por un sistema de acquisición digital formado por cuatro tarjetas Pixie-4 Digital Gamma Finder, diseñadas especialmente para la espectroscopía γ.

Desde el punto de vista estructural, los isotopos estudiados en este trabajo son sistemas relativamente sencillos, con tan sólo unas pocas partículas/huecos fuera del cierre de capas, siendo por tanto sistemas que pueden ser descritos por el modelo de capas nuclear con bastantee éxito. El caso más interesante es el $^{81}_{50}\mathrm{Ga}_{31}$, con solo 3 protones de valencia fuera del ^{78}Ni y órbitas más bajas en $p_{3/2}$ y $f_{5/2}$. La transición de carácter $M1$ que conecta estos estados tiene que ser l prohibida y, por lo tanto, considerablemnte lenta (decenas de picosegundos). Tras realizar el análisis de datos el esquema de niveles del ^{81}Ga se amplió con 47 niveles y 70 nuevas transiciones en el rango de energía de hasta 6.5 MeV. La vida

media del ^{81}Zn de 290(4) ms medida en nuestro trabajo concuerda bien con los valores de estudios previos. La población β directa al estado fundamental del ^{81}Ga determinada en nuestro experimento resulta compatibe con el cero y mucho más baja que la propuesta anteriormente. Este resultado es compatible con las asignaciones $5/2^+$ y $1/2^+$ del estado fundamental del ^{81}Zn. En nuestras medidas no hemos podido observar ni la población β ni la población γ al estado $9/2^+$ observado en isotonos con $N = 50$. El valor obtenido para la probabilidad de emisión retardada de un neutron ^{81}Zn es de 23(4)%. La vida media del primer estado excitado del ^{81}Ga fue medida a ser $T_{1/2} = 60(10)$ ps, lo que indica que la transición de 351 keV es efectivamente l prohibida con multipolaridad $M1$ y conecta las configuraciones $\pi p_{3/2}$ y $\pi f_{5/2}$. La vida media del segundo estado excitado de 23(16) ps permite proponer la configuración cluster $\pi(f_{5/2})^3$ construida sobre el core del ^{78}Ni. Por lo tanto, el espín y paridad asignados a estos estados es $3/2^-$.

El esquema de niveles del ^{81}Ge poblado en la desintegración β del ^{81}Ga ha sido ampliado en nuestro trabajo con 15 nuevas transiciones γ y 11 nuevos niveles energéticos, sumando en total 111 transiciones que desexcitan 47 niveles. Las medidas de coincidencias ultrrápidas nos han permitido medir tres vidas medias de 3.48(8) ns, 257(13) and 31(7) ps para los estados del ^{81}Ge a 711, 896 y 1723 keV. La información sobre la sistemática de las probabilidades de transición reducidas en la región cercana a $A = 81$ combinada con la multipolaridad $E1$ de la transición de 216 keV confirman las asignaciones $1/2^+$ y $5/2^+$ de espín-paridad en los niveles intrusos de 679 y 711 keV. Además, el bajo valor de la $B(E2)$ del rayo γ de 711-keV indica una debil colectividad y, por lo tanto, confirma la configuración de partícula independiente para el intruso $5/2^+$.

Finalmente, los niveles de ^{81}As fueron poblados simultaneamente en la desintegración β del isómero $1/2^+$ y del estado fundamental $9/2^+$ del ^{81}Ge, ambos de vida media larga. En total 5 niveles energéticos y 12 transiciones γ que no han sido observedas previamente fueron colocados en el esquema de desintegración del $1/2^+$ mientras que en el caso del la desintegración β desde el $9/2^+$ fueron 7 niveles nuevos y 12 transiciones γ. Las vidas medias de los estados de baja energía de 93, 290, 336, 738 y 1129 keV fueron medidas por primera vez, dando lugar a los valores de 113(9), 53(13), 170(5), $\leq$30 and 33(10) ps respectivamente. Nuestros resultados son consistentes con los espínes de $5/2^-$, $7/2^-$ y $9/2^-$ de los niveles de 336, 738 y 1129 keV. Las nuevas vidas medias de los estados de 93 y 290 keV proporcionan fuertes argumentos para asignar $1/2^-$ al primero y $3/2^-$ para el segundo. Nuestros datos confirman la multipolaridad $E2$ de las transiciones de 738 y 793 keV y la naturaleza mixta de los rayos γ de 197 y 336 keV. A partir de nuestras medidas se puede concluir que la transición de 93 keV, que conecta el primer estado excitado con el fundamental, es una $M1$ casi pura. Esto apunta a la configuración de partícula independiente en el estado de 93 keV.

En conclusión, los resultados de la tesis permiten aportan nuevos datos sobre la estructura de tres núcleos alrededor del doblemente mágico ^{78}Ni: ^{81}Ga, ^{81}Ge y ^{81}As. Nuestras medidas de vidas medias de los estados excitados ayudan aclarar la estructura nuclear de núcleos exóticos que se encuentrar lejos de la línea de estabilidad. Las nuevas propiedades del ^{81}Ga han sido recopiladas en un artículo científico que fue enviado a la revista *Physical Review C*, mientras que los resultados del ^{81}Ge y ^{81}As están en preparación. Nuestro amplio análisis de la desintegración β del ^{81}Zn al ^{81}Ga es el máximo acercamiento que pudo realizarse hasta hoy a la espectroscopía de la desintegración β del ^{79}Ni al ^{79}Cu, que tiene solo un protón más que el ^{78}Ni. Esto será el futuro reto para los experimentos de coincidencias ultrrápidas con la espectroscopía γ de alta resolucón.

Introduction

The atomic nucleus is a many-body quantum system with strong correlations between the constituent fermions. The interaction scale is such that nucleons (protons and neutrons) are the relevant degrees of freedom for the description of the nuclear physics phenomena in the low energy regime. Nevertheless, the basic interaction between the nucleons is not completely understood. The question of how the nucleon-nucleon interaction behaves and how it evolves when we move away from the stability valley still remains.

The pursuit of nuclear models with sufficient predictive power has triggered theoretical and experimental research in large-scale facilities around the world. Many important aspects of the interactions between the constituent protons and neutrons are revealed in nuclei with a large N/Z ratio. The properties of these exotic nuclei are key ingredients for the development of nuclear models that can be successfully applied at the limits of the nuclear chart. Experiments are steadily advancing to the exploration of key observables further and further off stability, at the extreme of isospin, where nuclear models can be put to the most stringent tests.

Although the excitation energies are the observables that provide the first guidance to the understanding of nuclei, since they can be directly measured by means of gamma and particle spectroscopy, the predictive power of nuclear models is subject to more demanding tests when dynamic properties are obtained. This can be achieved with the measurement of the electromagnetic transition probabilities connecting nuclear states. The direct measurement of excited-state lifetimes, together with the knowledge of the decay level schemes, provides a model-independent way of determining the transition probabilities, and thus they are key observables that can guide the models for a better understanding of atomic nuclei.

The modelling of the nucleus and the understanding of its properties has rekindled in the last years with the development of nuclear forces based on chiral effective field theory and the inclusion of larger and larger model spaces. In spite of the current progresses, ab-initio models are still limited to light nuclei or nuclei around closed shells. On the other hand, large-scale shell-model approaches based on configuration interaction have been able to explain in a quantitative manner many of the properties of stable nuclei and those close to stability. The nuclear mean field determines the single-particle motion and the effects due to the well-known nuclear shells, while collective aspects are due to correlations and to configuration mixing by coherent parts of the residual interaction beyond the mean field.

Striking modifications to the standard ordering of the single-particle energies have been observed in exotic nuclei that have a large disparity in proton and neutron numbers, giving rise to the disappearance of the conventional magic numbers and the appearance of new shell gaps. Understanding the underlying driving force causing such modifications

is one of the main subjects of nuclear structure physics.

These structural modifications are more prominent in neutron-rich exotic nuclei, and therefore these are critically scrutinized with the aim of realizing a predictive model for atomic nuclei that is valid across the nuclear chart. The regions around doubly-magic nuclei attract a strong interest from both experimental and theoretical points of view. They are the best suited to test the shell-model effective Hamiltonian, and allow important parameters such as single-particle energies, two-body matrix elements and effective electromagnetic operators to be obtained.

This PhD thesis focuses on the study of exotic nuclei in the region around the doubly-magic nucleus ^{78}Ni, with 28 protons and 50 neutrons ($Z = 28$ and $N = 50$). Although ^{78}Ni is to date difficult to reach (since it is 14 neutrons away from the heaviest stable nickel isotope ^{64}Ni), the properties of nuclei in this region can be studied far away from the valley of stability. A second motivation to study this region is that it is a crucial playground for nuclear astrophysics and in particular the rapid neutron capture process.

Specifically this work addresses the study of ^{81}Ga, with $N = 50$, three protons outside ^{78}Ni, with emphasis in half-life measurements of its excited states using the fast timing $\beta\gamma\gamma$ method [Mac89]. This is one of the most exotic experimentally accessible nucleus nowadays. Of particular interest is the measurement of reduced transition probability of the γ-ray that connects the lowest proton orbits $p_{3/2}$ and $f_{5/2}$ can shed light on the nature of the first excited state. The long half-life of this state would suggest $E2$ while the short value would support l-forbidden $M1$ transition.

The semi-magic ^{81}Ga was obtained via the β-decay of ^{81}Zn nuclides at ISOLDE (CERN). This opens the possibility of analysing also the β-delayed neutron emission branch of ^{81}Zn and explore the level scheme of ^{80}Ga populated in this process for the first time. Determination of the β-delayed neutron emission probability may have impact in the astrophysical r-process.

Due to its high production yield, ^{81}Ga produces intensively the $N = 49$ ^{81}Ge nuclide characterized by the low-lying long-lived $1/2^+$ and $5/2^+$ intruder states described by 1particle-2hole configuration of the $g_{9/2}$, $s_{1/2}$ and $d_{5/2}$ orbits. The systematic evolution of $1/2^-$ isomer is apparently broken in ^{81}Ge and the $p_{1/2}$ single-particle state turns out to have a half-life in subnanosecond range. Such modifications of the nuclear structure can be tested via the fast- timing method. Successively, the $1/2^+$ β-decaying isomer produces the $N = 48$ ^{81}As. Previous studies [Hof81] have shown that the decay of this level and the $9/2^+$ ground state, defined by a hole in the $g_{9/2}$ orbit, populates separate energy levels in ^{81}As. This fact opens the possibility to explore new structure in ^{81}As, specially at high energies. The sufficiently high yield permits to perform fast-timing investigation of the low-lying structure of ^{81}As and determine several lifetimes expected to lie in the subnanosecond range.

In Chapter 1 we describe the theoretical basis of the processes that take place in the decay of ^{81}Zn. The neutron-rich nuclei from this region are unstable and decay by emitting β particles with short decay half-lives. The excited products de-excite to the ground state by emitting γ radiation. In some nuclei this process competes at high-lying states with the emission of delayed neutrons. This chapter will be mainly focused on the physics laws that govern these processes. After that a brief introduction will be given for the shell model theory. As ^{81}Ga is believed to lie at the r-process path, some details on astrophysical nucleosynthesis will be given at the end.

In Chapter 2 we present some aspects of ^{78}Ni region that have strong impact on

the nuclei under study. In view of this description, the motivation of the thesis will be presented. Some general features of γ spectroscopy and Advanced Time Delayed Method will be given at the end of the chapter.

Chapter 3 contains the technical peculiarities of the production of ^{81}Zn at ISOLDE. First, the characterization of the ISOL technique will be given. Next, we will illustrate the experimental set up and properties of the detectors used in our experiment. The description of the data analysis will be right after. At the end of the chapter an additional section describes the energy and the time calibrations of the detectors used in the experiment.

Chapters 4, 5 and 6 address the main results of the thesis. In Chapter 4 the structure of ^{81}Ga populated in the β-decay of ^{81}Zn can be found. An expanded level scheme is constructed and low-lying level lifetimes measured. The results are compared to theoretical calculations. The novel results from the β-delayed neutron emission from ^{81}Zn to ^{80}Ga were also measured. Chapter 5 compiles the properties of ^{81}Ge populated in the β-decay of ^{81}Ga and Chapter 6 contains the structure study of ^{81}As populated in the β-decay of ^{81}Ge. Finally, the conclusions and possible future lines of work are presented in the last chapter Conclusions and Outlook.

Chapter 1

Theoretical Fundamentals

The study of exotic nuclei far away from the stability line in the nuclear chart provides key information for the investigation of shell-evolution. The very neutron-rich nuclei from this zone are unstable and decay by emitting β particles with short decay half-lives. The excited products reach the minimum energy state by γ de-excitations. In some cases a neutron can be emitted almost immediately after the β-decay and give a different daughter nucleus with the same number of protons but with one neutron less. This process is called β-delayed neutron emission. This chapter will be mainly focused on the physics laws that govern these processes.

All the experimental results must be verified with theoretical models which are used to describe it. In some cases the model is not well prepared for this task and the parameters which describe it should be modified in light of the experimental results. The Sec. 1.3 of this chapter will describe the theory of the shell-model calculations used in this work for verification of experimental data. Finally, in Sec. 1.4 we include a brief description of the r-process as the main application of the nuclei studied in the thesis.

1.1 Beta decay

The β particle is an electron or a positron emitted in a process called *beta decay*, which basically consists of conversion of nucleons one to each other, that is a neutron to a proton or a proton to a neutron. In the first case an electron is emitted and the reaction is denominated *negative* β-decay (β^-). The second type is called *positive* β-decay (β^+) because of the emitted positron. A third process exists called orbital *electron capture* (ϵ). It usually occurs in proton-rich nuclei and consists in absorbing of inner atomic electron changing a nuclear proton to a neutron. Both electron and positron guarantee the charge conservation but not the mass conservation. To balance out the missing energy the existence of a particle called neutrino (or antineutrino, depending on the process) was proposed by W. Pauli in 1930. In nuclear physics we are interested in the nuclear β-decay. Schematically, the three basic decays for an initial nucleus X that decays to a daughter nucleus Y can be represented by the following equations:

$$\beta^- : {}^A_Z X_N \rightarrow {}^A_{Z+1}Y_{N-1} + e^- + \overline{\nu}_e, \tag{1.1}$$

$$\beta^+ : {}^A_Z X_N \rightarrow {}^A_{Z-1}Y_{N+1} + e^+ + \nu_e, \tag{1.2}$$

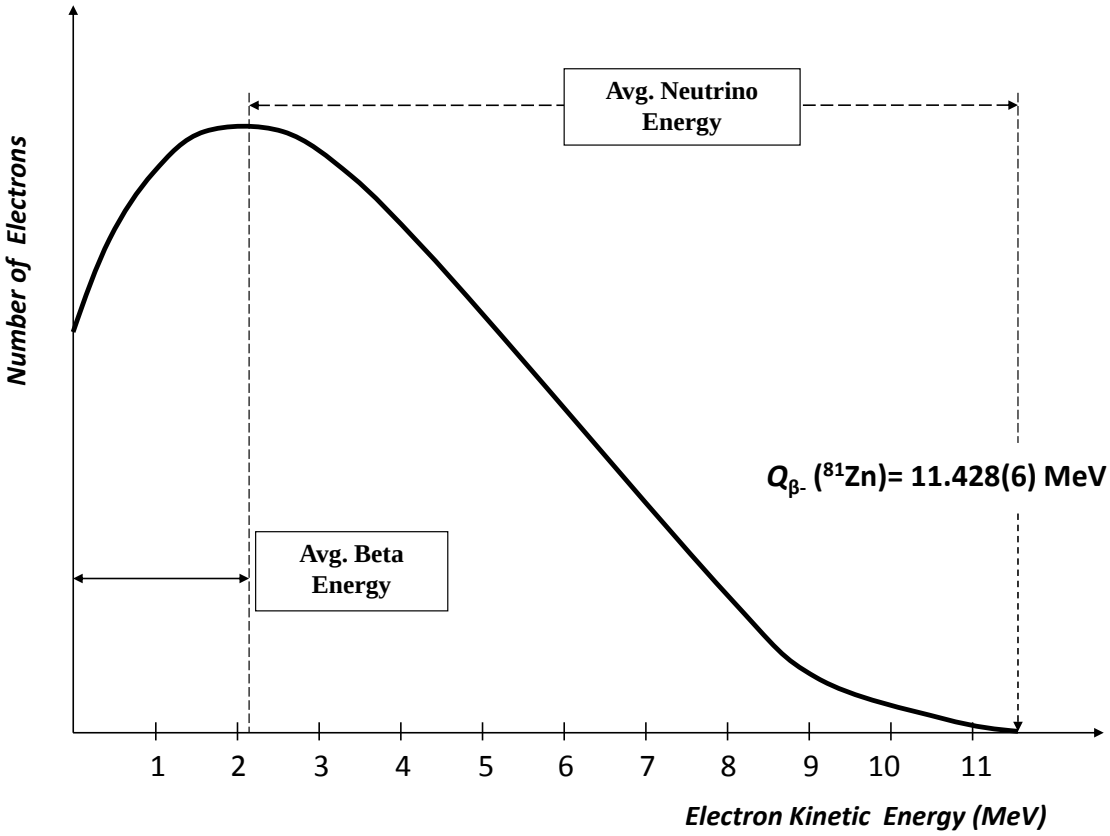

Figure 1.1: Continuous electron distribution from the β^--decay of ^{81}Zn. The updated Q_β value was taken from [Aud12a].

$$\epsilon : {}^{A}_{Z}X_N + e^- \rightarrow {}^{A}_{Z-1}Y_{N+1} + \nu_e. \tag{1.3}$$

As Z and N change by one unit the total number of nucleons A remains constant and we can talk about *isobaric decay*. It is important to note that the protons involved in the β^+ and ϵ decays are not free particles. Otherwise, they would not decay because of their stable properties (very large half-life) when no additional energy is put into play. In the other case, free neutrons are not stable, with about 15 minutes of lifetime [Nak10] and β^- decay does not require bound neutrons.

The emitted β particles have a continuous energy distribution, contrarily of discrete spectrum as with α or γ decay. This is due to the 3-body interaction between proton or neutron, electron or positron and neutrino or anti-neutrino respectively. A typical plot of the β^- distribution is shown in the Figure 1.1. The main difference between β^- and β^+ spectrum is that the kinetic energy of the first one can not be zero because the proton charge repulsion does not allow the electron to escape the nucleus while it does for the positrons. The decay energy is of order of MeV, so the non-relativistic approximation $T \ll mc^2$ is not valid and relativistic kinematics must be used.

An important requirement to have a spontaneous β-decay is a positive energy balance (Q value), that is, the difference between the initial and final nuclear rest energies must

be greater that zero. Neglecting the neutrino's mass the Q value has the following expressions:

$$Q_{\beta^-} = \left[M\left({}^{A}_{Z}X_N\right) - M\left({}^{A}_{Z+1}Y_{N-1}\right) - m_e\right]c^2 \tag{1.4}$$

$$Q_{\beta^+} = \left[M\left({}^{A}_{Z}X_N\right) - M\left({}^{A}_{Z-1}Y_{N+1}\right) - m_e\right]c^2 \tag{1.5}$$

$$Q_{\varepsilon} = \left[M\left({}^{A}_{Z}X_N\right) + m_e - M\left({}^{A}_{Z-1}Y_{N-1}\right)\right]c^2, \tag{1.6}$$

where M represents the nuclear masses. It is more frequent to find tabulated the neutral atomic mass $m\left({}^{A}X\right)$ instead of the nuclear mass [Aud12a]. Neglecting the binding energy between electrons and nucleons one can convert the expressions above into:

$$Q_{\beta^-} = \left[m\left({}^{A}X\right) - m\left({}^{A}Y\right)\right]c^2 \tag{1.7}$$

$$Q_{\beta^+} = \left[m\left({}^{A}X\right) - m\left({}^{A}Y\right) - 2m_e\right]c^2 \tag{1.8}$$

$$Q_{\varepsilon} = \left[m\left({}^{A}X\right) - m\left({}^{A}Y\right)\right]c^2 + B_n \tag{1.9}$$

The latter expression, which describes the Q value for electron-capture process, takes into account the binding energy B_n of the captured electron. All Q values described above refer to decays between the ground states. If the final nuclear state is an excited state, the Q value must be decreased by the excitation energy of the state. As it was mentioned before, the Q value must be positive. This means that starting with an initial nucleus we move to the final one with higher binding energy and thus more stable. In case of β^- decay, for example, the Q value also shows the energy shared by the electron and the anti-neutrino:

$$Q_{\beta^-} = T_{e^-} + E_{\overline{\nu}_e}. \tag{1.10}$$

When one member is zero the other reaches the maximum. This fact can be easily understood by analyzing the Figure 1.1.

The detailed description of the β-decay was carried out by Fermi in 1933 [Kra87]. Fermi's theory basically relies in considering the time-dependent perturbation theory in which the weak interaction is used as small perturbation applied to the nuclear stationary states. From the Fermi Theory and usual conservation laws one can deduce the selection rules that permit to judge whether a β transition is allowed or not. The so called *allowed approximation* entails that the only change in the angular momentum of the nucleus must result from the spins and the parities of the initial and the final states. In our case both particles (electron and neutrino or positron and anti-neutrino) have $1/2$ spin. The only two possibility after coupling leads to $S = 1$ (Fermi transitions) and $S = 0$ (Gamow-Teller transitions). Therefore, the main selection rules for allowed β-decay are:

	Fermi Transition	**Gamow-Teller Transition**
ΔJ	0	0, ± 1 ($0 \not\to 0$)
π	0	0
ΔT	0	0, ± 1 ($0 \not\to 0$)
ΔT_3	± 1	± 1

Table 1.1: Selection Rules for allowed β-decay transitions. T and T_3 represents the isospin and its projection.

$$\Delta J = 0, 1 \tag{1.11}$$

$$\Delta \pi = \text{no}, \tag{1.12}$$

where J is the nuclear spin and π reflects the parity which is given by the angular momentum (-1)^l. We can summarize thess rules including isospin in the Table 1.1. The conclusion is that the *allowed transitions* contain zero angular momentum for electron and neutrino in case of negative β-decay. They are the most probable and intense. There also exist the so called *superallowed Fermi transitions*, that is a special case of Fermi transitions $0^+ \to 0^+$. On the other hand, there are other types of transitions denominated *forbidden transitions*. The forbidden decays are not strictly prohibited but usually less probable than the allowed decays and generally lead to longer state half-lives. If the transition matrix elements M_{fi} vanish, then the forbidden transitions are the only ones that can occur. The angular momentum L in this case is higher than zero being 1, 2, 3, ... If $L_\beta = 1$ we talk about the *first-forbidden decay*, for $L_\beta = 2$ we have the *second-forbidden decay* and so on. The selection rules for the first two forbidden transitions are:

$$\text{First} - \text{forbidden} \qquad \Delta J = 0, 1, 2 \quad \Delta \pi = \text{yes}, \tag{1.13}$$

$$\text{Second} - \text{forbidden} \qquad \Delta J = 2, 3 \quad \Delta \pi = \text{no}. \tag{1.14}$$

The higher is the order of forbiddenness the more unlikely the decay is, and the nucleus prefers to decay by allowed or first-forbidden type.

Microscopic theory of β-decay was developed by E. Fermi in 1934. The decay probability was given by Fermi's Golden Rule:

$$\lambda = \frac{2\pi}{\hbar} |M_{fi}|^2 \rho_f, \tag{1.15}$$

where ρ_f represents the density of final states and $|M_{fi}|$ is the matrix element of nuclear interaction. It was demonstrated (see [Kra87]) that the partial decay rate for electrons and neutrinos can be expressed in terms of their momentum p and q respectively:

$$\lambda = \frac{2\pi}{\hbar} |M_{fi}|^2 g^2 \;\; 4\pi^2 \;\; \frac{p^2 dp}{h^6} \frac{dq}{dE_f}, \tag{1.16}$$

where the final energy $E_f = E_e + qc$ and qc is given by the difference between the decay energy Q and kinetic energy of electron T_e. Therefore, the total decay rate is calculated by integrating the Eq. 1.16 ever all values of p:

$\log ft$	Type	ΔJ	$\Delta\pi$
$2.9 - 3.7$	Super-allowed	0	no
$3.8 - 6.0$	Allowed	0, 1	no
≥ 5.0	l-forbidden allowed	0, 1	no ($\Delta L \neq 0$)
$6 - 8$	first-forbidden	0, 1	yes
$8 - 10 \pm 0.5$	first-forbidden	2	yes
$11 - 13$	second-forbidden	2, 3	no
$17 - 19$	third-forbidden	3, 4	yes
> 22	fourth-forbidden	3, 4	no

Table 1.2: Classification of the β transitions according to the $\log ft$ values [Suh07].

$$\lambda = \frac{g^2 \left|M_{fi}\right|^2}{2\pi^3 \hbar^7 c^3} \int_0^{p_{max}} F\left(Z^{'}, p\right) p^2 \left(Q - T_e\right)^2 dp \tag{1.17}$$

As can be seen Fermi function $F(Z', p)$ was introduced to reflect the effect of the nuclear Coulomb field on the electron wave function (see [Boh75] for details). Since $cp_{max} = \sqrt{E_{max} - m_e^2 c^4}$ the *Fermi intgeral* is defined as:

$$f\left(Z^{'}, E_{max}\right) = \frac{1}{\left(m_e c\right)^3 \left(m_e c^2\right)^2} \int_0^{p_{max}} F\left(Z^{'}, p\right) p^2 \left(E_{max} - E_e\right)^2 dp. \tag{1.18}$$

Some constants were included to make f dimensionless. This integral can be estimated numerically for a given atomic number of the daughter nuclear and maximum total energy of an electron or positron. As $\lambda = ln2/t_{1/2}$, the $ft_{1/2}$ or ft value can be calculated:

$$ft_{1/2} = ln2 \frac{2\pi^3 \hbar^7}{g^2 m_e^5 c^4} \left|M_{fi}\right|^2. \tag{1.19}$$

Changes in ft values indicates changes in nuclear matrix element $|M_{fi}|$ which represents nuclear wave function. In this way, the ft value permits make classification of β-decay transitions. The half-life may vary in a huge range, so the classification is usually done in terms of $\log ft_{1/2}$ values as shown in Table 1.2.

Figure 1.2 shows the distribution of $\log ft$ values from more than 4000 well-known β-decays. The plot represents the experimental results for allowed, first and second forbidden transitions between states with well defined angular momentum and parity.

1.1.1 β-delayed neutron emission

The daughter nucleus born from the β-decay usually ends in an excited state from that de-excites by γ decay. However, if the the energy is sufficiently high this γ emission competes with another process in which one or even few nucleons can be ejected from the excited state populated by the β-decay. Particularly, the β-delayed neutron emission ($\beta - n$) has a special interest in our work because its probability $P_1 n$ plays an important role in nucleosynthesis r-process path calculations (see 1.4 for details).

The schematic representation of this process is shown in Fig. 1.3. The $\beta - n$ emission will take place if the β-decay energy is greater than the neutron separation energy i.e $Q_\beta > S_n$ in the daughter nucleus, where S_n is given by:

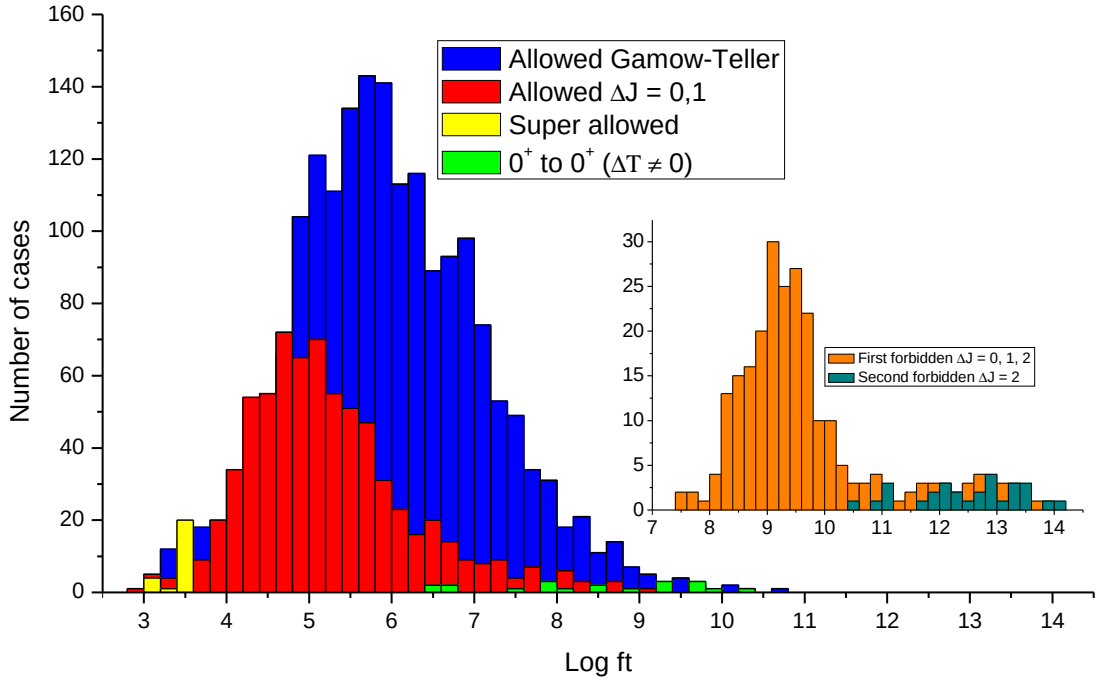

Figure 1.2: Summary plot of $\log ft$ values in β-decay based on Figure 1 from [Sin98].

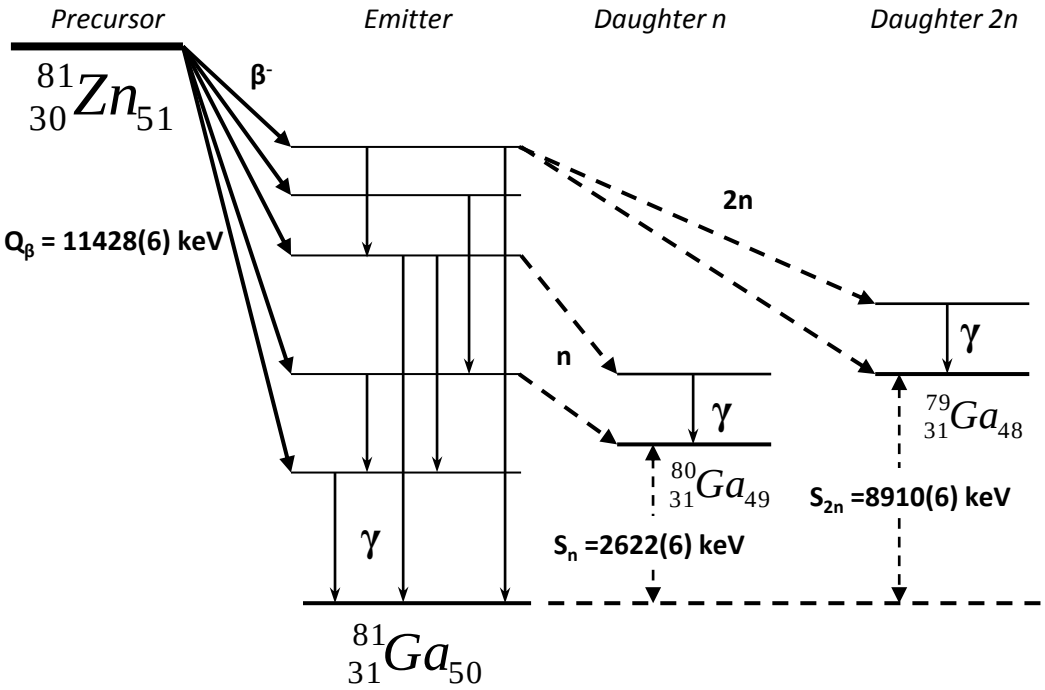

Figure 1.3: Example of β_n and β_{2n} emission in the decay of ^{81}Zn. The nucleon emission in this plot is produced from well-defined excited states in the emitter. In a real situation this states are so close one to another, that they form a continuum. The Q_β value and neutron separation energies S_n and S_{2n} were take from [Aud12a].

$$S_n = \left[M\left(Z, N-1\right) - M\left(Z, N\right) + m_n\right] c^2. \tag{1.20}$$

The difference between neutron separation energy and Q_β gives the available energy $Q_{\beta n}$ for this process. Whenever this process is energetically permitted, there will be competing processes, as the γ de-excitations from the states in emitter or β-decays to lower levels in the emitter that cannot decay by particle emission.

1.2 Gamma Decay

The next step is to analyse the *gamma emission* caused by the β-decay process. In most of the cases the product nucleus remains in an excited state and goes to the ground state by emitting one or more photons. The transition probability between excited states is described by Fermi's Golden Rule, that shows a strong proportional dependence of the transition rate from the transition matrix element $\langle J_f M_f \left| H_{int} \right| J_i M_i \rangle$ of the final and initial states. Neglecting the internal composition of nucleons and assuming that photon's wave length is much higher than the nucleus size one can describe the electromagnetic field in terms of multipoles of electric ($E\lambda$) and magnetic ($M\lambda$) components, where λ is the multipole order. With these assumptions, the *electric* and *magnetic multipole* operators can be written as [Ham75]:

$$\mathcal{M}\left(E\lambda, \mu\right) = \quad \rho\left(\mathbf{r}\right) r^\lambda Y_{\lambda\mu}\left(\hat{\mathbf{r}}\right) d\tau, \tag{1.21}$$

$$\mathcal{M}\left(M\lambda, \mu\right) = \frac{-1}{c\left(\lambda+1\right)} \quad j\left(\mathbf{r}\right) \cdot \left(\mathbf{r} \times \boldsymbol{\nabla}\right) r^\lambda Y_{\lambda\mu}\left(\hat{\mathbf{r}}\right) d\tau, \tag{1.22}$$

where $\rho\left(\mathbf{r}\right)$ is the charge distribution, $j\left(\mathbf{r}\right)$ is the current distribution and $Y_{\lambda\mu}$ are the spherical harmonics of order λ, μ. Parity properties together with conservation of angular momentum give the selection rules for γ transitions:

$$\Delta\pi = \begin{cases} \left(-1\right)^\lambda & E\lambda \\ \left(-1\right)^{\lambda+1} & M\lambda \end{cases} \tag{1.23}$$

$$\left|J_i - J_f\right| \leq \lambda \leq J_i + J_f (0^+ \not\rightarrow 0^+), \tag{1.24}$$

The photons are bosons and have spin $S = 1$. Thus the transitions $0^+ \rightarrow 0^+$ are forbidden. However, the transitions may occur by internal conversion of electrons, that always competes with gamma emission, in which the nucleus de-excites by transferring its energy directly to an electron, which is emitted from the atom. This competition is characterized by a factor α, that is ratio between their probabilities. This factor increases with Z and multipolarity λ and decreases with γ energy. The total γ transition intensity is given thus by

$$I = I_\gamma\left(1 + \alpha\right). \tag{1.25}$$

In general, α increases rapidly with increasing multipolarity and decreasing energy. Pure γ-transitions are dominated by low values of λ, and the electric channel dominates over the magnetic one.

1.2.1 Lifetimes of excited states

In most of the cases, a nucleus in an excited state is de-excited to low-lying energy levels by emitting photons of different energy, multipolarity and transition probability. The total transition probability P_{tot} can be determined by measuring the *mean lifetime*, *mean life* or simply *lifetime* τ of a certain nuclear energy level. The relation between the mean life, the half-life $T_{1/2}$ and, therefore, the total transition probability is given by:

$$\tau = \frac{1}{P_{tot}} = \frac{T_{1/2}}{ln2} \tag{1.26}$$

Since a given excited state can decay to more than one level the total transition probability is the summed transition probability of all depopulating transitions. If the de-excitation pattern is known, the partial mean life for a certain transition is $\tau_\gamma = \tau / I_{frac}$, where the fractional intensity I_{frac} is the γ-intensity of the particular transition divided by the total de-excited level intensity. Therefore, the partial mean life is given by:

$$\tau_\gamma = \tau \left(\frac{I_\gamma}{\sum_i I_{\gamma i} \left(1 + \alpha_i\right)} \right)^{-1} \tag{1.27}$$

The index i is over all the γ transitions depopulating the level, and the electron conversion branch is taken care of any α_i.

1.2.2 Transition probabilities and Weisskopf estimates

It is very useful to obtain an analytic expression for the transition probabilities between two states $|J_i M_i\rangle$ and $|J_f M_f\rangle$ characterized by its total angular momentum. To evaluate the transition matrix element it is necessary to sum over the magnetic quantum numbers M, given by the condition $M_i + \mu = M_f$, where μ is the index from equations 1.21 and 1.22. This gives the reduced transition probability [Boh75]:

$$B\left(X\lambda;\, J_i \to J_f\right) = \sum_{\mu, M_f} \left| \left\langle J_f M_f \left| \mathcal{M}\left(X\lambda, \mu\right) \right| J_i M_i \right\rangle \right|^2 = \frac{1}{2J_i + 1} \left\langle J_f \left| \mathcal{M}\left(X\lambda\right) \right| J_i \right\rangle , \tag{1.28}$$

where X is either E or M. The Wigner-Eckhart theorem [Ros57] was used in 1.28 to factor out M_i and M_f. The reduced matrix element is hence independent of the magnetic quantum numbers and contains the nuclear structure information. To compute these reduced matrix elements and, therefore, the reduced transition probability one should construct wave functions based on a particular model. In order to find the experimental values, we must find the contribution of each multipole order to the experimentally measured lifetime. For a transition with a multipole λ from an initial to a final state defined by their J, the partial mean life and the reduced transition probability are related by [Boh75]:

$$B\left(X\lambda;\, J_i \to J_f\right) = \frac{1}{\tau_\gamma} \left[\frac{\lambda \left((2\lambda + 1)!!\right)^2}{8\pi \left(\lambda + 1\right)} \hbar \left(\frac{\hbar c}{E_\gamma} \right)^{2\lambda + 1} \right], \tag{1.29}$$

where the energy transition energy appears as E_γ. The $B\left(X\lambda;\, J_i \to J_f\right)$ is a dimensional quantity, measured in $e^2 fm^{2\lambda}$ in the case of electric transitions and $\mu_N^2 fm^{2\lambda - 2}$ for the

magnetic transitions. As example, we calculate transition rates for the first four multipole orders:

$$\begin{aligned} B(E1) &= 6.29 \times 10^{-16} E_\gamma^{-3} \tau_\gamma^{-1} e^2 fm^2 & B(M1) &= 5.68 \times 10^{-14} E_\gamma^{-3} \tau_\gamma^{-1} \mu_N^2 \\ B(E2) &= 8.20 \times 10^{-10} E_\gamma^{-5} \tau_\gamma^{-1} e^2 fm^4 & B(M2) &= 7.41 \times 10^{-8} E_\gamma^{-5} \tau_\gamma^{-1} \mu_N^2 fm^2 \\ B(E3) &= 1.76 \times 10^{-3} E_\gamma^{-7} \tau_\gamma^{-1} e^2 fm^6 & B(M3) &= 1.59 \times 10^{-1} E_\gamma^{-7} \tau_\gamma^{-1} \mu_N^2 fm^4 \\ B(E4) &= 5.92 \times 10^{3} E_\gamma^{-9} \tau_\gamma^{-1} e^2 fm^8 & B(M4) &= 5.34 \times 10^{5} E_\gamma^{-9} \tau_\gamma^{-1} \mu_N^2 fm^6 \end{aligned} \tag{1.30}$$

A close agreement between the theoretical and experimental transition probabilities represents a more stringent test of the nuclear model wave function than for instance agreement for the level energies. The level energies, being static properties, are described by a wave function which normally is composed of many different components. If some of these components are strong they may dominate over the weaker ones in the contribution to the energy's eigenvalue. Thus, the energy may be correctly reproduced even if the detailed composition of the wave function is incorrect. On the contrary, the $B(X\lambda)$ are very sensitive to the detailed wave functions. Certain types of transitions are very susceptible to the structure of initial and final state. The most sensitive groups are the transitions which are enhanced due to collective admixtures and those which are forbidden by selection rules. The second part of Eq. 1.28 is generally valid for pure states only. If mixing is involved, the general expression needs to be modified.

The measured transition probabilities for a given type and multipolarity have been observed to vary by several orders of magnitude among different nuclei, and sometimes also within the same nucleus. In order to compare experimentally the measured and theoretical transition probabilities *Weisskopf estimates* were introduced [Wei51]. They give a simple physical interpretation of the transition strength. The Weisskopf estimates measure the transition probability if one particle is responsible of the transition, i.e. we assume the single particle approximation. To compute the estimates we consider the constant radial wave function, nuclear radius given by the usual expression $R \propto A^{1/3}$ and the fact that the transition is caused by only one nucleon which de-excites from one orbit to another without affecting the other nucleons. With these assumptions, the reduced transition probabilities for electric and magnetic multipolarities are given by:

$$B_W(E\lambda) = \frac{1}{4\pi} \left(\frac{3}{\lambda+3} \right)^2 (1.2)^{2\lambda} A^{\frac{2\lambda}{3}} e^2 fm^{2\lambda} \tag{1.31}$$

$$B_W(B\lambda) = \frac{10}{\pi} \left(\frac{3}{\lambda+3} \right)^2 (1.2)^{2\lambda-2} A^{\frac{2\lambda-2}{3}} \mu_N^2 fm^{2\lambda-2} \tag{1.32}$$

The *Weisskopf units W.u* provide a reference to compare the theoretical and experimental results. If a transition is enhanced by an order of magnitude or more over the Weisskopf estimate, many nucleons must be acting together in a coherent manner. Thus, these units serve also to indicate the magnitude of collectivity of the transition.

The measured lifetime of a certain energy level is employed to derive the transition rate of γ-rays that de-excite this level. In light of this, the transition multipolarity can be discussed and in some cases the spin of the de-excited state can be deduced or at least some values can be excluded.

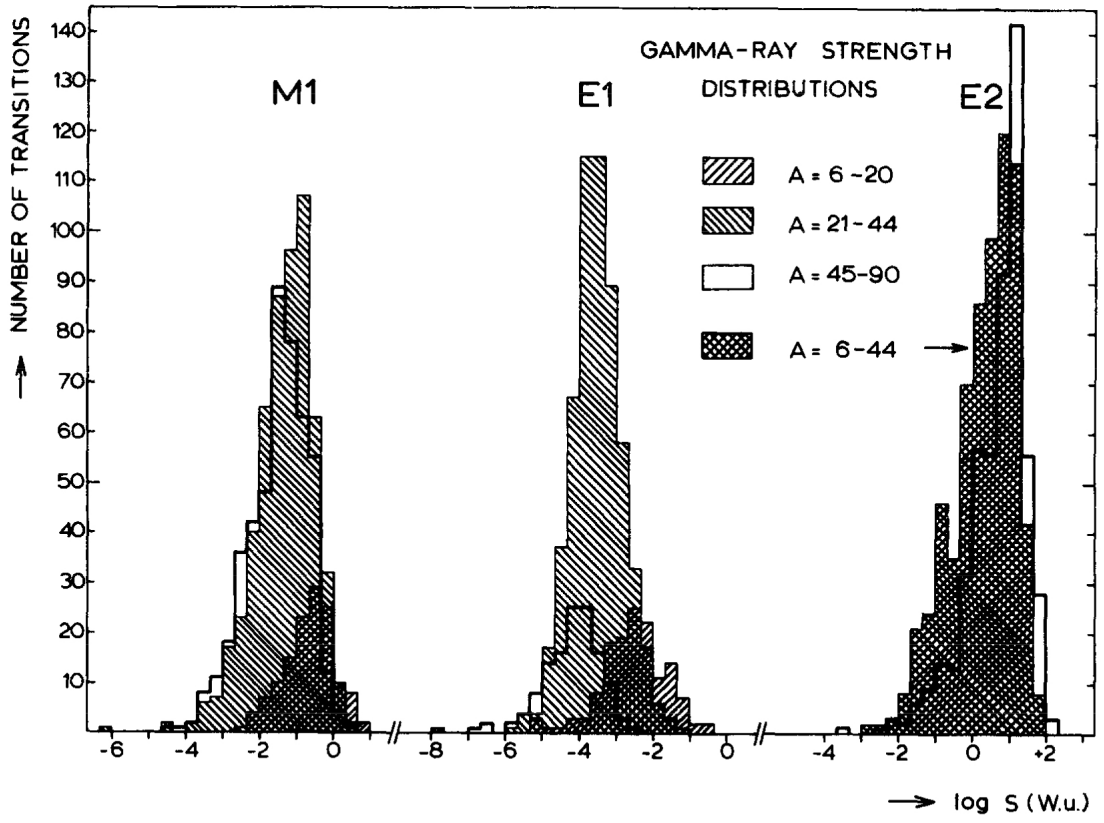

Figure 1.4: Strength histograms of M1, E1 and E2 γ transitions from light ($A = 6 - 20$), intermediate ($A = 21 - 44$) and intermediate-heavy nuclei ($A = 45 - 90$). Taken from [Sin98].

The transition rates denoted by $B(X\lambda)$ can be enhanced or quenched with respect to measured values from the systematics of the region or the expected values calculated with a given theoretical model. The latest compilation of γ-transition strengths in $A = 45 - 90$ nuclei, that is the transition rates of magnetic and electric multipolarities in W.u., was done in 1979 by P. M. Endt [End79]. It provides very useful information about experimental $B(X\lambda)$ values in nuclei closed to ^{78}Ni. Fig. 1.4 contains the comparison between the strength distribution for the most frequent transition ($M1$, $E1$ and $E2$) in different regions of nuclei. The Recommended Upper Limits (RUL) are shown in Tab.1.3. They provide a good indication that if the measured transition rate is higher than RUL the assumed multipolarity may be wrong. The $E2$ transitions are usually associated with the collectivity of the de-excited states due to quadrupole vibration or rotations of a deformed nucleus. The $E3$ also show the deformation as consequence of octupole vibrations. On the other hand, the most common $M1$ transitions are slow and normally do not exceed 1 W.u.

Character	$B(X\lambda)$ (W.u.)	Number of transitions
E1	0.01	127
E2	300	562
E3	100	45
E4	100	17
M1	3	470
M2	1	15
M3	10	7
M4	8	30

Table 1.3: Recommended Upper Limits for transition rates in in nuclei from $A = 45 - 90$ region [End79]. The third column shows the number of experimental transitions used to obtain the limits

1.3 The Shell Model

There exist many strong experimental evidences that shows the existence of *magic-number nuclei* in nature. The number of protons and neutrons in these nuclei can be 2, 8, 20, 28, 50, 82 and 126 in analogy with the number of electrons in noble gases (2, 10, 18, 36, 54 and 86). The same theoretical treatment as in multi-electronic atoms was applied to describe this new nuclear structure. In first approximation, it was assumed that each nucleon moves independently in a nucleus under the action of some central potential which represents the effect of the other nucleons. The easiest way to construct this potential is to try first with the spherical harmonic oscillator or the infinite well. The Schrödinger equation can be solved analytically in both cases. After applying the Pauli principle, the number of nucleons in each energy level characterized by the two quantum numbers n and l can be obtained. The first three magic numbers are reproduced well with this simple assumptions but the others differ considerably from the experiment. Studying the problem with a more realistic potential, such as Wood-Saxon [Woo54], this problem persists: only the first three magic numbers can be explained, but the higher ones do not appear from the calculations.

Brilliant solution of this question came independently from Maria Göppert Mayer, Hans Süess, Otto Haxel and Hans Jensen in 1949 and was published in different sources [May49, Hax49, GM55]. The idea was to include a strong attractive *spin-orbit* term $V_{so}(r)$ $\mathbf{l} \cdot \mathbf{s}$ plus the term proportional to $\mathbf{l^2}$ in the total potential:

$$V = V_{WS}(r) + V_l \mathbf{l^2} + V_{so}(r)\mathbf{l}\cdot\mathbf{s}, \tag{1.33}$$

where Wood-Saxon potential is given by

$$V_{WS}(r) = \frac{-V_0}{1 + exp(\frac{(r-R)}{a})}, \tag{1.34}$$

and the radial part of spin-orbit interaction can be approximated by $-24A^{-2/3}$. In this equation the nuclear radius is given by $R = 1.25A^{1/3}$ and $a = 0.524$. The well depth V_0 is

of the order of 50 MeV, adjusted to obtain the correct separation energies. The $\mathbf{l} \cdot \mathbf{s}$ term in Eq. (1.33) is the responsible of new reordering of the energy levels. Solving Schrödinger's problem with the new potential the energy spectrum is obtained (see Fig. 1.5). The states are labelled with three quantum numbers nl_j, where the total angular momentum or *nuclear spin* is given by $j = l + s$, and in each level there can be only $2j + 1$ nucleons of each type. A group of levels well-separated from the others constitutes a *shell*. The magic numbers are reproduced correctly now. Nuclei with nucleons located in closed shells are spherically symmetric and form an inert core with total nuclear spin $j = 0$. When nucleons are added to the closed-shell core the properties of the wave functions are determined essentially by the last unpaired nucleon and the excited states can be formed by simply elevating this nucleon to higher energy orbits.

This primordial shell model is nowadays called the *single or independent particle model* (SPM or IPM) due to the fact that the independent nucleons are confined by a surface-corrected isotropic potential, plus spin-orbit term. The main effect of this two-body interaction between nucleons is to generate a spherical mean field. The simplest shell-model calculations assume wave functions in which the nucleons fill the lowest available single-particle orbits, where this availability is determined by the Pauli principle.

In general, the Hamiltonian used to study nuclear properties can be written in terms of the one-body central potential H_1, which is determined by the sum of kinetic and potential energy of each nucleon, and the two-body residual interaction H_{12}, which is small enough to be treated in perturbation theory. In our example from the Eq. (1.33) no residual interaction was taken into account. In this way, the shell-model calculation procedure consist of correct choice of the dominant central field H_1, selection of the orbits from the one-particle eigenstates of H_1, calculation of the multinucleon eigenstates spectra of H_1, correct selection of the residual interaction H_{12} and diagonalization of this matrix between the multinucleon eigenstates of H_1.

Many nuclear properties can be described with this simple model. However, this scheme fails in determination of nuclear spectroscopy features specially in nuclei far away from stability. For that purpose, more detailed treatment of H_{12} is needed with the freedom to admix many different multiparticle configurations into a given eigenstate. The appropriate form of H_{12} and larger and larger configuration spaces make these new shell-model calculations (sometimes called *large-scale or many-body* shell-model calculations (LSSM)) more credible.

The LSSM correctly predicts many properties of the nuclei near the Valley of Stability, such as the spin-parity of the ground and the first excited states of even-even systems or the magnetic dipole and electric quadrupole moments. It is used in our work to perform calculations with good precision, in order to verify the experimental results. For this purpose, several state-of-the-art residual interactions employed with the ANTOINE [Cau05a] and NUSHELL**@**MSU [Bro14b] codes were used for calculations of the energy levels of nuclei studied in this thesis. All of them were specially constructed to operate in ^{78}Ni region.

One of the interactions, called JUN45, was developed by Honma *et al.* in 2009 [Hon09], and it was focused in the *pf* shell with ^{56}Ni core and $1p_{3/2}$, $0f_{5/2}$, $1p_{1/2}$ and $0g_{9/2}$ single-particle orbits. A microscopic interaction based on the Bonn-C nucleon-nucleon potential was taken as a starting point for a Hamiltonian which was characterized by 133 two-body matrix elements (TBME) and 4 single-particle energies (SPE). The effective interaction JUN45 was obtained after performing 45 linear combinations of these parameters and

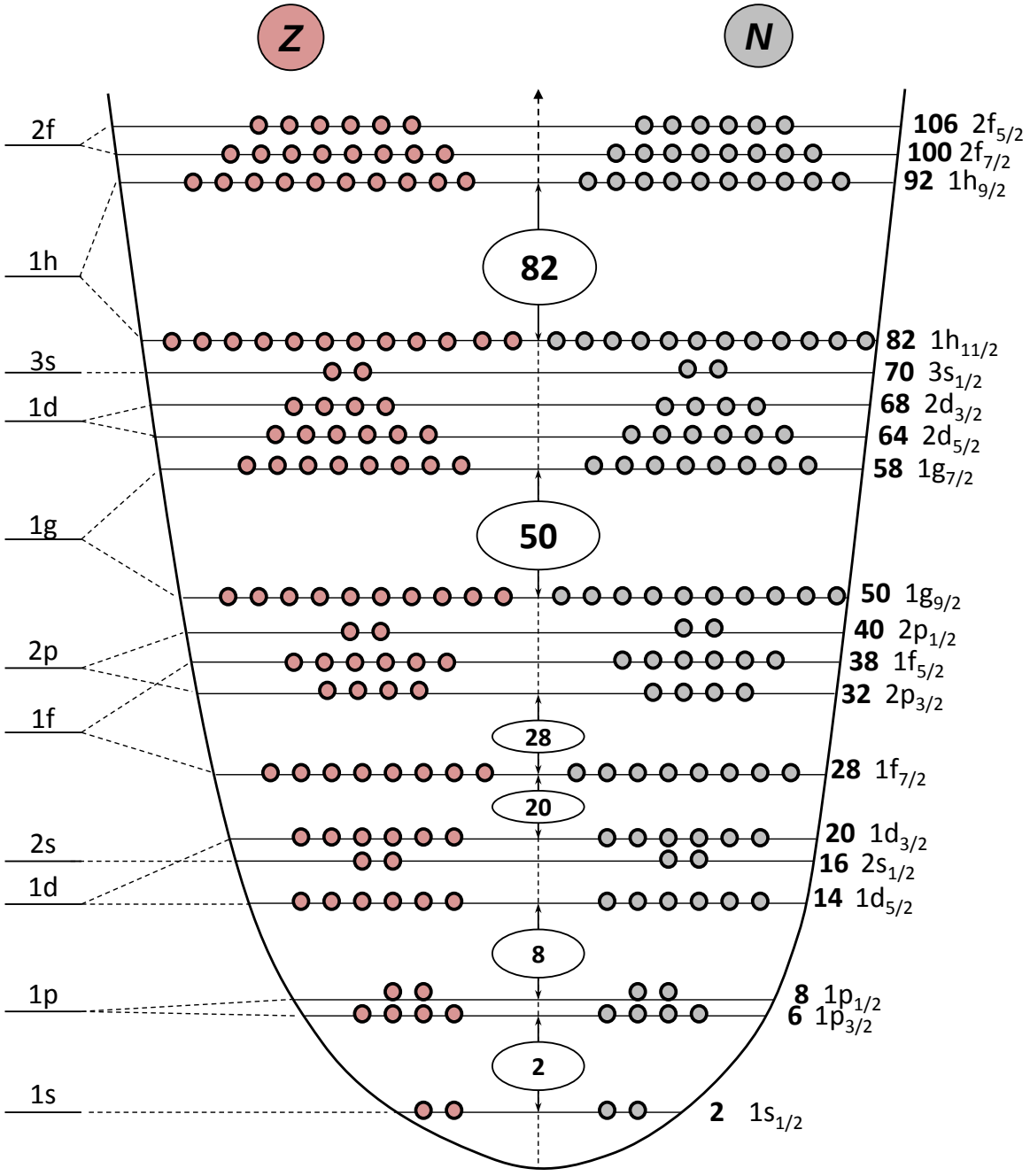

Figure 1.5: Energy levels calculated with Wood-Saxon plus spin-orbit interaction. It can be seen how the spin-orbit term splits the levels (except $l = 0$) into two new ones. In the right side of the plot the number of accumulated particles ($2j + 1$) is shown together with the label nl_j of each state.

fitting to more than 400 experimental binding and excitation energies. The interaction confirms specially well the experimental data of low-lying states in $N = 49$ isotones, Ge isotopes near $N = 40$ and $N = Z$ nuclei with $A = 64 \sim 70$.

Another effective interaction, called jj44b, which made successful prediction for nuclei near ^{78}Ni was created in 2004 by Lisetskiy *et al.* [Lis04]. It was constructed with the same effective core and model space. The Hamiltonian was also based on the Bonn-C NN potential including four single-particle energies and 65 $T = 1$ two-body matrix elements. The fitting to the experimental data was done with Linear Combination Method which leads to 20 linear combinations of SPE and TMBE. For the neutron interaction part 91 experimental energy levels from $^{60-72}$Ni and 15 binding energies from $^{57-78}$Ni were used while for proton interaction 113 energy levels and 19 experimental binding energies were needed. The detailed use of jj44b with some interesting results in ^{78}Ni and ^{100}Sn region can be found in [Lis04]. Theoretical calculations of Ga isotopes shows that jj44b reproduce better the heavier isotopes than JUN45 [Sri12].

1.4 The r-process path

Several nucleosynthesis processes are responsible of the creation of new atomic nuclei. In case of intermediate and heavy nuclei the neutron capture process plays an important role. This capture can be fast or slow. When a neutron is caught in conditions of relatively low neutron density and intermediate temperatures in stars we talk about the s-process (slow process). Its name comes from the neutron capture characteristic time, relatively lower than the half-life of the β^- decay which occurs after the slow capture. The s-process is the responsible of the production of more than half of the elements heavier than Fe.

On the other hand, a neutron capture process is called *rapid* or r-process when its characteristic time is much lower than the β-decay half-life. The mechanism of this process consists on rapid successive captures of neutrons by heavy neutron-rich seed nuclei. It occurs in stars with high neutron density at high temperatures. During the r-process the nuclei are strongly bombarded by huge fluxes of neutrons ($\sim 10^{22}$ neutrons$/cm^2 \cdot s$) producing neutron-rich unstable nuclei which decay successively by β^- decay to the stable ones.

Three peaks with double structure at $A = 80 - 88$, $A = 130 - 138$ and $A = 194 - 208$ can be observed in the curve of abundance of elements shown in Fig. 1.6. This means that there should exist some process which involves the rapid capture of neutrons which occurs before the nuclei can decay by the β process. The sharpness of these double peaks means that only a small amount of environments have contributed to the r-process.

Suess and Urey associate the heavier peak of each group from the Fig. 1.6 with neutron magic numbers 50, 86 and 126 and suggest to relate the lighter peaks with neutron-capture process which occurs under high neutron densities [Sue56]. In the first case we deal with s-process, in which generally predominates the β-decay before a neutron is captured, and in the second case the r-process predominates in which the characteristic time scale is lower than β-decay half-lives [Bur57].

The description of classical r-process calculations can be found in [Tri75, Mat85, Kra93] where the use of *waiting-point* approximation and β-flow equilibrium simplifies considerably the computation process. The first approximation includes basically two assumptions: a) the temperature and the neutron density are sufficiently high that the

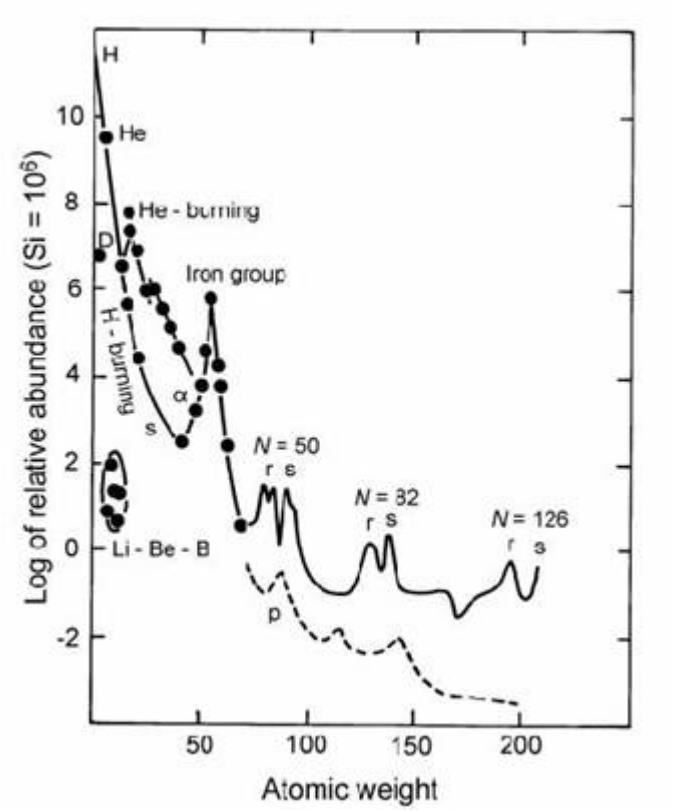

Figure 1.6: Abundances of the Elements based on the data from [Sue56]. Note the twin peaks at $A = 80$. Picture taken from [Bur57].

(n, γ) and (γ, n) reactions will be in equilibrium, and b) the time scale for β-decay is much lower than the scale for neutron capture. In this way, large abundances of elements will be created near the so called *waiting points* where the β-decay is faster than the neutron capture. The *steady* or β-flow equilibrium condition assumes that the β flow from each Z-chain to $(Z+1)$ is equal to the flow from $(Z+1)$ to $(Z+2)$. The nuclear Saha equation,

$$\frac{n_n N(Z, A-1)}{N(Z, A)} = \frac{2(2\pi\mu kT)^{3/2}}{h^3} \frac{G(Z, A-1)}{G(Z, A)} e^{-\frac{B_n}{kT}}, \tag{1.35}$$

which describes the abundance ratio of two adjacent isotopes A and $A-1$, includes the exponential dependence on the neutron separation energy B_n of an isotope with mass A, divided by the stellar temperature T [Mat85]. Neglecting differences in the ratios of the partition functions the maximum abundance in each isotopic chain is determined by the neutron number density n_n and the temperature. The exponential behaviour in Eq. 1.35 converts B_n in the most important parameter in the classical r-process calculations. The abundance peak varies sharply around a particular value of B_n constituting what is called *r-process path* (see Fig. 1.7).

Some nuclear parameters needed for the r-process path calculations from the classical point of view including ^{81}Ga and ^{80}Ga isotopes studied in this work can be found in the Table 1 of [Mat85]. When the neutron separation energy is small, the production of the next heavier isotope by the r-process must wait until the β-decay produces a new nuclide

[1]http://www.ph.sophia.ac.jp/ shinya/research/research.html

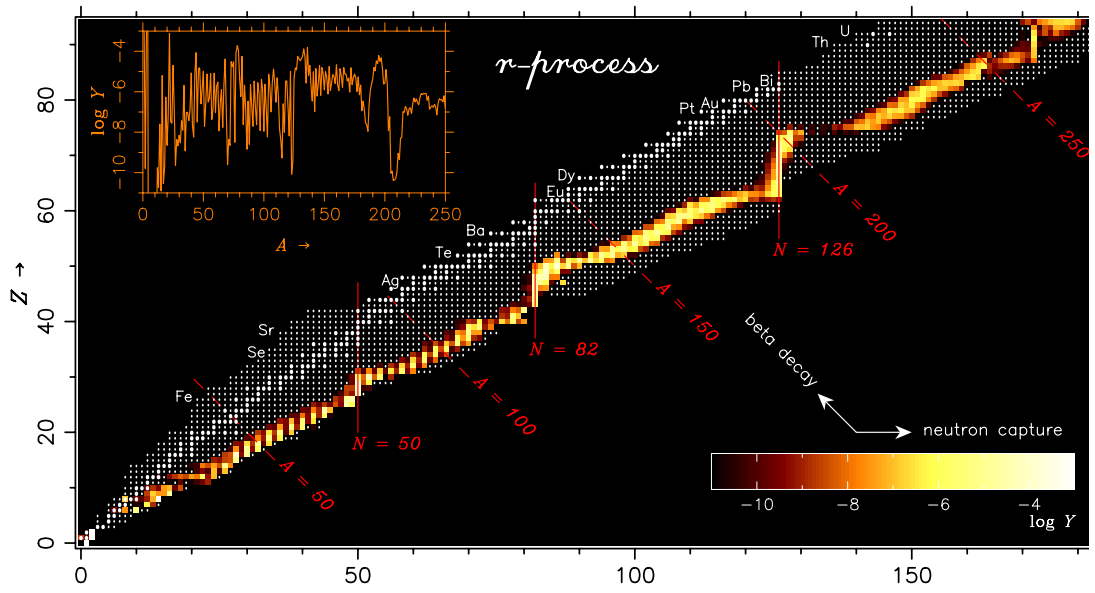

Figure 1.7: r-process Nucleosynthesis in Supernovae. Taken from Sophia University web page [1].

with higher B_n. Under this circumstances, the neutron closed-shell points of $N = 50$, $N = 82$ and $N = 126$, where the binding energy decreases precipitously, indicates the existence of three waiting-point nuclei: ${}^{80}_{30}\mathrm{Zn}_{50}$, ${}^{130}_{48}\mathrm{Cd}_{82}$ and ${}^{195}_{69}\mathrm{Tm}_{126}$.

The measurements of β-decay half-lives and β-delayed neutron branches are the most decisive for the correct calculation of the r-process path. These parameters can be obtained from the β-decay experiment such as explained in chapter 3 of this thesis (see chapter 3). In our case the β-decay half-life had been measured for r-process-path nuclide ^{81}Zn and ^{81}Ga. On the other hand, the probabilities of β-delayed neutron emission P_n, neutron-capture cross sections $\sigma_{n,\gamma}$ and ground- and excited-state spin-parities play also an important role in r-process calculations.

In the Saha equation (1.35) the partition function $G(Z, A)$ can be expressed in terms of the ground-state and excited-state spins and the energies of the first excited states:

$$G = \sum_i (2J_i + 1)e^{-E_i/kT}, \tag{1.36}$$

where the summation is done over all nuclear states. This shows that the characterization of the nuclear structure is also very important for r-process calculations. The total β-decay rate λ_β is also a very useful magnitude because it participates in the relative elemental abundances computation according to the following equation:

$$\frac{dN_Z}{dt} = \lambda_{Z-1}N_{Z-1} - \lambda_Z N_Z, \tag{1.37}$$

which shows that even if the r-process path passes through low β-decay-rate isotope the abundance of this element will build up as it waits to decay. This happens for the waiting-point nuclei with neutron-closed shells $N = 50$, $N = 82$ and $N = 126$, as was explained above. The β-decay rates are related to the half-lives of the exotic nuclei via $\lambda_\beta = ln2/T_{1/2}$.

In the general framework of the r-process, the β-delayed neutron emission must be taken into account when the nuclei decay from the r-process path back to the β-decay stability region. In case of high value of the β-delayed neutron emission probability $P_n(\%)$ an important smoothing of the final observed abundances may be noted. This effect can be shown in the Eq. (1.38) which expresses the general abundance change dY/dt of nucleus (Z, A) in r-process nucleosynthesis:

$$\begin{aligned}\frac{dY(Z,A)}{dt} &= n_n Y(Z, A-1)\sigma_{A-1} + Y(Z, A+1)\lambda_{A+1} \\ &-Y(Z, A)(n_n\sigma_A + \lambda_A + \lambda_\beta^A + \lambda_{\beta n}^A + \lambda_{\beta 2n}^A + \lambda_{\beta 3n}^A) \\ &+Y(Z-1, A)\lambda_\beta^{Z-1,A} + Y(Z-1, A+1)\lambda_{\beta n}^{Z-1,A+1} \\ &+Y(Z-1, A+2)\lambda_{\beta 2n}^{Z-1,A+2} + Y(Z-1, A+3)\lambda_{\beta 3n}^{Z-1,A+3},\end{aligned} \tag{1.38}$$

where up to three delayed neutrons were taken into account expressed by their β-delayed-neutron-emission rates $\lambda_{A_{\beta n}}$, $\lambda_{\beta 2n}^A$ and $\lambda_{\beta 3n}^A$. For deeper understanding of Eq. (1.6) see [Kra93].

Chapter 2

Half-life measurements of excited states around ^{78}Ni

One of the most important features in nuclear structure is the determination and experimental confirmation of magic numbers predicted by the spherical shell model. A special region of interest is situated near $N = 50$ and $Z = 28$ where the ^{78}Ni isotope is considered to be doubly magic. The neutron to proton ratio is considerably high at this location and the nuclei situated near ^{78}Ni are particularly exotic. This fact introduces many complications for their production and experimental analysis.

Studying the decay schemes of nuclides close to ^{78}Ni helps to understand the evolution for neutron-rich fp shells beyond $Z = 28$. In this chapter we will describe some irregularities occurring in this interesting region such as the *monopole migration* near $N = 50$, the anomalous variation of the first $9/2^+$ state in odd-Z isotopes and the inversion of states above $N = 40$. The reasons to measure the structure of ^{81,80}Ga, ^{81}Ge and ^{81}As will be presented in the second section as motivation of this thesis. Our tool to characterize the properties of this nuclei is the experiment measurements in the framework of the β-decay of ^{81}Zn. The determination of level schemes and half-lives of low-lying states is the strong point of our experimental technique which is described in details in the last section.

2.1 Exotic nuclei in the vicinity of ^{78}Ni

More than 6000 different nuclides with sufficiently large half-life are estimated to be created and studied nowadays. Fig. 2.1 shows the two-dimensional nuclear chart representing almost all those nuclear species according to their proton (Z) and neutron (N) number. Three dashed lines can be appreciated in the figure: two drip blue lines indicating the proton and neutron instability emission and one green drip line where the fission barrier becomes zero. In principle, all the nuclei that are in the region formed by these three lines can be produced, although some of them may have very short lifetimes. Different color codes are used to classify the decay of nuclei and to show special regions of interest. The nuclides in black constitute the valley of stability, that is, the region where stable nuclei are located. We call *exotic nuclei* those which are very far away from the line of stability and because of their nature cannot be studied as those which are inside or very close to the valley of stability. The properties of exotic nuclei allow to test the

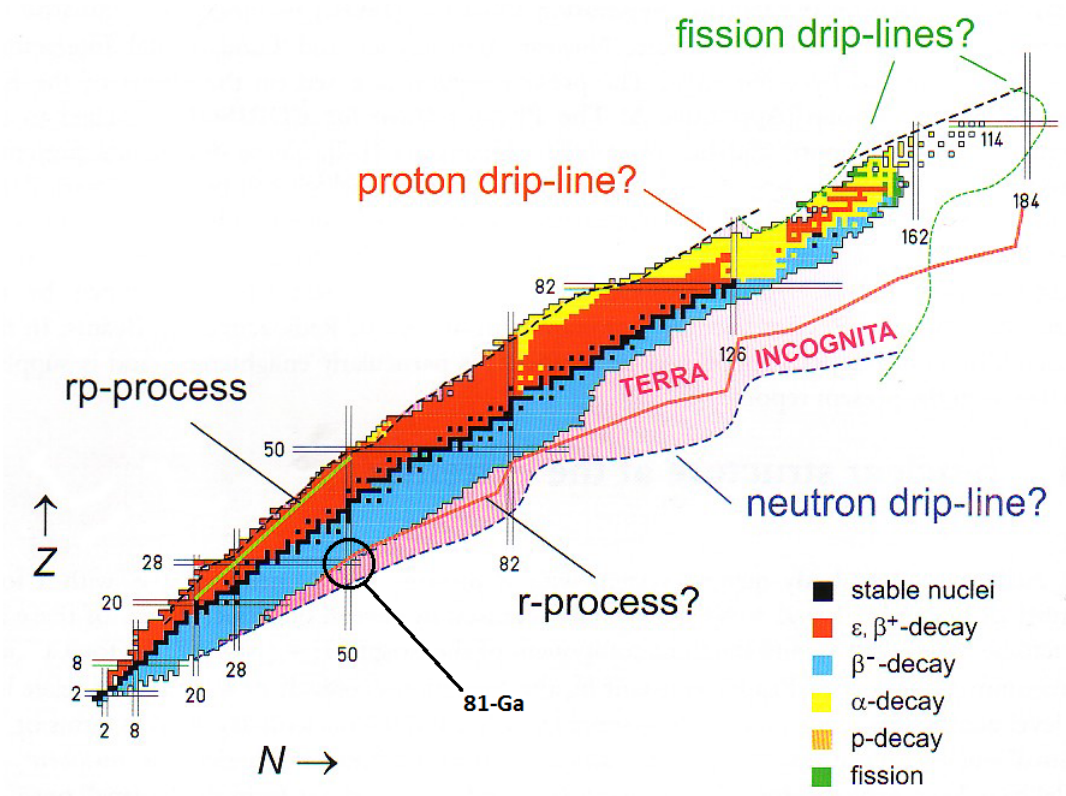

Figure 2.1: Chart of nuclides.

robustness of the theoretical models for species located far away from the stability.

This thesis is focused in the analysis of the exotic nuclides located in the border of β^--decay region, marked with blue, and Terra Incognita, only few nucleons away from the doubly magic ^{78}Ni, which has 28 protons and 50 neutrons.

The study of the exotic nuclei provides valuable information not only about nuclear structure models but also about nuclear interactions, decay models, nuclear reactions, etc. Some neutron-rich nuclei studied in this work play a role in Stellar Nucleosynthesis processes. Many of them cannot be produced at the laboratory conditions and have to be studied by theoretical models and systematics considerations. Due to their special properties they have to be produced at accelerators or neutron beam facilities and must be analyzed immediately on-line after the synthesis because of the very short lifetimes. According to the mass we can classify them in light exotic nuclei, intermediate mass nuclei, heavy and super-heavy exotic nuclei. There are few different ways to produce the exotic nuclei according to their mass and proton/neutron ratio (neutron fission, fragmentation by protons, heavy beam fission, etc.). The technique used to produce the nuclides studied in this work is based on a proton beam impacting on a fragmentation target and its detailed description will be provided in the next section.

The standard procedure to measure the properties of an exotic nucleus consists of few steps. The first and most important one is to prove the existence of such nuclei. After that the decay characteristics such as the half-life are measured. The intrinsic properties like nuclear mass or nuclear radius are also determined even before the decay properties. The measurement of the spectroscopic parameters (γ spectroscopy, energies of the excited states and their spin-parity assignations, electric and magnetic multipole moments of the

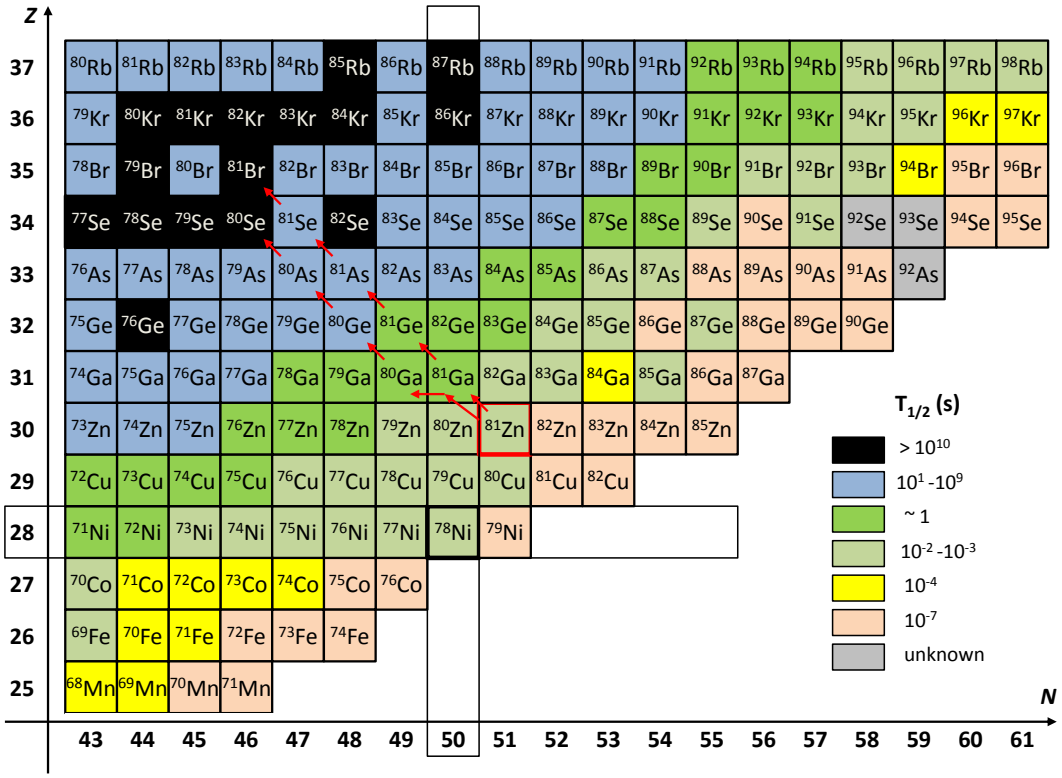

Figure 2.2: Region of nuclei closed to the doubly magic ^{78}Ni.

states, etc) which permit to construct the level scheme of the daughter nucleus requires higher production rates, and that typically occurs after few years of investigation.

The intermediate-mass nucleus ^{78}Ni, with $Z = 28$ and $N = 50$ is expected to be doubly magic since both N and Z are experimentally verified magic numbers in nuclei close to the stability [Xu14]. According to the shell-model picture from Fig. 1.5 the structure of nuclides closed to ^{78}Ni will be dominated by the occupation of $\nu g_{9/2,7/2}$ and $\pi p_{1/2,3/2} f_{5/2}$ orbits. The analysis of the $Z = 28 + 1$ copper isotopes [Fla09, Fra01b, Ste08] shows some modifications in the ordering of this single-particle levels. The ground state spin-parity of ^{69}Cu$_{40}$ is $3/2^-$ and the first excited $5/2^-$ state is located at 1214 keV. The $N = 40$ energy gap between this states decreases rapidly with the filling of the $\nu g_{9/2}$ orbital being 534 keV in ^{71}Cu$_{42}$ and 166 keV in ^{73}Cu$_{42}$. The spin-parity of the ground state and the first excited state is inverted in ^{75}Cu$_{44}$ where the energy separation becomes 62 keV (See panel (c) from Fig. 2.3). Such state migration associated with the occupation of $\pi f_{5/2}$ by the single proton is well explained by the strong attractive residual monopole p-n interaction [Ots05] which becomes significant when neutrons start to fill the $\nu g_{9/2}$ orbital [Smi04, Fra01b]. This order remains in ^{77}Cu$_{48}$ and ^{79}Cu$_{50}$. The energy gap between $p_{3/2}$ and $f_{5/2}$ grows whenever the occupation of $\nu g_{9/2}$ is getting bigger being 650 keV in ^{79}Cu$_{50}$. The so called monopole migration was not observed in the equivalent $Z = 50+1$ Sb isotopes, where the energy of the single-particle state $\pi d_{5/2}$ increases with growing occupancy of the $\nu h_{11/2}$.

The systematic decrease of the energy gap between the $5/2^+$ ground state and the $1/2^+$ excited state in $N = 51$ isotones from $Z = 38$ Zr (1205 keV) to $Z = 32$ Ge (247 keV) indicates the possibility of a reordering of these states in ^{81}Zn (see Panel (a) from

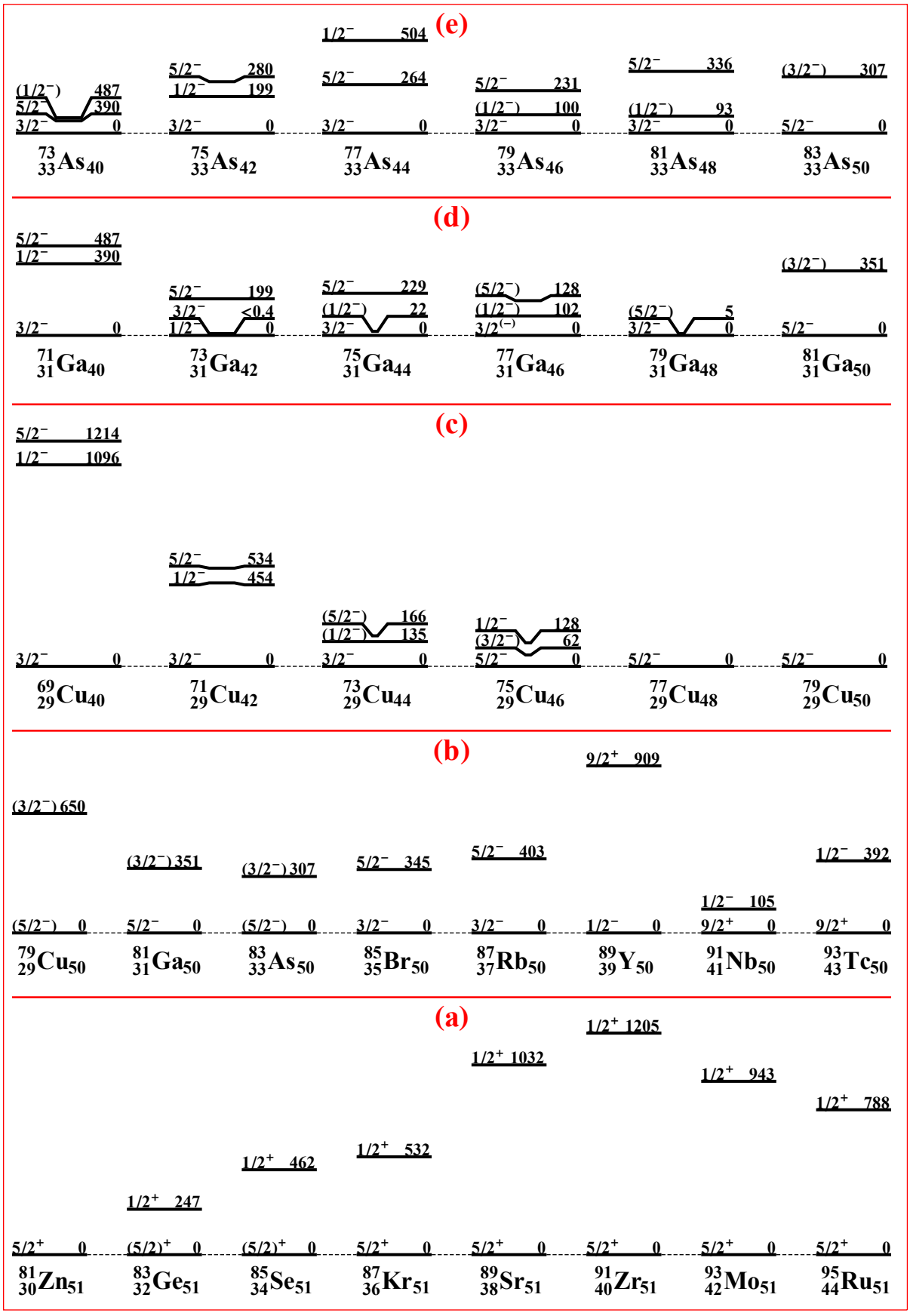

Figure 2.3: Systematic evolution of the low-lying states in $N = 51$ (a) and $N = 51$ (b) isotones. Panels (c), (d) and (e) show the ground state and the first excited states of Cu, Ga and As isotopes in the region between $N = 40$ and $N = 50$.

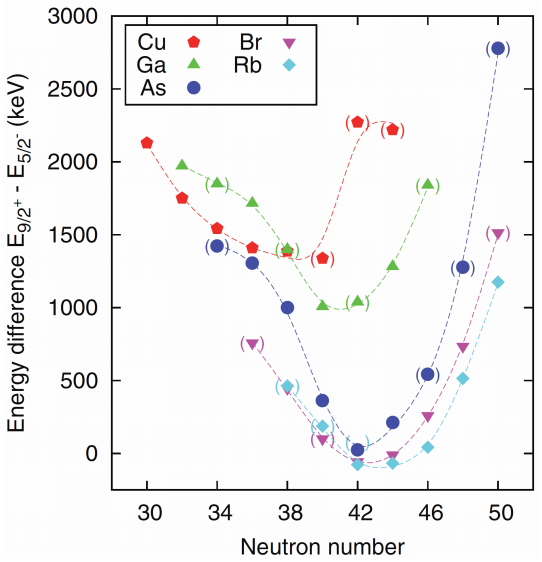

Figure 2.4: Systematics of $\pi g_{9/2} \rightarrow \pi f_{5/2}$ proton excitation energies from [Bac15].

Fig. 2.3). However, the preliminary results recently obtained in RIKEN [Nii14] seems to confirm the $5/2^+$ ground state of this nucleus, discarding the migration of the $1/2^+$ state due to the effect of monopole potential.

The structure of the odd-mass Ga nuclei has been of strong interest during the last years. One of the main objective of this works was the analysis of the evolution of single-particle states in Ga isotopes near the $Z = 28$ closed shell. The low-energy-level structure of $^{71-81}$Ga was studied with the β-decay of Zn isotopes ([**?** Run83, Eks86, Kra91b, Pad10]), as well as using particle transfer reactions ([Kay09b, Ver79]) and deep-inelastic reactions [Ste09]. All these isotopes are characterized by three valence protons in $\pi p_{3/2}$ orbit according to the standard shell-model configuration leading to $3/2^-$ ground state. However, the $N = 42$ and $N = 50$ Ga isotopes do not show these properties. The ground spin-parity of the first one, the ^{73}Ga, was recently measured to be $1/2^-$ by Coulomb Excitation technique [Dir10a] forming a doublet with $3/2^-$ with energy difference less then 0.4 keV [Ved16]. Collinear laser spectroscopy measurements [Che10] also confirm this value and propose the $5/2^-$ spin-parity assignment for the ground state of ^{81}Ga. The high abundance of experimental data allows to test the theoretical models. Large scale shell model calculations were performed by H. Jiang [Jia11] in 2011, P. C. Srivastava [Sri12] and P. Verma *et al.* [Ver12] in 2012. All theoretical results confirm the doublet in ^{73}Ga and that the $\pi p_{3/2}$ single particle state is higher in energy than the $\pi f_{5/2}$ in ^{81}Ga. The systematics of $N = 50$ isotones (see Panel (d) from Fig. 2.3) shows the $5/2^-$ predominance for the ground state in $^{79}_{29}$Cu$_{50}$, $^{81}_{31}$Ga$_{50}$ and $^{83}_{33}$As$_{50}$ where the valence protons are located in $\pi p_{3/2} f_{5/2}$ shells. The first excited state in these isotopes takes the $3/2^-$ spin-parity assignment indicating probably the $\pi p_{3/2}$ single-particle state. The panorama changes at $^{85}_{35}$Br$_{50}$ when the protons start to fill more the $\pi f_{5/2}$ shell and the ground state becomes $3/2^-$ while the first excited state takes $5/2^-$ value. This situation persists in $^{87}_{37}$Rb$_{50}$. Fig. 2.4 shows the systematics of proton energy excitations between $9/2^+$ and $5/2^-$ levels. The situation near $N = 50$ predicts significant increase of this gap from 1578 keV in ^{87}Rb to the recently measured 2779 keV in ^{83}As. The challenge of future work may be the determination of $9/2^+$ level in ^{81}Ga and ^{79}Cu nuclei.

The neutron-rich $Z = 32$ Ge isotopes with $40 \leq N \leq 50$ are characterized by four protons in the pf shell outside of the $Z = 28$ closed shell. Multiple experiments were performed with the purpose of measuring the properties of low-lying states in $^{73-81}$Ge. The structure of ^{73}Ge was studied from the β-decay of ^{73}Ga in 1976 by K. Forssten and M. Brenner [For76] as well as the structure of ^{75,77}Ge [Gra74] and ^{79,81}Ge by P. Hoff and B. Fogelberg in 1981 [Hof81]. Important information about the spin-parity assignments was determined via transfer-reaction data [Ahn13, Yoh76, Kay09a]. The $N = 41$ and $N = 49$ isotopes have $9/2^+$ ground states due to the particle/hole presence in $\nu g_{9/2}$. Both seem to have $1/2^-$ isomers and positive parity intruders of $5/2^+$ and $1/2^+$. However, measurements from Studsvik R2-0 reactor in 1981 performed by P. Hoff and B. Fogelberg affirm that the isomer is likely to be $1/2^+$. It is pertinent to mention here that the systemtics of $N = 49$ isotones does not support this proposition. All these isotones from ^{83}Se to ^{91}Mo have a long-lived $1/2^-$ isomer. The other two germanium isotopes, the $N = 43$ and the $N = 47$ one, have the same $1/2^-$ ground state and $7/2^+$ isomer at 140 and 190 keV while in the intermediate ^{77}Ge$_{45}$ the structure is inverted and the 54 s excited state at 160 keV takes $1/2^-$ value.

The next important isotope chain that can provide valuable information about the double magicity of ^{78}Ni is ^{81}As with only two protons more than Ga isotopes. These five valence nucleons are distributed in $2p_{3/2}$, $1f_{5/2}$, $2p_{1/2}$ and $1g_{9/2}$ states while the neutrons start to fill the $1g_{9/2}$ from ^{73}As to ^{83}As. The low-spin structure of these nuclei has been an important research target of many experimental groups making use of the β-decay study [Sch92, Ng68, Bha79, Mei12, Win88a, Hof81], (^{3}He, d), (α, p) and (p,n) reactions [Bet71, Mor82, Rot80, Rot83], fusion reactions [Por11, Orl09] and neutron-induced fission [Bac15]. The main feature is the $3/2^-$ ground state of $^{73-79}$As and migration of this state to $5/2^-$ in ^{83}As as shown in Panel (e) of Fig. 2.3. It has been found that the low-lying negative-parity structures consist of single-particle and rotational bands characterized by the $p_{1/2}$, $p_{3/2}$ and $1f_{5/2}$ orbitals. The $9/2^+$ level, originated most probably from the transition of an unpaired proton into the $g_{9/2}$ orbital, was found in all odd-A arsenic isotopes in $40 \leq N \leq 50$ region lying from 428 keV in ^{73}As to 2779 keV in ^{83}As (see Fig. 2.4). The half-lives of these levels were found to be in μs range except for the most neutron-rich nuclei ^{81,83}As, that have not been measured yet.

2.2 Motivation of the experiment

We propose to measure the level lifetimes and determine new properties of the nuclear structure in the exotic nuclei of ^{81,80}Ga, ^{81}Ge and ^{81}As by the $\beta\gamma\gamma$(t) time-delayed (ultra-fast timing) technique and $\gamma\gamma$ coincidence spectroscopy. These isotopes are relatively simple nuclear systems with few particles and/or holes outside of the doubly-magic core and thus can be treated rather precisely within the shell model. The anticipated new structure information, and in particular the lifetime results will put constrains on the model parameters and will serve to verify their predictions. The selected nuclei are some of the most exotic ones just above ^{78}Ni, where the transition rates can be studied at present.

The semi-magic $^{81}_{50}$Ga is the most interesting case. It has only 3 valence protons outside of ^{78}Ni core with the lowest proton orbits being $p_{3/2}$ and $f_{5/2}$. The $M1$ transition between these states, although allowed by the selection rules, should be l-forbidden and therefore

significantly slow. This should increase the lifetime up to the subnanosecond range. The investigation of systematic $9/2^+$ intruder is also very important because it sheds light in the single-particle excitations between $\pi g_{9/2}$ and $\pi f_{5/2}$ orbitals. We expect to extend the level scheme with high energy γ transitions up to the neutron separation energy at 6476 keV [Aud12b]. Confirmation of the $5/2^+$ character of the ground state of ^{81}Zn can be obtained from $\log(ft)$ values of the β-decay population of ^{81}Ga. The sufficient production of ^{81}Zn will provide the determination of the β half-life of its ground state which has being investigated during last years. It is well known that ^{81}Zn and ^{81}Ga lie along the r-process path only one proton above the waiting-point ^{80}Zn nucleus. Thus, the precise determination of its nuclear structures is crucial for r-process calculations.

As ^{81}Zn also decays by the β-delayed neutron emission the levels of ^{80}Ga can be populated. The level scheme of this process will be obtained for the first time and new measurement of P_n value will contribute for abundance change of ^{81}Zn in r-process nucleosynthesis. Opening the $A = 80$ decay chain we can also perform the half-life measurements from ^{80}Ga to the stable ^{80}Se.

We do not expect big improvements of the γ spectroscopy in ^{81}Ga's daughter ^{81}Ge because the yields included in the previous study performed by Hoff and Fogelberg in 1981 [Hof81] are similar to those included in our measurements. However, we believe to have enough statistics to clarify the half-life of the 679-keV isomer as well as to precise the half-lives of 711-, 896- and 1724-keV levels. This data can help to understand whether the spin-parity assignment of the isomer follows the systematic evolution or its value is changed to $1/2^+$ as predicted by Hoff and Fogelberg. Once the isomer is characterized the pair of intruders $1/2^+$-$5/2^+$ will be assigned. The strongest γ lines in ^{81}Ge the β-decay half-life of the ground state of ^{81}Ga which is very useful in r-process calculations.

Finally, the experimental yield of ^{81}As populated in the β-decay of ^{81}Ge is sufficiently high to expect enough statistics of γ rays to improve the previous measurements from Studsvik [Hof81], specially at the energies above 2 MeV. The main objective here is to measure the half-lives of the first three excited 93-, 290- and 336-keV states, that are expected to lie in the subnanosecond range due to the effects of collectivity caused by the interaction of neutrons from $g_{9/2}$ and protons in pf shell. More clear assignments of the β transitions may be done based on the lifetime measurements and $\log ft$ values. As in ^{81}Ga, it would be interesting to analyse the $9/2^+$ state established to lie at 2625 keV [Por11].

2.3 Gamma-ray spectroscopy

The detailed characterization of γ-rays emitted from the energy states populated by the β-decay is done in the framework of γ-ray spectroscopy technique. It is based on the characterization of γ transitions according to their energy (peak positions) and intensity (peak area). The semiconductor high pure Ge spectrometer, whose properties will be discussed in chapter 3, is involved in the detection of γ-rays. This detector is mainly characterized by its excellent energy resolution in a large energy range.

The energy spectra are the one-dimensional histograms which represent the number of counts distributed according to the amplitude of the signal which characterize the count. The accumulated counts are classified in bins (channels) of the internal device memory according to the height of the signal. The channels can be associated with the energy of

signals by determining the energy calibration of the detector.

When a γ-ray interacts with the detector it can be totally absorbed by an electron from the medium. This situation is well described by the photoelectric effect and a photoelectric peak or photopeak appears in the energy spectrum. The other possibility is to be Compton scattered by the electron partially transferring its energy. Compton effect provide a continuum of counts in the energy spectrum characterized by the Compton edge at E_c given by:

$$E_c = \frac{E_\gamma^2}{E_\gamma + m_e/2}, \tag{2.1}$$

where E_γ is the photopeak energy and m_e is the electron mass. Obviously Compton events have lower energies and appears on the left side of the photopeak. Sometimes the Compton scattered photons can come back to the detector via frontal collision in the shielding walls. If it is totally absorbed by photoelectric effect again in the detector the produced *backscatter* peak will lie at $E_\gamma - E_c$, i.e. in the low energy part of the spectra.

For higher energy γ-rays ($\geq 2m_e = 1.022$ MeV) pair production of e^- and e^+ can also occur. The produced positron is rapidly annihilated with an electron from the medium giving two 511-keV photons. The probability to detect both of them at the same time is very low and normally one escapes the detector and a peak of $E_\gamma - 511$ keV will be displayed in the spectrum. This is so called the *first escape* peak (FE). If the high energy γ is strong enough even two 511-keV γ-rays can escape and we will see a peak at $E_\gamma - 1022$ keV denominated as the *second escape* peak (SE).

If an intense nuclear source is exposed close to the detector a large number of counts will be accumulated in the energy spectrum during a long period of time as can be seen in Fig. 2.5. The peaks below 1 MeV are narrow (<2 keV FWHM for these energies) and most of them are completely resolved. Their energy and intensities can be studied by analyzing them directly from the spectrum.

For determination of energy it is enough to select the limits of a peak in the spectrum and find the centre of gravity or the centroid:

$$\bar{c} = \frac{\sum_i n_i c_i}{\sum_i n_i}. \tag{2.2}$$

The n_i represents the number of counts in channel c_i. The uncertainty is obtained via the standard deviation:

$$\Delta\bar{c} = \frac{\sum_i n_i \left(c_i - \bar{c}\right)}{\sum_i n_i}. \tag{2.3}$$

The ideal response function of a γ detector is a Gaussian peak. In some cases small tails in the low energy side of the peaks can appear due to the non-uniform deposition of the energy by the γ rays. Sometimes, specially at low energies, peaks are seated on big Compton background. This effect can also alter the symmetry of the peak. For all these reasons, we do not use Gaussian fit for the centroid determination in this work .

The intensities of the γ-rays measured with high pure germanium detectors are given by the corresponding peak areas. For the absolute γ-ray intensities it is necessary to know the source-detector distance, counting rate, determine the peak areas and the absolute efficiency of the detector. An appropriate corrections for dead time must be done. To

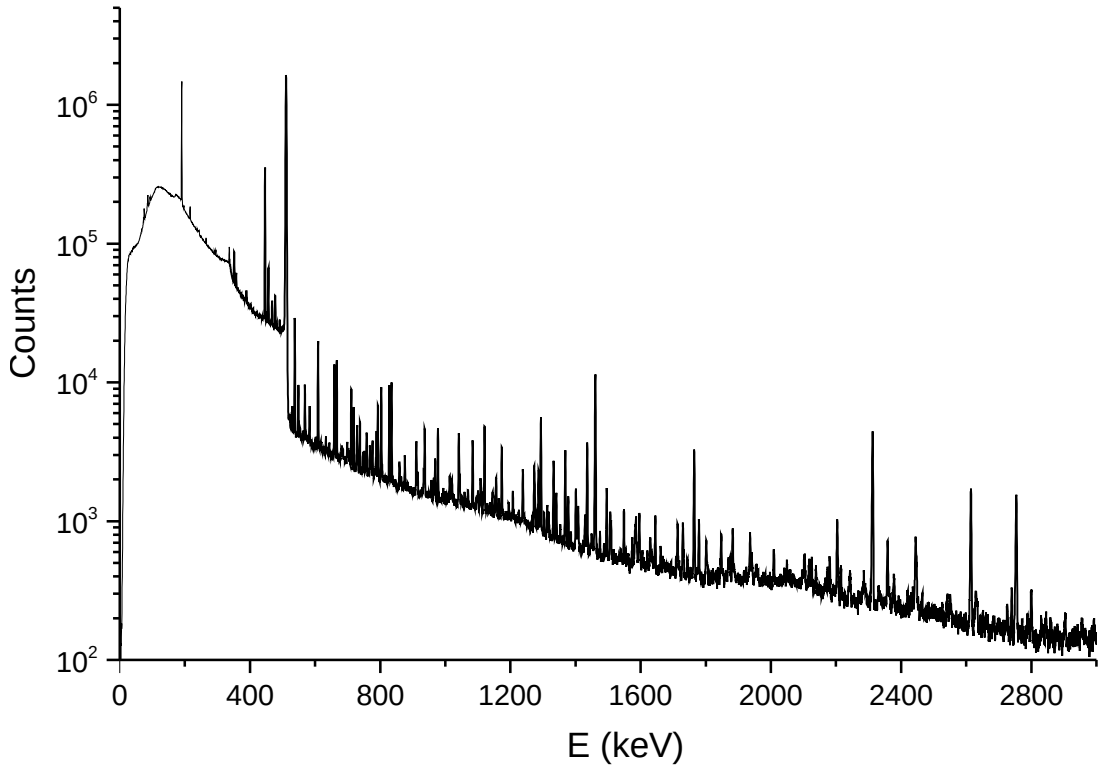

Figure 2.5: Characteristic energy spectrum obtained with a high pure germanium semiconductor spectrometer.

obtain peak areas the simple procedure of summing all the counts in the selected energy range and subtracting the background contribution is employed. Slope linear function between the minimum values on each side of the peak is chosen as the background function. The uncertainty is estimated as the square root of quadratic sum of the number of counts (n_i) in each channel. Once the efficiency is determined the intensity is calculated by dividing the area of the peak by the efficiency.

In the β-decay, which is studied in this work, a parent nucleus decays by populating several states of the daughter nucleus. The de-exciting γ transitions from higher levels also contribute to this population. Once the intensities are calculated it is very useful to normalize them to the nominal one, which is normally the strongest one.

Frequently the absolute radiation intensity is required, specially in calculation of the β feeding of the populated levels which leads to $\log ft$ values. The β intensity coming out from the parent nucleus is distributed between the intensity which feeds the ground state (I^{β}_{gs}) of the daughter and the intensity carried by the γ transitions from the higher excited states directly to the ground state:

$$I^{\gamma}_{gs} = \sum_i I^{\gamma}_i(1+\alpha_i), \tag{2.4}$$

where the index i enumerates the γ lines directly populating the ground state and α is the total conversion coefficient of the i-th γ-ray. In this way, the following relation must be achieved for 100 initial β-decays of the parent:

$$100 = N(I^{\gamma}_{gs}) + I^{\beta}_{gs}, \tag{2.5}$$

where the normalizing factor N shows the relation between the relative and absolute scales. Therefore, the absolute intensity of a certain γ transition A is calculated by simply multiplying its relative intensity by the normalizing factor:

$$I_A^{abs}(\%) = NI_A^{rel}. \tag{2.6}$$

When there is no β feeding to the ground state the normalizing factor is easily computed from the Eq. (2.5). However, if the β feeding to the daughter ground state is non-zero its value must be computed from the next decay product.

A very common situation is when the parent nucleus decays by more than one mode, for example by β^- and β-delayed neutron emission. In this case the branching ratio of β is not 100%:

$$B_{\beta^-} = \frac{I_g^{\gamma} s(\beta^-) + I_g^{\beta} s(\beta^-)}{I_g^{\gamma} s(\beta^-) + I_g^{\beta} s(\beta^-) + I_g^{\gamma} s(\beta^- n) + I_g^{\beta} s(\beta^- n)}. \tag{2.7}$$

The uncertainty of the absolute intensity of a given γ-ray A when only one decay mode is presented is calculated by using the standard error-propagating technique:

$$\Delta I_A^{abs} = I_A^{abs} \cdot \sqrt{D_A^2 + \left(\frac{\Delta I_A}{I_A}\right)^2 + \left(\frac{\Delta G}{G}\right)^2}, \tag{2.8}$$

where I_A is the relative intensity. The coefficient D_A represents the relation between the summed errors of the total transition intensities and their values:

$$D_A^2 = \frac{{}_i \Delta T_i^2 (1 - \delta_{iA})}{(\ {}_i T_i)^2}. \tag{2.9}$$

The parameter G represents the fraction of intensity that does not populate the ground state of the daughter. The detailed demonstration of Eq. (2.8) can be found in [Bro86].

Once we know the fraction of intensity that populate directly the ground state we can determine the β *feeding* (i.e. the number of times the level is populated by the direct feeding from the parent) of the rest of levels and normalize them. The β feeding of the excited states is calculated by finding the balance between the γ intensity that de-excites the level and the γ intensity that populates it. With the β feeding, the Q_β value, the energy of the state from which the parent decays together with its half-life $T_{1/2}$ and the $\log(ft)$ values for each state can be computed.

For decays with large Q_β value many nuclear configurations in the daughter nucleus are possible. That means that many high energy levels will be available. The γ-ray which depopulate this levels will be weak and the high resolution detectors as HPGe used in this work will not be able to detect them because their efficiency at high energies is only few percent. As consequence, much of the β feeding to these high energy states will not be registered as well as the intensity of the transitions which de-excite them. This is so called *Pandemonium effect*. It specially affects to the low-lying states because the intensity that feeds them form higher levels is not considered. To avoid the Pandemonium effect the Total Absorption Spectrometer (TAS) can be used. It is made of scintillator materials and has a very good efficiency for high energy γ-rays covering 4π solid angle. The disadvantage of TAS is its bad energy resolution.

2.4 Advanced Time Delayed $\beta\gamma\gamma(t)$ method

Lifetime measurements of the excited states in an atomic nuclei provide a key information about the structure of a given nucleus. Measuring half-lives permits to determine the *reduced transition probability* $B(X\lambda; i \rightarrow f)$ between two states. The spin-parity assignments in a certain nuclear level can be extracted from the γ decay selection rules determining previously whether the γ transition de-exciting the level is magnetic or electric with each corresponding multipolarity λ. According to the Eq. (1.29) the $B(X\lambda)$ can be calculated knowing the excitation energy E_γ, the multipolarity and the half-life of the de-excited state measured experimentally. On the other hand, its value can be determined theoretically by performing shell-model calculations.

Nowadays the range of nuclear lifetimes that can be determined experimentally comprises 54 orders of magnitude from 10^{-23} seconds in ^{7}H [Til02] to 10^{31} seconds in ^{128}Te [Tak96]. Thus, there is more than one technique to perform these measurements. For long lifetimes the procedure is considerable simple and consists in measuring the number of nuclei after a certain period of time. The decay constant is inversely proportional to this time and its precision will depend on how precise is the measurement of the initial and the final number of the species under study. The situation is different when we try to analyse shorter half-lives. Many techniques and methods had been developed in order to determine half-lives below the ms range. Most of them can be grouped in two large branches: *time-delayed methods* and methods based on *Doppler effect*. The first one has been successfully employed in microsecond, nanosecond and sub-nanosecond range while the second one is more sensible for obtaining lifetimes down to picoseconds and femtoseconds. Both methods overlap in the 1-10 ps range.

In this work the ATD (Advanced Delayed Timing) $\beta\gamma\gamma(t)$ method was used to determine lifetimes from few picoseconds to tens of nanoseconds in nuclei arising from the decay of ^{81}Zn. The principle of operation consists on using coincidences of electronic signals, which define the creation of a certain nuclear state and its decay, in order to calculate the time space between them. The moment of formation of such state is described by the *start event* which populates it. This event can be a γ-ray or a β-particle. The *stop event* is produced by a signal which comes from the decay product and normally is a γ transition or a conversion electron. The set of coincidences is usually composed by a slow part where the transition energy can be selected with good precision and a fast part responsible for the timing signals. In this way, the ATD method works with triple coincidences between a β-particle, detected by a thin plastic scintillator which acts as start and two γ-rays. One of them comes from a scintillator crystal with good timing resolution (BaF_2 or $LaBr_3$) and will act as a stop signal. The time distribution between these two events is recorded by a Time-to-Amplitude-Converter (TAC) and provides the way to measure the half-life of a nuclear level. The second γ-ray comes from the high-energy resolution detector (typically HPGe) and will be used to make the energy spectrum of the fast-timing detector cleaner in order to select the correct energy gate and reduce Compton contribution of others γ-rays. The technical aspects of the experimental setup and the structure of events will be explained in the next chapter.

The ATD or fast-timing $\beta\gamma\gamma(t)$ method was specially developed as a general tool for the half-life measurements in the subnanosecond range in neutron-rich nuclei. It was invented by Henryk Mach in 1986 while he was working at the TRISTAN facility at Brookhaven Nation Laboratory (USA) [Mac86]. This method is designed to avoid the

traditional complications in the time-delayed methods allowing lifetime measurements in levels with weak branches. Technical aspects were developed during the period 1986-1989 by H. Mach, M. Moszynski and R. Gill and showed up in scientific community with two publications in 1989 [Mac89, Mos89]. The fast-timing method has been applied in many nuclei populated in β-decay in different regions of the nuclear chart. One of the first results was the $B(E2; 0_1^+ \rightarrow 2_1^+)$ rates measurements in $^{90-96}$Sr isotopes [Mac91] and interpretation of 0^+ bands in heavy Sm and Gd isotopes [Mac92]. Few years later the technique was used to study the Sb, Ba and Ce neutron-rich nuclei near the doubly magic ^{132}Sn [Mac95b, Mac95a, Sim07]. Many lifetime measurements in heavy nuclei region were performed during 1996-2002. The octupole correlations in ^{227,229,231}Ra and ^{229,231}Th were investigated by A. J. Aas *et al.* [Aas96, Aas99], K. Gulda *et al.* [Gul02] and L. M. Fraile *et al.* [Fra99, Fra01a]. During last years the ATD method was successfully extended to $N = 40$ region where the exotic neutron-rich isotopes of Fe and Mn were analyzed by B. Olaizola *et al.* [Ola13]. The experimental campaign IS590 at ISOLDE was intended to characterize via fast-timing setup the low-lying 0^+ and 2^+ states of the doubly magic candidate ^{68}Ni. Scarce information about lifetime measurements in the pico and nanosecond range is available in the region of the doubly magic ^{78}Ni and this thesis will contribute to correct this deficiency measuring half-lives of Ga, Ge and As isotopes.

One of the biggest challenges of a general time-delayed method is the time/energy resolution of the detector which is responsible for the selection of the stop signal generally characterized by a de-excited γ-ray. The energy resolution must be as good as possible in order to precisely impose the desired energy gate in the timing detectors maintaining acceptable resolution in time. At the beginning of the fast-timing era truncated-cone BaF_2 scintillators were used. Throughout the last years a new generation of fast scintillators appeared in the market. The $LaBr_3$(Ce) and $CeBr_3$ inorganic crystals were discovered to have better energy and time resolution than BaF_2 and were incorporated in the ATD method as timing detectors. The detailed properties of these crystals will be described in the next chapter. However, the decisive tool of this method is the use of thin ΔE plastic scintillator which absorbs the β radiation homogeneously. This detector assures to have the uniform time response for full range of β radiation. Small deviations can be corrected by constructing the β-walk curve which describes the evolution of time response for a whole β energy range. This correction is described in more details at the end of the next chapter.

For half-life determinations the fast-timing method includes two different tools: the *Convolution technique* and the *Centroid Shift technique*. The use of one or another depends on the range of the lifetime.

2.4.1 The Convolution Technique

The Convolution technique is used to measure half-lives of a certain level when its value is long enough to appear as a slope on the delayed part of the time spectrum. Even when the radiation is emitted simultaneously the time distribution is not a delta because of statistical fluctuations and electronics instabilities of pulses in the detector. When a certain nuclear state has a very short half-life the time distribution does not show any delayed part and we talk about *Prompt time distribution* or $P(t)$. The full width at half maximum (FWHM) of this distribution represents the real time resolution of the detector chain and the ability to distinguish the $P(t)$ curve from the exponential tail and fixes the

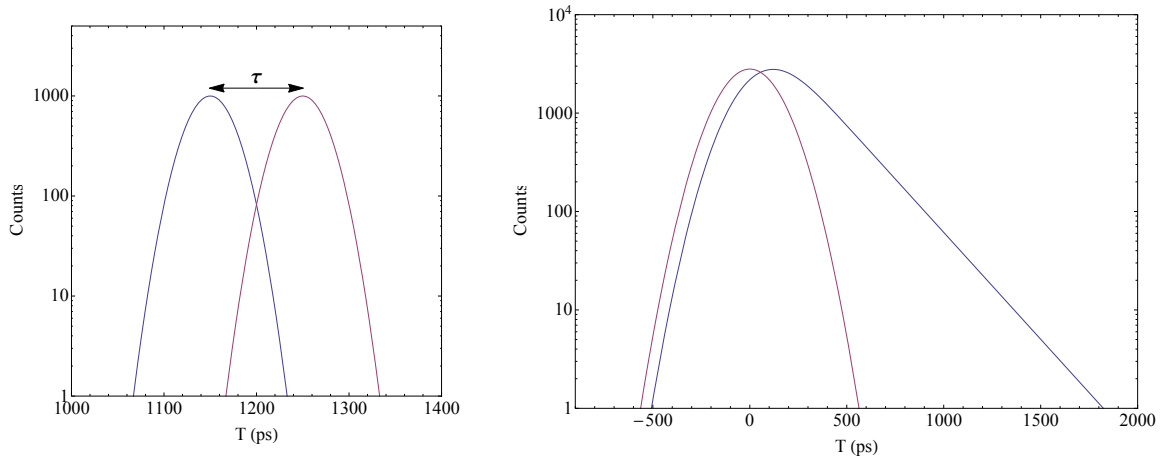

(a) (b)

Figure 2.6: Two procedures used for the lifetime measurements. Panel (a) illustrates the Centroid Shift technique where the deviation of the time distribution of studied half-life with respect to the prompt reference gives the desired lifetime. Panel (b) shows the convolution technique where the lifetime is being obtained from the slope in time delayed part of the spectrum.

lower limit of lifetimes that can be measured with this technique (see Fig. 2.6). Ideally the prompt curve can be fitted to the Gaussian function but more realistic situation is a quasi-Gaussian curve with irregularities and tails.

The response of a timing detector, which registers a γ-ray coming from a state with sufficiently large half-live to appear as a slope component on the delayed part, will be the convolution of the decay function $f(t)$ and the prompt time distribution $P(t)$:

$$F(t) = N \int_0^\infty P(t-t')f(t')dt', \tag{2.10}$$

where N is the total number of counts in the time spectrum. The integral represents the number of counts at time t due to the shifted events at time t'. This displacement is due to the time jitter explained in [Ham75]. As was already mentioned, it is a good approximation to use Gaussian function to represent the $P(t)$. The $f(t')dt'$ indicates the probability of producing the stop signal after being started by the β-event. Taking into account the exponential decay in the delay part the Eq. (2.11) takes the analytical form:

$$F(t) = \gamma \int_A^\infty e^{\delta(t-t')^2} e^{\lambda(t'-A)} dt', \tag{2.11}$$

where γ and δ represent the parameters from the normalized Gaussian approximation and $\lambda = 1/\tau$ is the decay constant of a given nuclear state. Note that the lower limit of the integration now is A instead of $t = 0$ which is related but not necessarily equal to the centroid of the prompt distribution. The Eq. (2.11) can be integrated giving the combination of the exponential decay and the Gauss error function $erf(t)$:

$$F(t) = \frac{\gamma\sqrt{\pi}}{2\sqrt{\delta}} e^{-\lambda t - A + \frac{\lambda^2}{4\delta}} erf \quad \frac{2\delta(t-t') - \lambda}{2\sqrt{\delta}} \Bigg|_{t'=A}^{t'=+\infty}. \tag{2.12}$$

In the region out of prompt distribution the er$f(t)$ function tends to 1 and $F(t)$ takes a very simple form in logarithmic scale:

$$\ln\left[F(t)\right] = -\lambda t - A + \frac{\lambda^2}{4\delta}\ln \quad \frac{\gamma\sqrt{\pi}}{2\sqrt{\delta}} \quad \cdot \tag{2.13}$$

Thus, the time distribution is given by a simple line with a slope represented by the decay constant λ. The experimental determination of the lifetime is summarized therefore in fitting the time distribution from the Eq. (2.11) with a standard χ^2 program employing an iterative procedure [Bev92]. The half-life is extracted from the linear fit in logarithmic scale described by the Eq. (2.13).

When a half-life reaches the nanosecond range and the data presents low statistics the χ^2 test underestimates the lifetime and the fit must be done using Poisson statistics. However, some tricks can be applied in order to avoid this problem. The first solution for increasing the statistics is to measure the half-life by selecting several gammas in timing detector and add together the timing spectra. Another way to tackle this problem is to work with the systematic compression of the time distribution spectra fitting each time to the convolution function. The final result is obtained by reaching a stable value or by selecting the fit with the lowest χ^2 value maintaining the same slope λ. Another alternative is to ignore the Ge detector and perform the data analysis in $\beta\gamma$(t) mode selecting the energy gates directly in $LaBr_3$ detector. However, this can be done only when the desired γ peak is not mixed in the energy spectrum. Moreover, the systematic compression must be also used in this analysis in order to get a stable value.

When the slope of the delayed part becomes comparable to the apparent slope of the prompt distribution the convolution method can not be used. It is very difficult to determine the numerical limit of this situation because it depends strongly on the statistics of data or how good is the semi-Gaussian approximation in the prompt distribution. The triple coincidences $\beta\gamma\gamma$(t) normally allows to reduce the background Compton contribution to neglected amounts. However, if we work with double coincidences $\beta\gamma$(t) the ratio between the background area and the peak area can be large and greatly affect the time resolution usually represented by the FWHM of the time peak in the TAC spectrum. Deeper study of limitations of Convolution Technique are discussed in [Mac89].

Nevertheless, a simplified example can be shown in order to illustrate the order of magnitude of the apparent mean life of the prompt response. From the Fig. 2.6 the slope in the delayed part is given by λ. Lets find the slope of the line tangent to the prompt function represented by Gaussian distribution centred in $t = 0$:

$$g(t) = Ne^{-\frac{t^2}{2\sigma^2}}. \tag{2.14}$$

Calculating the derivative of $\ln\left(g(t)\right)$ we obtain the straight line given by the following equation:

$$g'(t) = -\frac{t}{\sigma^2}. \tag{2.15}$$

This function represents the slope of the tangent line to the prompt curve. It is a good approximation to evaluate it in the point of half of the maximum $\ln N$ of $\ln\left(g(t)\right)$, i.e.

$$0.5 \cdot \ln\left(g(t_{max})\right) = \frac{1}{2}\ln(N) = -\frac{t^2}{2\sigma^2} + \ln(N) \rightarrow t^{+}_{0.5max} = \pm\sigma\sqrt{\frac{\ln(N)}{2}}. \tag{2.16}$$

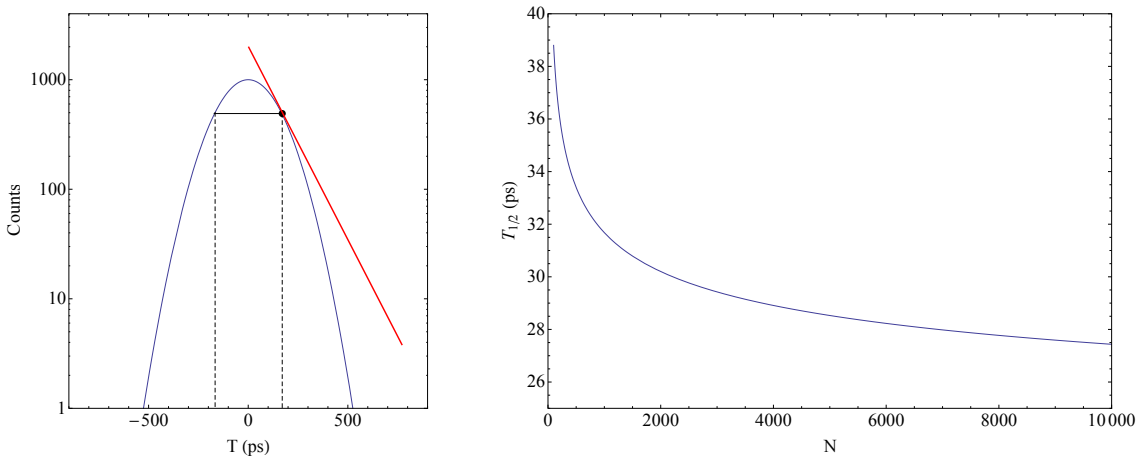

(a) (b)

Figure 2.7: (a) Gaussian function that represents a prompt time response. The slope of the tangent line at the half of the maximum permits to estimate the apparent mean life of the Gaussian function. (b) Evolution of the limit of Convolution Technique for 200 ps of FWHM in time distribution function (see text for details)

.

Evaluating the Eq. (2.15) at the point defined by Eq. (2.16) we get the slope of the tangent line in terms of FWHM evaluated at 50% of the maximum (see Panel (a) from Fig.2.7):

$$g'(t^{+}_{0.1max}) = -\frac{1}{\sigma}\sqrt{\frac{\ln(N)}{2}}. \tag{2.17}$$

This value is the apparent half-life of prompt function and serves to establish a limit for the decay slope $\lambda = \ln 2/T_{1/2}$ in terms of FWHM$= 2\sigma\sqrt{2ln2}$:

$$\frac{ln2}{T_{1/2}} = \frac{1}{\sigma}\sqrt{\frac{\ln(N)}{2}} \rightarrow T_{1/2} = \frac{ln2\sqrt{2}}{\sqrt{\ln(N)}}\sigma \simeq 0.42 \cdot \frac{FWHM}{\sqrt{N}}. \tag{2.18}$$

The parameter N reflects the maximum of peak of time distribution. In order to have some numbers which represent the real case we can assume 200 ps of FWHM for transitions at around 300 keV. The plot (b) from Fig. 2.7 shows the lower limit of the half-life obtained with Convolution Technique as function of N which was varied between 100 (low statistics) and 10000 (very high statistics). This example shows that we will be able to detect slopes with half-lives longer than 40 ps.

2.4.2 The Centroid Shift technique

In general, when the desired lifetime does not manifest itself as a slope in the time-delayed part of the timing spectrum it can be deduced from the relative shift between centroids from time response curves.

Let us consider a general situation when the low-spin β-emitter populates levels in a certain nucleus (see Panel (a) in Fig. 2.8). The simplest way to measure τ_1 is making use of two sequential transitions γ_1 and γ_2. As was mentioned in previous section, the ATD method works with triple coincidences $\beta\gamma\gamma$(t). In our example the β branch is

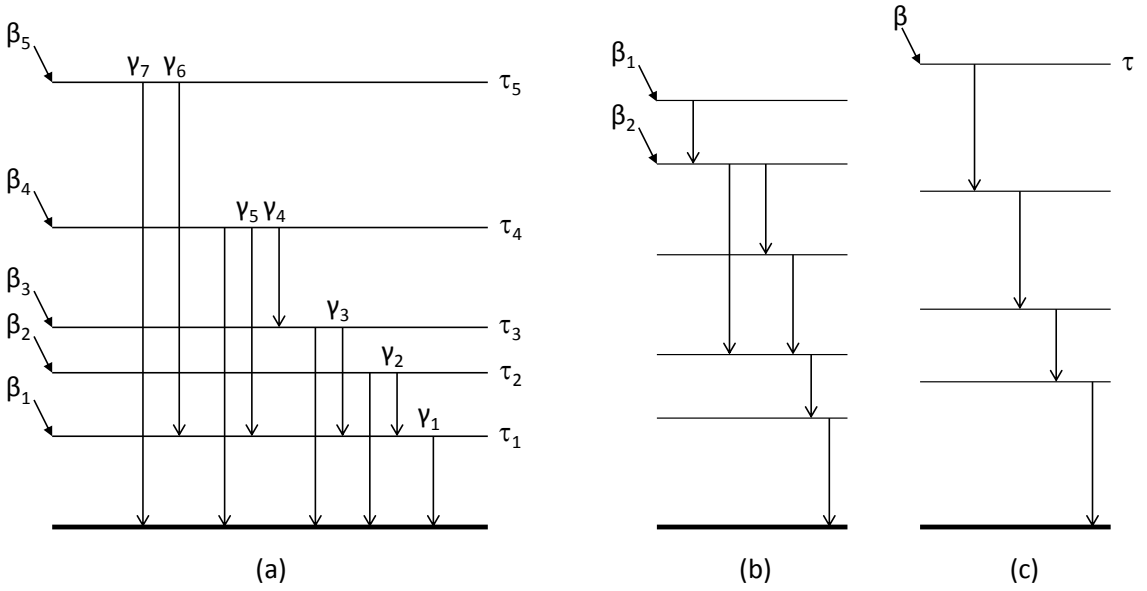

Figure 2.8: Level schemes populated in β-decay from low- (a) and high-spin (b) and (c) emitters.

selected in a plastic scintillator while γ radiation is treated by HPGe and $LaBr_3$. If γ_1 is selected in Ge detector γ_2 will be seen in coincidence in $LaBr_3$ which acts as stop signal for TAC. In this situation the feeding β_1 will not play any role and only β_2 is recorded in coincidence in β detector which provides signals to start the event in the TAC. Thus, the time distribution will be given by the convolution of two Gaussian curves centred in τ_2 and τ_0 respectively and therefore the time delay observed between timing detectors is the sum of this two quantities [Bro14a], that is $t_1 = \tau_2 + \tau_0(E_2)$. The prompt component τ_0 is a fixed time delay between timing detectors and is energy dependent. The mean life τ_1 does not contribute to the delay because is selected in Ge detector which is much slower than $LaBr_3$ and the event will arrive much later. Changing the selecting order, i.e. γ_1 in $LaBr_3$ and γ_2 in Ge, the time delay t_2 will include now both τ_1 and τ_2 because the event from Ge detector comes first. In this way, $t_2 = \tau_1 + \tau_2 + \tau_0(E_1)$. Subtracting t_2 and t_1 gives τ_1:

$$\tau_1 = \Delta t - \Delta\tau_0, \tag{2.19}$$

where Δt is the difference between the centroids from the time response of γ_1 and γ_2 and $\Delta\tau_0 = \tau_0(E_1) - \tau_0(E_2)$ is obtained from the *Prompt Calibration Curve* (see below).

When parallel instead of sequential transitions are taken into account we can avoid the correction for τ_0 as a function of energy because $LaBr_3$ detector will record exactly the same γ line. Such is the case of selecting γ_4 and γ_5 in Ge and the γ_1 in $LaBr_3$. The difference between time delays τ_3:

$$t_4 - t_5 = (\tau_0(E_1) + \tau_1 + \tau_3 + \tau_4) - (\tau_0(E_1) + \tau_1 + \tau_4) = \tau_3\,. \tag{2.20}$$

The high energy states, usually above 2 MeV, except isomers, are characterized by very short half-lives, normally in femtosecond region. This fact can help us to measure τ_2 from Fig. 2.8. Assuming that γ_6 depopulates nuclear levels above 2 MeV τ_6 can be

approximate to zero. The time distribution t_6 will be obtained by taking γ_6 in Ge and γ_1 in $LaBr_3$, that is $t_6 = \tau_0(E_1)$. On the other hand, $t_2 = \tau_0(E_1) + \tau_1 + \tau_2$. Subtracting again both time responses we obtain the desired mean life:

$$\tau_2 = t_2 - t_6 \,. \tag{2.21}$$

More complex cascades can be studied with sequential or parallel transitions as shown in (b) and (c) from the Fig. 2.8. However, the examples shown above illustrate the most simple situations and can fail when the level scheme is more sophisticated. A very typical case is when there is not enough statistics to calculate the time distribution centroid given by γ_2. To solve this problem the fast-timing method makes use of the already mentioned Prompt Calibration Curve. Taking an appropriate calibration we can construct a set of points that represent prompt position for a given energy. This data can be estimated from γ-rays depopulating the excited states with short and precisely known half-life. Therefore, the prompt time response is measured by simply subtracting the mean life of the level de-excited by a γ line of energy E to the time response centroid corresponding to the same transition. In this way one can determine the prompt position for a certain energy and use it for the lifetime measurements in levels with weak γ population. The calibration isotopes of ^{138}Cs and ^{140}Ba were used for timing corrections in this thesis.

Apart from the prompt correction which play the most important role in ATD method, Compton background can also introduce modifications in time response of $LaBr_3$ and its effect should not be neglected. As there is no way to select Compton events below a FEP we consider the region immediately close to the peak on the right or left side to find its time response and then we shift this value by using the *Compton Response Curve*.

There is a third correction curve called *Compton Correction Curve* describing the time difference between Compton events of the same energy, but coming from different prompt γ transitions. This curve had not been used in this thesis because it represents a minor correction.

More details and real examples of the calibration curves are presented in section 3.5.

2.5 Summary of the chapter

The aim of this work is to apply the ATD $\beta\gamma\gamma$(t) method to perform half-life measurements in nuclei populated in the β-decay of very exotic neutron rich ^{81}Zn located close to the doubly-magic ^{78}Ni. These measurements will provide key information about shell evolution in this region and will test the robustness of theoretical models. Using a suitable set of γ detectors in combination with a plastic β scintillator we will be able to extend considerably the level scheme of the most exotic ^{81}Ga. As ^{81}Ga is found to be at r-process path novel properties in the structure of this nucleus and its daughters will be very useful for astrophysical nucleosythesis calculations. Apart from the recent results on measurements of nanosecond half-lives in the ^{80}Zn decay chain obtained from the same experiment by our collaboration [Lic14] this is the first time that fast-timing method in picosecond range is used in the vicinity of ^{78}Ni.

Two different techniques have been explained as the part of ATD method, which works very well with simple level schemes and is very powerful in half-life measurements in subnanosecond range with sufficient statistics, as we expect to reach in the decays of ^{81}Zn, ^{81}Ga, ^{81}Ge and ^{81}As. However, some sophisticated timing calibrations must be

performed in advance in order to guarantee the correct results. The detailed examples of such calibrations are explained at the end of the next chapter. We are also limited to the energy resolution of timing detectors and the precise selection of the energy gates will depend on how good the peaks are resolved in the spectrum. The precision of our measurements, specially when the Centroid Shift techniques is used, is mostly determined by the precision of calibration curves and determination of centroid positions. In case of the Convolution Technique the most important role in error bar of lifetimes will play the number of counts in the energy spectrum. In our experiment we will not able to measure half-lives longer that 30 ns and shorter than 10 ps due characteristics of the setup and low count rate for neutron-rich nuclei.

The experimental campaign which lead for obtaining ^{81}Zn included only few γ detectors. However, it is possible to improve this situation by adding more detectors as was done in our FATIMA (FAst-TIMing Array) experimental campaign which has been already successfully performed at ILL (Grenoble, France) in 2013 using the EXOGAM array of Ge detectors combined with 16 $LaBr_3$ [Rég14]. In this case the ATD method has been extended to several detectors and the Generalized Centroid Difference Method [Rég13] was applied for lifetime measurements. A special design of the experimental setup used in EXILL-FATIMA permits to reach linear time response of $LaBr_3$ with the Compton events. The next step of ATD method is to be utilized with FATIMA in the facility of FAIR at GSI (Darmstadt, Germany) which is planned to be built from 2017 onwards.

Chapter 3

Experiment and data analysis

The study of the neutron-rich exotic nuclei requires its production in excited states. The final point of the investigation of this PhD thesis is to measure the half-lives of exited states and the determination of the reduced transition probabilities in nuclei from the ^{78}Ni region. The most decisive condition for successful analysis is the precise knowledge of the decay level schemes and high production count rate of the desired isotopes in order to guarantee good statistics in time and energy spectra. To reach this objective the experimental measurements must be performed in large-scale facilities equipped with modern instrumentation and state-of-the art detectors. For radioactive ion beam (RIB) production a proton beam impinging in a target is normally used. Different reactions (fission, fragmentation, spallation, etc.) can take place in this process depending on the target and intrinsic beam properties. The purity of the desired isotope beam and their production yield play an important role when choosing the facility.

The RIB can be produced following two complementary ways: *Isotope Separator On Line method (ISOL)* and *In-Flight Recoil Separation method (In-Flight)*. Both methods are based on the transportation of nuclei from the target to the experimental area reducing the amount of background species generated after the beam has impacted onto the target. The In-Flight technique is characterized by selecting the short-lived nuclei even at μs while the ISOL cannot work in the range below ms. This property depends on the time employed in the extraction and transportation of the isotopes of interest. The driver beam used in ISOL method is generally composed by light charged particles as protons or neutrons. The primary beam and reaction products are stopped directly inside the thick target and the extraction is done by using chemical procedures that lead to high purity of the beam and small energy and space degeneration. However, the production is strongly affected by the chemical properties of the target and its complex design. On the other hand, the beams utilized by the In-Flight method are usually composed by heavy ions that impact onto thin targets. This technique relies on the forward focusing of the reaction products emitted from the target. The set of nuclei of interest are selected in-flight by charge and mass separation. This method permits the detection of isotopes without significant losses. Nevertheless, the secondary beam obtained in this way has bad optical properties and the cross section of the target reaction is strongly limited by the type of the reaction (see [Mor04] for a deeper study). The ISOL method was used to generate ^{81}Zn and it is detailed in the next two sections.

The data analysed in this work come from the experimental campaign performed at ISOLDE (CERN) RIB facility in 2011 as part of the fast-timing measurements in exotic

nuclei populated in the decay of isotopes of Zn[1]. During one week of the experiment there were produced isotopes of Zn from $A = 82$ to $A = 71$. This chapter is devoted technical details of the experiment and data analysis procedure.

3.1 The ISOL method

When the radioactive beam of protons or heavy ions hits the target many type of reactions can occur. The choice of the reaction usually depends on the location of the desired nucleus on the chart of nuclei. In this way, light- and heavy-ion fusion evaporation reactions were used for the nuclei close to the line of stability on the neutron-deficient side. When a high energy proton beam hits a target the most probable reactions that can take place are fission, spallation and fragmentation. Fission reactions on ^{235,238}U or ^{232}Th targets are usually used to produce neutron-rich nuclei in the intermediate mass range from $A = 70$ to $A = 100$. Spallation products can cover a wide range of neutron-deficient isotopes, while the fragmentation is mostly used for the study of light nuclei. In some cases a suitable converter can be used before the target to change the primary proton beam into neutrons.

The determination of the *target* plays a very important role in the minimization of contaminants and when optimizing the beam-target combination for the highest cross-section of the reaction. The general objective of the target is to produce as many isotopes as possible. Special designs are made to maximize the power dissipated by radiation in case the target heating is to high. For 1 mA intensity proton beam at 1 GeV the dissipated power reaches 100 kW. External water or liquid-lithium cooling can also be used. Finally, one has to take into account, that the yields from different targets can drop even an order of magnitude after few days of operation and it must be changed after this period of time.

In some facilities, as for example in IGISOL, the exotic nuclei are thermalized after their production in a solid o gaseous *catcher*. In this process the radioactive products are cooled down loosing several orders of magnitude of their kinetic energy. In some facilities the target and the catcher are mounted in the same system. In case of solid catchers the speed of radioactive atoms is increased by heating the target/catcher system in order to avoid effusion towards the ion source. After thermalization process the radioactive beam is transported to the *ion source* through the *transfer line* generally kept at a high temperature to minimize the lingering of atoms on the walls of the line. The radioactive atoms suffer the ionization procedure (electron impact ionization, surface ionization, laser ionization, etc.) and normally singly-charged ions are produced. The target, catcher, transfer line and ion source form the *target-ion system* which is put to high voltage typically between 20 and 60 kV.

The next important step is the *mass separation*. After the ion source the low-energy ion beam passes through the dipole magnets where it is mass separated and after that it is transported to the focal plan where it is focused. The resolving power defined as $R = M/\Delta M$ measures the quality of the separation system exceeding 5000 in case of

[1]The whole list of collaborators who took part in the experiment is: V. Paziy, H. Mach (spokeperson), L.M. Fraile (spokeperson), A. Aprahamian, C. Bernards, J.A. Briz, B. Bucher, C.J. Chiara, Z. Dlouhý, I. Gheorghe, D. Ghiţă, P. Hoff, J. Jolie, U. Köster, W. Kurcewicz, R. Lică, N. Mărginean, R. Mărginean, B. Olaizola, J.-M. Régis, M. Rudigier, T. Sava, G. Simpson, M. Stănoiu, L. Stroe, W.B. Walters and ISOLDE collaboration team.

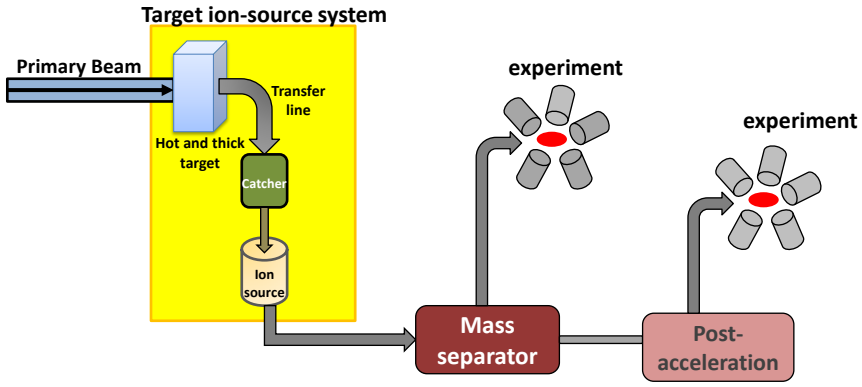

Figure 3.1: ISOL method. Steps followed by the radioactive ion beam generated by the primary beam bombarding the target.

HRS at ISOLDE. After the mass separation the beam is normally transported to the measurement station where the detector system is mounted to measure nuclear properties of the separated isotopes. However, in case of experiments where the separated radioactive ions are utilized to produce more nuclear reactions the post-accelerating step is needed. First, the mass separated species are cooled down in a *cooler/bancher* in order to improve their optical properties and bunch the beam. Before injecting into an accelerator it is useful to transform the singly charged ions into multiply charged ones. This task is done by the *charge-state breeder*. The singly or multiply charge ions are transported to the acceleration system (cyclotron, tandem accelerator or linear accelerator) and the final energetic beam is delivered to the experimental area. The schematic representation involving different members of ISOL method can be found in the Fig. 3.1.

During the last fifty years many ISOL facilities have been built in different countries in all over the world. Most of them are located in Europe (ISOLDE, GSI, LISOL, IGISOL, OSIRIS PARNNE, IRIS, etc) and some in Canada (ISAC-TRIUMF) and Japan (JAERI). A large description of ISOL technique with much more detailed information and the overview of the ISOL facilities can be found in [VD06] and [Kös02].

3.2 ISOLDE facility

The ISOLDE RIB facility was approved by the European Organization for Nuclear Research (CERN) the 19th of December 1964 and the first experiment started three years later. Presently it is situated at the Proton-Synchrotron Booster (PSB) of the CERN accelerator complex. The 1.4 GeV pulsed proton beam is delivered by the PSB injector containing the order of 3×10^{13} protons per pulse with a minimum spacing of 1.2 s. This gives the average intensity of 2 μA. The high proton energy and the target ion-source system allow to extract and separate more than 1000 different isotopes of more than 70 elements ($Z = 2$ to 88). This number of isotopes available for users is by far the highest at any ISOL-facility in the world and together with the excellent beam quality thus makes

ISOLDE ideally suited for nuclear structure and reactions studies. The on-line separation method uses the spallation, fission and fragmentation reactions with thick targets. The reaction products are stopped inside of the target and diffuse outside by thermal processes to be ionized and accelerated to form an ion beam. A substantial and rapidly increasing fraction of the radioactive isotopes have been accelerated up to 3 MeV/u with the REX-ISOLDE post-accelerator. REX-ISOLDE can operate all the way up to mass number 238, thereby increasing drastically the boundary of physics which may be inspected in the installation. Present experiments mainly deal with nuclear structure questions, explored via measurements of ground state properties (mass, radii, moments), via decay studies or Coulomb excitation and transfer reaction studies at low energy. A sizeable part of the program is devoted to other fields, such as nuclear astrophysics and fundamental physics research.

The most important installations at ISOLDE include two mass separators GPS and HRS, the REX-ISOLDE and HIE-ISOLDE post-accelerators, the ISOLDE decay station (IDS), high-precision mass spectrometers (ISOLTRAP Penning trap, transmission spectrometer), UHV experimental chambers for surface and interface studies, high-resolution laser spectroscopy set-ups as COLLAPS and shielded collection points and special laboratories for the handling of radioactive samples and various beam lines for experiments. Several detector arrays as segmented Si-detector array, state-of-the-art germanium detectors for nuclear spectroscopy and MINIBALL, a highly efficient germanium array placed at target station after REX. Some new instrumentation as a beta-NMR platform for nuclear and solid state physics with polarized radio-nuclides and a new laser spectroscopy set-up CRIS for low intensity beams is going to be installed. On the Fig. 3.2 one can see the schematic view of some parts of the ISOLDE facility. Our experiment was performed at LA1 area.

The main characteristics of the ISOLDE facility are the ability to produce a spot like radioactive beams with excellent emmitance thanks to the high quality optics, large variety of beams, with many target and ion-source combinations, selective ionization and beam purity, including RILIS, high mass resolution due to the HRS separator, which permits to reach highly pure low-energy beams, very important in the β-decay experiments, and combination of many experimental set-ups and techniques.

3.2.1 The CERN accelerator complex

The large accelerator complex of CERN is shown in Fig. 3.3. It consists on different accelerating machines that boost successively the beam of particles. The protons are initially obtained by removing the electrons from hydrogen atoms applying an electric field. After that the protons are injected into the Linac-2 where the first acceleration step takes place and the particles reach 50 MeV. The second machine, the Proton Synchrotron Booster (PSB), accelerates protons up to 1.4 GeV. From this point the particles are transported to ISOLDE. If higher energy is needed the protons can be post-accelerated in the third accelerator called Proton Syncrotron (PS). The PS pushes the beam to 27 GeV. Next accelerator, the Super Proton Syncrotron (SPS), can accelerate particles up to 450 GeV. For further high-energy physics experiments this energy is not enough, reason why the LHC (Large Hadron Collider) was built in 2008. It consists of two beam pipes where the protons circulates in opposite directions. The record energy reached in LHC was 6.4 TeV and the energy of collision inside of ALICE, ATLAS, CMS and LHCb detectors

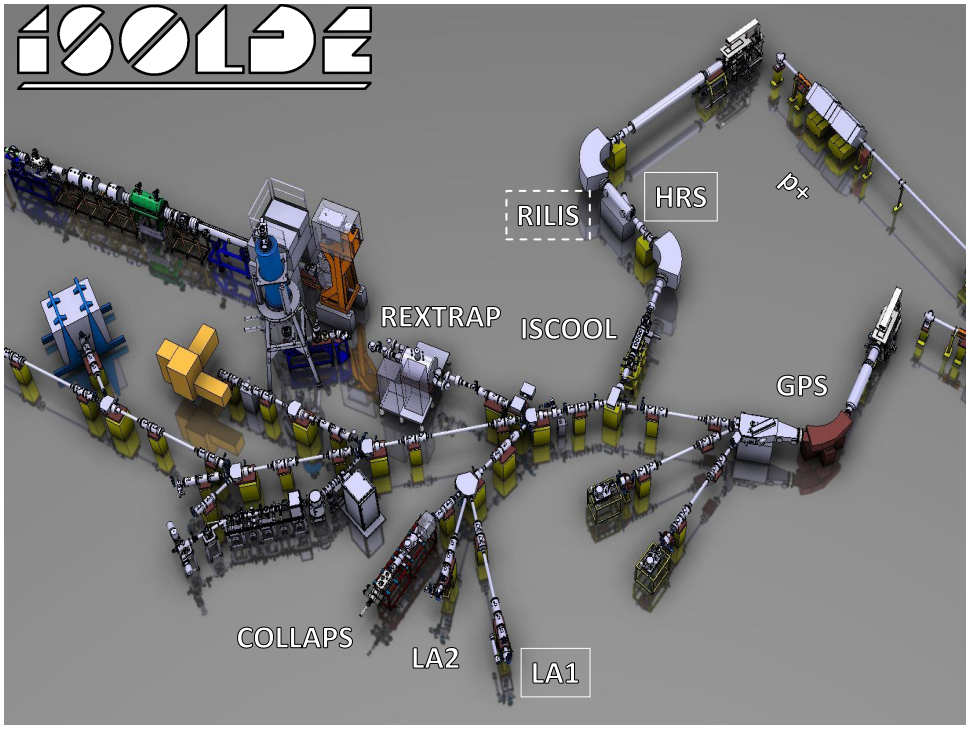

Figure 3.2: Layout of the ISOLDE facility without post-accelerator complex. See text for details.

ascends to 13 TeV in 2015. Lead ions can also be accelerated in CERN complex. After being created in a vaporized source they enter into Linac-3 to be post-accelerated in the Low Energy Ion Ring (LEIR). Then, the lead ions can continue the same way as protons to reach the maximum energy at LHC.

For experiments at ISOLDE the 1.4 GeV is the most suited proton energy for radioactive ion beam production in order to perform all kind of experiments in nuclear physics or material science. Initially, the protons are generated in a Duoplasmatron ion source where the electrons are separated from the hydrogen atoms with 92 kV extraction potential and up to 300 mA of proton beam current can be reached. The first proton accelerating element at CERN is the linear accelerator Linac-2, which replaced in 1978 the Linac-1 built in 1959. The Linac-2 is of the Alvarez Proton Linac design and consists of three accelerating tanks (see Fig. 3.4) which push successively the proton to 10.3, 30.5 and finally 50 MeV. The beam passes through pulsed electromagnetic quadrupoles situated inside the drift tubes in order to minimize the emittance below 50% of the accepted limit. An 80 meter transport line carries the beam up to the PSB passing through the additional magnets to minimize the dispersion. During last years the new Linac-4 accelerator has been developed to increase the beam energy up to 160 MeV and will replace Linac-2 in 2017-2018.

The Proton Synchrotron Booster (PSB) is the first and the smallest circular proton accelerator in the accelerator chain at the CERN LHC injection complex as shown in the Fig. 3.3. The 50-MeV protons that come from Linac-2 are accelerated up to 1.4 GeV before being injected at the Proton Synchrotron (in which they can reach 27 GeV) or being directed to the ISOLDE installation. The synchrotron includes four superimposed rings of 25 meters of diameter with 32 dipoles and 48 quadrupoles each. Pulses of 2.4

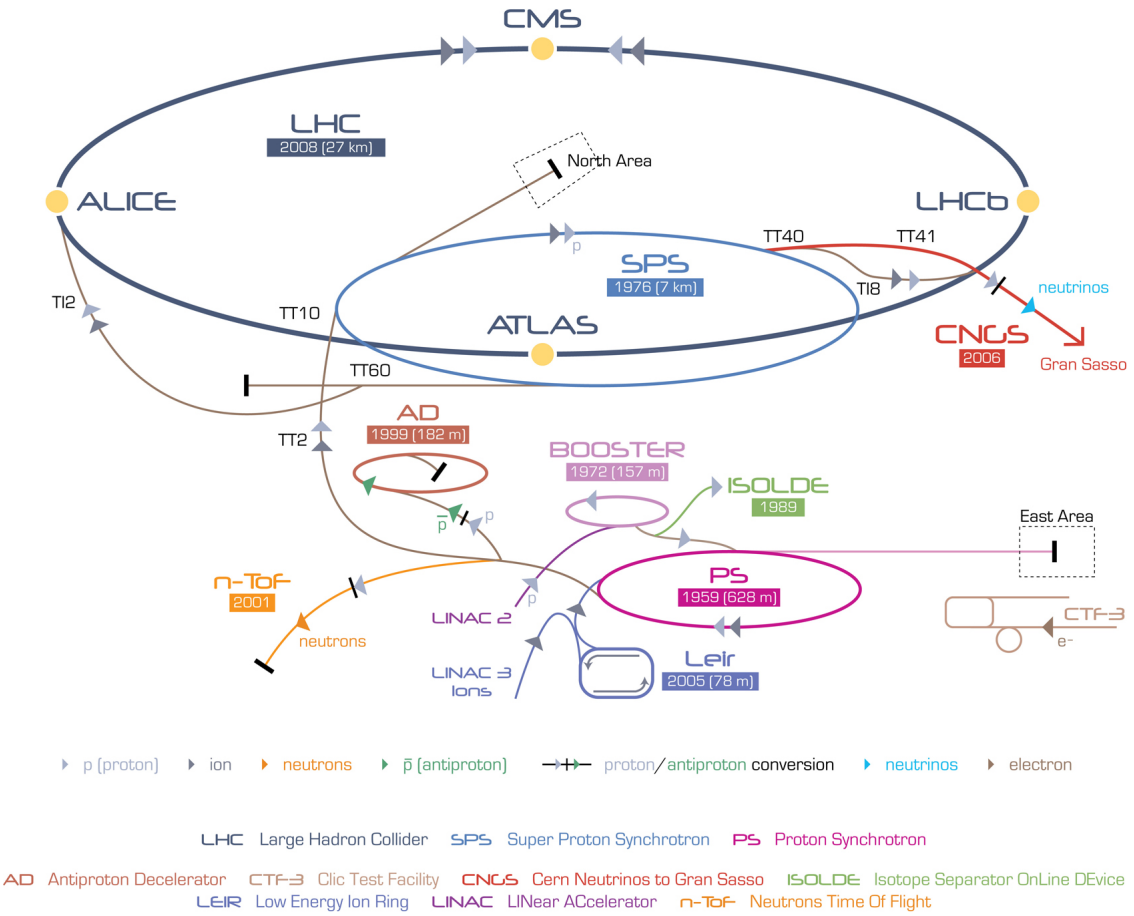

Figure 3.3: Schematic representation of several accelerating machines which take part in the set of CERN accelerators. Picture taken from http://cern.ch.

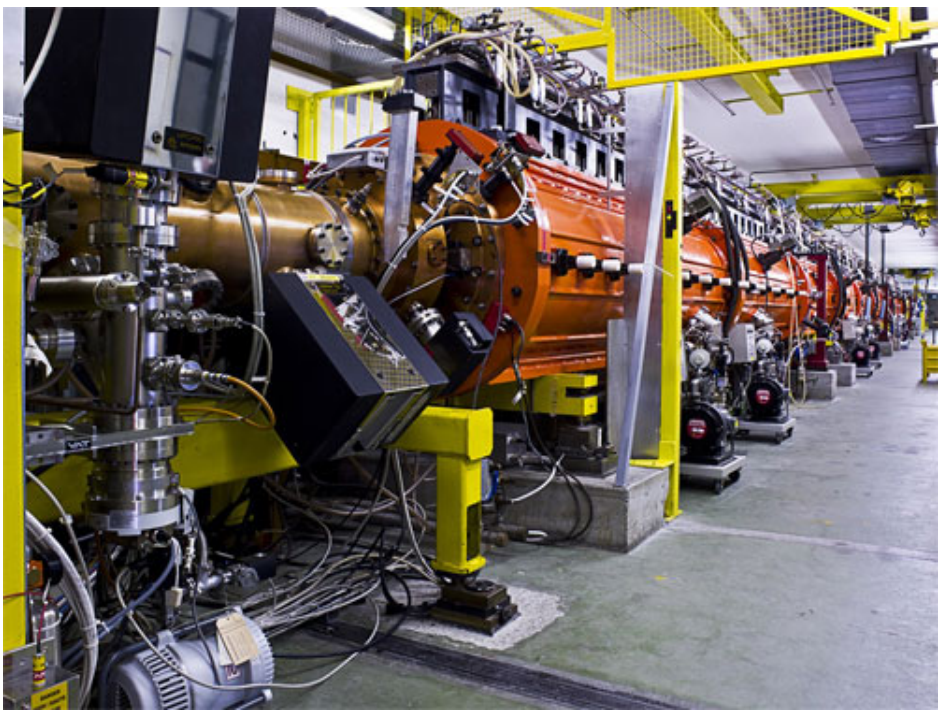

Figure 3.4: Linac-2 accelerating tanks.

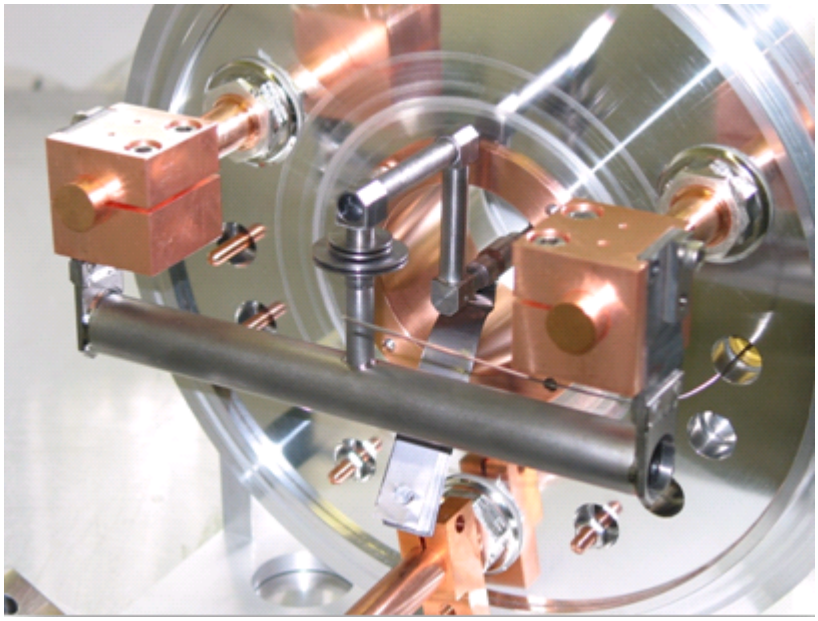

Figure 3.5: Target from ISOLDE. Picture Taken from the ISOLDE web page http://isolde.web.cern.ch

μs length emitted by the PSB come every 1.2 seconds and are very intensive (about 3.6×10^{13} protons/pulse). These pulses are collected in supercycles or superpulses, containing between 30 and 50 cycles or pulses. ISOLDE has at its disposal between 30% and 50% of all pulses produced at PSB. This corresponds to about 2 μA of electric current. Thanks to this short pulses the diffusion of radiation increases and, thus, the production of short lived isotopes is also increased. During our experiment the supercycle length was 40-50 pulses.

3.2.2 Target ion-source system and mass separators

The combination of the target and the ion-source system forms one of the most decisive part of ISOLDE facility. The target is the first element found by the proton beam coming from the PSB through the transfer line. The target is not a simple plate or rod placed in an accelerator beam but is a complex system which produces the desired nuclear species via different reactions such as fission, fragmentation or spallation. A wide range of isotopes can be produced by playing with the beam energy, target thickness or its chemical structure. The objective of the target is to produce as many isotopes as possible and extract them in the fastest way, specially in the case of short-lived nuclides.

Normally, and specially in fission reactions, thick targets in combination with the high-energy proton beam are used. Some experiments make use of a neutron converter in order to perform the fission with neutrons instead of protons. This helps to reduce the number of isobaric contaminants and minimize the probability for spallation and fragmentation reactions that can also take place together with the fission. Fig. 3.5 shows a picture which describes the most important parts of the target-ion system used at ISOLDE. The target container is represented by the gray horizontal tube with a reaction material inside. It can be foils, fibers, liquids or powders. The typical thickness of the target is few tens of g/cm^2.

The container is heated up to about 2000 Celcius degrees by applying an electrical current through the tube. When the protons hit the target material the reaction products diffuse by a small vertical tube towards the ion-source system. When the proton-to-neutron converter, based on a solid tantalum or tungsten rod, is used it is located immediately below the target container and the incident particles impinge on it first.

Passing through a transfer line the radioactive products are ionized following different mechanisms: *Electron Impact Ionization*, *Surface Ionization*, *Laser Ionization*, etc. ISOLDE is characterized by the RILIS (Resonance Ionization Laser Ion Source) which is based on the photo-ionization technique [Mis93]. Isobar contamination can be one of the disadvantages of the ISOL technique and even a high resolution system of magnets cannot separate isobars with very similar masses. RILIS provides very effective isobaric separation based on Z-selective resonant ionization. The atoms diffused in the target are effused towards the hot cavity where they are maintained in gaseous state. Laser pulses with more than 10 kHz of frequency irradiate the atoms during 10-100 μs. The role of the cavity is to keep ions confined in a compact volume before they are extracted from the target ion-source system by creating a gradient after reaching high temperatures inside the cavity. In atoms with low ionization potential thermal ionization can take place due to the heating, and perfect isobaric separation cannot be performed. During the resonant laser ionization atoms are gradually excited by laser photons up to states close to the ionization limit where the electrons can be separated from the atom by applying an electric field or through infra-red irradiation. The yield of ionized atoms depends on the flux of laser photons, the cross section for ionization from the excited states to higher excited states close to continuum and decay rate of the excited states of an atom. Normally, the efficiency of the laser ionization is higher than 10%.

The confinement inside the hot cavity is achieved with electrons naturally emitted from the metallic walls of the cavity while it is heated. For that reason materials with low electron work function as niobium or tantalum are used in RILIS. The complete setup consists on optical elements to focus the laser beams, three tunable dye lasers and three tunable Ti:Sa lasers, all of them Nd:YAG pumped. The spectral range covered by RILIS is 210-950 nm. A very special design of quartz glass transfer line in combination with RILIS is used to get an addition selectivity of the desired nuclei [Bou07]

Once the atoms are ionized and isobarically separated as well as possible the mass separation take place. The ions are extracted into the beam line with a 60-kV potential applied between the target and the end point of the line before separators. The ionization of the air around the target can alter this potential. Nevertheless, this effect is minimized when the pulsed high voltage supply is interrupted 35 μs before the impact of the beam and it is restored to the regulated value 6-7 ms after.

As can be seen in Fig.3.2 there are two separators at ISOLDE. The General Purpose Separator (GPS) is the smallest one and more simple to use. It contains a double focus magnet of 70° which has 1.5 meters of mean radius curvature which allows to select three ion beams in $\pm$15% mass range from the central mass and channelling these beams to three different experimental points at the same time. This machine consists of pairs of cylinder-shape deflector plates, one to each side of the central line. Moving this deflectors in parallel with the focal plane we can perform the mass selection. This smaller beam lines are mainly used for collecting ions or small experimental set-ups in nuclear and solid state physics.

The High Resolution Separator (HRS) is more complex but it has higher resolution. It

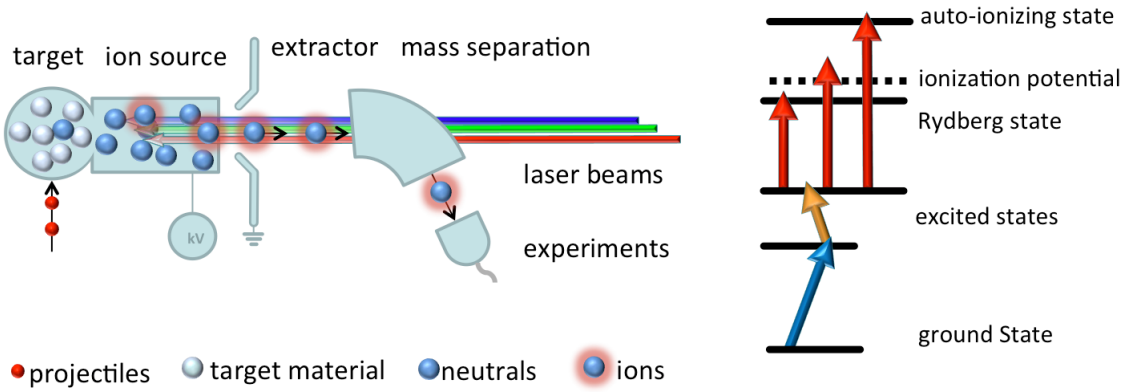

Figure 3.6: Schematic representation of the target ion-source system, resonant ionization process and mass separation at ISOLDE. The process of ionization of an atom from the ground state to the levels in the ionization region is shown in the right hand side (taken from http://rilis.web.cern.ch).

consists of two C-type dipoles (the first of 90° and the second of 60°) dispersing the beam in opposite directions, electrostatic quadrupole lenses and few magnetic and electrostatic elements that correct the aberration effects. As the two magnets twist the beam in opposite direction there is no need to additional intermediate focus before the second dipole. The maximum resolution of this separator is thereby $\triangle M/M = 15000$, but only 5000 have been reached at the moment. More technical details about GPS and HRS can be found in [Kug00]. Fig. 3.6 summarizes the trip of initially created atoms in the target after being ionized by lasers and mass separated afterwords.

The target ion-source system situated in air is managed by a robot due to the high radioactivity presented around even after several days of the experiment. Starting from the ion source the system is immersed in vacuum to avoid the interaction with particles from the air. In order to make the best use of the space available in the experimental hall, a central beam line is constructed to allow ions from either of the two separators to be used (see Fig. 3.2). The beams are merged together with cylinder shaped electrostatic deflectors, combined with a final parallel plate condenser used as the final beam-kicker, steering the beam into the central beam line. The loss of a fraction of beam intensity in different parts of the beam line (focusing points, mass selection segments, Coulombian repulsion, etc.) constitutes a crucial step for unsuccessful experimental campaign and must be cared with big attention. To regulate the injection of reaction products created in the target into the beam line the so called beam gate composed by a 4.5-kV electrostatic deflector is installed. Any isotope that remains in the target after a relatively long period of time can be considered as a contaminant. To avoid its diffusion into the beam line the beam gate can be closed. The characteristic beam gate time depends on the half-life of the desired isotope which is planned to be studied at the experimental area. For beam intensity monitoring many Faraday cups, moving wire scanners and wire grids are installed along all the beam lines. In this way, the user can control and optimize the beam intensity for his specific experiment.

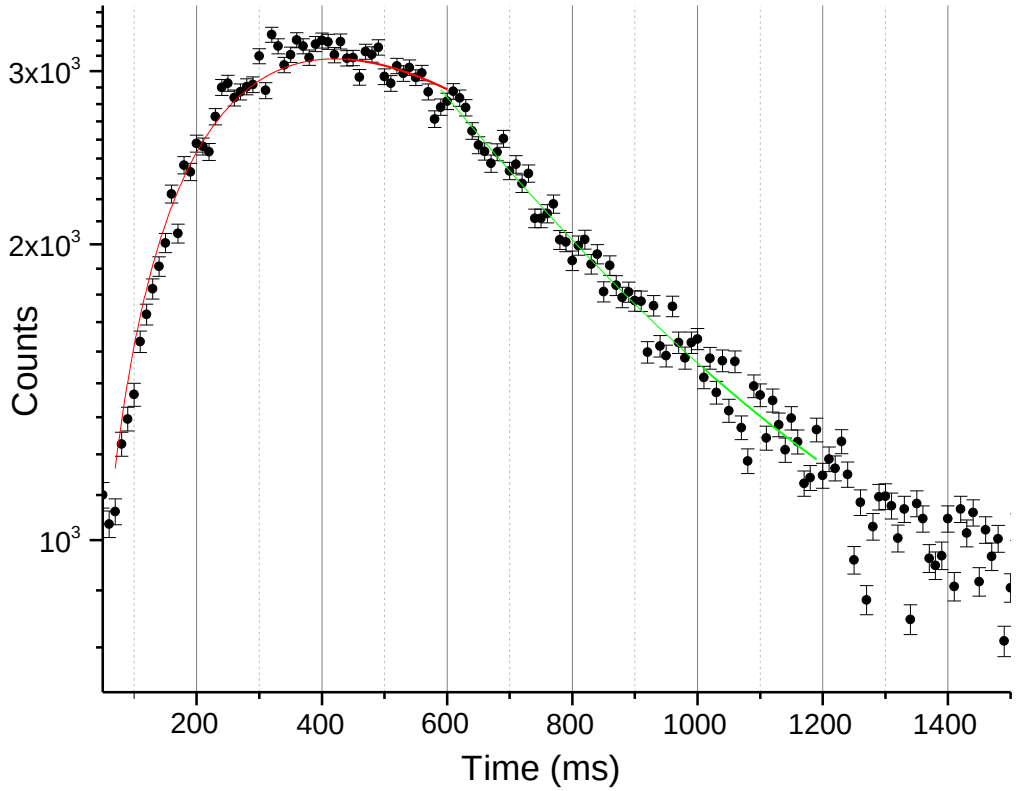

Figure 3.7: Release curve (red) of ^{81}Zn fitted to the experimental data with a gate in the 351-keV transition of ^{81}Ga. The fitted release time is in the order of tens of ms. The decay part of ^{81}Zn (green) was fitted from 600 ms, after the beam gate was closed.

Target release

The ion-beam intensity as function of time since last proton impacts into the target is called *target release curve*. It plays an important role in the development and characterization of thick targets used at ISOLDE. In general, it is difficult to find analytical expression that describes properly the diffusion of isotopes created inside the target due to many boundary conditions, complex diffusion process at variable temperatures, for which most of the coefficients and potentials are unknown. The release function $P(t)$ is given by the probability density for an atom generated at $t = 0$ of a given element to be released at time t. When the half-life of the desired isotope is in the millisecond range, significant part of nuclei will decay before reaching the experimental area. For that reason, the correct description of the release curve must include the decay part. The curve proposed by Lettry *et al.* in 1997 [Let97] is based on many experimental data fittings and shows that, almost all the release processes, start with with a sharp rise given by a time-constant-like parameter $\lambda_r = ln2/t_r$ and followed by the decay characterized by a fast and slow components represented by λ_f and λ_s:

$$P(t) = \frac{1}{N} \quad 1 - e^{-\lambda_r t} \quad \alpha e^{-\lambda_f t} + (1-\alpha)e^{-\lambda_s t} \quad e^{-\lambda t}. \tag{3.1}$$

The normalization factor N and weighting parameter α were also included in $P(t)$. Some measured release parameters for even-even ^{74,76}Zn isotopes were measured by Köster *et al.* and published in 2005 [Kös05]. Unfortunately, there is no previously measured release

parameters for ^{81}Zn. Gating in the strongest γ line from the β-decay of ^{81}Zn to ^{81}Ga we can fit the experimental data to the Eq. (3.1). Fig. 3.7 shows the release curve $P(t)$ for ^{81}Zn in red. The data were fitted avoiding the range of γ-rays from neutron capture (first 50 ms) and only until the beam gate was open (600 ms). After that, the free decay of ^{81}Zn takes place (green curve). This fit was done from the beam gate until 1200 ms, when the next consecutive proton pulse impact the target. Fitting parameters are represented in the same plot. In our case, the weighting parameter α was very close to zero. This means that only one exponential decay components of the release takes place. The obtained decay time t_f was very small and in our case there were no sufficient data for correct fitting. The obtained release time that corresponds to the rise time t_r from the Eq. (3.1) was quite large, in the order of tens of milliseconds. This effect can be attributed to the quartz transfer line, which retains the nuclei diffused out the target.

Production rates

The intensity of a radioactive beam received by the ISOLDE user in the experimental area depends on the production of the radioactive species in the target and transportation efficiency. In nuclear spectroscopy experiments the total rate of particles detected in the experimental set-up is given by the following equation:

$$I = \int_0^l \Phi \cdot \sigma(E) \cdot N \cdot \quad dx, \tag{3.2}$$

where Φ is the flux of the primary beam, σ is the reaction cross-section and N is the number of atoms per surface area present in the target. The cross-section depends on the energy that is lost when the particles go through the target. That is why the intensity is calculated by integrating over the target thickness l. The last term of Eq. (3.2) represents the total efficiency of the process and can be separated as the product of the target extraction efficiency ($_{target}$), the efficiency in the ionization procedure ($_{ion-source}$), the transportation efficiency ($_{trasp}$) which accounts for losses in the mass separator (normally close to the unit) and reduction of transmission to the experimental set-up and finally the detection efficiency ($_{set-up}$). If additional elements as coolers or breeders are used in the experiment its efficiencies must be also taken into account in Eq. (3.2). Some extra ideas on how to optimize and purify the intense ISOL beam can be found in [Kös01].

3.3 Experimental setup

The aim of this thesis resides in the study of nuclear structure of nuclides obtained from the decay of ^{81}Zn. It is a very exotic isotope with considerably short half-life, about 300 ms, and its production requires a sophisticated technique. The main problem in producing Zn isotope is to achieve a pure beam without isobaric contaminants. An important progress has been reached with the use of the ISOLDE RILIS but the elements with low ionization potential as Rb, Ga or Sr, ionized on the walls of the hot ionizer cavity, remained in the beam line. Even when using the RILIS the Rb/Zn ratio is more than 10^5 in case of $A = 81$. To enhance this value all state-of-the-art techniques as the use of neutron converter [Got14], a fast beam chopper gated on the RILIS pulses, the use of macro-gates on the Zn release and High Resolution Separator were employed, but at least a

factor of 30 of Rb/Zn remained. Thus, an additional optimization method was required. The *isothermal vacuum chromatography* technique with the combination of quartz glass transfer line were added to the previous techniques and the ^{81}Rb background obtained at the end was similarly intense as ^{81}Zn. Hence, the great reduction of contaminant of five orders of magnitude allows us to perform our experimetnal campaign, which is described in the following. More details about yield and release optimization of neutron-rich Zn isotopes can be found in [Kös05, Kös08].

The experiment IS441 in which almost pure beam of Zn ions was created has been performed at ISOLDE in October 2011 in the framework of a systematic ultra-fast timing investigation of neutron-rich nuclei populated in the decay of Zn. The 1.4-GeV proton pulses with average intensity of 2 μA coming from PS Booster every 1.2 seconds were converted into fast neutrons [Kös02] before being impacted on the hot 2000 °C 50 g/cm^2 UC_x/graphite target inducing spontaneous fission reaction. The extracted fragments were accelerated up to 60 keV and guided through the cooled quartz glass transfer line into a tungsten ionizer where Z-separation was preformed by using the RILIS (Resonance Ionization Laser Ion Source). The beam gate, as defined before, was established to avoid the accumulation of long-lived activity delivered from the target and in case of ^{81}Zn it was set to 600 ms. The obtained ions were transported to magnetic HRS for selection of ^{81}Zn nuclei. The separated ^{81}Zn were sent to the experimental area where they were collected in an aluminum stopper creating a saturated source. The average activity of the β particles registered during the experiment was about 10000 cps for ^{81}Zn.

3.3.1 Detectors

The experimental setup includes two high-purity Germanium (HPGe) detectors, two lanthanum bromide doped with Ce ($LaBr_3$(Ce)) and one plastic scintillator NE111A for β particle detection. They were positioned in a close geometry around an aluminum foil. Lanthanum bromides and NE111A plastic detector were placed in a vertical plane, while both HPGe were located in a horizontal plane as shown in Fig. 3.8.

The cylindrical 3-mm thick and 22-mm in diameter organic plastic scintillator NE111A [nuc] was mounted on Photonis XP2020 photomultiplier (PMT) and situated less than 1 mm away from the stopper in order to obtain an efficiency as high as possible. For correct use of ATD method the β detector must be as thin as possible to guarantee an homogeneous energy and time response. The thin detector provides quite uniform time response for a wide range of β energy (see section 3.5), being almost insensitive to γ radiation. The XP2020 URQ manufactured by Philips is a 12-stage PMT with 2-inch diameter and very fast response. The internal studies performed in Grupo de Fı́sica Nuclear (UCM, Madrid) reports the time resolution of NE111A+XP2020 well below 50 ps and a rise time below 1 ns.

BaF_2 scintillators were the traditional crystals used for fast-timing measurements [Mos89] in the picosecond range. These crystals present a very fast component in timing signal which permit to reach 120 ps for time resolution at ^{60}Co energies when coupled to XP2020Q PMT and close to 10% of energy resolution for 662-keV γ-ray from ^{137}Cs. During the last years new fast response crystals of $LaBr_3$ doped with Ce appeared as a good substitute for BaF_2 due their high light output (63 photons/keV), much better energy resolution (around 3% at 662-keV γ-ray of ^{137}Cs), short decay time, weak temperature dependence, high density (5 g/cm^3) and radiation tolerance [Owe07]. It has a very good

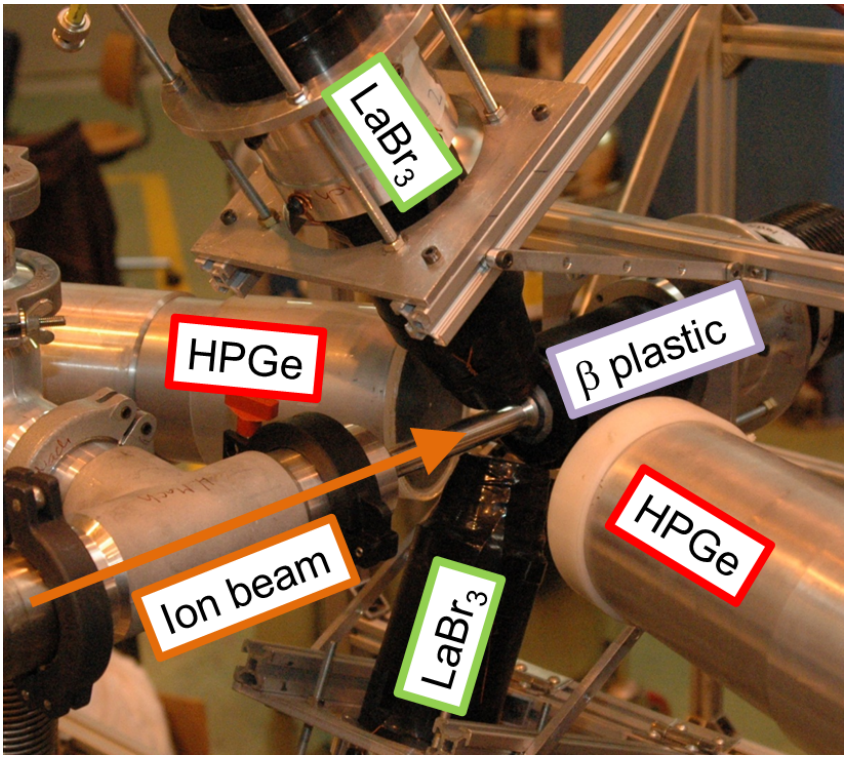

Figure 3.8: Set-up of five detectors used in IS441 experiment.

timing properties in addition to high γ-ray efficiency and good stopping power. Large and detailed study of 1-inch $LaBr_3(Ce)$ has been performed in Grupo de Física Nuclear (UCM, Madrid) by V. Vedia *et al.* and published in [Ved15]. Great improvements in energy resolution of 2.8% for ^{137}Cs 662-keV transition and even better timing resolution below 100 ps were achieved. The crystals were produced by different manufacturers with distinct Ce dopant concentration, but having the same cylindrical shape with nominal size of 1-in. in height and 1-in. in diameter. They were hermetically encapsulated inside an aluminium frame which had a thin aluminium window at the entrance, and was fitted with a glass light guide at the coupling side to the photosensor. Inside the case several layers of light reflector and shock absorbing material assure the stability of the crystal and minimize photon losses.

In IS441 we used a new generation of $LaBr_3(Ce)$ crystals with truncated cone shape as shown in Fig. 3.9. The time and energy resolution are similar to the 1-inch crystal. The dimension parameters were optimized for detection efficiency without deteriorating the time resolution. This geometry permits to place the crystals very close to the radioactive source covering about 7% of the total solid angle. Several layers of Pb were used to cover the crystal in lateral faces in order to absorb the backscattered gammas. The two truncated cone shape $LaBr_3(Ce)$ used in our experimental campaign were mounted on 8-stage Photonis XP20D0 fast-response 2-inch photomultiplier tube optimized to give fast time response at the cost of lower gain. However, in case of $LaBr_3(Ce)$ the gain is not needed because these crystals have very high proton yield.

For precise selection of γ rays with excelent resolution two HPGe detectors from LPSC (France) were employed. While one of them is p-type (labelled as HPGe1) and the other n-type (labeled as Ge2), both are manufactured by Ortec and have $\sim$60% of efficiency.

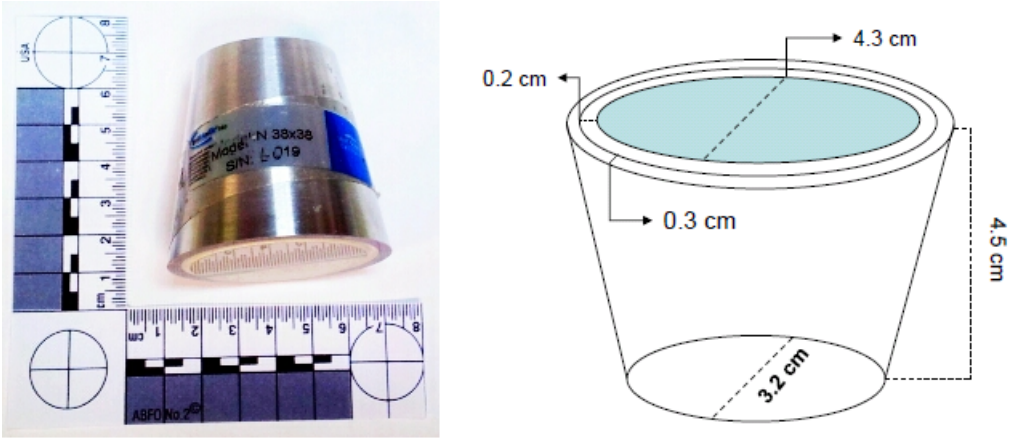

Figure 3.9: A picture of truncated $LaBr_3(Ce)$ with aluminum encapsulation used in our experiment (left) and its dimensions (right). Taken from [Mam13].

The energy resolution of HPGe1 is 0.15% at 1.33-MeV ^{60}Co γ-ray while Ge2 has 0.17% at the same energy. The peak-to-Compton ration of the first one is also higher at the same energy being 70:1 and 56:1 respectively. On the other hand, the efficiency of Ge1 above 2 MeV is much higher than in Ge2 which is more efficient at energies below 50 keV. Their poor timing resolution (the best value of 8 ns was published in [Mih07]) does not allow us to employ them for half-life measurements in picosecond range. However, if it had existed any isomer in nano- or microsecond range we would have been able to detect half-life by timing with HPGe.

The detector signals were processed by a complex electronic system which can be divided in two parts. The first one, the energy branch (see (a) from the Fig. 3.10), incorporates NE111A and Ge detectors. Working in coincidence mode the $\beta\gamma$ or $\gamma\gamma$ spectroscopy analysis can be performed in order to place γ lines in a level scheme and calculate their intensities. The signals are slow with the rise time of hundreds of picoseconds and go directly to the acquisition system. The other branch corresponds to the timing part (picture (b) from the Fig. 3.10), which includes the plastic scintillator and both $LaBr_3(Ce)$ detectors. The signals treated with these detectors are fast (few nanoseconds of rise time) but with worse shapes than in HPGe. Time to Amplitude Converter (TAC) was utilized in this branch for measuring time response. In requires a start and stop signal to form timing event. Five TACs were placed in our set-up. The start signal in four of them was coming from the β detector. In case of picosecond half-lives the signal from each $LaBr_3(Ce)$ crystal served as stop. The signal from HPGe detectors was used as stop for the analysis of longer half-lives. The fifth TAC, also used for short lifetimes, was started by the signal from one of $LaBr_3(Ce)$ detectors and stopped by the other. In this way, the $TAC_{\beta-LaBr}$ and $TAC_{LaBr-LaBr}$ are called fast TACs (FTAC) and $TAC_{\beta-Ge}$ is called slow TAC (STAC).

3.3.2 Electronics and Data Acquisition System

The signals from detectors were guided to the NIM standard (Nuclear Instrument Module) that is a modular system formed by specific bins (rectangular boxes of 8.75 inches tall and 1.35 or 2.7 inches width) and crates where the bins are mounted on. The crate provides

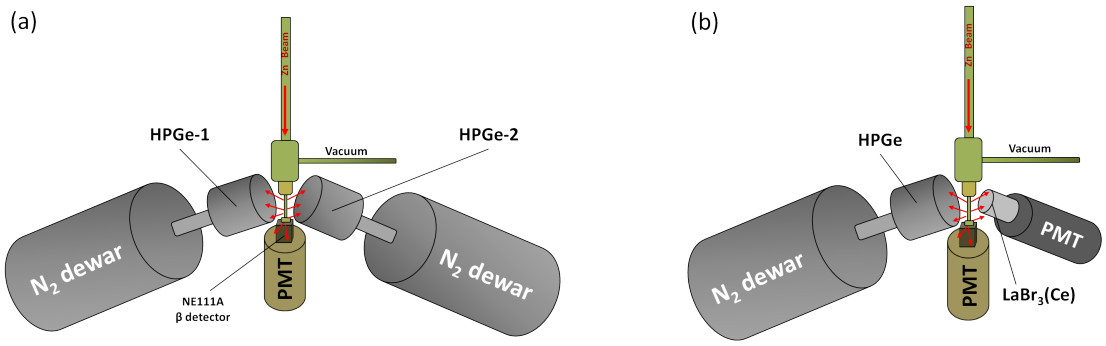

Figure 3.10: The whole set-up of five detectors can be divided in two branches and perform the data analysis separately. For spectroscopy measurements the energy part (a) must be used where HPGe detectors plays the most important role. Timing measurements were done following the scheme from (b) in which NE111A plastic scintillator and $LaBr_3(Ce)$ crystal act as the start and the stop signal in Time to Amplitude Converter.

a fix voltage for each bin module. Under the crate there is a slot to put fans and the air can flow towards all the modules fixed in the crate to prevent their burn. When more than one crate is needed it is useful to put them into a rack. Fig. 3.11 shows the complete analogue electronic scheme followed in the experiment IS441.

The β detector participates as a start signal in four 567 ORTEC TACs. There are two signals that leave the PMT to which it is coupled. One of them, coming from the last dynode, is used to characterize the energy of β particles. It is pre-amplified by ORTEC 113 module and amplified by ORTEC 572 Amplifier. Before getting to the Data Acquisition system (DAQ) it is passed through the Linear Gate Stretcher ORTEC 542 module which permits the signal to pass if it receives a coincidence from the corresponding TAC. All the signals from TACs are collected by the Universal Coincidence Device in order to gate signals with coincidence conditions. Negative signal from the PMT goes directly through 10-ns cable to the Constant Fraction Discriminator (CFD) ORTEC 935 Quad. CFD gives an additional internal delay of 2.5 ns and triggered output signal with the low time walk is transported to Time-to-Amplitude Converters by a 2-ns cable where it starts rising a voltage. This voltage is proportional to the time until the stop signal arrives and the amplitude of the output signal will be characterized by the increase voltage difference.

The signals from $LaBr_3(Ce)$ receive similar treatment. The anode one is used for timing and it goes to the CFD with 2.5 ns internal delay through the 10-ns delay cable and after it is connected to the TAC by a 2-ns cable where it acts as a stop signal. The dynode signal, used for the energy, is amplified in the same way as in β detector and 16-ns cable transports it directly to the DAQ system. In our experimental set-up one additional TAC was used for fast-timing measurements. It was started by the scintillator crystal labeled as LaBr-1 and stopped by LaBr-2. The signal from the first detector was carried to the TAC through a 10-ns cable while the signal from the second one was guided by a 48-ns cable. The $LaBr_3$-$LaBr_3$ is utilized to perform $\gamma\gamma$(t) coincidences when the desired transitions are resolved in the energy spectrum.

HPGe crystals produce a weak signal, so the amplification process takes place in the integrated system inside the detector. Two identical signals are emitted. One is used for the energy and the other serves for timing. The energy part is carried directly to the

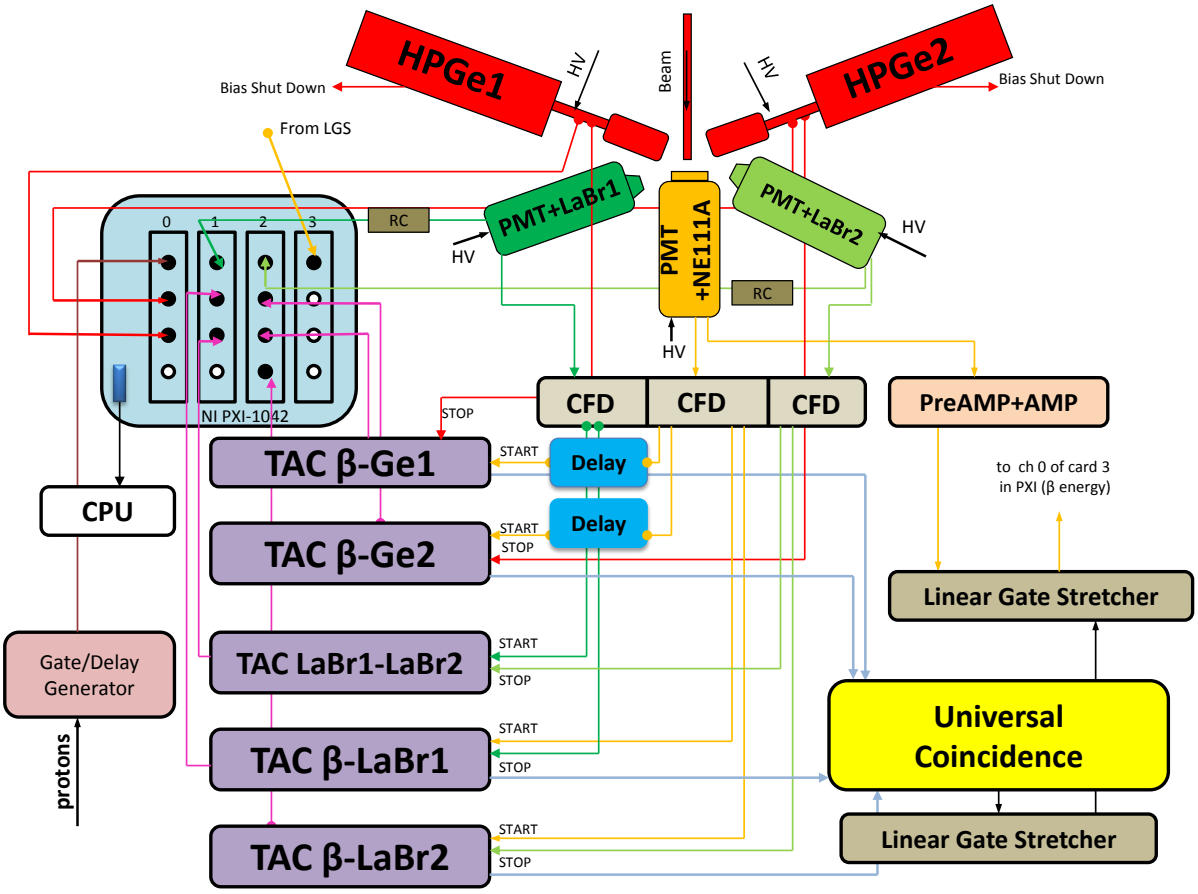

Figure 3.11: Full electronic scheme used in IS441 experiment. It includes four detectors of γ radiation (two hiper-pure Ge and two lanthanum bromide scintillators doped with Ce) and one plastic scintillator for β detection. Each scintillator crystal was coupled to a photomultiplier and in combination with Constant Fraction Discriminators provided signals for fast-timing. Five TACs, three fast and two slow, were placed for half-life measurements. All the signals were processed by a Digital Gamma Finder connected to a CPU.

DAQ, while the timing signal passes through 6-ns cables by the TAC where it serves as the stop signal started by the β detector. The input channel in the DAQ system is labeled as β-STAC.

The data acquisition system used in experiment IS441 was PIXIE-4 Digital Gamma Finder from XIA LLC [LLC13]. This is a digital system designed specially to deal with the high resolution γ spectroscopy using HPGe. It is also compatible with scintillators or other semiconductor detectors when the signals are properly prepared. It can acquire 75 millions of samples (75 MHz) with 14-bit Analog-to-Digital Converters (ADC) working as a waveform digitizer.

The most appropriate signal for PIXIE-4 is the signal that outcomes directly from Pre-AMP or AMP without any additional treatment. This system permits signal amplitude measurements at the same time that its shaped in each input channel. Fig. 3.12 shows 4 cards labelled with 0, 1, 2 and 3 containing 4 input channels each one. Each card can execute acquisition as well as signal processing. The diagram below the picture of

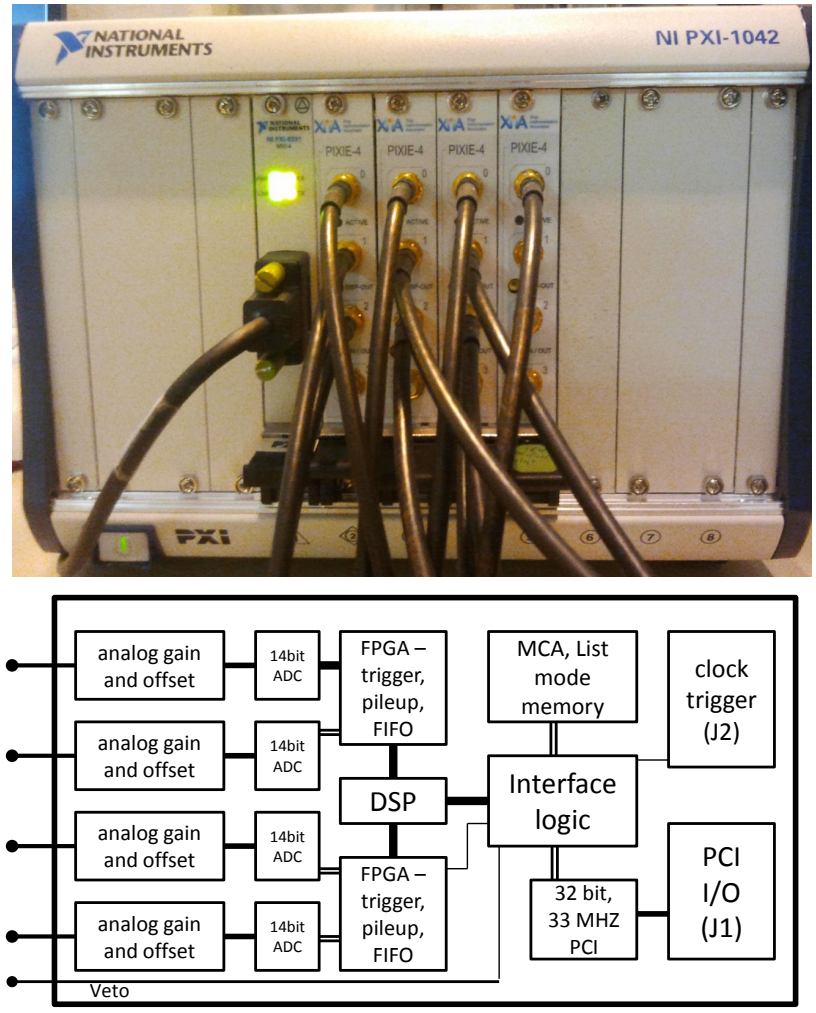

Figure 3.12: A picture of PIXIE-4 with four cards, each of them composed by four input channels. The figure below shows the internal composition of each card (see text for details).

PIXIE-4 shows all the internal electronic devices that each card is made up of. Each analogue input has its own signal conditioning unit (**Analog Signal Conditioning**). The task of this circuitry is to adapt the incoming signals to the input voltage range of the ADC, which spans 2V. The 14-bit ADC converts the input analog signal into a digital one characterized by 16-bit digital word. The maximum of 2V corresponds to $2^{16} = 65536$.

The **Real-time Processing Units**, one per two channels, is represented by FPGA box in Fig. 3.12 and consist of a field programmable gate array (FPGA) which also incorporates a FIFO memory for each channel. The RTPUs apply digital filtering to perform essentially the same action as a shaping amplifier transforming a signal with a trapezoidal filter. The flat top will typically cover the rise time of the incoming signal and makes the pulse height measurement less sensitive to variations of the signal shape. The RTPUs contain a pileup inspector which ensures that if a second pulse is detected too soon after the first one, so that it would corrupt the first pulse height measurement, both pulses are rejected as piled up. If a pulse was detected and passed the pileup inspector, a

trigger will be issued. That trigger would notify the DSP that there are raw data available now. If a trigger was issued the data remain latched until the RTPU has been serviced by the Digital Signal Processor (DSP).

The third component of the RTPU is a FIFO memory, which is controlled by the pile up inspector logic. The FIFO memory is continuously being filled with waveform data from the ADC, only stopped to avoid overwriting of data for valid events. On a trigger the read pointer is positioned such that it points to the beginning of the pulse that caused the trigger. When the DSP collects event data, it can read any fraction of the stored signal, up to the full length of the FIFO.

The DSP controls the operation of the PIXIE-4, reads raw data from the RTPUs, reconstructs true pulse heights, applies time stamps, prepares data for output to the host computer, and histograms spectra in the on-board memory. The host computer communicates with the DSP, via the PCI interface, using a direct memory access (DMA) channel. Reading and writing data to DSP memory does not interrupt its operation, and can occur even while a measurement is underway.

As can be seen in the following scheme not all of the 16 input channels were used:

Card 0

- Channel 0: Proton pulse from PS Booster.
- Channel 1: Gamma energy from HPGe1.
- Channel 2: Gamma energy from HPGe2.
- Channel 3: Empty

Card 1

- Channel 0: Gamma energy from $LaBr_3$-1.
- Channel 1: β-$LaBr_3$-1 FTAC.
- Channel 2: $LaBr_3$-1-$LaBr_3$-2 FTAC.
- Channel 3: Empty.

Card 2

- Channel 0: γ energy from $LaBr_3$-2.
- Channel 1: β-$LaBr_3$-2 FTAC.
- Channel 2: β-HPGe-1 STAC.
- Channel 3: β-HPGe-2 STAC.

Card 3

- Channel 0: β energy from NE111A.
- Channel 1: Empty.

- Channel 2: Empty.
- Channel 3: Empty.

This distribution was optimized according to count rates and type of the detectros. The energy signals from HPGe detectors and the proton pulses, i.e. the signal triggered by the proton beam that impacts on the uranium target, were collected in the same unit to be in coincidence while the signals from the other three detectors and five TACs were distributed separately between the remaining three blocks of PIXIE-4. The triggered beam pulses (channel 0 from the first card) are very important for the lifetime measurements because they define the starting time for the ^{81}Zn accumulation and were used to rule the large half-life contaminants through the time gates taking this signal as a reference. The acquisition system was configured to write the data independently whether the detectors were in coincidence or not. In order to permit an easy imposition of coincidence, energy or time restrictions the data has to be organized properly. For this purpose it was necessary to develop many computer tools made in FORTRAN77 and programmed by H. Mach and B. Olaizola with several upgrades made by L. M. Fraile and V. Paziy.

3.4 Data Analysis Technique

The data was collected in two different modes: *List Mode (LMD)* and *MCA* 32k-histograms mode. The MCA histogram stores data histograms for all channels. The MCA block is fixed to 32768 words (32-bit deep) per each channel, i.e. total 128K words per card. In the List Mode Data format the data is organized by time and channels, giving the information in list format. Each of 4 modules of PIXIE-4 is composed of 32 memory *buffers* and each buffer can accumulate up to 744 events. When one of the modules fills the first buffer with 744 events the rest of the modules will close their current buffer independently of the number of events reached in this buffer. In our experiment the HPGe detectors, stored in the first card, had buffer priority over the scintillator detectors because of their higher count rate. Thus, every time the first module buffer was full the buffers of the other three modules were closed and started new ones started.

The output data are available in 3 different memory blocks (1 for MCA and 2 for LMD). The MCA block resides in memory external to the DSP (Digital Signal Processor). There is a local I/O (input/output) data buffer (virtual memory) for LMD located also in the DSP and consisting of 8192 16-bit words and the extended I/O data buffer in the external memory, holding up to 32 local buffers follow immediately one after other. The normal procedure is to fill first the local I/O. However, the readout process of the data is slow. During the readout the acquisition of data is halted. That gives the readout dead time of about 30 ms per module and buffer. The optimal solution is to transfer the data to the external memory when the local buffer is full. This is repeated 32 times (32 buffers per card) until the external memory is full, and only then the run is halted and data is read out by the host PC (hardware disk). The size of a data file was set to 64000 buffers. With the usual β activity it corresponds to about one hour data file. In this way, if something is going wrong in the experiment and the file becomes corrupt it can be stopped and only a small portion of data is lost.

The 32 buffers in external memory follow immediately one after another. The buffer content always starts with a buffer header of the first module. Each buffer header

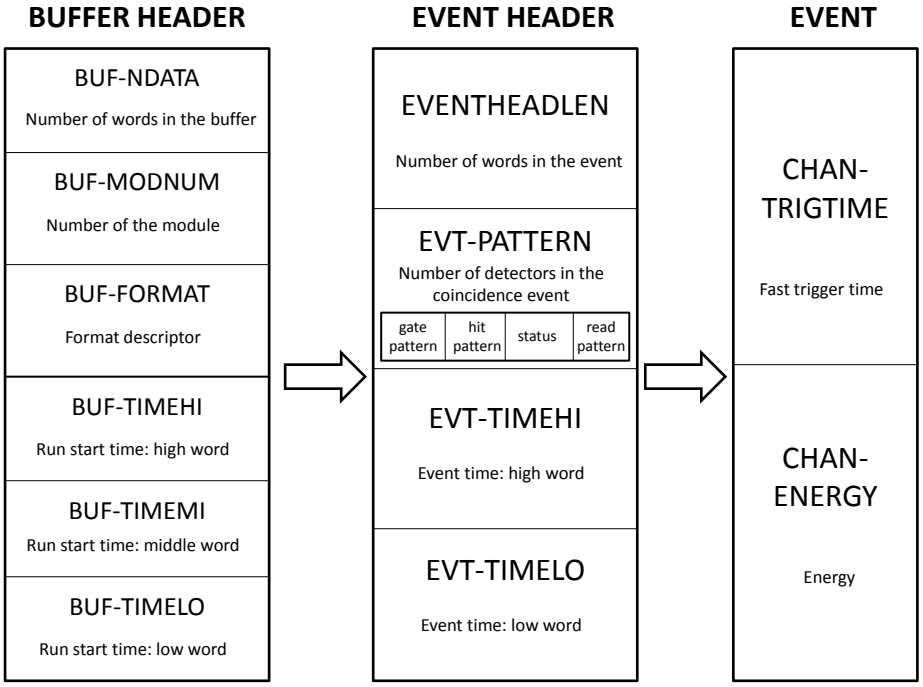

Figure 3.13: Content of the buffer header (6 ordered words), event header (4 words) and event itself (2 words).

contains six words: BUF-NDATA, BUF-MODNUM, BUF-FORMAT, BUF-TIMEHI, BUF-TIMEMI and BUF-TIMELO. The first word represents the number of words in a buffer, that is, the total number of event words plus the total number of event headers. The second one shows the modules number (0-3). The data from our experiment were written in the simplest List Mode with Comression 3 that recorders only energy and time. It has been labeled as RUNTASK = 259. The remaining three words represents the starting time of the buffer according to internal PIXIE-4 clock. All of them are 16-bit long, so each of them can accumulate $2^{16} - 1 = 65535$ events or time ticks. The procedure to work with the time words consists on sequential filling of them. As PIXIE-4 working frequency is 75 MHz each event or tick will be separated by 13.3 ns from the next one. Thus, the low time word (BUF-TIMELO) will be full after 0.87 ms. In this moment the medium time word (BUF-TIMEMI) counts 1. The maximum of BUF-TIMEMI corresponds to 57.3 seconds and is not enough to perform experiments. For that reason the high time word is used when the medium one is full extending the operation time of the experiment up to 43.4 days.

In data analysis different types of *events* can be treated. In physics the *nuclear event* usually corresponds to the nuclear decay, normally observed through emission of γ or β particle. When this event is detected in the experimental set-up it is called *detector event* which can be divided in a *single event*, which is normally corresponds to the energy or time observed in one detector, and a *coincidence event* or simply a *coincidence*, which is constructed from the information coming from several detectors. In this case time requirements between detectors are needed such as the time window between single events. Sometimes accidental events, which occur in a very small interval of time, can obey the coincidence condition but not correspond to the desired nuclear event. They are called

random events and must be suppressed in the data analysis procedure.

When signals from the detectors comes to the channels within the same module PIXIE-4 can record them in coincidence mode applying a ± 8.107 μs time window. For example, in IS441 the first card contained signals from HPGe detectors and, thus, the coincidence event between them was stored as a single event. However, the $LaBr_3(Ce)$ detectors were situated in different cards and the coincidences between them had to be done with additional software.

After the buffer header, the events are stored in sequential order. Each event starts out with an event header of length EVENTHEADLEN. Currently, EVENTHEADLEN=3, and the three words are: EVT-PATTERN, EVT-TIMEHI and EVT-TIMELO. The first one is a 16-bit word and describes the number of detectors that take part in the coincidence event. It is subdivided in 4 smaller 4-bit words: gate pattern, hit pattern, status and read pattern. The hit pattern is a bit mask, which tells which channels were read out plus some additional status information. After the event header follows the channel information as indicated by the hit pattern, in order of increasing channel numbers. For example, 1110 in module 0 would mean that the first three input channels are recorded in coincidence while the fourth one is not used. The rest of 12 bits of EVT-PATTERN were not utilized in the data acquisition of our experiment. The event header contains two time words which acts in the same way as medium and low times in buffer header. The beginning time of the event can be calculated with the BUF-TIMEHI from the buffer header and EVT-TIMEHI and EVT-TIMELO from the event header.

After the event header comes the event itself (channel header) represented by two words: CHAN-TRIGTIME and CHAN-ENERGY. The first one represents again the time word called *fast trigger time* and it is equivalent to the low time from the buffer header. With channel header the time stamp of the event can be constructed by simply using the high time (BUF-TIMEHI) from the buffer header, the high time (EVT-TIMEHI) from the event header and fast trigger time (CHAN-TRIGTIME) from the event itself or channel header. Finally, the second word of the event called CHAN-ENERGY contains the information about the channel contents (not necessary the energy itself, it can be the time) which is converted to a digital representation by the ADC. Schematic representation of the buffers and events content is shown in Fig. 3.13.

In general, the output spectrum from PIXIE-4 can contain between 1024 and 32768 channels with 32-bit deep word containing 0 or 1. So the maximum number of counts per channel is $2^{32} = 4294967296$.

Data sorting

The data treatment can be described in two *sorting* steps. The first one, usually called *presorting*, consists in ordering the data according to the detectors and assigning a time stamp to each event. The code, based on FORTRAN77, makes use of the input text file where we indicate the name of the input data files and names of the desired output files, the information about proton pulses, the gain shift correction of energy or time peaks obtained from the raw data, etc. The programme reads the data file first and then loads a buffer from each card to the RAM memory of the PC. After that it looks for coincidences between channels inside the same module or between different modules. Finally, the events are written in different output files applying the gain shift correction o reconstructed proton pulse pattern. Normally, the experiments go on for several days and the data are

stored in many portions called *runs*. In this situation, the presorting programme repeats the procedure above and adds all runs together, giving a single presorted output file.

The simplest single event is constructed with 4 parameters: time since last proton impacted in the target (proton time), proton pulse pattern, energy and total time since the beginning of the experiment (long time). PIXIE-4 assigns time stamps to events according to its internal clock which is referred to the long time. However, it is more appropriate to work with the proton time which indicates the instant of creation of isotopes in the target. In order to build the time spectrum since last proton the presorting code searches for proton pulse and sets it as a reference time. Next pulse will come 1.2 s at the earliest. That is why the input channel 1 from the first card of PIXIE-4 was prepared for proton pulses and the other two for HPGe detectors. All the detector events between these two proton pulses will have the time stamp assigned as the difference between their own time and the reference proton and will be expressed in PIXIE-4 units in milliseconds. However, due to the internal dead time in PIXIE-4 (when 32 buffers of the external memory are full) some protons were missed and the time spectrum had to be reconstructed with the information from the whole proton list provided by the ISODLE.

Fig. 3.14 shows 4 histograms which corresponds to 4 parameters of a single event of HPGe. The data are accumulated during all the time. However, it is much useful to reconstruct the proton time in such a way that when a proton pulse impacts on the target we start to accumulate data in the time spectrum (see plot (a) from Fig. 3.14). If the second proton pulse impacts 1.2 s after the first one the counter is set to zero and the process is repeated. This is done by the presorting code offline. When the consecutive proton is missed and the next one impacts 2.4 seconds after the first proton pulse we observe the first "tread" in the proton time plot. Finally, the graph takes a stepped form due to more than one missed proton pulses and the plot in (b) presents the number of counts accumulated in each proton pulse type. In this way, the maximum number of counts was accumulated during the period when only one proton pulse was missed (second red bar in (b)). The third plot labeled with (c) shows γ peaks registered during all the experiment. Huge amount of new transitions were detected up to very high energy (channel 20000 corresponds to 8 MeV as will be shown in next section). Finally, the last picture (d) contains all the events accumulated according to the total experiment time, scaled to 1 second per channel. Several time gaps can be appreciated when the data acquisition was stopped due to experimental problems or maintenance.

For β-decay experiments the γ decays follows the β particle. This constitutes a very useful tool for decreasing background employing the β detector in coincidence with a γ detector. In this case, the presorting procedure will operate between two different modules as the signal from the β detector was sent to the card 3 from PIXIE-4. Coming back to the example with HPGe the event now is extended with two parameters more. The first one is the β energy and the second one is the difference between the time stamp of HPGe and β detector. The β-gated presorting was used in our data analysis to determine energies and intensities of γ transitions.

For the correct placement of γ lines in a decay scheme the $\gamma\gamma$ coincidences between two HPGe detector was needed. This task was already done internally by PIXIE-4 with ± 8.107 μs coincidence window. The coincidence event in this case will contain similar information as in the single event explained above. The main difference here is the use of two γ detectors and thus, two parameters for the energy. The last parameter measures the time difference between the events of HPGe detectors and is characterized by a narrow

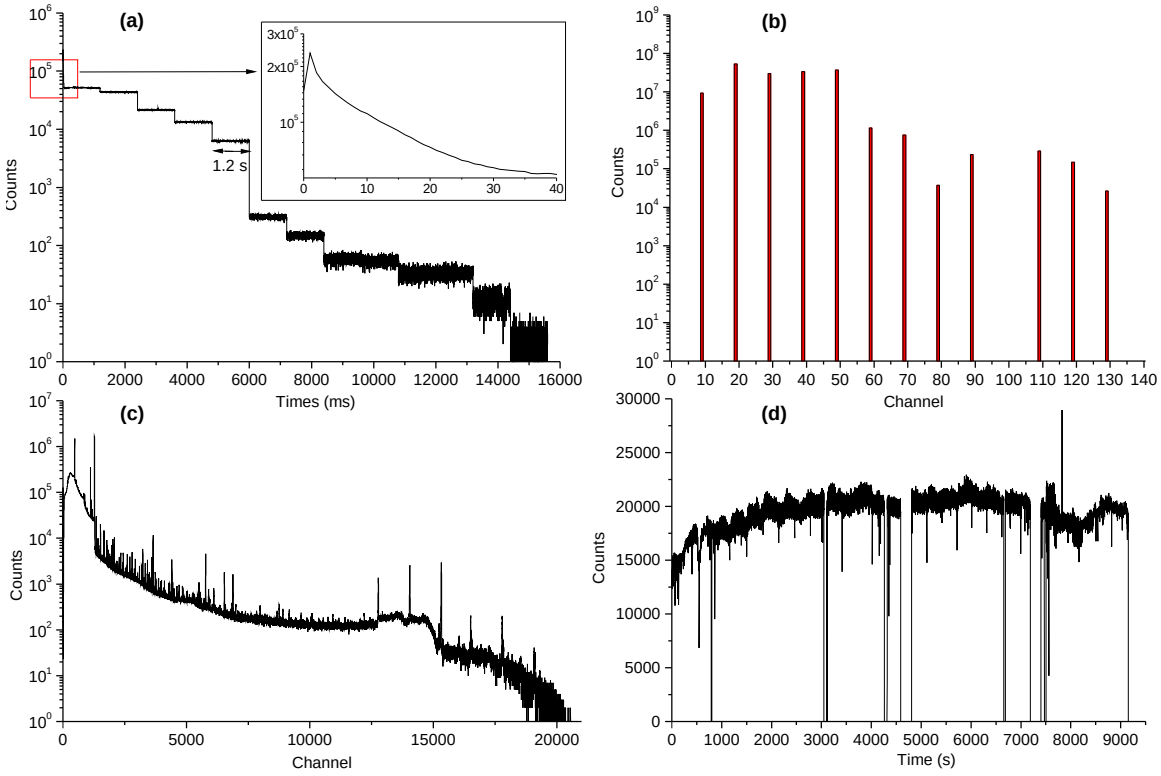

Figure 3.14: 4-parameter single event from HPGe detector. Proton time is shown in (a), proton pattern in (b), energy spectrum in (c) and long time in (d).

event peak and random coincidences represented by a flat background on the sides (see Fig. 3.15). An additional coincidence with β detector can be added in the presorting of $\gamma\gamma$ giving β-HPGe-HPGe event. It will reduce the statistics but will ensure that all γ rays de-excite levels populated by β-decay.

For half-lives measurements with Convolution Technique or Centroid Shift technique the presorting is more complex because it includes more parameters and therefore the coincidences must be done between channels of three different cards. The presorting includes the β detector in coincidence with $LaBr_3$(Ce) and FTAC. The HPGe detector can be used for precise selection of γ lines in $LaBr_3$ and coincidences with proton pulses must be taken into account for correct time spectra. In this way, the event will be characterized by the proton-β-$LaBr_3$-FTAC-HPGe coincidences. In the case of longer half-lives (tens of nanoseconds) the Slow-TAC was employed and only HPGe detectors were employed for γ-ray selection. For each situation, sophisticated data analysis codes were written and the events could contain between 5 and 9 parameters.

Once the presorted files are generated we can classify and identify nuclear events by imposing several conditions in the event parameters and explore the related information. Random subtraction is performed at this part. This step is usually called *sorting* and the imposed conditions take the name of *gates*, which act as filters for the event parameters. In this way, if we want to measure a certain nanosecond half-life by fitting the delayed part of the time response spectrum the energy gate must be set in the desired γ transition that de-excites the nanosecond energy level. That means that we have to locate this γ peak in $LaBr_3$ detector and select the corresponding range of channels in the ADC. This process is called *projection*. The time spectrum seen in FTAC will contain a slope

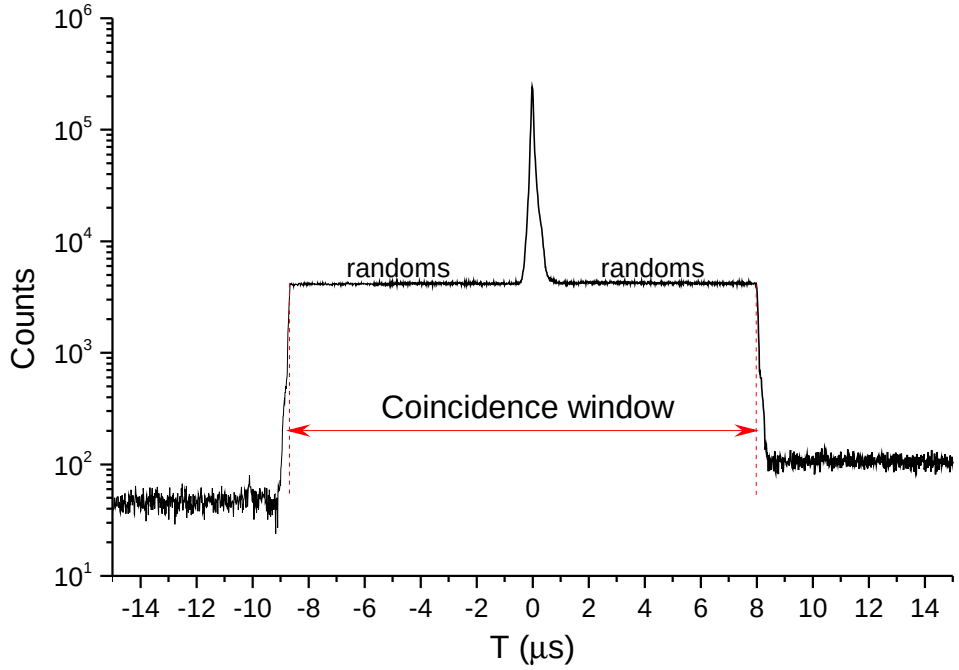

Figure 3.15: Time difference between HPGe detectors in $\gamma\gamma$ coincidence event. Random counts should be subtracted in the data analysis during sorting process.

which characterizes the half-life. Another simple example of projection can be found in $\gamma\gamma$ coincidences when a certain energy gate is established in one HPGe and projected into another. The resulting gated spectra will contain all γ lines which are in coincidence with the one where the gate was set.

When the presorted file contains more parameters, as in case of β-$LaBr_3$-FTAC-HPGe, several levels of gates can be used. The code which performs this sorting was programmed by H. Mach and can perform projections with up to 8 parameters. All the spectra obtained in our work have 32768 channels. For plotting, the graphical selection of the gates, centroid and area calculations of the peaks and many other graphical tasks, the DMP.exe programme written also by H. Mach was used.

3.5 Calibrations

Before starting the data analysis the HPGe and $LaBr_{Ce}$ detectors must be energy calibrated for accurate determination of the peaks. That means that the correct relation between the energy and the channels from ADC must be found. The intensity of the γ transitions placed in the decay scheme of a certain nucleus requires a precise determination of the efficiency of HPGe detectors since their response changes a lot with the energy. The efficiency curves must be constructed for each HPGe detector. The efficiency calibration of $LaBr_3$(Ce) detectors is not performed because they are only used for timing measurements in our work. However, time calibrations of these detectors is the decisive part for the fast-timing method specially when the Centroid Shift technique is applied. The so called *walk curves* that represents the time response as function of energy of the full energy peak or Compton event must be built for the combination of $LaBr_3$(Ce) crystal and FTAC. The time calibration, i.e. ps/channel, of the Time-to-Amplitude-Converters must

be performed previously. The β detector must be also time calibrated as it presents a non-linear response with the energy deposited by the β particle.

3.5.1 Energy Calibrations and stability

For quick identification of γ lines a preliminary energy calibration of the semiconductor detectors was performed at the beginning of the IS441 experiment at ISOLDE. Transitions from background contaminants and known decay chains were used for that. The obtained energy-channel relation was $E(keV) = 0.299 \cdot Chan + 0.19$. However, during the presorting step we switched to more comfortable value of 0.4 keV/channel with zero offset for both detectors. This allows both HPGe to be treated simultaneously.

For precise placement of γ transitions in a level scheme, a careful energy calibration was needed. It is well known from the previous studies of the decay of ^{81}Ga to ^{81}Ge [Hof81] that HPGe will detect high energy gammas of more than 4 MeV. Taking into account the large Q_β value of ^{81}Zn we expect to see γ rays with even higher energy. Therefore, the range of the HPGe γ-spectrum was extended to 6-7 MeV. The conventional calibration sources of ^{152}Eu, ^{60}Co, ^{140}Ba or ^{138}Cs can not provide such high energy gammas. Because of that we had to turn to the use of γ rays from neutron capture process. Thermal neutrons escape from the target converter and may reach the experimental area where they are captured by different atomic nuclei which form materials that surround the experimental setup (Cl, O, H, Al, Fe, etc.) or elements that compose the detectors (Ge, La, Ce, etc.). The energy excess released from neutron capture is transformed in γ decay which can be detected by our germanium detectors. The advantage of using these lines is their intensity in the energy range up to 8 MeV. Tab. 3.1 collects the energy values used for the calibration. The gap between 2.5 y 4.3 MeV was filled with gammas from known β-decay of ^{81}Ga to ^{81}Ge (2444, 3503 and 4035 keV) and ^{81}Ge to ^{81}As (2800 and 3195 keV). First escape peaks of 6018- and 6419-keV lines were used to cover 4.4-6.4 MeV range.

The zoomed picture of the first 40 ms in the time spectra (a) of the Fig. 3.14 shows a fast buildup during the first 2 ms and a smooth decay in the range of 2-40 ms. This region precisely corresponds to neutron-capture activity. Setting a narrow gate of the first 50 ms in time since last proton spectrum and projecting into the energy we obtain the desired γ transitions that comes from the neutron capture process. The resulting spectra was analysed directly with DMP.exe programme calculating the centroid position of each energy peak and their corresponding energies were obtained from the National Nuclear Data Center of Brookhaven National Laboratory[2]. Tab. 3.1 collects all the γ-rays used in the energy calibration of HPGe. The second column explains the process γ line comes from. The resulting points were fitted to a straight line $E = m \cdot Chan + n$ as shown in Fig. 3.16. As shown with residual plot for each detector the fitting was very precise. The fitting parameters with their uncertainties are collected in Tab. 3.2.

Lanthanum bromides are not so efficient at high energies and, thus, were calibrated with the standard calibration sources. Moreover, they were not used for precise determination of γ lines but only for peak selection in the timing measurements. The β-decay of ^{138}Cs to ^{138}Ba provides sufficient number of strong γ transitions for energy calibration of $LaBr_3$(Ce) up to 2.6 MeV. The high light output (63 photons/keV) and short decay time (16 ns) cause an intense scintillation, which can create saturation in the

[2]http://nndc.bnl.gov/capgam/

E_γ(keV)	Process
23.43(5)	^{70}Ge(n,γ)^{71}Ge
52.50(10)	^{74}Ge(n,γ)^{75}Ge
175.05(3)	^{70}Ge(n,γ)^{71}Ge
198.48(6)	Sum ^{70}Ge(n,γ)^{71}Ge
253.01(10)	^{74}Ge(n,γ)^{75}Ge
326.86(3)	^{70}Ge(n,γ)^{71}Ge
499.97(2)	^{70}Ge(n,γ)^{71}Ge
595.85(1)	^{73}Ge(n,γ)^{74}Ge
692.03(2)	^{56}Fe(n,γ)^{57}Fe
708.14(3)	^{70}Ge(n,γ)^{71}Ge
867.90(1)	^{73}Ge(n,γ)^{74}Ge
1019.02(2)	^{56}Fe(n,γ)^{57}Fe
1095.47(5)	^{70}Ge(n,γ)^{71}Ge
1164.850(7)	^{35}Cl(n,γ)^{36}Cl
1260.60(30)	^{56}Fe(n,γ)^{57}Fe
1298.56(5)	^{70}Ge(n,γ)^{71}Ge
1378.66(7)	^{70}Ge(n,γ)^{71}Ge
1463.75(1)	Sum ^{73}Ge(n,γ)^{74}Ge
1612.78(2)	^{56}Fe(n,γ)^{57}Fe
1725.29(3)	^{56}Fe(n,γ)^{57}Fe
1942.61(17)	^{40}Ca(n,γ)^{41}Ca
2223.250(5)	^{1}H(n,γ)^{2}H
2444.15(4)	^{81}Ga β-decay
2800.20(20)	^{81}Ge β-decay
3195.10(20)	^{81}Ge β-decay
3503.24(8)	^{81}Ga β-decay
4035.20(7)	^{81}Ga β-decay
4217.98(11)	^{56}Fe(n,γ)^{57}Fe
4418.6(5)	^{40}Ca(n,γ)^{41}Ca
5507.39(7)	FE of 6018 keV
5907.65(5)	FE of 6419 keV
6018.42(7)	^{56}Fe(n,γ)^{57}Fe
6418.68(5)	^{40}Ca(n,γ)^{41}Ca
7631.18(10)	^{56}Fe(n,γ)^{57}Fe

Table 3.1: Neutron capture γ lines and some transitions from the decay of ^{81}Ga and ^{81}Ge [Bag08] used for HPGe energy calibration.

Detector	a_4 (keV/ch^4)	a_3 (keV/ch^3)	a_2 (keV/ch^2)	a_1 (keV/ch)	a_0 (keV)
HPGe-1	0	0	0	0.40001(1)	-0.0067(468)
HPGe-2	0	0	0	0.39990(2)	-0.0854(807)
$LaBr_3$-1	$-3.4(8)\cdot10^{-12}$	$3.0(7)\cdot10^{-8}$	$-1.0(2)\cdot10^{-5}$	0.403(21)	14.1(83)
$LaBr_3$-2	$-3.2(2)\cdot10^{-13}$	$5.9(2)\cdot10^{-9}$	$1.7(9)\cdot10^{-5}$	0.259(14)	18.0(74)

Table 3.2: Parameters from the polinomial fits $E = a_4 \cdot Ch^4 + a_3 \cdot Ch^3 + a_2 \cdot Ch^2 + a_1 \cdot Ch + a_0$ which gives the energy calibration for HPGe (linear) and $LaBr_3$(Ce) (forth order polinomial).

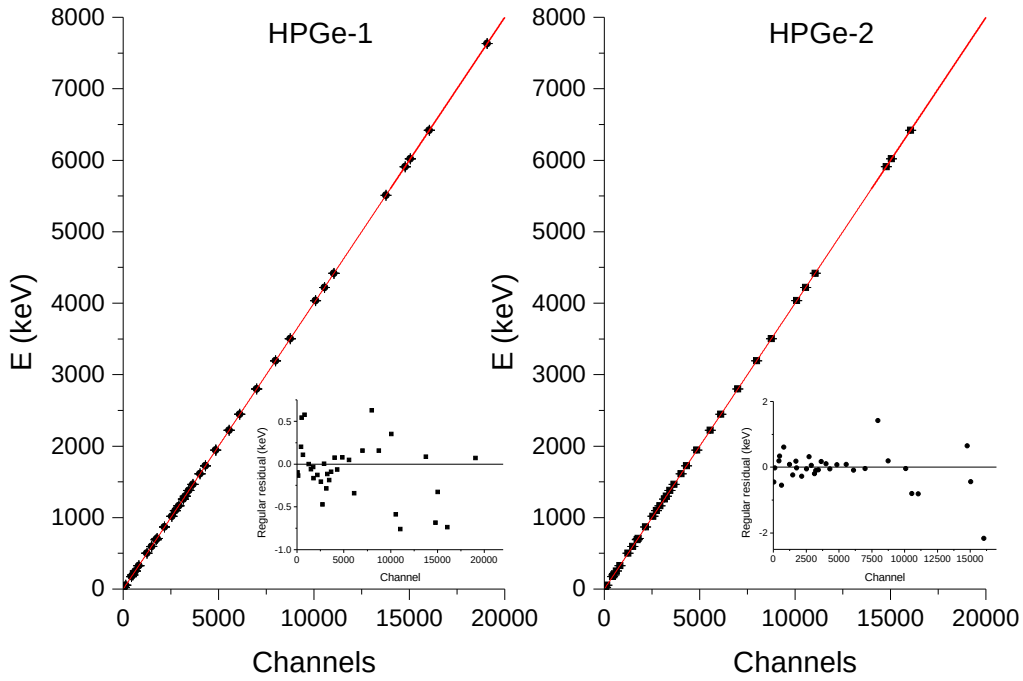

Figure 3.16: Energy calibration of HPGe detectors with neutron capture γ lines. The residual plot indicate goodness of the fitting.

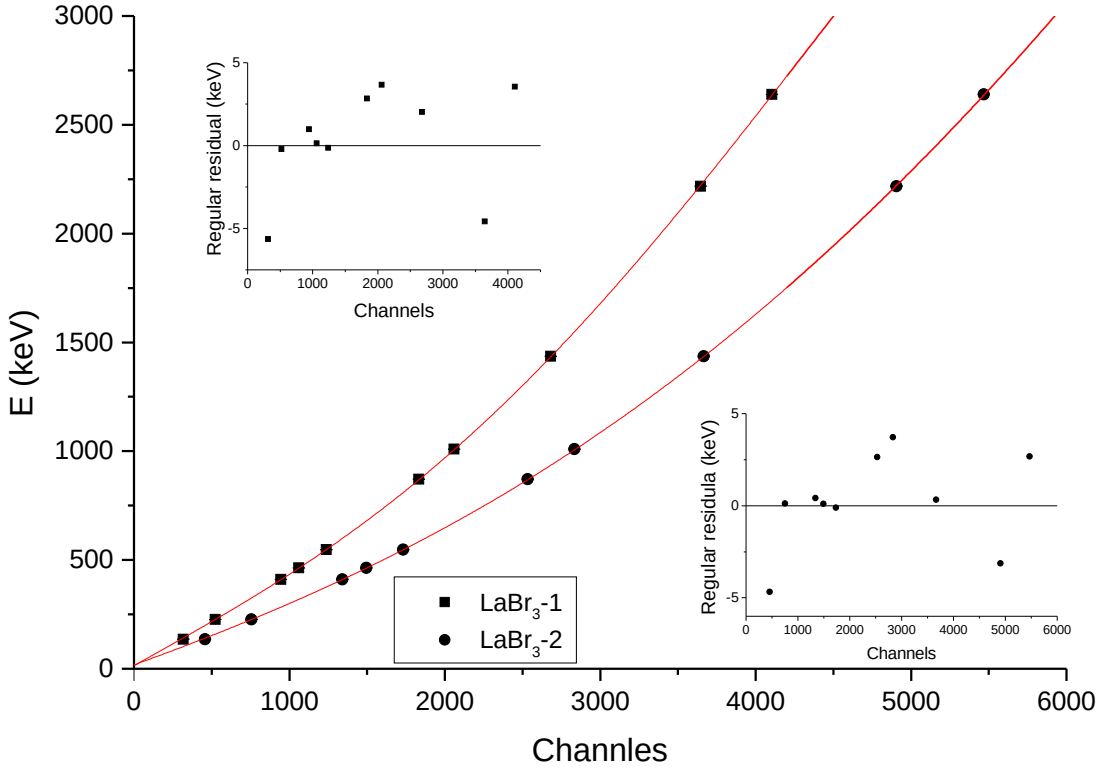

Figure 3.17: Energy calibration of $LaBr_3(Ce)$ detectors with the γ transitions from the β-decay of ^{138}Cs to ^{138}Ba. The residual plot indicate goodness of the fitting.

PMT and, therefore, non-linear energy response of the combination $LaBr_3(Ce)$+PMT. This effect was carefully investigated in a wide range of energy by Trofimov, Lupara and Yurov and their results were published in 2013 [Tro13]. Fig. 3.17 shows how the points from ^{138}Cs calibration source were fitted with good precision (see residual plot from the same figure) to a forth order polynomial for both crystals used in our measurements. The offset in each fitting is very close to zero and does not disturb the calibration. The calibration was enough for identification of the strongest peaks from the decay of ^{81}Zn detected previously with the high resolution germanium detectors.

Stability

Power supply fluctuations or changes in the temperature during several days of experiment may cause drifts in electronic devices. Thus, all the detectors employed in our experiment must be checked for the stability, specially those which take part in timing analysis. As the data were acquired in portions of approximately one hour we can easily check the energy and time spectra directly without presorting. In the case of energy, it was sufficient to verify the centroid position of few peaks preferably at low and high energy in each portion of data. For ^{81}Zn decay no significant fluctuations were observed in HPGe detectors and TACs during 30 runs and, thus, we can consider them stable. However, a pronounced drift was detected in one of lanthanum bromides. Fig. 3.18 reflects this fact. As a test, the centroid position of the intense peak 190-keV γ line from the decay of ^{81}Rb contaminant was chosen because is the strongest one from the background contamination. To the contrary, LaBr3-1 did not show any significant drift and was considered stable. On the

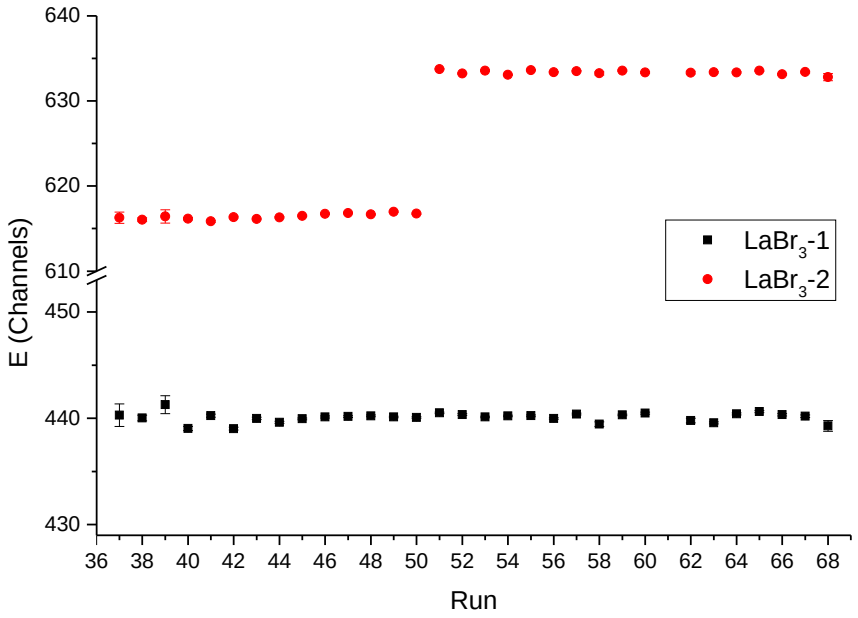

Figure 3.18: Centroid position of 190-keV peak in $LaBr_3$(Ce) detectors. The drift of more than 30 channels can be observed in the detector labeled with 2.

other hand, in the second scintillator a big shift of more than 30 channels can be seen. This irregularity was corrected during the presorting process.

3.5.2 Efficiency Calibration

The efficiency of germanium detectors plays an important role in the determination of intensities of γ transitions which de-excite energy levels populated in the β-decay. The number of counts of a certain γ-ray registered in one of the HPGe detectors can be calculated by measuring the peak area in the energy spectrum. This is done again directly in DMP.exe graphic display. Once the limits of a peak are established the programme calculates the area by summing the number of counts of each channel in the selected range. Sometimes we deal with mixed peaks, that is several γ-rays from different decay chains have a very similar energy and the area of the desired transition constitutes only a part of the total area of the peak. For precise calculation of this area we make use of $\gamma\gamma$ coincidences. When a certain γ line A de-excites an energy level populated by γ transition B and C the ratio of their areas in $\beta\gamma$ spectrum is equal to the ratio of areas in the spectrum gated by the line A in $\gamma\gamma$, i.e.:

$$\left(\frac{A_B}{A_C}\right)_{\gamma\gamma} = \left(\frac{A_B}{A_C}\right)_{\beta\gamma}. \tag{3.3}$$

When more than two transitions feeds the level which de-excites the γ-ray A the two transitions B and C are selected following the criteria of proximity (the energy of B and C must be as close as possible), intensity (both transitions must be intense in order to precisely select the peaks) and cleanliness (the γ-ray B and C should not be mixed with another transitions).

The background contribution, which is considered as linear, is subtracted in the same step. Since the semiconductor detector is not equally efficient at high than at low energies

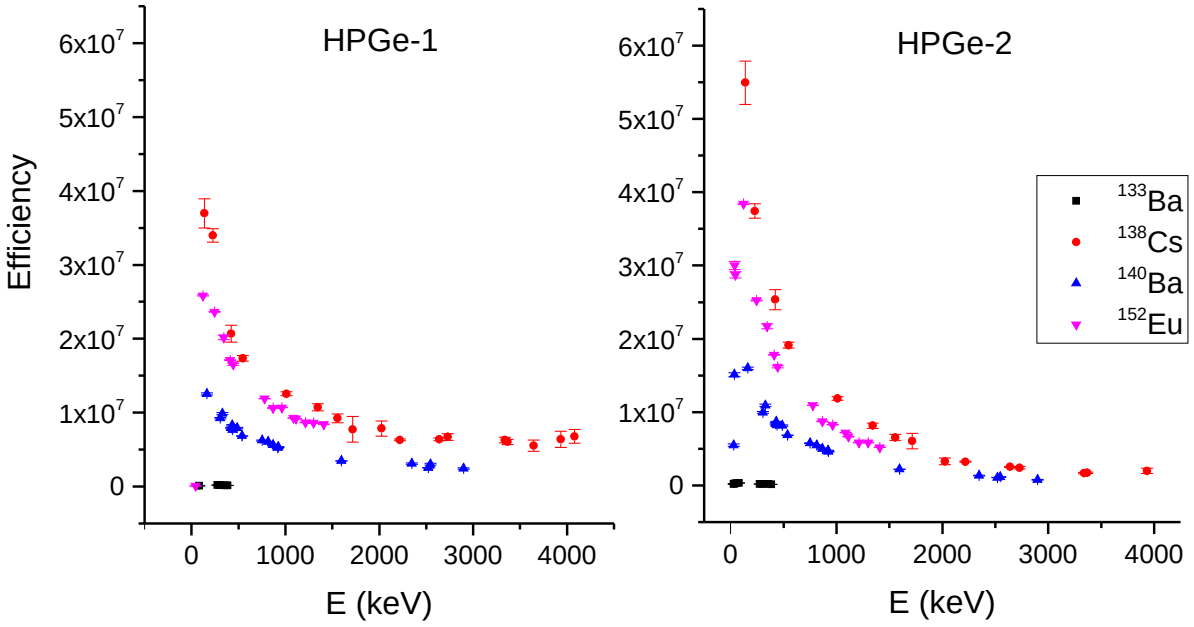

Figure 3.19: Efficiency in arbitrary units for both germanium detectors in linear scale.

the efficiency curve is determined for each detector. The intensity γ with energy E is given by the area corrected by the efficiency at the same energy:

$$I(E) = \frac{A}{(E)} \tag{3.4}$$

In our study we will work with relative intensities, it is not necessary to determine the absolute efficiency of the detector. In order build the efficiency curve of HPGe we used four different and standard calibration sources: ^{133}Ba, ^{138}Cs, ^{140}Ba and ^{152}Eu. The energies of γ-rays from these sources cover a wide range between 30 and 4080 keV. In each case the presorting process was performed first in order to correct possible energy shifts and sum all the runs in one to accumulate the whole statistics. As the absolute intensities were precisely measured previously [Kha11, Son03, Nic07, Mar13] we can extract the efficiency from the Eq. (3.4) and plot it as the function of energy in Fig. 3.19. The area of each peak was calculated directly from the energy spectra. The efficiency units are arbitrary.

In order to get one curve with four sources we performed a vertical displacement of all points towards the ^{152}Eu source. This is a standard procedure to obtain the efficiency curve in a wide range of energy using different calibration sources. The attempt to fit all points to a single analytic function [Gra85, Jäc87] in logarithmic scale has not led to any satisfactory results. Thus, we decided to break the points in three regions and fit to the 1st-, 2nd- or 4th-order polynomials in $\log_{10}$-$\log_{10}$ display [McC75, Ram00]. The results are shown in Fig. 3.20.

The analytical form of the fitted polynomials is the following:

HPGe-1

- 45-121 keV $log(\ ) = -295.47 + 496.12logE - 301.96(logE)^2 + 80.83(logE)^3 - 8.02(logE)^4$

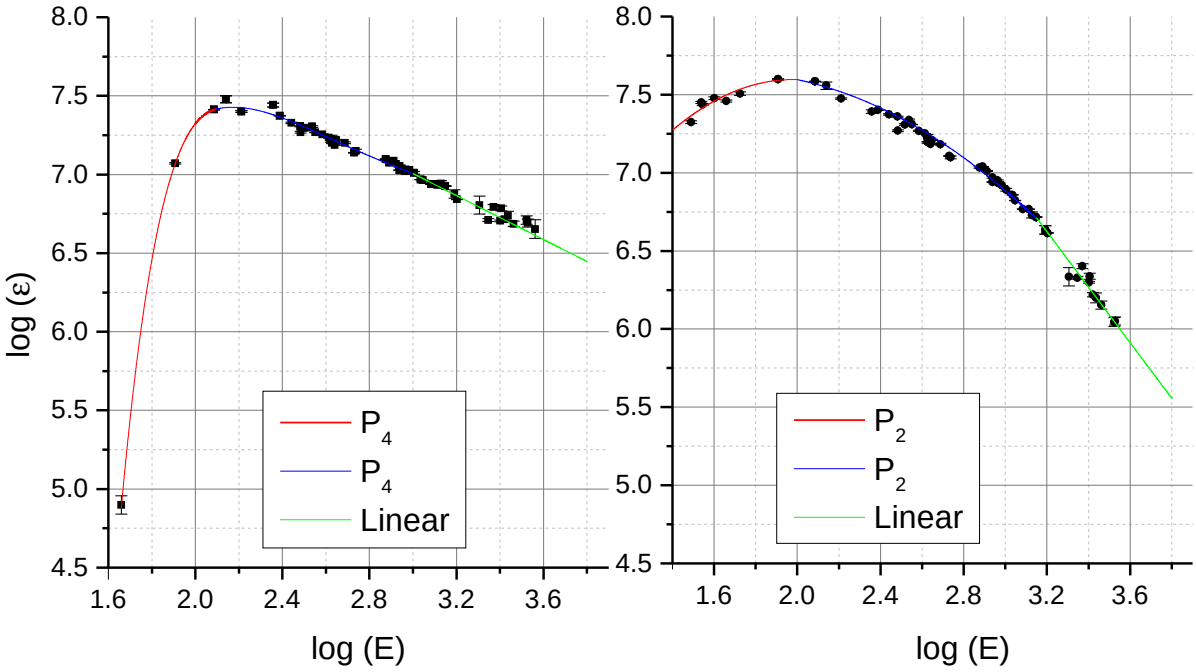

Figure 3.20: Relative efficiency of HPGe detectors.

E(keV) HPGe-1	Error		
45-85	30%	E(keV) HPGe-2	Error
85-121	10%	30-100	10%
121-1010	5%	100-3367	5%
1010-3650	10%	3367-6450	15%
3650-6450	15%		

Table 3.3: Efficiency uncertainties.

- 121-1010 keV $log(\ ) = -39.42 + 69.15logE - 37.68(logE)^2 + 9.01(logE)^3 - 0.80(logE)^4$
- 1010-6450 keV $log(\ ) = 9.10 - 0.70logE$

HPGe-2

- 30-100 keV $log(\ ) = 3.79 + 3.85logE - 0.97(logE)^2$
- 100-1408 keV $log(\ ) = 6.46 + 1.42logE - 0.43(logE)^2$
- 1408-6450 keV $log(\ ) = 12.31 - 1.78logE$

The error bars are summarized in Tab. 3.3 and were assigned based on the goodness of fit, the error of points and the dispersion.

3.5.3 Time calibrations

Since timing detectors involved in ATD method do not have a constant time response with energy several timing calibrations must be performed. As the Time-to-Amplitude Converter is the module which provides timing spectrum it must be calibrated first, i.e. the relation between channels and time must be found. The β plastic scintillator NE111A is not an ideal thin ΔE detector, and thus, it gives slightly non-linear timing response in the whole energy range of β particles. This inhomogeneity may shift in few ps the final value of the half-life of a certain energy level. The time response of $LaBr_3$ detectors is complex and more sophisticated to deal with. It constitutes the most important correction in the lifetime measurements with ATD method. Moreover, as we analyse γ transitions, the time response of Compton events must be treated separately from the events of full energy peaks (FEP), which can differ by tens of ps depending on the geometry. In this way, the curve of Compton walk and the Prompt Response Curve must be constructed. Compton events of the same energy but coming from different FEPs will have distinct response in the time spectrum. As this effect provides 1-2 ps of difference we consider it as negligible and it will be not used in this work.

Calibration of TACs

The NIM module responsible to measure time response of different energy events is the Time-to-Amplitude Converter (TAC). As it has been already mentioned, there were five TACs in our experiment. In order to find a linear connection between channels and time the TACs were calibrated using a Time Calibrator ORTEC 462 which emits start and stop signals with a very precise frequency and adjustable period and range. In this way, the time spectrum obtained from a TAC will contain several equidistant Gaussian peaks and the period divided by the distance in channels provides the calibration in ps/channel. For FTACs this period was chosen to 10 ns while in case of STACs it was 160 ns. Linear fit of data was performed to get the final value for the calibration. Table 3.4 summarizes the results for all TACs.

FTAC1(ps)	**FTAC2(ps)**	**FTAC3(ps)**	**STAC1(ps)**	**STAC2(ps)**
3.913(1)	3.908(1)	3.843(1)	76.94(1)	76.70(1)

Table 3.4: Time calibration of Time-to-Amplitude Converters in ps/Channel. Following labeling has been used: FTAC1 = $TAC_{\beta-LaBr1}$, FTAC2 = $TAC_{\beta-LaBr2}$, FTAC3 = $TAC_{LaBr1-LaBr2}$, STAC1 = $TAC_{\beta-HPGe1}$ and STAC2 = $TAC_{\beta-HPGe2}$

For verification of the values from the table above two well known half-lives very utilized. The β^- decay of ^{138}Cs to ^{138}Ba indicated the existence of a nanosecond isomer at 1898.7 keV [Car74]. The half-life of 2.164 ns was precisely measured at OSIRIS facility in 1995 by H. Mach and B. Fogelberg and reported in [Mac95a]. The decay scheme of ^{140}Ce populated by the β-decay of ^{140}La shows another nanosecond isomer at 2083.3 keV [Ada82] whose 3.474(10)-ns half-life was also measured by H. Mach and B. Fogelberg. In both cases the Convolution Technique described in Chapter 2 was employed for half-life fitting.

Once the β-walk correction (see next section) was done for β-$LaBr_3$-FTAC-HPGe coincidences in ^{138}Cs decay data, the gates on 409.0, 547.0 and 1435.9 keV were selected

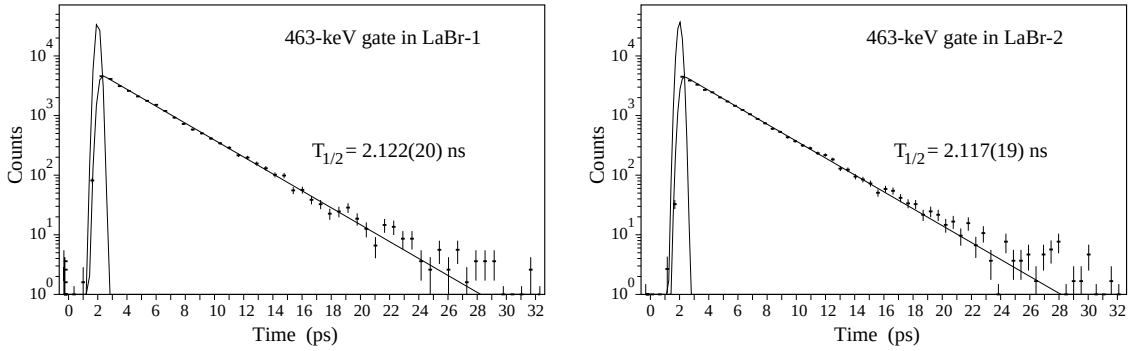

Figure 3.21: Time response of 463-keV transition from ^{138}Ba selected in $LaBr_3$ detectors and projected into the corresponding FTAC. The half-life of corresponding 1899-keV state is shown.

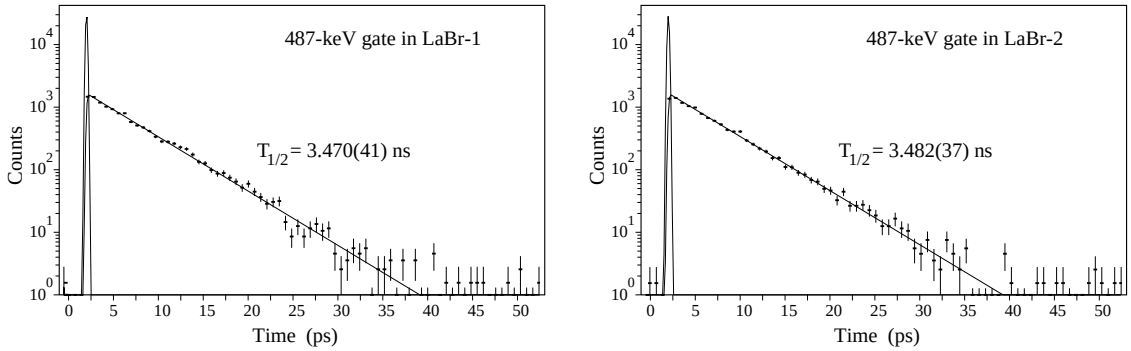

Figure 3.22: Time response of 487-keV transition from ^{138}Ba selected in $LaBr_3$ detectors and projected into the corresponding FTAC. The half-life of corresponding 2083-keV state is shown.

in the energy spectrum of HPGe. This generated the coincidence spectrum in $LaBr_3$(Ce) with a very clean peak of 462.8-keV transition which de-excites the 1898.7-keV state. After projecting this energy gate into the TAC corresponding time delayed spectrum was constructed. Fig. 3.21 displays the time spectra of FTAC1 and FTAC2 and fitted curves of 1898.7-keV level lifetime. Both values are very close one to each other but the mean value of 2.119(20) ns is slightly lower that 2.164(11) ps measured by Mach and Fogelberg in 1995 [Mac95a].

The same procedure was followed to get the half-life of 2083.3-keV state in ^{140}Ce nucleus. Three strongest lines of 328.8, 432.5 and 1596 keV and in coincidence with 487.0 keV were gated in high resolution germanium detector. The clean peak of 487.0 keV obtained from these three gammas was projected from $LaBr_3$(Ce) into the FTAC1 and FTAC2 and the fitted time delayed spectra can be seen in Fig. 3.22. The average 3.476(39)-ns half-life is in very good agreement with 3.474(10) ns from [Mac95a].

In view of these results we can say that the calibration has been calculated correctly and can be adopted for measurements in the decay of ^{81}Zn. We note that both $LaBr_3$(Ce) detectors give very similar results with completely different detection conditions.

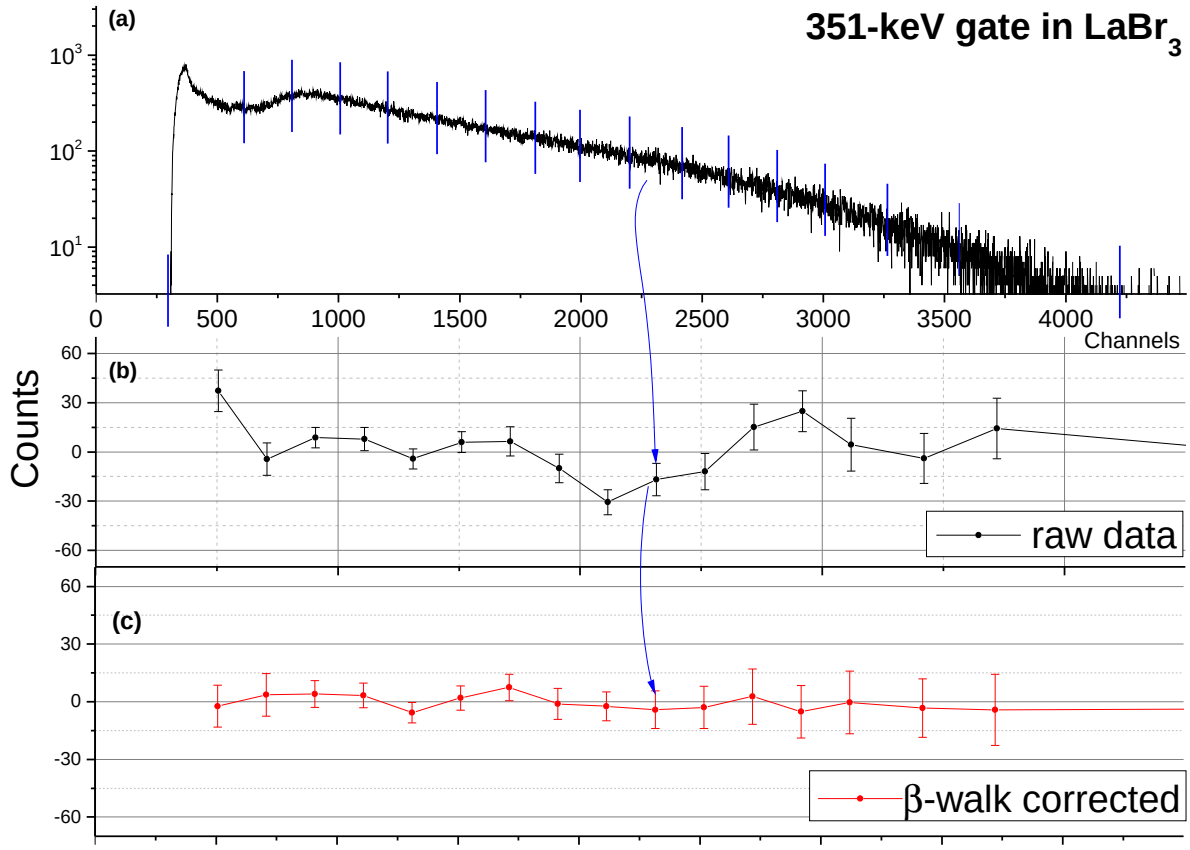

Figure 3.23: The β energy spectrum (a) obtained by projecting the strongest γ line from the decay of ^{81}Zn to ^{81}Ga. The β-walk curve (b) presents oscillations with 60 ps range. After doing corrections the time response curve (c) is practically flat.

Beta-walk

The time response of the β detector is not completely uniform and slightly depends on the energy distribution and on Q_β value of the decay. In our experimental set-up the use of a very thin 3-mm detector permitted to obtain a continuous energy distribution of β particles as only a fraction of their energy was deposited. However, not all of them penetrate the detector perpendicularly and some of them can collide with particles inside the detector. On the other hand, not only β particles are detected in NE111A plastic but also γ-rays and even fast neutrons, which deposit very small amount of energy. All of these possible interactions produce some irregularities in the β-decay spectrum specially at the low energy range (plot (a) from the Fig. 3.23). Moreover, the digital processing may have same input on the energy spectrum due to the pile-up rejection filter.

In practice, the time response is not so flat as we expect and even after taking all necessary precautions in the experimental set-up there is a *walk* in the β detector. The non-uniformity of its timing response is shown in the plot (b) of Fig. 3.23. This is so called the β-walk curve. In our example it was obtained by projecting the small portions of the β spectrum into the FTAC. This procedure is done with triple $\beta\gamma\gamma$ coincidence presorted file which involves two γ detectors in coincidence with a FTAC and NE111A plastic. Once a strong γ-ray that de-excited a short lived level is selected in $LaBr_3(Ce)$ and projected into the β spectrum several intervals can be chosen. If the statistics is

high enough to include HPGe detector in the sorting a gate in a γ transition which is in coincidence with the first one can be established. This will permit to obtain a clean energy peak in lanthanum bromide energy spectrum. After breaking the β spectrum in intervals we project all this information into a corresponding FTAC. The resulting plot constitutes the β-walk curve. In the lower part of Fig. 3.23 (plot (c)) we show the β-walk corrected time response curve produced by the selecting 351-keV transitions in the energy spectrum of the decay of ^{81}Zn to ^{81}Ga. It was necessary to write a code in FORTRAN77 which operates in the presorted file and simply adds or subtracts a certain number of channels in the FTAC parameter which corresponds to a given interval of channels in β spectrum. The number of channels to move and the limits of the interval are indicated in the input file.

As the walk of the β detector is very sensible to the Q_β value the β-walk correction must be done for each decay in the chain. Nevertheless, since the β produces an energy distribution for a given β-decay energy, the walk effect will averaged out.

Compton Response Curve $LaBr_3$(Ce)

Once the TACs are calibrated and the walk of the β detector is optimized the timing corrections for $LaBr_3$(Ce) can be performed. Normally, the FEPs are sitting on the background which is mainly composed by Compton events coming from transitions of higher energies. Therefore, the centroid position of the time response of the composed peak (FEP+Compton) will be given by the following equation:

$$A_{c+p}C_{c+p} = A_pC_p + A_cC_c, \tag{3.5}$$

where the A_i represents the area and C_i the centroid position of timing response. In addition, the centroid position of Compton and FEP (prompt peaks) have energy dependence, different for each type of event. As there is no way to select directly the Compton events below a FEP, we consider the region immediately close to the peak in the right or the left side. Let us call C_c' the centroid position of the time peak which corresponds to this interval of channels. As the response is not identical C_c and C_c' will be shifted and in order to find this difference and extract the desired C_c the general time response curve for Compton events must be calculated as a function of energy.

For that purpose the already mentioned calibration source of ^{138}Cs was employed again. The Compton background of 1436-keV full energy peak will be analyzed. After the usual $\beta\gamma\gamma$(t) data presorting and the β-walk correction in ^{138}Cs decay data the gate optimization in the sorting process was applied. If 1009-keV transition is chosen in HPGe and projected into the $LaBr_3$ only 1436-keV line with its corresponding Compton background should appear in the energy spectrum. Fig. 3.24 shows the resulting spectra.

Small X-ray peak appears at low energy and the peak around 240 keV corresponds to the backscatter emission. The timing response of Compton events is obtained by projecting small portions of Compton background from the Fig. 3.24 into a corresponding FTAC. The constructed Compton Response Curve for both $LaBr_3$(Ce) detectors is displayed in Fig. 3.25. The plot is done in the way that the end point of 1436 keV, which is a FEP, is shifted to zero. Both curves are smooth but present a pronounced slope. The time difference in the whole energy range is around 1 ns and is about 500 ps between 250 and 1250 keV. This calibration curve will be used to perform Compton correction from Eq. (2.2) for all measurements in the decay ^{81}Zn.

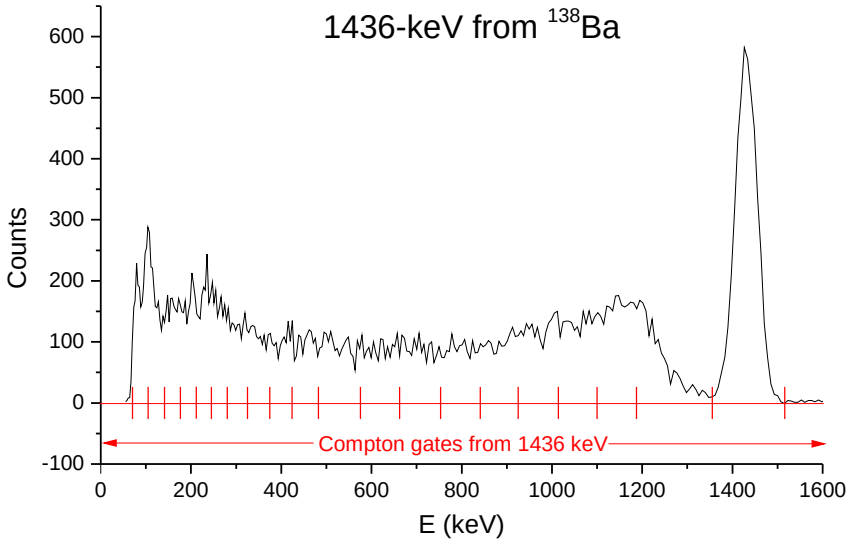

Figure 3.24: Energy spectra containing the full energy peak at 1436 keV with its corresponding Compton background, the X-rays in low energy range close to 100 keV and a backscatter peak around 240 keV.

Prompt Response Curve

Once Compton Response Curve is determined the timing walk of $LaBr_3$ of the photopeak events can be analyzed. The distribution of centroids obtained by projecting several γ-rays from the decays of ^{138}Cs and ^{140}Ba as a function of the energy is called Prompt Response Curve. Any transition that de-excites a level with well known half-lives in the range below 10 ps can be considered prompt in our experiment because it is lower than the sensitivity of the ATD method. The calibration sources mentioned above present many prompt or quasi-prompt (with slightly higher half-life) γ lines with well known lifetimes. Their energies and lifetimes of de-excited levels are summarized in Tab. 3.5.

The presorted data file used for Comptom walk correction was also used for prompt walk. The corresponding centroids in the time spectrum were obtained after sorting with gates set on the FEPs in $LaBr_3$(Ce) gated by HPGe and β plastic scintillator. The obtained positions of the centroids after projecting into a FTAC were Compton corrected with the use of Eq. (2.2) and finally shifted by the lifetimes from Tab. 3.5. Each calibration nucleus involved in the experiment has the same shape of the time response for prompt gammas [Mac91]. This fact constitutes the fundamental feature of the ATD method for a given experimental set-up. In this way, the prompt curves obtained with γ-rays from ^{138}Ba and ^{140}Ce must be shifted by a constant in order to get a unique relative prompt calibration curve. Fig. 3.26 shows the final Prompt Response Curve after displacing points from ^{138}Ba to ^{140}Ce. The data were normalized to the response of 2218-keV line.

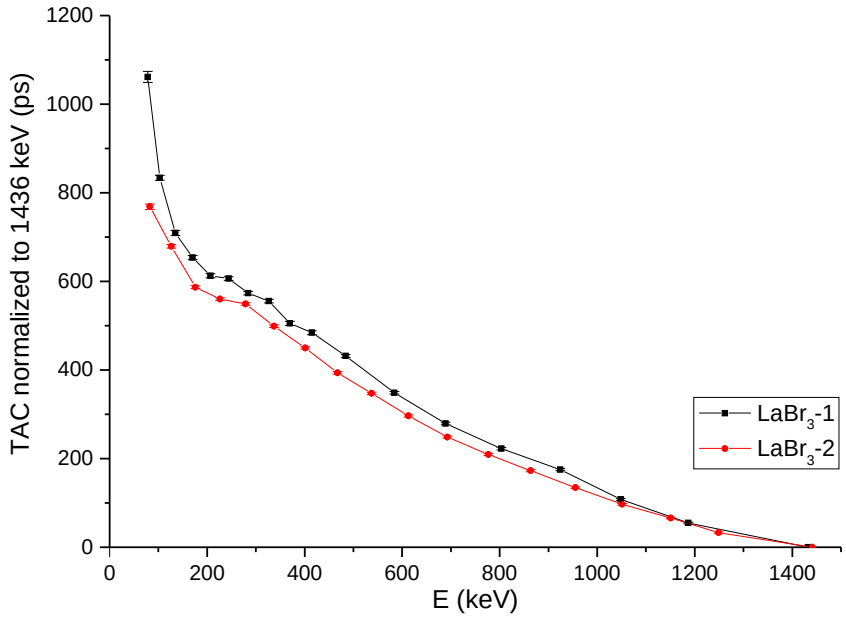

Figure 3.25: Compton walk curve for $LaBr_3$-1 and $LaBr_3$-2 obtained with ^{138}Ba. Due to different energy calibration the points from both curves do not match.

E_{level} (keV)	E_γ (keV)	Nucleus	Absolute Intensity (%)	Half-life (ps)
2445.72	138.10(6)	^{138}Ba	1.49(8)	4.9(36)
2445.72	227.76(6)	^{138}Ba	1.51(4)	4.9(36)
2412.02	328.762(8)	^{140}Ce	20.3(3)	1.3(4)
2307.66	408.98(6)	^{138}Ba	4.66(9)	7.0(26)
2515.77	432.493(12)	^{140}Ce	2.90(3)	1.3(4)
2445.72	547.001(5)	^{138}Ba	10.8(2)	4.9(36)
2347.89	751.637(18)	^{140}Ce	4.33(4)	0.15(10)
2412.02	815.772(19)	^{140}Ce	23.3(2)	1.3(4)
2307.66	871.80(8)	^{138}Ba	5.1(1)	7.0(26)
2541.43	925.189(21)	^{140}Ce	6.90(7)	0.8(7)
2445.72	1009.78(8)	^{138}Ba	29.8(6)	4.9(36)
1435.91	1435.86(9)	^{138}Ba	76.3(16)	0.202(8)
1596.24	1596.21(4)	^{140}Ce	95.4(1)	0.0916(19)
2217.97	2218.00(10)	^{138}Ba	15.2(3)	0.123(14)

Table 3.5: γ transitions employed for Prompt Response Curve. The energy values, intensities and lifetimes were taken from [Mac95a], [Son03] and [Nic07].

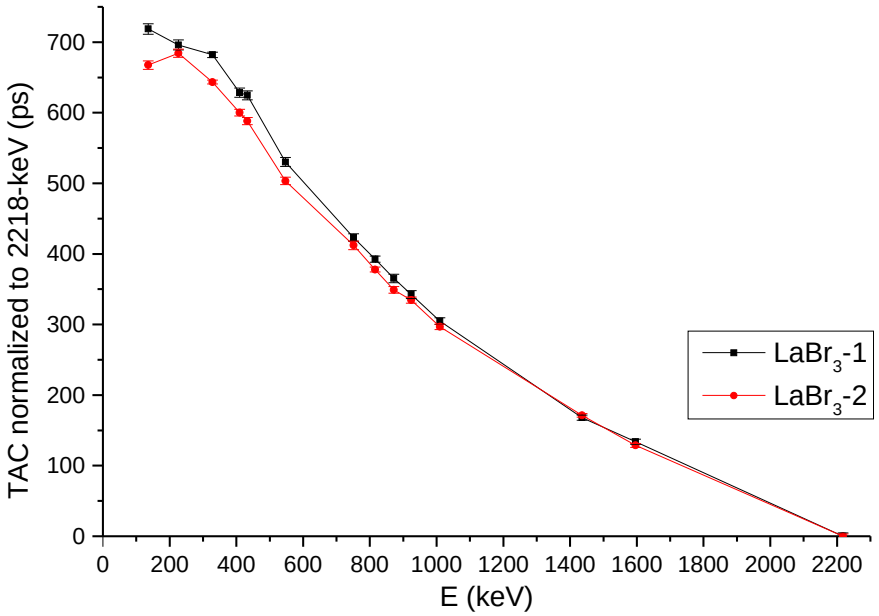

Figure 3.26: Prompt walk curve of two $LaBr_3$ scintillator crystals as a function of prompt γ-ray energy. The curves are smooth but with a slope of 700 ps in 2.2 MeV energy range.

3.6 Summary of the chapter

The experimental campaign, where almost pure beam of isotopes of Zn was obtained, had been performed at the ISOLDE Radioactive Beam Facility situated at accelerating complex of CERN (Switzerland). A general overview of the facility was presented at the beginning of the chapter providing technical details of the incident proton beam, target-ion-source and mass separators. The elements used for production of Zn were described in depth focusing in the techniques used to reduce the otherwise high Rb contamination.

The experimental set-up included five detectors: two with excellent energy resolution for γ detection (HPGe), two scintillator crystals with very good timing properties ($LaBr_3$(Ce)) and one thin plastic scintillator for measurement of β particles. The combinations HPGe-HPGe and β-HPGe were employed for the level scheme determination and the use of β-$LaBr_3$-FTAC and β-$LaBr_3$-HPGe-FTAC was applied for lifetime measurements in subnano- and picosecond range. In the first case the measurements were performed with Convolution Technique while for triple coincidences the Centroid Shift technique was used as explained in Chapter 2. All the detectors and the rest of elements from the setup (Time-to-Amplitude Converters, Constant Fraction Discriminators, Amplifiers, etc) were shown in the electronic scheme of Fig. 3.11. All the signals were guided to the data acquisition system PIXIE-4. Signal treatment process required new programmes written in FORTRA77 for the data presorting.

Several calibrations of detectors were explained in the last section of the chapter. The energy calibration of HPGe was done with neutron capture γ-rays which cover the range up to 7 MeV while for $LaBr_3$ energy calibration the sources of ^{138}Cs and ^{140}Ba were employed. Special attention was payed to the efficiency calibration of HPGe detectors which leads to measure intensities of γ transitions which de-excite the β populated levels. This step was performed with standard calibration sources of ^{133}Ba, ^{138}Cs, ^{140}Ba and ^{152}Eu.

For precise lifetime measurements several timing calibrations were needed. First of all, the TACs were calibrated and the resulting relation between time and channels was successfully verified with known lifetimes from ^{138}Ba and ^{140}Ce. After that, the procedure for walk correction of the β detector was shown. For each analysis it is necessary to make β-walk correction separately. Because of nonlinear timing response to the full energy peak and Compton events two timing calibration curves were constructed: Compton Walk Curve and Prompt Response Curve. These corrections are the most important when short half-lives at the picosecond region are measured.

Chapter 4

Nuclear structure of ^{81}Ga and ^{80}Ga

Modifications to the standard ordering of the single-particle energies have been observed in exotic nuclei with a large N/Z ratio. They give rise to the disappearance of the conventional magic numbers and the appearance of new shell gaps. Magic nuclei are key players for the mapping of the single-particle degrees of freedom around closed cores, as an important ingredient to theoretical models. In addition, the evolution of the proton-neutron interaction and the role of neutron excitations across neutron shell gaps can be studied in these nuclei.

Although ^{78}Ni, with 28 protons and 50 neutrons ($Z = 28$, $N = 50$), is expected to show the characteristics of a doubly magic nucleus, it is located 14 neutrons off the stability line and it is to date barely reachable. Nonetheless, the properties of some exotic nuclei around ^{78}Ni can be studied far away from the valley of stability. Core properties of these nuclei play a role in the astrophysical rapid neutron capture process [Hos10]. This is why neutron-rich nuclei around ^{78}Ni have motivated recent experimental and theoretical studies, aimed at the understanding of the nuclear structure in this region with a large neutron excess.

In this chapter we address the neutron magic nucleus ^{81}Ga, with $N = 50$, three protons outside ^{78}Ni, to provide information about proton single-particle configurations. In our study we have produced ^{81}Zn isotopes at ISOLDE, CERN to populate ^{81}Ga in the β^--decay of ^{81}Zn and ^{80}Ga via the β-delayed neutron emission. We use γ-ray spectroscopy to greatly extend the known level scheme and the Advanced Time Delayed $\beta\gamma\gamma$(t) method [Mac89, Mos89] to measure excited level lifetimes, and deduce transition probabilities to help understand the ^{81}Ga structure. The level scheme of ^{80}Ga populated in the β^-n decay of ^{81}Zn was obtained for the first time.

Figure 4.1 shows the decay chain of ^{81}Zn produced in our experiment. All known structure data were taken from the latest Nuclear Data Sheets for $A = 81$ and $A = 80$ [Bag08, Sin05]. As can be seen from the figure, in addition to ^{81}Ga the decay chain also contains ^{81}Ge, ^{81}As and ^{81}Se and γ-rays that de-excite their levels will be seen in the detection system. Moreover, ^{81}Zn and ^{81}Ga are open to decay by emitting β-delayed neutrons, to the channel to mass 80 channel. In this way, γ transitions from another four nuclei will contribute to the energy spectrum. Finally, β^+ decay of ^{81}Rb contaminant to ^{81}Kr provides some strong γ-rays, which must be also taken into account.

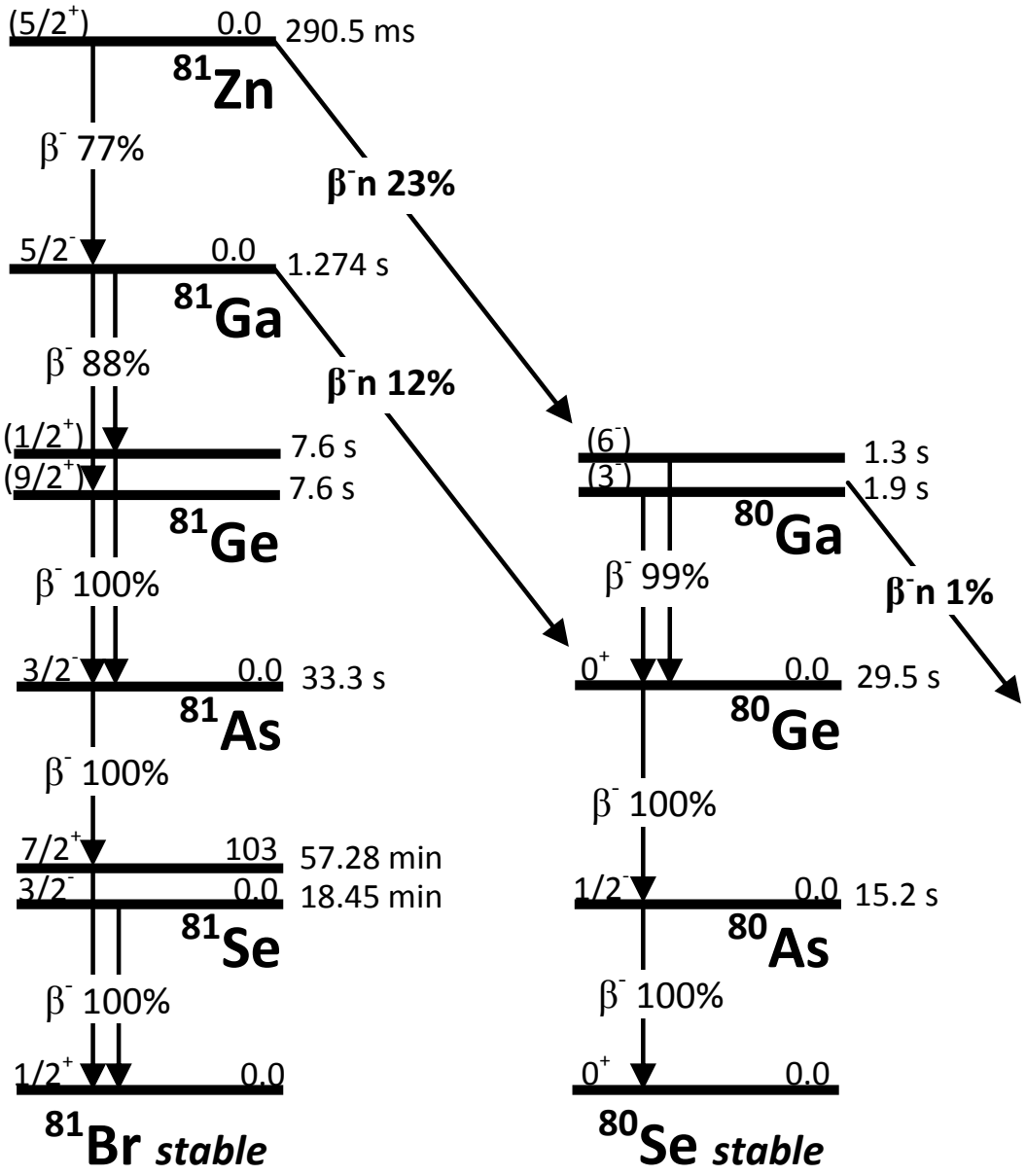

Figure 4.1: Decay chain of ^{81}Zn. Most of data were take from Nuclear Data Sheets for $A = 81$ and $A = 80$ [Bag08, Sin05]. The structure of ^{80}Ga is based on [Lic14] and [Ver13] while the P_n branching and half-life of ^{81}Zn is taken from our work.

4.1 Production of ^{81}Zn

The experiment was performed at the ISOLDE, CERN facility in the framework of a systematic fast-timing investigation of neutron-rich nuclei populated in the decay of Zn. The selectivity and efficiency for the production of Zn ion beams had been previously studied [Kös08] in order to guarantee the purest beam of $^{77-82}$Zn nuclei. The separated ^{81}Zn nuclei were collected on an aluminium stopper creating a saturated source. The average activity of β particles registered during the experiment was about 10^4 counts per second. The estimated yield of ^{81}Zn was around 600 ions/μC. Since Rb atoms partially survived the quartz transfer line selection and were surface ionized on the walls of the ionizer, the long-lived 4.57-h ^{81}Rb contaminant was present in the beam. Our estimations lead to 5000 ions/μC, about five times higher than production of ^{81}Zn. A beam gate blocking the delivery of ions to the experimental station was established to avoid the accumulation of long-lived activity coming from the target, and in case of mass 81, it was set to close 600 ms after proton impact.

In the first ∼50 ms after proton impact on target neutron capture γ-rays are observed in the HPGe spectra. This is due to neutrons that escape the converter in the target area, thermalize and reach the measurement station. These capture lines were used for high energy calibration of the HPGe detectors. The energy spectra also contain γ lines from the ^{81}Zn decay chain and also a small fraction of contaminant lines from the β^+ decay of ^{81}Rb to ^{81}Kr. The strongest 446-keV transition of this decay constitutes around 4% of intensity of the 351-keV transition of ^{81}Ga. In addition, the subtraction of the long-lived activity (using a delayed time window after proton impact) provides an energy spectrum containing gammas from the β-decay of ^{81}Zn, including the β-delayed neutron emission branch (see Fig. 4.4). The gammas from the decay can be assigned to de-excite energy levels in the ^{81}Ga and ^{80}Ga nuclei and their daughters.

4.2 Previous studies on the decay of ^{81}Ga

First studies of the half-life and the β-delayed neutron emission probability of ^{81}Zn were obtained at ISOLDE (CERN) facility in 1991 by Kratz *et al.* [Kra91a]. The reported values were $T_{1/2}$ = 290(50) ms and P_n = 7.5(30)%. The first level scheme of ^{81}Ga populated in the β^- decay of ^{81}Zn was constructed from the data of PARRNe experimental program [Ver07] at the IPN Orsay in 2004. Sufficient statistics was reached in this experiment to determine the 351.1-keV transition attributed to ^{81}Ga due to the new half-life value of 391(65) ms of ^{81}Zn. The existence of the second exited state of 802.8 keV level was confirmed by observing the 451.7 keV γ-ray in coincidence with 351.1-keV one. The first exited state was characterized by the 351.1-keV transition of large intensity. A third weak transition was detected at 1621.6 keV and thus a level of the same energy was tentatively added to the level scheme. Tentative spin-parity assignments of $5/2^-$, $3/2^-$ and $3/2^-$ were proposed for the ground, the first and the second excited states of ^{81}Ga, according to the shell-model calculations and the systematics of the region. The authors attributed $1/2^+$ for the ground-state spin. Both 351- and 452-keV γ-rays were also identified as the decay of ^{81}Zn to ^{81}Ga by Köster *et al.* [Kös05] again at ISOLDE in 2005. The lover limit of 10% for P_n value of ^{81}Zn was proposed. Newer measurements performed at NSCL and published in 2010 by Hosmer *et al.* [Hos10] propose considerably

larger ground state half-life of 474^{+93}_{-83} ms and higher $P_n = 30(13)\%$ value for ^{81}Zn. The theoretical calculations made by Borzov in 2005 [Bor05] predicted $P_n = 13\%$.

The most recent data of the β-decay of ^{81}Zn comes from HRIBF at Oak Ridge National Laboratory. The results were published in 2010 by Padgett *et al.* [Pad10]. The decay scheme shows 6 new energy levels and 9 new γ transitions. Transitions of 452, 916, 1108, 1585 and 2358 keV were observed in coincidence with the strongest 351-keV peak. The 802 keV line were rejected to be the sum of 351 and 452 in the germanium crystal because of its low intensity. Other four gamma transitions, only observed in the singles γ spectrum with 1458, 1936, 4294 and 4880 keV were set to feed directly the ground state (g.s.). A new $304(13)ms$ half-life of ^{81}Zn was established. A beta-delayed neutron branch of 12(4)% was determined using the 1083-keV transition in ^{80}Ge. In this work a spin-parity assignment for the ground state of ^{81}Zn of $5/2^+$, different from the earlier value, was proposed, based on the $J^\pi = 5/2^-$ ^{81}Ga g.s. [Che10] and the beta-feeding. The first and the second excited states both received a tentative $J^\pi = 3/2^-$ assignment.

4.3 β decay of ^{81}Zn to ^{81}Ga

For single γ-ray analysis the data presorting included HPGe detectors and protons. As discussed in Chapter 3, the events triggered by the proton signals were sorted offline in a three-parameter data set including the HPGe energy, the time since last proton impact on the target and the proton pattern. Fig. 4.2 contain two plots in the energy range up to 3 MeV in which single γ-rays are compared to those obtained after including an additional coincidence with β detector. The energy spectrum contains many γ lines from the β^- and the β^-n decay chain of ^{81}Zn, the β^+ decay of ^{81}Rb to ^{81}Kr, decays from the background nuclei and neutron capture γ-rays. The strongest peaks of each decay are indicated. In some cases peaks are overlapping and an addition step of sorting is needed to separate them. Picture (a) shows the energy spectrum registered by HPGe in coincidence with proton pulses. There is a large background contamination in the low energy part and some peaks even can not be seen. The peaks corresponding to the decay of background nuclei are very strong and marked with grey boxes in the spectrum. Many counts corresponds to 511-keV γ-ray which is produced in electron-positron annihilation. A big amount of positrons comes from the β^+ decay of ^{81}Rb. In order to considerably reduce this contamination the coincidence with β detector was added in the presorting of data. The resulting energy spectrum is shown in the picture (b) of Fig. 4.2. Only γ-rays corresponding to the events from the β-decay process are shown here. All the background contamination was totally suppressed with exception of 511-keV peak and some γ lines from the decay of ^{81}Rb. High statistics obtained specially for transitions from ^{81}Ga provide good prospects for extending the previous level scheme and perform the half-life measurements.

In view of the results, the analysis of the β-gated γ-ray singles was done. The multiparameter data set included the information about the time of proton impact on the target, proton pattern, γ and β energies and time difference between events from NE111A and HPGe detectors. In order to minimize the presence of long-lived activity a time gate between 50 and 1200 ms after proton impact was set.

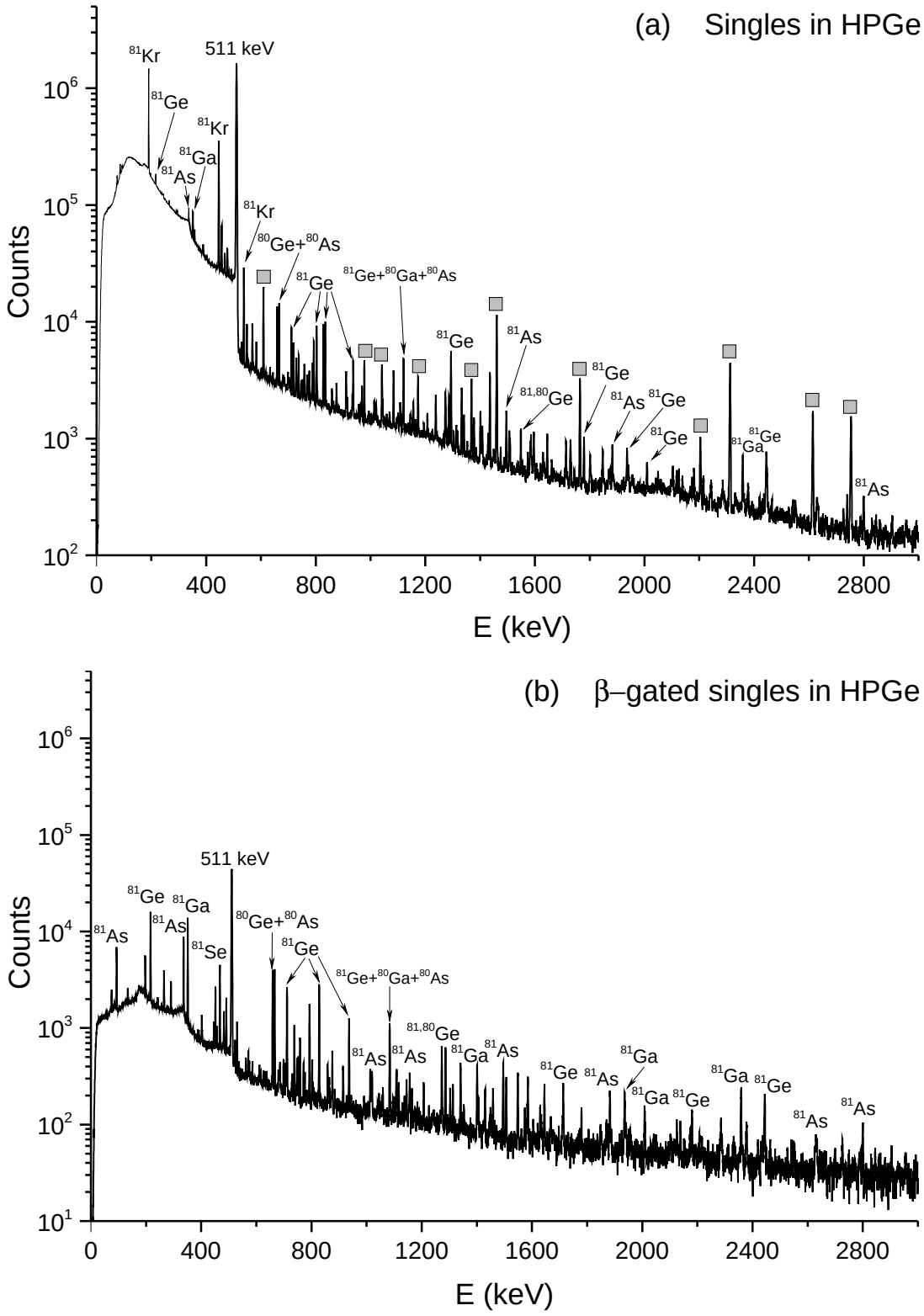

Figure 4.2: Two spectra of single γ-rays from the decay chain of ^{81}Zn. In the first plot (a) the HPGe data were presorted in coincidence with proton signals. Energy peaks of all nuclei from the decay of ^{81}Zn can be seen. The spectrum is characterized by a huge background in the low energy part and very intense γ transitions coming from background contamination and ^{81}Kr decay (marked with grey boxes). This contamination is highly reduced with an additional coincidence with the β detector is used in the presorting. Its energy spectrum is shown in the plot (b). Note the logarithmic scale used for the plots.

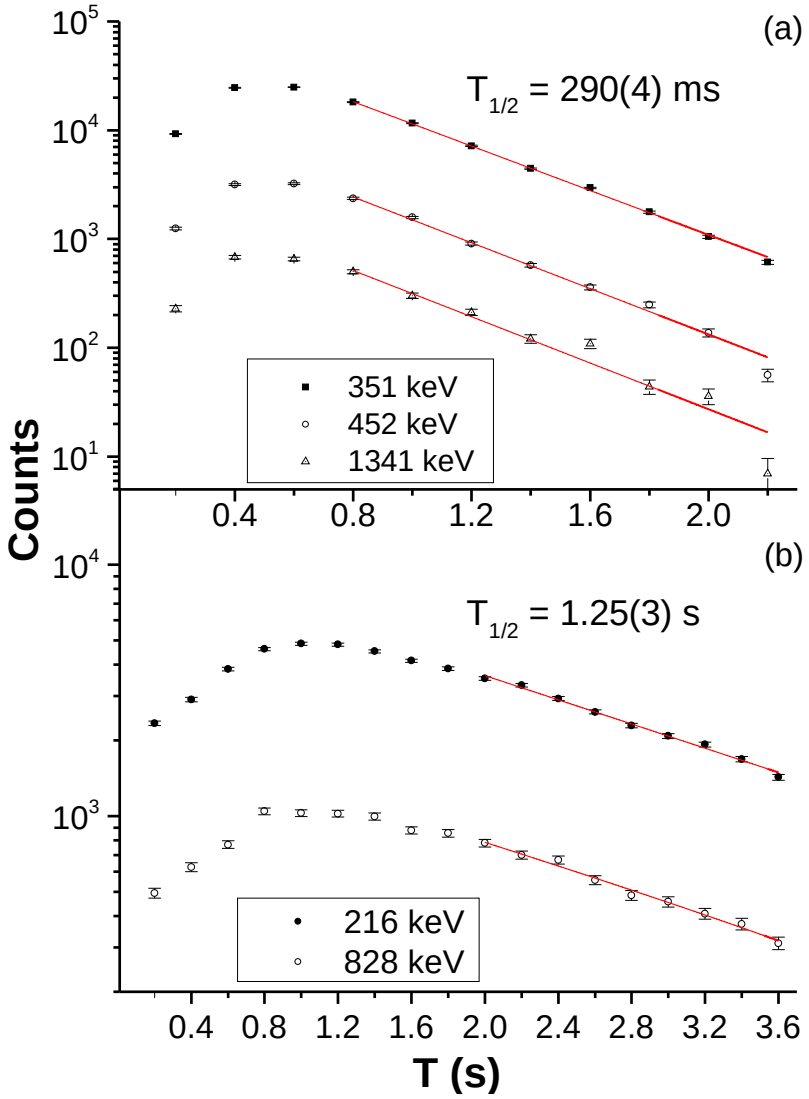

Figure 4.3: Half-life measurements of ^{81}Zn (a) and ^{81}Ga (b). The strongest γ peaks of ^{81}Ga and ^{81}Ge were directly selected in the β-gated energy spectrum and projected into the time spectrum. A simple exponential decay plus a constant was used for fitting.

4.3.1 Half-life of ^{81}Zn and ^{81}Ga

In our experiment the half-life of ^{81}Zn has been measured in the β-gated time spectrum selecting directly the strongest ^{81}Ga transitions of 351, 452 and 1341 keV. A simple exponential decay plus a constant has been used in the range from 700 to 2400 ms. The plot can be seen in Fig 4.3. The lower limit was set with a slight delay after the beam gate closing at 600 ms to minimize the DAQ dead time while the upper one corresponds to two proton cycles. The weighted mean value obtained after fitting yields $T_{1/2} = 290(4)$ ms, in good agreement with the recent literature value [Pad10, Xu14].

For the ^{81}Ga half-life the 216- and 828-keV transitions in ^{81}Ge [Hof81] were used. A simple exponential fit was used by limiting the lower limit of 2000 ms after proton impact, which correspond to 6.9 half-lives of ^{81}Zn, when less than 1% remains. The fitted slope leads to $T_{1/2} = 1.25(3)$ s for ^{81}Ga as depicted in (b) of Fig. 4.3, consistent with the literature value of 1.217 s [Bag08].

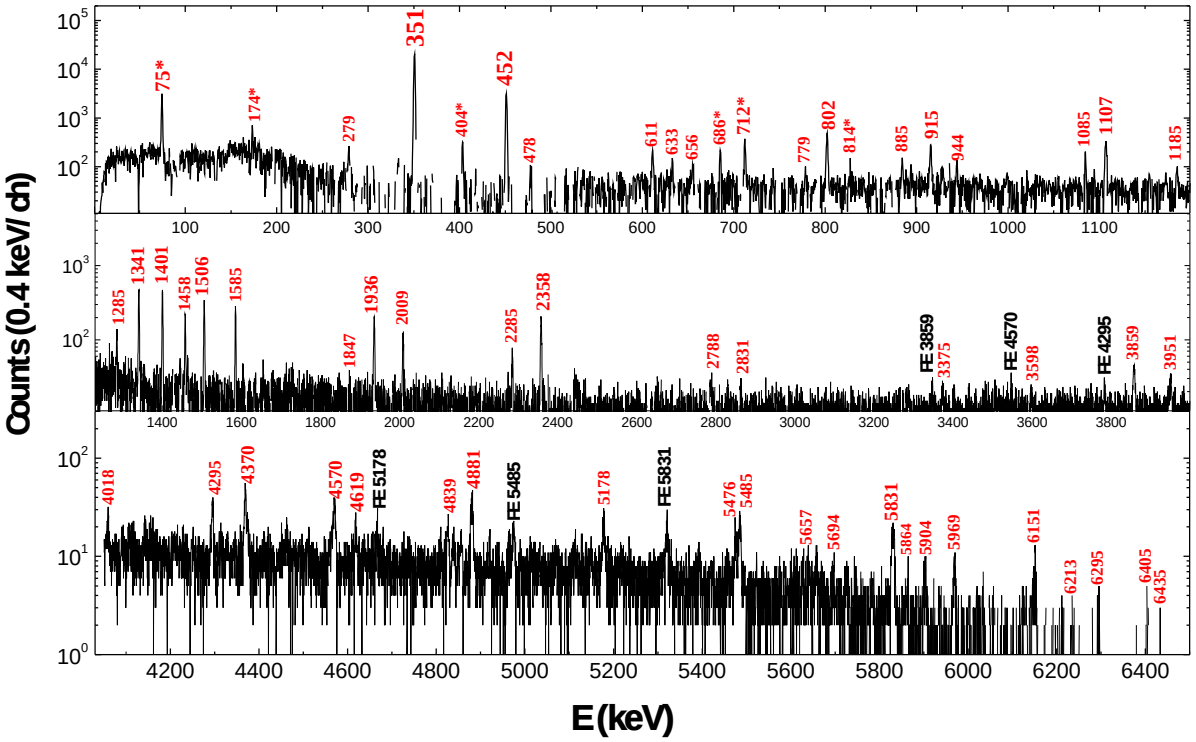

Figure 4.4: The most pure β-gated γ-ray singles spectrum of ^{81,80}Ga obtained by subtracting the long-lived activity.

4.3.2 Level scheme of ^{81}Ga

For complete suppression of long-lived activity from the energy spectrum of HPGe an additional sorting step was needed. It consisted in subtraction of the long-lived activity directly during the sorting, that is, the activity corresponding to the period of 1800-8400 ms normalized to the period of 50-1200 ms. In this way, energy peaks from long-lived activity were eliminated and only peaks from ^{81}Ga and ^{80}Ga remain in the energy spectrum.

The significantly improved statistics compared to the previous work [Pad10] is illustrated in Fig. 4.4. Gamma lines up to 6.5 MeV are observed along with the strongest lines at 351 and 452 keV. More than 20 transitions with sizeable intensity are detected beyond 4 MeV. Transitions arising from the β^- decay of ^{81}Zn have been identified by their time behaviour after proton impact, which is consistent with the measured half-life of ^{81}Zn of 290 ms (see Sec. 4.3.1), and the γ-γ coincident spectrum between both HPGe detectors, based on coincidences with previously known transitions.

Figure 4.5 shows the energy spectra acquired in coincidence with the 351- and 2358-keV transitions. Note that γ-rays up to 5 MeV were registered in coincidence with the strong 351-keV line. Table 4.1 collects the information about the γ transitions associated to the decay of ^{81}Zn to ^{81}Ga. The relative intensities were extracted using the full-energy peak areas from the β-gated γ-ray spectrum (consisted with γ-ray singles spectrum) and the HPGe detector efficiencies determined in Sec. 3.5.2.

E_γ(keV)	$E_{in.level}$ (keV)	$E_{fin.level}$ (keV)	I_γ (%)[a]	γ-γ
279.3[b] *3*			0.64 *4*	
333.3 *2*	2285.6 *1*	1952.4 *2*	0.80 *4*	611, 1341, 2009
351.1 *1*	351.1 *1*	0.0	100 *4*	452, 633, 655, 915, 1085, 1107 1155, 1185, 1250, 1285, 1585 1847, 2065, 2358, 2807, 2838 3375, 3402, 3558, 3598, 3763 3858, 3943, 3950, 4018, 4250, 4463, 4570, 4761, 4827, 4839 5024, 5072
451.6 *1*	802.5 *1*	351.1 *1*	20.1 *7*	351, 633, 4619, 4857
478.2[c] *2*	1936.4 *1*	1458.3 *1*	0.35 *3*	
505.1[b] *4*			0.39 *3*	
611.4 *1*	1952.4 *2*	1341.0 *1*	1.8 *1*	333, 1341
626.7[b] *5*			0.42 *4*	
632.9 *1*	1435.5 *1*	802.5 *1*	0.90 *7*	351, 452
655.8[c] *2*	1458.3 *1*	802.5 *3*	0.59 *6*	351
778.6[b] *3*			0.49 *5*	
802.4 *1*	802.5 *3*	0.0	4.9 *2*	
884.8 *2*	2285.6 *1*	1400.7 *2*	0.95 *8*	1400, 2009
894.1[c] *1*	2830.7 *3*	1936.4 *1*	0.84 *7*	
915.5 *4*	1266.7 *3*	351.1 *1*	3.0 *2*	351
944.4 *4*	2285.6 *1*	1341.0 *1*	1.33 *8*	1341
1084.7 *5*	1435.5 *1*	351.1 *1*	3.0 *2*	351
1107.4 *2*	1458.3 *1*	351.1 *1*	5.7 *3*	351
1155.0 *2*	1506.3 *1*	351.1 *1*	0.68 *8*	351
1185.2 *2*	5485.9 *3*	4301.6 *4*	0.8 *1*	351
1250.9 *2*	2686.5 *2*	1435.5 *1*	0.58 *7*	351, 1285
1266.9 *6*	1266.7 *3*	0.0	0.79 *8*	
1285.3 *1*	1636.4 *2*	351.1 *2*	2.7 *2*	351
1341.0 *1*	1341.0 *1*	0.0	10.5 *6*	333, 611, 945, 2009
1400.7 *1*	1400.7 *2*	0.0	11.0 *6*	884
1458.3 *2*	1458.3 *1*	0.0	5.0 *3*	
1506.4 *1*	1506.3 *1*	0.0	8.5 *5*	
1585.5 *1*	1936.4 *1*	351.1 *1*	7.0 *4*	351, 2358

Continued on next page

Table 4.1 – *Continued*

E_γ(keV)	$E_{in.level}$ (keV)	$E_{fin.level}$ (keV)	I_γ (%)[a]	γ-γ
1847.2 *4*	2198.3 *4*	351.1 *1*	0.9 *1*	351
1936.3 *2*	1936.4 *1*	0.0	8.1 *5*	2358
2009.2 *2*	4294.9 *1*	2285.6 *1*	4.8 *3*	333, 611, 885, 1341, 2285
2065.5 *3*	2416.6 *3*	351.1 *1*	0.57 *8*	351
2285.5 *2*	2285.6 *7*	0.0	3.7 *2*	
2358.4 *2*	4294.9 *1*	1936.4 *1*	10.9 *7*	351,1585,1936
2627.8[b] *4*			0.5 *1*	
2686.6 *4*	2686.5 *2*	0.0	1.8 *2*	
2788.4 *3*	2788.4 *3*	0.0	1.8 *2*	
2807.0 *3*	3158.1 *4*	351.1 *1*	1.0 *1*	351
2830.7 *3*	2830.7 *3*	0.0	1.5 *2*	
2838.2 *7*	3189.3 *7*	351.1 *1*	1.0 *1*	351
2943.1[b] *4*			1.2 *2*	
3374.7 *6*	3725.8 *6*	351.1 *1*	2.4 *3*	351
3402.7 *4*	3753.8 *4*	351.1 *1*	2.1 *3*	351
3558.5 *5*	3909.6 *4*	351.1 *1*	1.5 *2*	351
3598.2 *5*	3949.3 *5*	351.1 *1*	2.1 *3*	351
3763.6 *7*	4114.7 *7*	351.1 *1*	1.4 *3*	351
3858.5 *4*	4209.3 *3*	351.1 *1*	4.1 *6*	351
3909.7 *8*	3909.6 *4*	351.1 *1*	1.0 *3*	
3943.9 *5*	4294.9 *1*	351.1 *1*	2.2 *4*	
3950.5 *4*	4301.6 *4*	351.1 *1*	2.8 *4*	351
4017.8 *5*	4369.0 *4*	351.1 *1*	4.2 *6*	351
4208.5 *6*	4209.3 *3*	0.0	1.1 *2*	
4250.5 *5*	4601.6 *5*	351.1 *1*	0.5 *2*	351
4295.4 *4*	4294.9 *1*	0.0	4.6 *6*	
4328.9 *6*	5131.4 *4*	802.5 *1*	1.0 *3*	351, 452
4369.2 *4*	4369.0 *4*	0.0	2.9 *6*	
4374.6 *7*	5177.8 *3*	802.5 *1*	1.3 *3*	351, 452
4463.2 *6*	4814.3 *8*	351.1 *1*	1.9 *3*	351
4570.0 *4*	4921.1 *4*	351.1 *1*	6.8 *8*	351
4618.9 *7*	5421.9 *2*	802.5 *1*	1.7 *3*	351, 452
4761.9 *10*	5113.2 *8*	351.1 *1*	1.9 *3*	351

Continued on next page

Table 4.1 – *Continued*

E_γ(keV)	$E_{in.level}$ (keV)	$E_{fin.level}$ (keV)	I_γ (%)[a]	γ-γ
4826.9 *4*	5177.8 *3*	351.1 *1*	2.4 *3*	351
4839.8 *7*	5190.9 *7*	351.1 *1*	2.9 *4*	351
4856.6 *5*	5658.6 *3*	802.5 *1*	2.7 *4*	351, 452
4880.4 *4*	4880.4 *4*	0.0	7.2 *9*	
5024.0 *5*	5375.1 *5*	351.1 *1*	0.5 *1*	351
5072.0 *5*	5421.9 *2*	351.1 *1*	1.1 *2*	351
5113.6 *6*	5113.2 *8*	0.0	1.3 *3*	
5178.2 *5*	5177.8 *3*	0.0	4.5 *6*	
5421.6 *3*	5421.9 *2*	0.0	0.8 *2*	
5475.5 *5*	5475.5 *5*	0.0	2.5 *4*	
5485.1 *5*	5485.9 *3*	0.0	4.6 *6*	
5657.4 *5*	5658.6 *3*	0.0	0.7 *2*	
5694.8 *7*	5695.5 *7*	0.0	0.7 *2*	
5726.9 *4*	5726.9 *4*	0.0	0.6 *1*	
5831.0 *5*	5831.0 *5*	0.0	4.4 *6*	
5863.5 *3*	5863.5 *3*	0.0	0.6 *1*	
5903.9 *8*	5903.9 *8*	0.0	2.0 *3*	
5936.1 *6*	5936.1 *6*	0.0	0.4 *1*	
5969.2 *7*	5969.2 *7*	0.0	2.3 *3*	
6150.5 *7*	6150.5 *7*	0.0	1.8 *3*	
6212.8 *4*	6212.8 *4*	0.0	0.29 *6*	
6236.1 *5*	6236.1 *5*	0.0	0.24 *6*	
6295.3 *5*	6295.3 *5*	0.0	0.26 *6*	
6405.2 *5*	6405.2 *5*	0.0	0.27 *6*	
6434.6 *4*	6434.6 *4*	0.0	0.09 *3*	

Table 4.1: Gamma transitions populated in the decay of ^{81}Zn to ^{81}Ga. For those placed on the decay scheme the initial and final level energies are given (2^{nd} and 3^{rd} columns). Relative intensities normalized to 100 units for the 351-keV transition are provided. The strongest transitions observed in γ-γ coincidences are given in the last column. Some transitions were not seen in coincidences but fit well between two energy levels. The intensity of the unplaced transitions amounts to 1.1 % of the total γ intensity.

[a] For absolute intensity per 100 decays, multiply by 0.37 *2*

[b] Not placed in the level scheme.

[c] Weak transition, not observed in γ-γ coincidences. Tentatively placed in the level scheme.

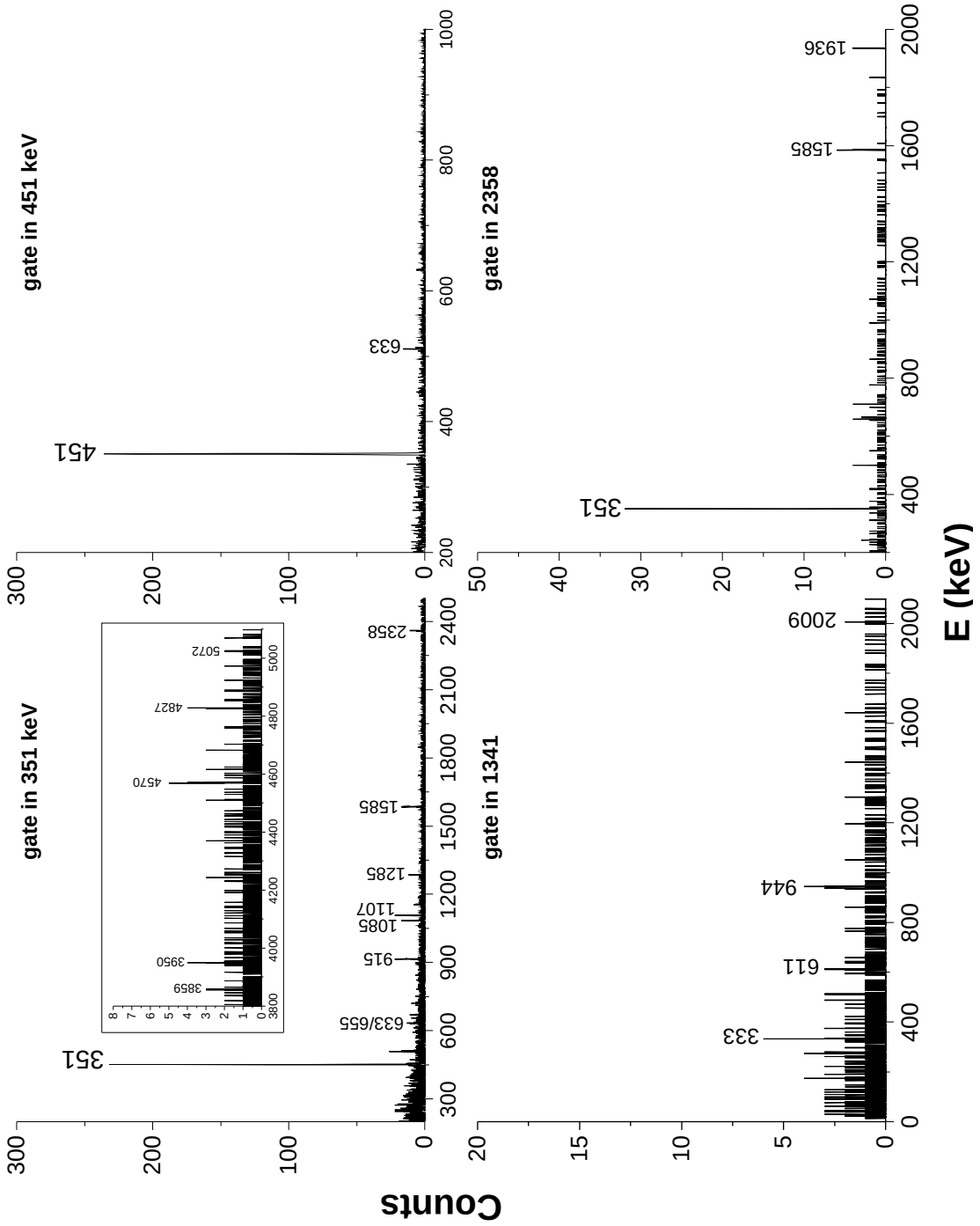

Figure 4.5: A $\gamma\gamma$ coincident spectrum gated by the strongest 351-keV transition (up) and the 2358-keV line (down).

Based on the γ-γ coincidences 70 transitions that had not been observed in [Pad10] have been placed

in the level scheme (Fig. 4.6 and Fig. 4.7). Weak transitions that were not observed in coincidence with strong ^{81}Ga γ-rays were not placed in the level scheme. However, some of them fits well between already established levels and were tentatively marked with broken lines. The high-energy gammas not observed in coincidence with 351- and 452-keV were placed as de-exciting the state with the same energy. We note that the available energy window for β^- decay is $Q_{\beta^-} = 11428(6)$ keV [Aud12a], compared to a value of $Q_{\beta^- n} = 4953(6)$ keV [Aud12a] for β-delayed neutron emission. Therefore γ-rays with energy above 5 MeV that follow the ^{81}Zn half life must belong to ^{81}Ga and not to ^{80}Ga, and most likely also γ-rays with energies larger than approximately 3.5 MeV. In this way, 47 excited states of ^{81}Ga in the energy range up to 6.5 MeV have been observed, 40 of them for the first time. We confirm the existence of 351-, 802-, 1266-, 1458-, 1936-, 4295- and 4881-keV levels from the previous study.

4.3.3 Absolute β feeding

For the absolute β feeding intensities to be calculated it is necessary to obtain the ground state β feeding, $I^{Ga}_{\beta,gs}$. Since there is no isomeric state observed in ^{81}Ga, the total g.s. intensity –both γ ($I^{Ga}_{\gamma,gs}$) and β– proceeds further from the ^{81}Ga ground state to states in ^{81}Ge via β-decay, and to states in ^{80}Ge via the β-delayed neutron emission. A β-decaying isomer exists in ^{81}Ge at 679 keV [Hof81], for which no γ-ray branch was observed. Therefore, both states need to be considered in the β-decay of ^{81}Ga, both for gamma ($I^{Ge}_{\gamma,gs+679}$) and beta ($I^{Ge}_{\beta,gs+679}$) feeding. In addition, the β-n branch from ^{81}Zn ($I^{Zn}_{\beta-n}$) needs to be taken into account, together with the already mentioned ^{81}Ga β-n branch ($I^{Zn}_{\beta-n}$).

The intensity balance for $A = 81$ can thus be summarized in the following expression:

$$I^{Zn}_{\beta-n} + I^{Ga}_{\gamma,gs} + I^{Ga}_{\beta,gs} = I^{Ga}_{\beta-n} + I^{Ge}_{\gamma,gs+679} + I^{Ge}_{\beta,gs+679} \tag{4.1}$$

For the β-n branch from ^{81}Ga we take the P_n branch of 11.9(7)% from the adopted value [Bag08] and for the ^{81}Zn the P_n value of 23(4)% that is calculated in Sec. 4.4 below.

In our experiment the ^{81}Zn ions were collected in a fixed catcher, creating a saturated source that included the short-lived and long-lived decay products from ^{81}Zn and its daughters. Therefore, the spectra without time gating conditions can be analysed to obtain the intensities in ^{81}Ga and ^{81}Ge in arbitrary units normalized to the strongest 351-keV γ-rays as shown in Tab. 4.1. The total gamma intensity that feeds the ground state of ^{81}Ga is measured to be $I^{Ga}_{\gamma,gs}$=203(4). In the decay of ^{81}Ga, the gamma intensity that goes directly to the 679-keV isomer state and the ground state amounts to 101(3) and 95(3) respectively, and thus $I^{Ge}_{\gamma,gs+679}$=196(4).

For the $I^{Ge}_{\beta,gs+679}$ we take the spin assignments of $9/2^+$ and $1/2^+$ [Hof81] for the lowest-lying states in ^{81}Ge, which are thus β-fed from the ^{81}Ga $5/2^-$ via two first-forbidden unique β transitions with $\Delta J = 2$ according to the β-decay selection rules. It is then reasonable to consider a lower limit of $\log^{1U} ft = 8.5$ (see Fig. 1 of [End79]) for both states. The β feeding calculated with these assumptions gives corresponding upper limits of 11.3 % for the $9/2^+$ g.s. and 6.6 % for the 679-keV isomer represented in absolute units (5.7(56) % and 3.3(33) % were used for calculations). Therefore, the final value of the ground state beta feeding in ^{81}Ga is extracted from the Eq. 4.1 and is given by an

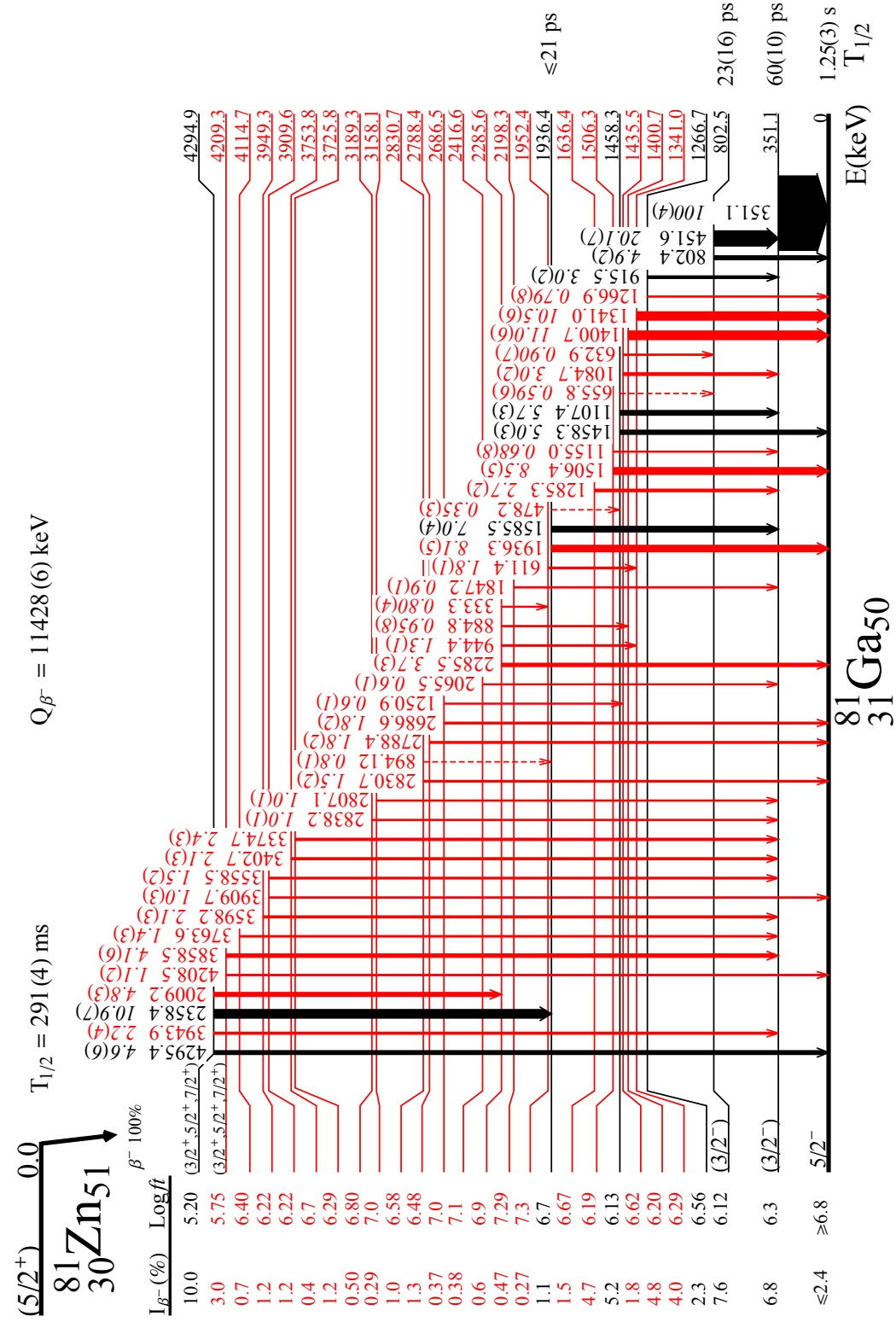

Figure 4.6: Level scheme of ^{81}Ga. States up to 4.3 keV are represented with their corresponding γ transitions.

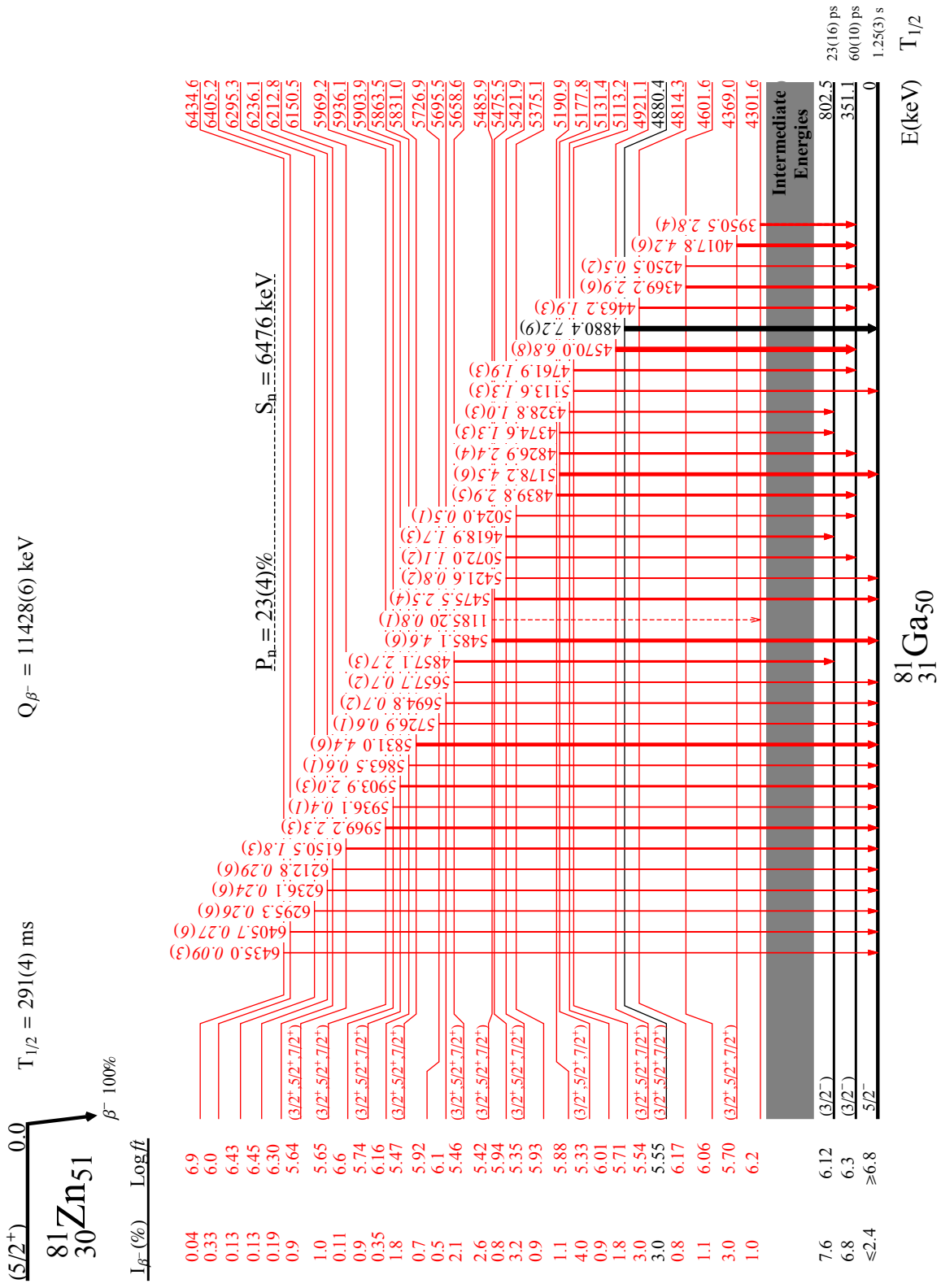

Figure 4.7: Level scheme of ^{81}Ga containing the high-lying states between 4.3 and 6.5 keV.

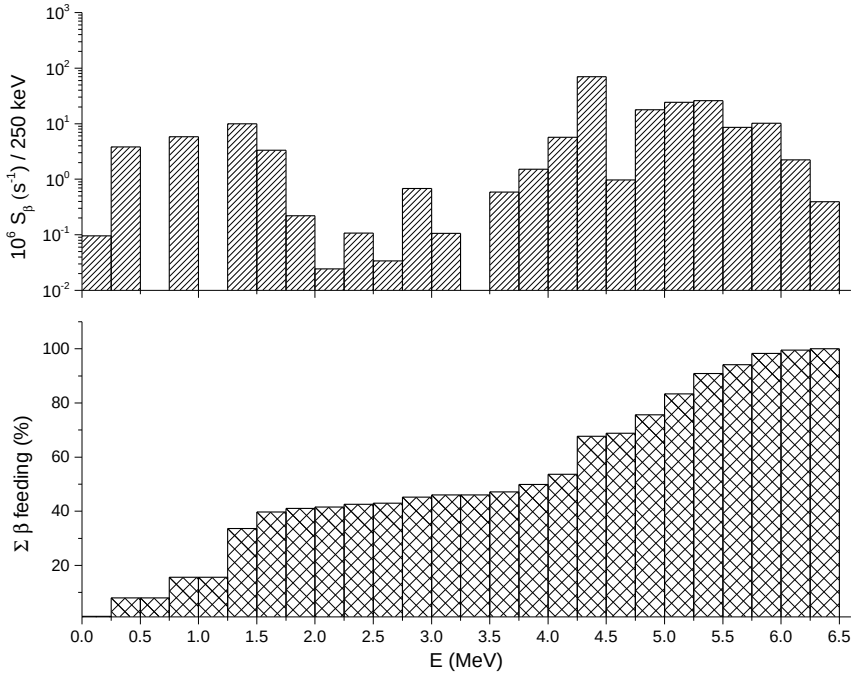

Figure 4.8: Accumulated absolute β feeding (lower panel) and β-decay strength distribution of ^{81}Ga levels represented in 250-keV bins.

upper limit of 2.4 % This leads to log$ft \geq 6.8$, in good agreement with the systematics and selection rules for the first-forbidden non-unique β-decay transition.

Using this value the apparent β feeding intensity of the rest of levels, $I_\beta(E)$, is obtained by intensity balance between feeding and de-exciting γ-rays. The results including energy and logft values for each state are shown in Tab. 4.2. Figure 4.8 depicts the corresponding β-decay strength distribution in the upper panel and accumulated absolute β-feeding distribution. The β-decay strength S_β of each state was computed as the quotient between the absolute β feeding and the ft value taken from Tab. 4.2. The data of both plots were binned to 250 keV. High-energy transitions could have been missed or misplaced if coincidences are not observed, which means that the β feeding would be slightly modified. We note the small energy gap between the highest level at 6435 keV and the recently reported neutron separation energy, S$_n$=6576(4) keV, still far from the available β-decay window, Q_{β^-} = 11428(6) keV [Aud12a]. However, we do not observe gamma emission from levels above the $S_n = 6.476(4)$ MeV [Aud12b]. Complementary techniques, as Total Absorption Spectroscopy (TAS) for example, might correct this failure.

With the Zn β-delayed neutron emission probability $P_n = 23(4)\%$ and the ground state feeding (taking $I^{Ga}_{\beta,gs}$= 1.2(12)%) an absolute normalization factor of 0.37(2) is obtained for the γ intensities in the decay of ^{81}Zn to ^{81}Ga from the relative ones tabulated in Tab. 4.1.

E_{level}(keV)	Abs. β feeding (%)	logft^a
0.0	$\leq$ 2.4	$\geq$ 6.8
351.1 *1*	6.8 *21*	6.25 *14*
802.5 *1*	7.6 *6*	6.12 *4*

Continued on next page

Table 4.2 – *Continued*

E_{level}(keV)	Abs. β feeding (%)	logft^a
1266.7 *3*	2.3 *2*	6.56 *5*
1341.0 *1*	4.0 *3*	6.29 *4*
1400.7 *2*	4.8 *4*	6.20 *3*
1435.5 *1*	1.8 *2*	6.62 *6*
1458.3 *1*	5.1 *4*	6.13 *4*
1506.3 *1*	4.7 *3*	6.19 *3*
1636.4 *2*	1.5 *2*	6.67 *7*
1936.4 *1*	1.1 *6*	6.73 *24*
1952.4 *2*	0.27 *7*	7.34 *12*
2198.3 *4*	0.47 *6*	7.29 *6*
2285.6 *1*	0.6 *3*	6.92 *22*
2416.6 *3*	0.38 *8*	7.09 *10*
2686.5 *2*	0.37 *8*	7.04 *10*
2788.4 *3*	1.3 *2*	6.48 *8*
2830.7 *3*	1.0 *1*	6.58 *6*
3158.1 *4*	0.29 *7*	7.03 *11*
3189.3 *7*	0.50 *7*	6.80 *7*
3725.8 *6*	1.1 *2*	6.29 *7*
3753.8 *4*	0.4 *1*	6.73 *15*
3909.6 *4*	1.2 *2*	6.22 *7*
3949.3 *5*	1.2 *2*	6.22 *7*
4114.7 *7*	0.7 *1*	6.40 *8*
4209.3 *3*	3.0 *3*	5.75 *5*
4294.9 *1*	10.0 *6*	5.20 *3*
4301.6 *4*	1.0 *2*	6.20 *10*
4369.0 *4*	3.0 *4*	5.70 *6*
4601.6 *5*	1.1 *2*	6.06 *7*
4814.3 *8*	0.7 *1*	6.17 *8*
4880.4 *4*	3.0 *4*	5.55 *6*
4921.1 *4*	3.0 *4*	5.54 *6*
5113.2 *8*	1.8 *2*	5.71 *6*
5131.4 *4*	0.9 *2*	6.01 *9*
5177.8 *3*	4.0 *4*	5.33 *4*

Continued on next page

Table 4.2 – *Continued*

E_{level}(keV)	Abs. β feeding (%)	logft^a
5190.9 *7*	1.1 *2*	5.88 *7*
5375.1 *5*	0.9 *1*	5.93 *7*
5421.9 *2*	3.2 *3*	5.35 *5*
5475.5 *5*	0.8 *1*	5.94 *8*
5485.9 *3*	2.6 *3*	5.42 *5*
5658.6 *3*	2.1 *2*	5.46 *5*
5695.5 *7*	0.5 *1*	6.05 *10*
5726.9 *4*	0.7 *1*	5.92 *9*
5831.0 *5*	1.8 *2*	5.47 *6*
5863.5 *3*	0.35 *7*	6.16 *9*
5903.9 *8*	0.9 *1*	5.74 *7*
5936.1 *6*	0.11 *4*	6.64 *16*
5969.2 *7*	1.0 *1*	5.65 *6*
6150.5 *7*	0.9 *1*	5.64 *7*
6212.8 *4*	0.19 *3*	6.30 *7*
6236.1 *5*	0.13 *2*	6.45 *7*
6295.3 *5*	0.13 *2*	6.43 *7*
6405.2 *5*	0.33 *7*	5.99 *10*
6434.6 *4*	0.04 *1*	6.89 *11*

Table 4.2: Energy levels of ^{81}Ga with absolute β feeding percentages and logft values.

[a] Computed using logft online calculator from http://www.nndc.bnl.gov/logft/

4.4 Level scheme of ^{80}Ga populated in the βn decay of ^{81}Zn

As already discussed, the β-delayed neutron emission is energetically allowed in the decay of ^{81}Zn, with a ^{81}Ga neutron separation energy S_n=6576(4) keV [Aud12a], well within the Q_{β^-} window. The analysis of the β-gated γ spectrum has allowed 11 γ transitions to be obtained (they were marked with an asterisk in Fig. 4.4. They were assigned to ^{80}Ga populated in β^-n decay of ^{81}Zn. The nuclide ^{80}Ga was studied at ISOLDE during the same experimental campaign, populated in the β^- decay of ^{80}Zn and the results of the analysis were published in [Lic14]. The γ-γ coincidence analysis provides the information to place the observed transitions ^{80}Ga de-exciting 9 known low energy levels (see Fig. 4.10).

Our new level scheme of ^{80}Ga populated from the β^-n decay of ^{81}Zn is consistent with the structure from [Lic14]. Table 4.3 contains the detailed information about the γ transitions and fed energy levels. The direct feeding of the ground and the first isomeric

E_γ(keV)	$E_{in.level}$ (keV)	$E_{fin.level}$ (keV)	I_γ (%)[a]	γ-γ
74.9 *1*	96.8 *3*	0.0	100 *12*	307, 1117
173.8 *4*	577.5 *2*	403.7 *2*	25 *2*	404
176.6 *1*	911.1 *4*	734.5 *3*	6.3 *6*	713
306.9 *2*	403.7 *2*	96.8 *3*	7.4 *5*	75
403.7 *2*	403.7 *2*	0.0	28 *2*	174
685.7 *1*	707.6 *3*	21.9 *3*	28 *2*	
712.6 *6*	734.5 *3*	21.9 *3*	47 *3*	177
814.2 *2*	911.1 *4*	96.8 *3*	6.5 *7*	
888.9 *3*	911.1 *4*	96.8 *3*	11 *1*	
928.7 *5*	950.6 *6*	21.9 *3*	12 *1*	
1116.7 *3*	1213.5 *4*	96.8 *3*	13 *1*	75

Table 4.3: Gamma transitions in ^{80}Ga populated in the β^--n decay of ^{81}Zn. Their relative intensity, placement in the level scheme, and main γ-γ coincidences, when available, are listed.

state is assumed to be zero. The second 1^+ isomer is confirmed at 708 keV. We measured its $T_{1/2} = 18.3(13)$ ns half-life using triple coincidences between β and two HPGe detectors, which replace the $LaBr_3$(Ce) scintillators when a determined γ line is selected for the fast-timing measurements. Since HPGe detectors are much slower they can be used for lifetime measurements beyond 5 ns. Therefore, the selection of energy gates was applied in the HPGe detector and projected onto the slow TAC, which was started by the β signal and stopped by the signal from HPGe. The time distribution was fit to a prompt Gaussian plus the exponential decay. The Fig. 4.9 shows the fitting which yields to $T_{1/2} = 18.3(13)$ ns, in good agreement with [Lic14].

The β-delayed neutron emission probability from ^{81}Zn is an important magnitude, which may have an astrophysical impact since ^{81}Ga is located along the r-process path [Mum16]. To obtain this value we compare the number of decays arising from the direct ^{81}Zn β-decay chain and the ^{81}Zn βn decay branch to the $A = 80$ chain as shown in Fig. 4.1. The following balance equation in arbitrary units:

$$P_n^{^{81}Zn} = N^{^{80}Ga} + P_n^{^{80}Ga} = \left[N^{^{80}Se} - P_n^{^{81}Ga}\right] + P_n^{^{80}Ga} \tag{4.2}$$

shows that the number of decays of ^{81}Zn that populate ^{80}Ga is equal to the number of decays of ^{80}As to the stable ^{80}Se corrected by the factor arising from the ^{81}Ga β^-n decay probability of 11.9(7)% [Bag08] and ^{80}Ga β^-n decay probability of 0.86(7)% [SIN02]. The 11.9(7)% value was not verified with data from our work because is used as input parameter for the computation of P_n branching of ^{81}Zn. The Eq. 4.2 is valid when a long period of time (much higher than individual half-lives of species in a sample) was left for nuclei to decay. The reason to take ^{80}Se is that the absolute intensity of γ-rays per 100 parent decays [Mcm71, Kra75] is well-known, contrary to ^{80}Ge or ^{80}As. Since the discovery of the long-lived isomer in ^{80}Ga [Ver13] the intensities of γ transitions in

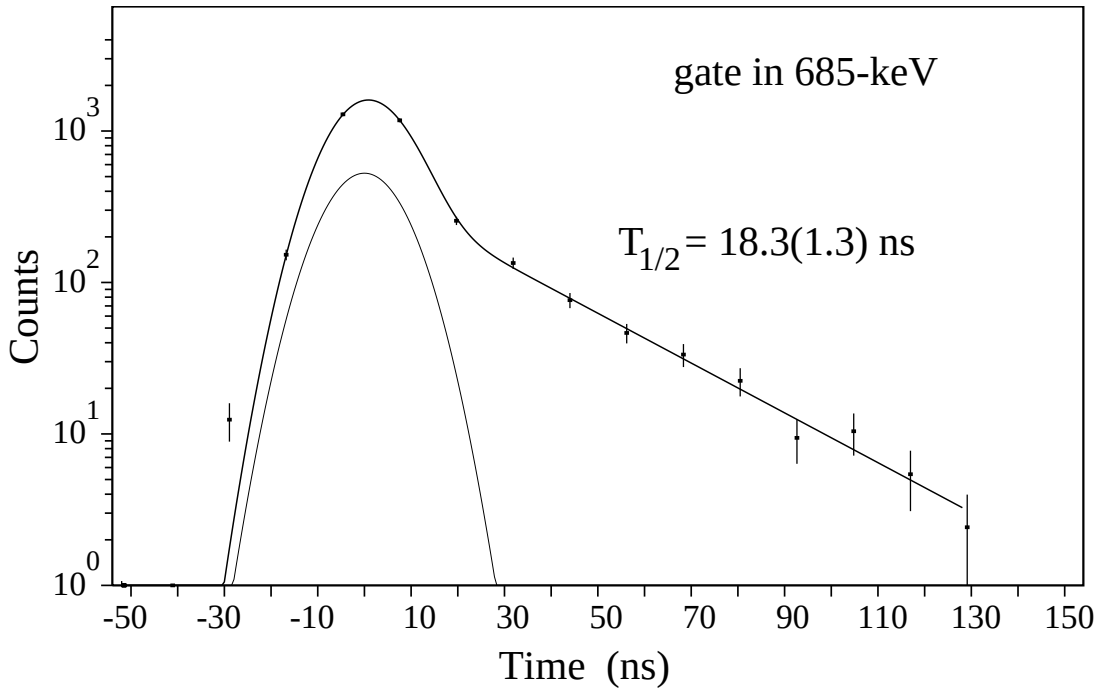

Figure 4.9: Time-delayed spectrum gated by 685-keV transition from ^{80}Ga.

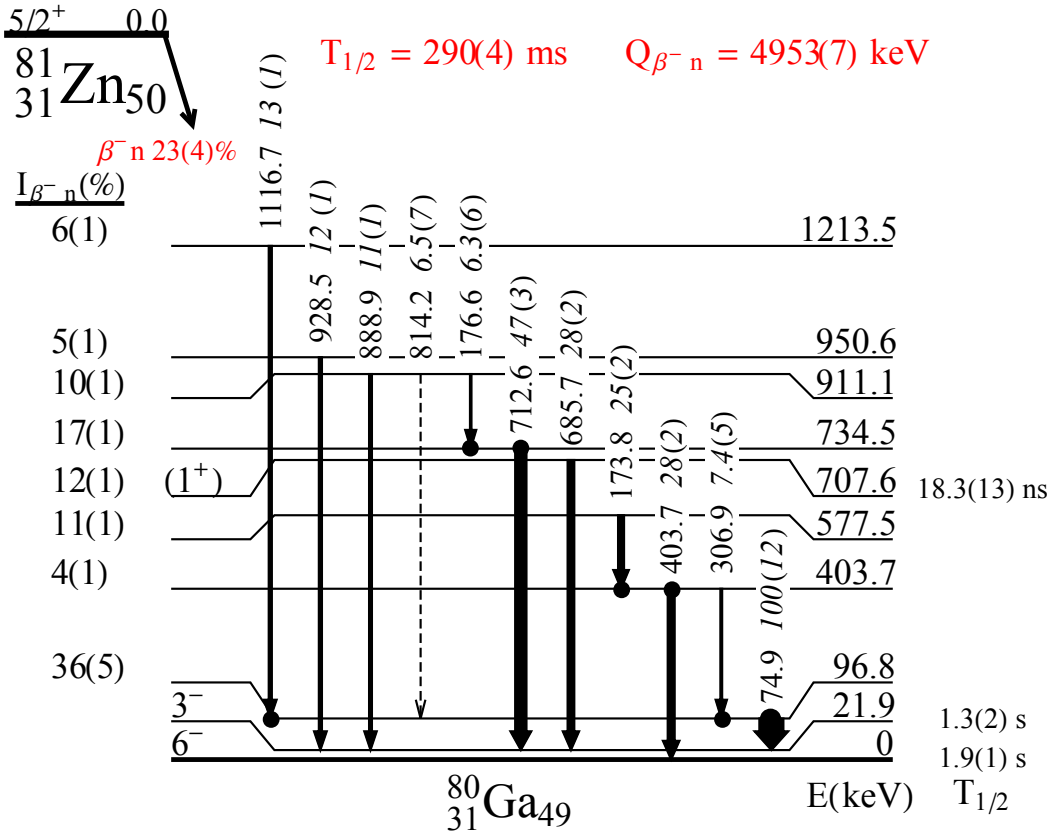

Figure 4.10: Levels in ^{80}Ga populated in the β^-n decay of ^{81}Zn.

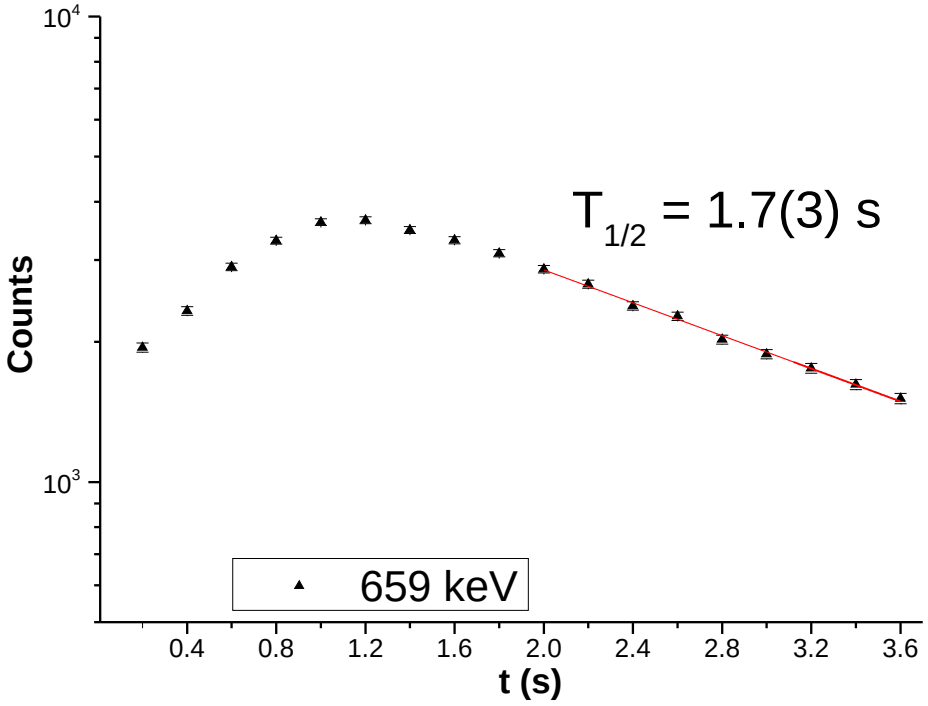

Figure 4.11: Apparent half-life of ^{80}Ga calculated by fitting in the β-gated time spectrum obtained by projecting the strong 659-keV transition in the time since last proton impacted the target. A simple exponential decay plus a constant was used for fitting.

^{80}Ge from [Hof81] should be updated. Large discrepancy between absolute intensities of 27(5)% and 48(2)% for 265-keV line of ^{80}As measured by P. Hoff and D. Fogelberg [Hof81] and M. Leino *et al.* [Lei91]. Determining the areas directly from the β-gated spectrum and taken into account the absolute intensities per 100 parent decays of 666-, 1207- and 1645-keV lines from ^{80}Se we computed the $P_n^{^{81}Zn}$ in arbitrary units. Normalizing to the total number of decays of ^{81}Zn we get P_n=23(4)%. The number of β-decays of ^{81}Zn to ^{81}Ga was obtained with the absolute intensities of 216- and 828-keV transitions from ^{81}Ge [Hof81].

As ^{80}Ga decays to ^{80}Ge its half-life can be measured following the same procedure than in Sec. 4.3.1. Gating on the 659-keV gamma which de-excites the 659-keV level in ^{80}Ge we get the apparent half-life of ^{80}Ga, where a 22-keV 3^- isomer has been identified above the 6^- ground state [Lic14]. The half-lives of these states were previously measured as 1.9(1) s and 1.3(2) s respectively [Ver13]. Since the first 659-keV excited state in ^{80}Ge is not β-fed the 659-keV spectrum of the time elapsed from the last proton pulse yields the combination of the ground state and the 22-keV isomer half-lives. Fig. 4.11 shows the result of fitting to a simple exponential decay plus a constant. Employing the same time condition for fitting limits than used in Sec. 4.3.1 we get $T_{1/2}$ = 1.70(3) s, which is in good agreement with the adopted value of 1.676(14) [Sin05] and with the average half-life of 1.71(2) calculated by Verney *et al.* [Ver13] using all γ of ^{80}Ge observed in their experiment.

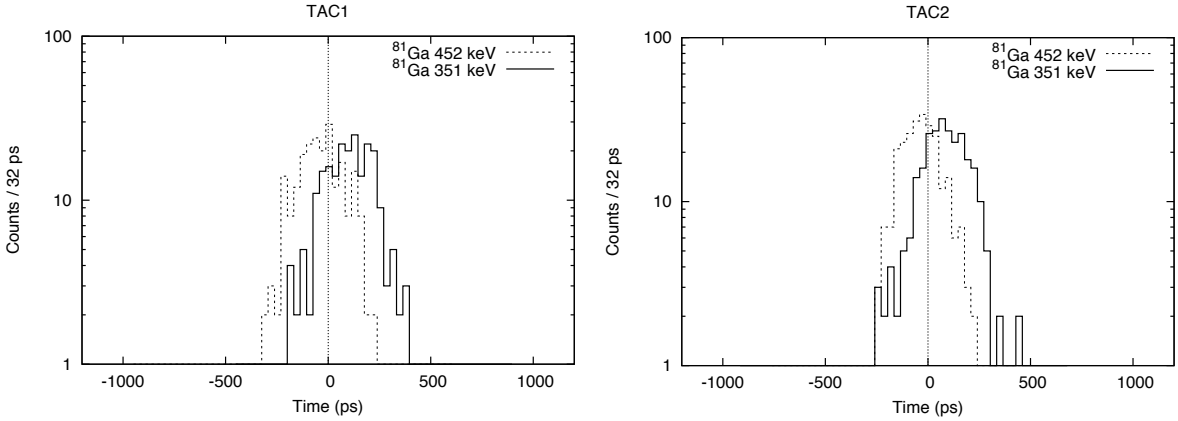

Figure 4.12: Mean life of 351-keV state determined with centroid shift method using sequential transitions of 351 and 452 keV in triple $\beta\gamma\gamma$(t) coincidences. The energy gates were set in $LaBr_3$(Ce) and projected into corresponding fast time-to-amplitude converter (FTAC). The time difference value between both time distribution centroids shown in the plot does not include timing correction of the prompt positions and Compton background contribution.

4.5 Lifetime measurements

Excited state lifetimes have been measured using the advanced time-delayed $\beta\gamma\gamma$(t) fast-timing method [Mac89, Mos89, Mac91] explained in details in Sec. 2.4. For shorter half-lives (from 60 to 10 ps) we will use the Centroid Shift technique while for longer half-lives the Convolution technique will be more appropriate. Peak and background centroid corrections are made separately according to their respective Prompt and Compton response walk curves. Peak and background centroid corrections are made separately according to their respective walk curves studied in Sec. 3.5.3. Normally FEPs seat on background arising mainly from Compton events coming from transitions of higher energies. In order to correct for this effect, the energy dependence of the background component is corrected with the help of the Compton correction curve and the peak to background ratio. The resulting centroid of the FEP time distribution is then compared with the baseline given by the FEP correction curve. Any delay relative to the curve is then due to the lifetime carried by the transition giving rise to the FEP and can be related to levels in the nuclide of interest. In addition, the timing analysis includes standard corrections for the small depended of the β time response with energy, and if needed for small electronics drifts during the measurement.

4.5.1 Half-lives of the excited states of ^{81}Ga

The special situation of 351-keV level in ^{81}Ga allows to use the Centroid Shift technique by using the relative comparison technique with sequential transitions of 451 and 351 keV. Assuming no long half-life of the high energy levels in ^{81}Ga the mean-life of 351-keV level is simply the difference between the centroid positions in FTAC gated by 351-and 451-keV lines in $LaBr_3$(Ce). However, as the time-response of the Compton and Full Energy Peaks (FEP) in $LaBr_3$(Ce) crystals is not linear with the energy some timing calibrations must be performed as well as the corrections of beta-walk curve non-linearity.

According to the level scheme of ^{81}Ga (see Fig. 4.6) the 351-keV line de-excites the first excited state of the same energy while the 451-keV transition comes from 802-keV energy level. Selecting the 351-keV one in Ge detector and the 452-keV one in $LaBr_3$(Ce), the time delay observed in the FTAC is due to the mean-life of the 802-keV level plus the contributions from the lifetime of high-lying levels. By reversing the gates, selecting the 452-keV line now in the Ge and 351-keV in the $LaBr_3$(Ce), the time delayed spectra observed in the FTAC is due to the mean-life of both 802-keV and the 351-keV levels, plus contributions from high-lying states. The time difference between both time distribution centroids, conveniently corrected for the different prompt positions at 351 and 452 keV (using the FEP response curve) and subtracting the Compton response for the background (see Eq. (3.5)), yields the mean-life of the 351-keV level. Figure 4.12 contains the difference between time distributions of 351- and 451-keV transitions in FTAC-1 and FTAC-2 obtained directly after projecting the energy gates set in $LaBr_3$(Ce) into FTAC. The mentioned time corrections were applied after determining the centroid positions of the peaks in time distribution. In this way, the Centroid Shift technique gives $\tau = 92(14)$ ps for the first $LaBr_3$(Ce)) and 80(10) ps for the second one. The average of both leads to $T_{1/2} = 60(8)$ ps half-life.

This value was verified with the Convolution technique fitting to the slope from the time spectrum in $\beta\gamma$(t). Figure 4.13 shows on the left hand side the energy spectrum of $LaBr_3$(Ce). A suitable gate in time parameter was set in order to minimize the 336-keV line mixture from the 351-keV one and sufficiently strict gate in β spectrum was established to reduce 511-keV contribution. The energy gate was set in $LaBr_3$(Ce) as shown in the plot and projected into the FTAC illustrated on the right hand side of the figure. As can be seen, a slope of the order of 60 ps appears on the time delayed part of the time spectrum. Small contribution of 336-keV peak, which could not be totally suppressed from the energy spectrum and whose half-life was measured to be 170(5) ps (see Chapter 6), can be observed in the time spectrum on the right hand side of the slope. Moreover, Compton background selected on the right hand side of the energy spectrum of $LaBr_3$(Ce) from Figure 4.13 gives also a small slope in FTAC. Due to these reasons, we can not adopt the precise value of 59(3) ps for the half-life of the 351-keV state. On the other hand, in case of triple $\beta\gamma\gamma$(t) coincidences, the energy gate in 452-keV line was set in HPGe for more precise selection of 351-keV transition in $LaBr_3$(Ce). This also helps to minimize Compton contribution for the 351-keV peak. However, low statistics of the 351-keV peak does not permit to observe any pronounced slope on the delayed part of the time spectrum.

A similar procedure was applied to measure the half-life of the 1936-keV state, using the coincident 1585- and 2358-keV lines. The results from the time spectra from the two $LaBr_3$(Ce) detectors are $\tau = 20(16)$ ps and $\tau = 6(14)$ respectively. We take the average value of $\tau = 13(15)$ ps or $T_{1/2} \leq 28$ ps for this level.

The half-life of the second excited state at 802 keV was measured using parallel transitions. The high-lying states in ^{81}Ga are characterized by short half-lives well below 1 ps. From the level scheme of ^{81}Ga (Fig. 4.6 and Fig. 4.7) several strong high energy γ lines are in coincidence with the 351-keV γ-ray. By selecting those in the HPGe detectors and the 351 keV in $LaBr_3$(Ce), the time response will be due to the 351-keV state mean-life. This can be compared with the time spectrum resulting from the selection of the 452-keV line in the Ge and the 351-keV in the $LaBr_3$(Ce), which is due to both the 351- and 802-keV states. The difference between centroid positions gives the average $\tau = 34(22)$

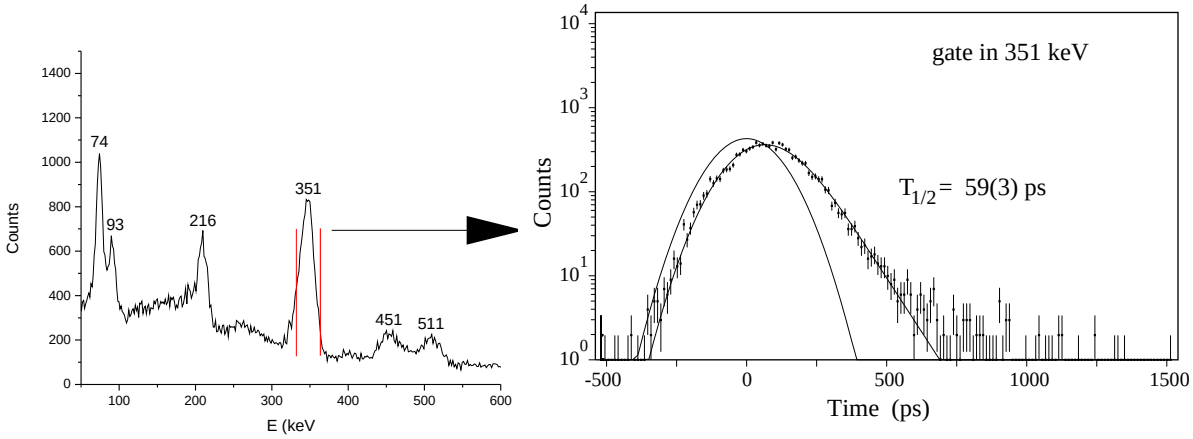

Figure 4.13: Energy spectrum of $LaBr_3$(Ce) from the $\beta\gamma$(t) coincidences (left) and time spectrum after projecting the 351-keV peak (right). Counts from 500 to 1000 ps are due to the small contribution of 336-keV line which de-excite the 336-keV level of ^{81}As with 170(5) ps half-life, also measured in our experiments and explained in details in chapter 6.

E_{level}	$T_{1/2}$	E	B(M1) W.u.			B(E2) W.u.		
(keV)	(ps)	(keV)	EXP	JUN45	jj44b	EXP	JUN45	jj44b
351	60(10)	351	$8.5(14)\times10^{-3}$	0.002	10^{-4}	85(14)	2.5	3.5
802	23(16)	452	$8(6)\times10^{-3}$	1.0	0.06	51(35)	2.1	0.8
		802	$4(2)\times10^{-4}$	0.04	0.02	6.1	10.6	0.7(5)
1936	≤ 21	1586	$\geq 1.8\times10^{-4}$			$\geq 9\times10^{-2}$		
		1936	$\geq 7.7\times10^{-5}$			$\geq 3\times10^{-2}$		

Table 4.4: Summary of half-lives of the excited states in ^{81}Ga, and experimental $B(M1)$ and $B(E2)$ reduced transition probabilities for the de-exciting transitions, compared to the theoretical values calculated with JUN45 and jj44b effective interactions (see text for details).

ps or $T_{1/2} = 23(15)$ ps half-life for the 802-keV level.

The measured half-lives of ^{81}Ga states obtained in this work are summarized in Tab. 4.4. Using the lifetimes and γ-ray branching from our level scheme the transition probabilities for the de-exciting lines have been calculated for the most probable multipolarities. The theoretical calculations of conversion coefficients for these transitions [Kib08] show that all of them are below 10^{-2} and thus were neglected in the computation of transition probabilities. Pure transitions are assumed for the calculations. According to the measured $B(XL)$ values both the 351- and 452-keV transitions are consistent with predominant $M1$ character as it happens with the 307-keV transition in ^{83}As [McC15] and the 345-keV line from ^{85}Br [Sin14], both connecting $3/2^-$ and $5/2^-$ as shown in Fig. 4.14.

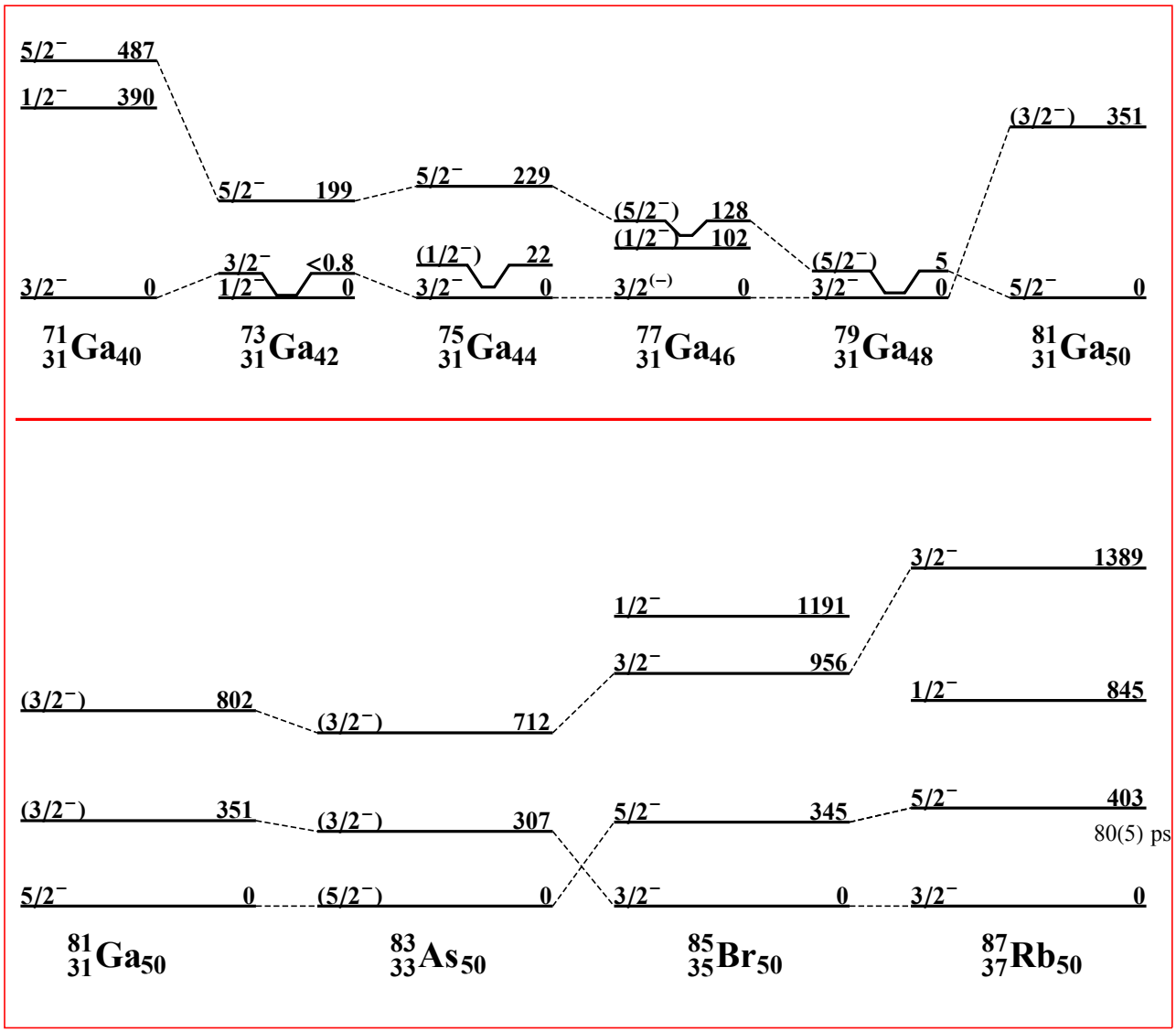

Figure 4.14: Above: level systematics of $N = 40 - 50$ Ga isotopes. Below: $N = 50$ isotones. The low-lying levels of Ga isotopes are taken from references [Zol70, Dir10b, Eks86, Hof81], except for ^{81}Ga from this work, while the structure of the $N = 50$ isotones is based on [Win88a, Zen80, Woh73].

4.6 Shell-model calculations

Large-scale shell-model calculations of nuclear states of ^{81}Ga have been performed. Two effective state-of-the-art interactions were implemented into the NUSHELL@MSU [Lis04] and ANTOINE [Cau05b] codes. The first interaction, labelled JUN45, was developed by Honma *et al.* in 2009 [Hon09] and it was focused in the *pf* shell with ^{56}Ni core and $1p_{3/2}$, $0f_{5/2}$, $1p_{1/2}$ and $0g_{9/2}$ single-particle orbits. A microscopic interaction based on the Bonn-C nucleon-nucleon potential was taken as a starting point for Hamiltonian which was characterized by 133 two-body matrix elements (TBME) and 4 single-particle energies (SPE). The interaction confirms specially well the experimental data of low-lying states in $N = 49$ isotones, Ge isotopes near $N = 40$ and $N = Z$ nuclei with $A = 64 \sim 70$. Another effective interaction, called jj44b, which made successful prediction for nuclei near ^{78}Ni was created in 2004 by Lisetskiy *et al.*. It was constructed with the same effective core and model space. The Hamiltonian was also based on the Bonn-C NN potential including four single-particle energies and 65 $T = 1$ two-body matrix elements. The detailed description of the jj44b was published in 2004 [Lis04] and it is quoted to reproduce better the heavier isotopes of Ga [Sri12].

The energy levels of ^{81}Ga obtained with JUN45 and jj44b are compared to our experimental results in Fig. 4.15. Both set of calculations reproduce satisfactorily the structure of this $N = 50$ nucleus. The calculations using the JUN45 interaction achieve a better agreement with experiment in the excitation energies, compared to jj44b. The calculated negative level density is consistent with the experimentally observed one. Both set of calculations give the lowest-lying positive parity state, a $9/2^+$ that will arise from the $\pi(g_{9/2})$ configuration, at around 3000 keV.

The occupation probabilities with both calculations for the lowest-lying states are summarized in Table 4.5. The shell model with both interactions are able to properly calculate the ground state spin-parity to be $5/2^-$, in agreement with the experimental value [Che10]. The proton occupation probability for the $\pi(f_{5/2})^3$ configuration is 80% with JUN45 and 75% with jj44b. Spin-parity of $3/2^-$ is calculated for the first and the second excited states in both calculations, although their energies differ considerably. According to the calculations the 351-keV level will have a single-particle $\pi(p_{3/2})$ character, with a large occupation value for the $\pi(f_{5/2})^2 \otimes \pi(p_{3/2})$ configuration, whereas the 802-keV level will have a preferred $\pi(f_{5/2})^3$ configuration.

The calculated reduced transition probabilities for the gammas de-exciting the lowest-lying excited states are given in Table 4.4 and compared with the measured values based on the experimental lifetimes and branching ratios. Only parity conserving transitions of

Table 4.5: Occupation probabilities for the proton configurations obtained with the JUN45 and jj44b interactions for the first three states in ^{81}Ga.

$\mathbf{E}_{level}$	**JUN45**		**jj44b**	
(keV)	$\boldsymbol{\pi(f_{5/2})^3}$	$\boldsymbol{\pi(f_{5/2})^2 p_{3/2}}$	$\boldsymbol{\pi(f_{5/2})^3}$	$\boldsymbol{\pi(f_{5/2})^2 p_{3/2}}$
0	80%	—	75%	—
351	28%	51%	—	78%
802	48%	41%	76%	—

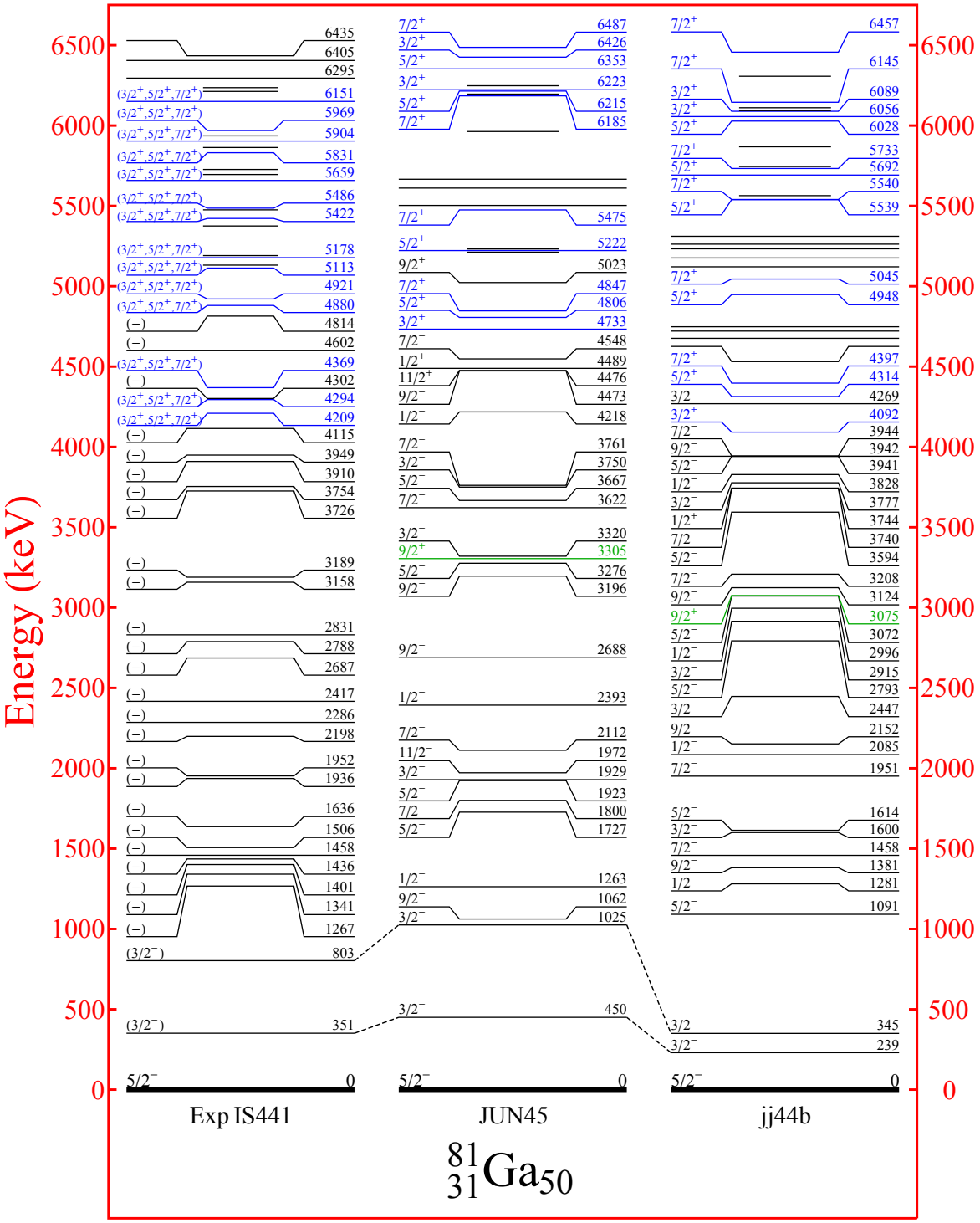

Figure 4.15: Shell-model calculations with JUN45 and jj44b interactions compared to the experimental data measured in this work.

the lowest multipolarities are considered due to the negative parity nature of the low-lying states.

4.7 Discussion

4.7.1 Ground state feeding and ground-state spin-parity of ^{81}Zn

The structure of the nuclei neighbouring ^{78}Ni is defined by the ordering and occupation probabilities of the $d_{5/2}$, $s_{1/2}$, $g_{7/2}$, and $h_{11/2}$ neutron orbitals, and the $f_{7/2}$, $p_{3/2}$, $p_{1/2}$, and $f_{5/2}$ proton orbitals (see Fig. 1.5 from Sec. 1.3). For the Cu ($Z = 29$) isotopic chain, an inversion of the ordering of the $p_{3/2}$ and $f_{5/2}$ states above ^{75}Cu has been observed, when the neutron $g_{9/2}$ orbital is being filled. This has been interpreted as the effect of the tensor interaction [Ots05].

The ^{81}Ga ground state spin-parity has been established as $5/2^-$ from collinear laser spectroscopy performed at ISOLDE [Che10]. The β-decay pattern from ^{81}Zn has been used by Padgett and co-workers [Pad10] to infer the ground-state spin of ^{81}Zn, which could be either $1/2^+$ based on extrapolation of the $1/2$ states in the region [Ver07] or $5/2^+$ based on the systematics of $N = 51$ isotones. These states will have a single-particle character, $\nu s_{1/2}$ and $\nu d_{5/2}$ respectively, and thus positive parity. Beta-decay transitions to low-lying states in ^{81}Ga are expected to proceed via forbidden transitions, since the Gamow-Teller operator will populate daughter states at much higher energy. Using the systematics for forbidden decays [End79] and based on the firm spin-parity assignment $5/2^-$ for the ground state of ^{81}Ga, two options are possible: the first one is a first-forbidden decay from $5/2^+$ to $5/2^-$ and with $\log ft$ >5.1, and the second one a first-forbidden unique decay from $1/2^+$ to $5/2^-$, more hindered and with $\log ft$ >7.5.

Our experimental data yield a β ground-state feeding compatible with zero, with a $\log ft$ larger than 6.8. We note that high-energy transitions can be still be missed in our detection set-up [Har77] and that, on the contrary, some of the high-energy transitions that are unambiguously identified to belong in ^{81}Ga have been tentatively placed in the level scheme as feeding the ground state based on the lack of observed coincidences. Thus the experimental value needs to be taken with caution.

Nonetheless, the observed negligible direct beta feeding to the ground state is in contrast to the previous experiment [Pad10]. This is because many weak γ transitions depopulating high-lying states in ^{81}Ga have been added in our study, which has a dramatic effect in the ground state γ feeding and decrease the apparent ground-state beta branching from 52% to $\leq$2.4%. This points to the well-known fact that the Pandemonium [Har77] effect occurs in this type of measurements. It is therefore very risky to base spin-parity assignments on the apparent beta-feeding. From our measurement none of the possible spin-parity assignments of ^{81}Zn can be ruled out based on systematics, although a first forbidden unique transition $1/2^+$ to $5/2^-$, and thus a $1/2^+$ ground-state spin-parity is very well possible. However, new β-decay experiment performed in RIKEN [Nii14] shows the decay of ^{81}Cu to ^{81}Zn. The preliminary data analysis indicates the strong possibility of $5/2^+$ assignment for the ground state of ^{81}Zn.

4.7.2 Low-lying structure of ^{81}Ga

In our experiment we have measured the first-excited 351-keV state half-life to be $T_{1/2} = 60(10)$ ps. Assuming that the transition connects states of negative parity, the $B(M1)$ rate for pure $M1$ multipolarity is $8.5(14) \times 10^{-3}$ W.u., whereas the pure $E2$ rate would be very collective. The reduced transition probabilities thus point to a moderately slow $M1$ transition according to the systematics [End79], which is consistent with the shell model calculations (Table 4.4). This suggest a $p_{3/2}$ dominant configuration for the 351-keV level, well described by the calculations (see Table 4.5). Owing to this fact, the 351-keV gamma would be slightly hindered due to the l-forbidden character of the $f_{5/2}$ to $p_{3/2}$ transition. The $E1$ multipolarity for 351-keV line is considered unacceptable due to its high $B(E1)$ value of 1.4×10^{-4} W.u. and the low probability to have positive-parity low-lying states in ^{81}Ga. The low lying states of the odd-mass Ga nuclei could be described through the weak coupling between an unpaired valence proton and the neighbouring even-even Zn "cores".

A very similar structure is found in $N = 50$ odd-A nuclei with $Z > 28$ as shown in Fig. 4.14, in particular for the two-proton neighbour ^{83}As. For the $Z = 37$ ^{87}Rb isotone, the $p_{3/2}$ and $f_{5/2}$ are already reversed due to the filling of the orbitals, the ground-state being a $3/2^-$ state. The 403-keV $5/2^-$ level has a very similar half-life of $T_{1/2} = 80(5)$ ps [Joh15], which gives a $B(M1)$ within a factor of 2 for the 403-keV transition to the ground-state compared to the 351-keV transition in ^{81}Ga. The shorter lifetime may be explained by the higher degree of mixing in ^{81}Ga. The $p_{3/2}$ single-particle assignment to the 351-keV level supports a narrow proton gap of the order of 500 keV between the $f_{5/2}$ and $p_{3/2}$ orbitals, as predicted for ^{79}Cu by shell model calculations [Smi04, Fla09], but at odds with what was claimed in [Dau10].

For the second excited state at 802 keV the calculations, specially those with the JUN45 interaction (which achieve a better agreement with the experimental excitation energies) show an admixture of the $\pi(f_{5/2})^3$ cluster configuration and the $\pi(f_{5/2})^2 p_{3/2}$ one. This gives rise to a $3/2^-$ spin-parity. Our measured half-life for this level is consistent with the $3/2^-$ assignment, and a $M1$ 452-keV de-exciting transition, whereas for the 802-keV transition the experimental result allows for a $E2$ component.

Both 351- and 802-keV levels are fed from positive-parity high-energy levels characterized probably by proton occupation of the $g_{7/2}$, $d_{5/2}$ and $d_{3/2}$ single-particle states. The de-excitations from these high-lying states, dominated by $3/2^+$, $5/2^+$ and $7/2^+$ spins, to $3/2^-$ 351- and 802-keV states take place via $E1$ or $M2$ high energy transitions beyond 3.8 MeV. Moreover, in view of the 3.5-MeV $N = 50$ energy gap measured in 2008 for ^{81}Ga by Hakala *et al.* [Hak08] the 3858-keV transition which connects the 4209- and 351-keV levels gives an idea of the $N = 50$ energy gap from our data.

The $3/2^-$ value of the first and the second excited states calculated by the shell model is in good agreement with our lifetime measurements. In this case, the occupation probability obtained with JUN45 interaction for the first excited state indicates 51% for the mixing configuration between $\pi(p_{3/2})^1$ and $\pi(f_{5/2})^2$ and 28% for $\pi(f_{5/2})^3$. In case of the second excited state this percentages are more similar: 41% and 48%, respectively. The calculations made with jj44b shows 78% probability for $\pi(f_{5/2})^2 \otimes \pi(p_{3/2})^1$ configuration of the 351-keV state and 76% for the case of $\pi(f_{5/2})^3$ situation in 802-keV level.

Table 4.4 collects the experimentally measured reduced transition probabilities of 351-, 452- and 802-keV gammas compared to the theoretical values. The $B(M1)$ value

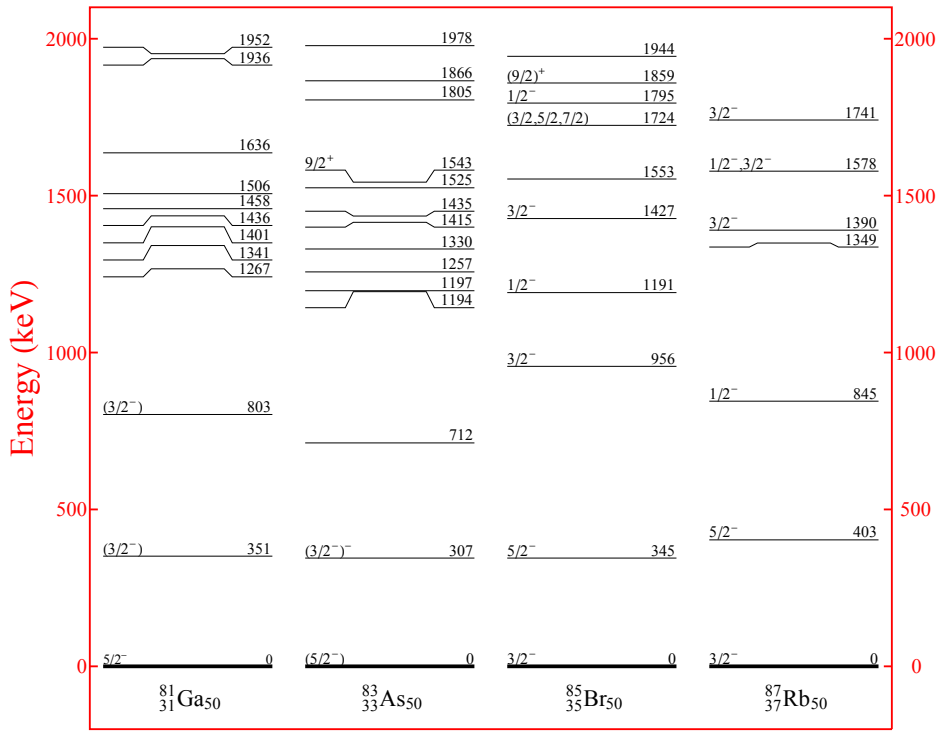

Figure 4.16: Levels of ^{81}Ga obtained in this work compared to the levels of ^{83}As, ^{85}Br and ^{87}Rb populated in the β-decay [Win88b, Sin14, Joh15].

calculated with JUN45 for the 351-keV transition is closer to the experimental value than the result obtained with jj44b which differs an order of magnitude. The $B(E2)$ value calculated with both interactions is also an order of magnitude lower than the experimental one. This fact reinforces our lifetime measurements which lead to assign 351-keV line as $M1$. Similar situation occurs with 452-keV gamma where the $B(M1)$ value is in agreement with experimental results but the $B(E2)$ does not. For 802-keV line the theoretical values are compatible with the experimental results.

Nine other excited states are experimentally found in ^{81}Ga below 2 MeV. The calculations reproduce the level density of these negative parity states. In a simplistic model where a quasiparticle is coupled to the ^{80}Zn core four states arising from the coupling of the $\pi(p_{3/2})$ to the 2^+ core in ^{80}Zn would have spins $1/2^-$, $3/2^-$, $5/2^-$, and $7/2^-$, whereas the $\pi(f_{5/2})$ coupling to the 2^+ will give rise to the 5 states with spins ranging from $1/2^-$ to $9/2^-$. This alternative description based on the $\pi(f_{5/2})^3$ cluster configuration provides a similar picture. The $\pi(f_{5/2})^3$ yields $3/2^-$, $5/2^-$ and $9/2^-$ spins, with the $9/2^-$ found at higher energies, and their couplings to the 2^+ of ^{78}Ni in this case will provide the observed levels.

A high density of levels in the region of 1 to 2 MeV can be observed as well in the level scheme of ^{83}As, with striking similarity to ^{81}Ga (see Fig. 4.17. The level scheme of ^{85}Br [Sin14] populated by the β-decay of ^{85}Se has also very similar structure. Out of these levels the 1936-keV state is strongly populated from the 4295-keV positive parity state above. We have measured a 30 ps half-life limit which does not allow to unambiguously

identify the multipolarity of the de-populating 1936- and 1586-keV transitions, but the decay pattern to the ground and first-excited level and the direct feeding from positive parity states makes a spin-parity assignment of $3/2^-$ or $5/2^-$ very likely for this state.

4.7.3 Positive parity states

As mentioned above, the lowest positive parity state is the $9/2^+$ state as predicted at energies close to 3.0 MeV and 3.3 MeV, depending on the interaction, originated from the $\pi(g_{9/2})$ orbital. This state would not be directly populated by the ^{81}Zn β-decay from a $1/2^+$ ground state and would have a limited feeding from a $5/2^+$ g.s., yielding a high logft value. The systematics near $A = 81$ suggests a long half-life for this state due to the $M2$ behaviour of the gamma line which would connect it to the $5/2^-$ ground state. No such long lifetime was observed in our measurement.

The allowed Gamow-Teller beta decay from the ^{81}Zn ground state neutron $\nu(d_{5/2})$ or $\nu(s_{1/2})$ configuration populates high-energy states in the ^{81}Ga daughter, since there are no low-lying positive parity states available. The positive states will have to arise from the coupling of the odd proton orbitals ($p_{3/2}$, $f_{5/2}$ and $p_{1/2}$) to neutron hole - neutron particle states, therefore implying the break-up of a neutron pair in the $N = 50$ shell. These cross-shell states arising from the excitation of the ^{78}Ni core will give an idea of the $N = 50$ shell gap, as discussed by Winger et al. [Win88b] in the beta-decay of ^{83}Ge to ^{83}As, and Padgett and co-workers in ^{81}Ga [Pad10].

Due to the Fermi factor, the β feeding and logft values to such states will be reduced, but they will be still favored in spite of their high energy. Several levels with low apparent logft values can be identified in the 4 – 5 MeV region. In our work we observe strong population to the 4209-, 4295-, 4369-, 4880-, 4921-, 5178-, 5422-keV levels, and some other ones at higher energies. This scenario is supported by the shell-model calculations, with several positive parity levels above 4 MeV. Assuming a $5/2^+$ g.s. state of ^{81}Zn, positive-parity assignments for these levels with 3/2, 5/3 and 7/2 spin values can be made. Identical situation can be observed in the $N = 50$ isotones ^{83}As [Win88b] and ^{85}Br [Sin14], populated respectively in the decay of ^{83}Ge and ^{85}Se (see Fig. 4.16) .

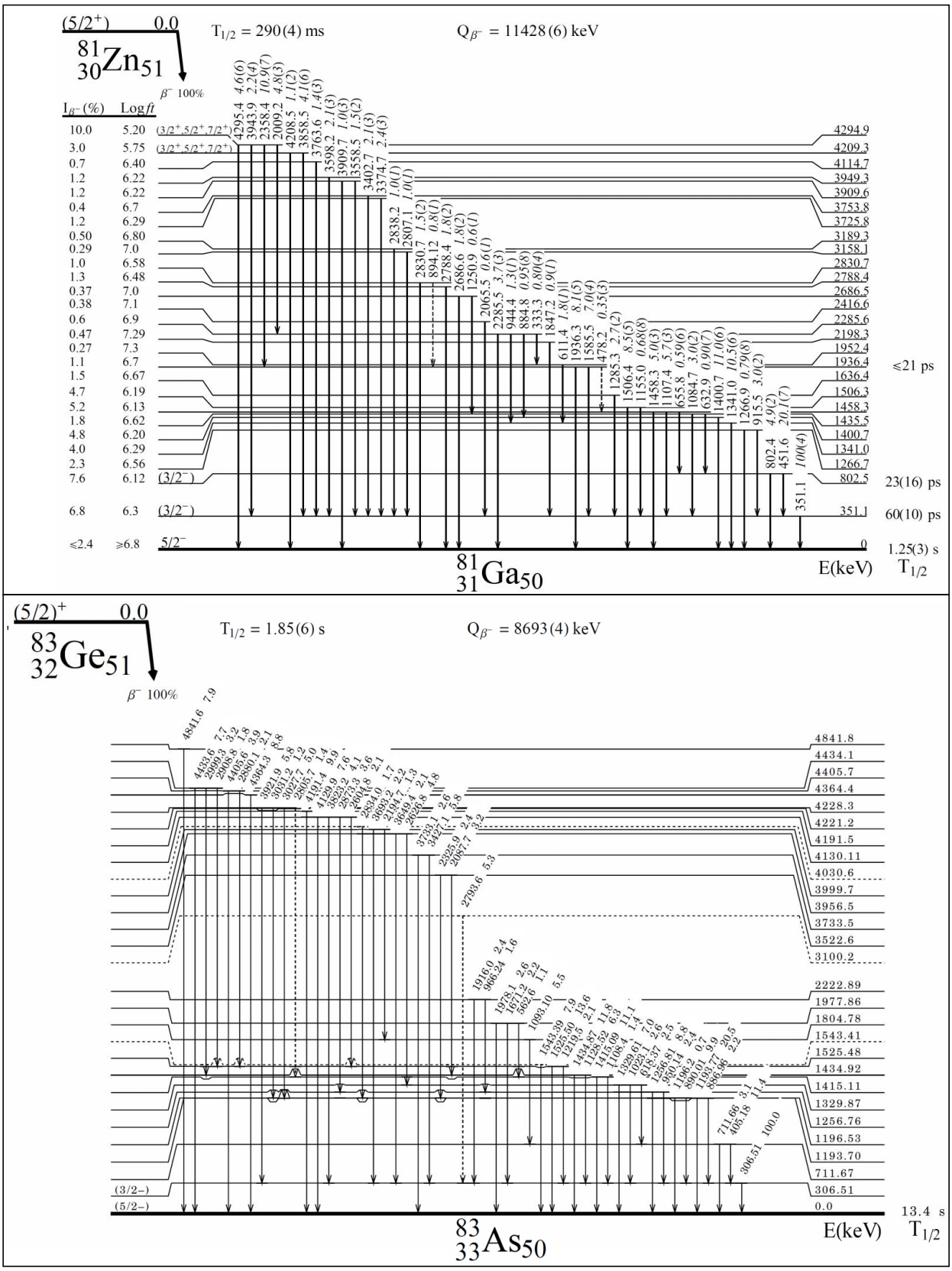

Figure 4.17: Comparison of the level scheme of $N = 50$ ^{81}Ga (up) measured in our work and the level scheme of ^{83}As isotone populated in the β-decay of ^{83}Ge [McC15].

4.8 Summary and conclusions

The high purity and intensity of Zn beams delivered by the ISOLDE facility at CERN have made it possible to obtain about ten-fold higher statistics than previous studies [Pad10]. The level scheme of the semimagic $N = 50$ nucleus ^{81}Ga has been significantly expanded with 47 new levels and 70 transitions in the energy range up to 6.5 MeV, very close to the neutron separation energy. The half-life of ^{81}Zn measured in this work is in good agreement with previous works [Pad10, Xu14]. Our measured 1.25(3) s half-life of ^{81}Ga fits to the adopted value of 1.217(5) s [Bag08].

The direct β feeding to the ^{81}Ga ground state measured in our experiment is negligible within the error bars, and much lower than proposed previously [Pad10], thus compatible with both $5/2^-$ and 1/2- assignments for the ^{81}Zn ground state. We do not observe beta nor gamma population to the the $9/2^+$ state seen in other $N = 50$ isotones and also predicted by our shell-model calculations to at around 3 MeV. We have measured the β-delayed neutron emission probability value of 23%, in agreement and more precise that 30(13) % measured by Hosmer [Hos10] and compatible with the low limit of 10 % obtained by U. Köster [Kös05].

The level scheme of ^{80}Ga populated in the β-delayed neutron emission from ^{81}Zn was built for the first time and it is in agreement with that described in [Lic14] from the β-decay of ^{80}Ga, including the low-lying 22-keV isomer. Our measurements also confirm the existence of 708-keV isomer with 18.3(13) ns half-life.

We have measured the half-life of the first excited state in ^{81}Ga to be $T_{1/2} = 60(10)$ ps, which indicates a l-forbidden $M1$ transition of 351 keV to the $5/2^-$ ground state, which points to a transition from the $\pi p_{3/2}$ to the $\pi f_{5/2}$ configuration. This is supported by our shell-model calculations, where the dominant occupations for the ground and first-excited states are found. The occupation probability and our experimental results strongly suggests the $\pi(f_{5/2})^2 \otimes \pi(p_{3/2})^1$ configuration for the first excited state of ^{81}Ga. The calculated transition rate supports this assignment too. For the second excited state a half-life of 23(16) ps is found. This value allows to obtain $B(M1)$ and $B(E2)$ (Table 4.4) reduced probabilities which together with the shell-model results allows to propose $\pi(f_{5/2})^3$ cluster configuration and $3/2^-$ spin-parity assignment for this state.

A high density of negative-parity levels can be observed in the region from 1 to 2 MeV of the level scheme of ^{81}Ga. This is consistent with $\pi(p_{3/2})$ and $\pi(f_{5/2})$ single-particle states coupling to the 2^+ core in ^{80}Zn, and it is well reproduced by the shell-model calculations. These states will be of negative parity and should be populated by first-forbidden β transitions. The level scheme of the $N = 50$ isotone ^{83}As [Win88b] also shows a similar high density around 1400 keV and it is much like ^{81}Ga. A similar structure is found in the $N = 50$ $Z = 35$ ^{85}Br nucleus populated by the β-decay of ^{85}Se [Sin14].

The situation changes beyond 5 MeV where we observe several states with sizeable apparent β feeding, which should arise from allowed transitions from the ^{81}Zn positive-parity ground sate. These levels of positive parity are confirmed by theoretical calculations made with JUN45 and jj44b effective interactions. They can be interpreted as neutron particle-hole excitations from the ^{78}Ni core.

Chapter 5

Nuclear structure of ^{81}Ge

The $N = 49$, $Z = 32$ Ge was populated from the β-decay of ^{81}Ga which was obtained from the β-decay of ^{81}Zn produced at ISOLDE. The properties of low-lying structure of ^{81}Ge may play a role in the r-process calculations since this is one of the nuclei that can affect the final abundance pattern. As ^{81}Ga is believed to be in r-process path [Mat85] its decay properties such as half-life and the β-delayed neutron emission probability play an important role in abundances calculations of ^{81}Ga. Moreover, theoretical simulations performed by Surman *et al.* [Sur13] indicate that the increase of capture rate of ^{81}Ge by a factor of 100 produces a change of more than 15% in the final abundance pattern in r-process.

Furthermore, the spin-parity assignments are crucial for understanding the shape coexistence of $N = 49$ isotones, where the systematic evolution of the low-lying $1/2^-$ isomer is apparently broken when comes to ^{81}Ge. The previously-known level scheme has been extended in our work with several new γ transitions and energy levels. By gating on the ^{81}Ge strongest gamma, we were able to measure the ^{81}Ga ground state half-life. For the first time we obtained a precise value for the half-lives of the first and second excited states in ^{81}Ge. This has allowed to confirm the spin-parity assignment of the 711-keV intruder. New half-lives of 1724- and 1832-keV levels were also measured. The determination of $B(XL)$ values of the γ transitions that depopulate these states opens the way to discuss the credibility of the $1/2^+$ assignment for 679-keV isomer.

5.1 Previous information about ^{81}Ge and considerations on the systematics

The spherical shell-model picture from Fig. 1.5 for $N = 49$ ^{81}Ge strongly suggests the $g_{9/2}$ ground state due to the unpaired neutron. The excited states will be dominated by neutron excitation to $g_{7/2}$, $d_{5/2}$, $d_{3/2}$ or $s_{1/2}$ providing $7/2^+$, $5/2^+$, $3/2^-$ and $1/2^+$ states and hole excitation to $p_{1/2}$ and $f_{5/2}$ leading to $1/2^-$ and $5/2^-$ spin-parities. No strong deformation is expected in this case because ^{81}Ge is very close to ^{78}Ni. The excitation of protons from $f_{5/2}$ or their interaction with neutrons from $g_{9/2}$ can provide an additional information to explain the spin-parity assignments in ^{81}Ge.

The first and the most complete study of ^{81}Ge was performed by P. Hoff and B. Fogelberg in 1981 [Hof81] via the β-decay of ^{81}Ga which was produced at the OSIRIS fission product mass separator. The decay scheme of the ^{81}Ga, whose 1.23(1) s half-life

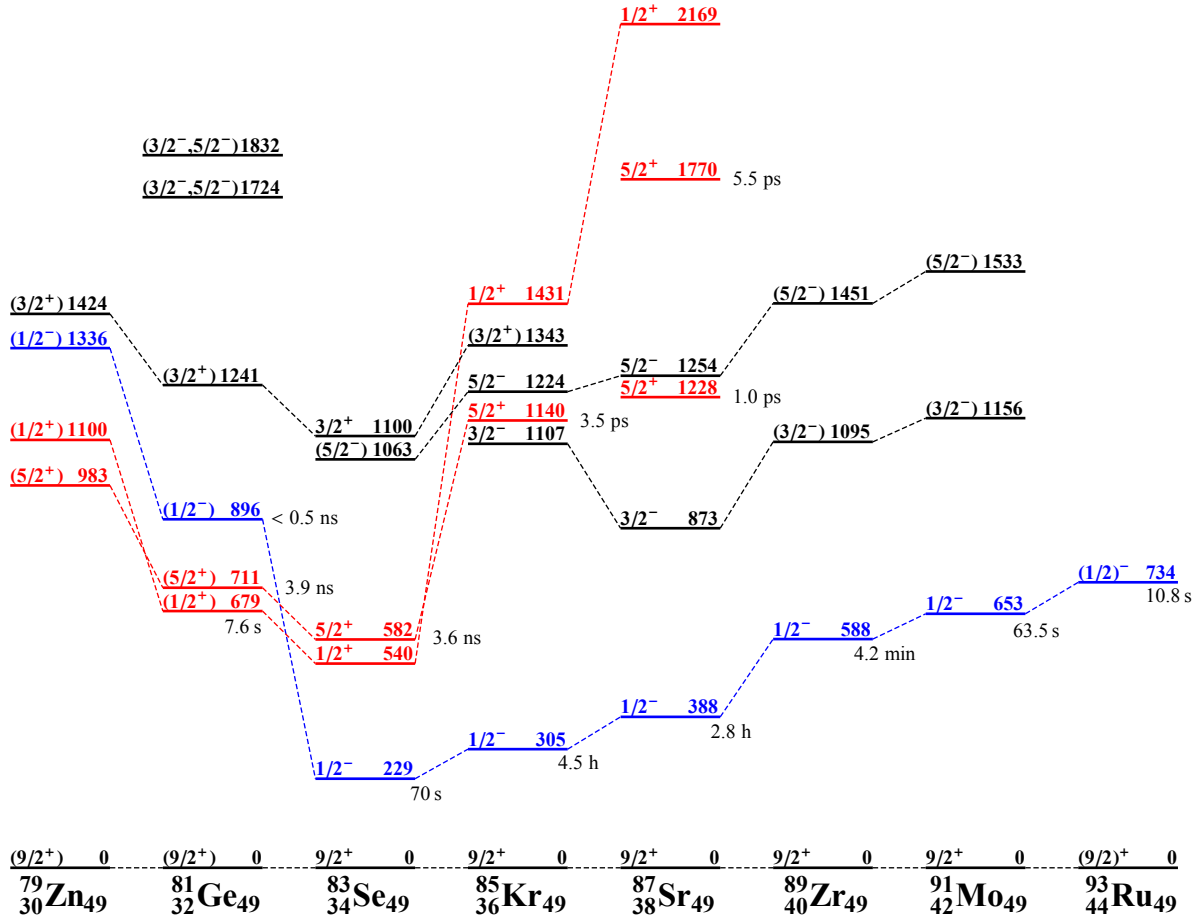

Figure 5.1: Level systematics for the odd-mass $N = 49$ isotones. The low-lying isomers are marked with blue colour while the levels marked with red colour correspond to the $1/2^+$ and $5/2^+$ intruders [Orl15, Hof81, McC15, Mey82, Hur75, Joh15, Kaw92, Kaw90, Lan76]. The long-lived $1/2^-$ states, characterized by single-particle $p_{1/2}$ configuration, change drastically the systematic evolution in ^{81}Ge. A pair of intruder states was observed in nuclei with $Z < 40$ starting from ^{87}Sr and are created by one-particle two-hole interaction between excited neutron and two $g_{9/2}$ holes giving $1/2^+$ and $5/2^+$ states.

was already measured in 1976 [Rud76], was built for the first time. It included 96 γ-rays that de-excite 36 energy levels extending up to 4.5 MeV. The authors did not find any indication for more than one β-decaying state in ^{81}Ga. This fact was also confirmed with our measurements in the previous chapter of this thesis. The J^π of the ^{81}Ga ground state has been measured to be $5/2^-$ [Che10].

A β-decaying isomer was observed in ^{81}Ge at 679-keV with no γ-ray branching. Its half-life was quoted to be 7.6(6) s, equal to the half-life of the ground state, which could not be distinguished from the isomeric one. The systematics of the odd-mass $N = 49$ isotones shown in Fig. 5.1 strongly suggests a $9/2^+$ assignment for the ground state and $1/2^-$ for the 679-keV isomer. However, the authors decided to assign $1/2^+$ for this state due to the lower limit of the partial half-life of the isomeric transition which resulted more than an order of magnitude higher than expected form the $M4$ transitions in the other isotones. Other indirect evidences are the measured $E1$ multipolarity for the 216-keV γ

line which connect the 896-keV and 679-keV states [Hof81], and a weak β population of the $1/2^+$ state in ^{83}As. Some additional arguments were given based on the levels of ^{81}As populated in the β-decay of ^{81}Ge from the ground state and the 679-keV isomeric state. The first one is the weak population of the $1/2^-$ excited state of ^{77,79}As from the $1/2^-$ isomeric states in ^{77,79}Ge. This is in contrast to the measured β feeding of the assumed $1/2^-$ 93-keV level of ^{81}As and thus indicates different nature of the low-lying isomer of ^{81}Ge.

A doublet of states strongly populated in the β-decay was discovered at 1724 and 1832 keV, both decaying by the strong 828- and 936-keV γ transitions to the 896-keV level whose spin is $1/2^-$. A 3.9(2)-ns isomer lying at 711 keV was considered as the intruder state with 1p-2h configuration at $d_{5/2}$ and de-excited to the g.s. by an almost pure E2 transition. Similar situation occurs in ^{83}Se [Mey82]. As both of them lie around 700 keV and the $N = 50$ shell gap for Ge isotopes was measured to be 3.15 MeV [Hak08] we can assume that the $Z = 40$ becomes stronger in this region blocking protons to reach $N = 50$. The decay properties of the states at 1286, 1303 and 1548 keV strongly suggest that they arise from the coupling of $g_{9/2}$ quasi-particle to a phonon. The 1303-keV one, with small β-feeding, was assigned tentatively $9/2^+$ and the other two states may have either $5/2^+$ or $7/2^+$ spin-parity.

A recent investigation of the structure of ^{81}Ge was performed from the ^{80}Ge$(d,p)^{81}$Ge transfer reaction via inverse kinematics at the Holifield Radioactive Ion Beam Facility at Oak Ridge National Laboratory in 2011. The results are summarized in the PhD thesis of Sunghoon Ahn published in 2013 [Ahn13]. The author confirms the existence of the doublet of $1/2^+$ and $5/2^+$ intruder states at 679 and 711 keV respectively assigning a spin-parity $1/2^-$ to the 896-keV level.

5.2 Level scheme of ^{81}Ge

The aim of our work is to verify the assumptions about the spin-parity assignments to the 679-, 711- and 896-keV states by determining the precise values not only of these levels but also of higher energy states connected to them by intense γ lines whose $B(XL)$ is expected to be measured in an experiment. We do not count on large improvements of the level scheme of ^{81}Ge as the production yield of ^{81}Ga in our experiment was very similar to that obtained by P. Hoff and B. Fogelberg in 1981 at OSIRIS.

The identification of γ transitions that belong to ^{81}Ge was mainly based on the $\gamma\gamma$ coincidences. As many of these transitions were already known our task was to confirm their existence and explore the possibility to find new γ lines in coincidence with the known ones. The analysis of γ lines was performed after the data presorting which consisted in constructing coincidences between the two HPGe and the β detector. This allows eliminating the background activity, including that coming from the β-decay of ^{81}Rb to ^{81}Kr. Only events from HPGe in coincidence with the β detector within 20 μs were recorded in the presorting. In this way, the multi-parameter data set was obtained. It consisted of the energy of events from the HPGe, energy of events from the β detector and the time elapsed between the event and the last proton pulse. Some additional parameters as the proton pattern (used in half-life determination of ^{81}Ga) and the time difference between events from HPGe and β detectors (employed for subtraction of random events) were included as well. The details were given in Chapter 3

Unlike ^{81}Ga, no longer lived activity was subtracted to obtain a pure spectrum of ^{81}Ge, because in this case we were losing information when weak peaks were over-subtracted. Figure 5.2 shows summed energy spectrum from both HPGe detectors in coincidence with β. All strong lines observed by P. Hoff and B. Fogelberg can be identified. The most intense peaks from ^{81}Ge are marked in the plot. The energies and relative intensities of all γ-rays can be found in Tab. 5.1. The last column indicates transitions seen in $\gamma\gamma$ coincidences with a given γ-ray. In case of mixed peaks the relative intensity and energy values were obtained from the $\gamma\gamma$ coincidences as explained in Sec. 3.5.2 Eq. 3.3. This generally increases the error bars.

E_γ(keV)	$E_{in.level}$ (keV)	$E_{fin.level}$ (keV)	I_γ (%)[a]	γ-γ
212.1[b] ***5***	1935.8 *5*	1723.7 *2*	0.4 *1*	216,828
216.5 ***1***	895.5 *2*	679.0 *2*	100 *4*	212, 644, 731, 776
				805, 828, 865, 920, 937
				991, 1164, 1189, 1273, 1406
				1605, 1615, 1633, 1668, 1713
				1779, 1941, 2049, 2095, 2126
				2181, 2312, 2336, 2444, 2542
				2554, 3273
256.7 ***2***	1805.1 *2*	1548.6 *1*	0.9 *2*	
262.3 ***4***	1548.6 *1*	1286.4 *1*	0.5 *1*	
357.8[b] ***6***	2081.5 *6*	1723.7 *2*	0.4 *1*	216, 828
437.3 ***5***	1723.7 *2*	1286.4 *1*	0.5 *1*	1286
482.2 ***2***	1723.7 *2*	1241.4 *1*	5.4 *10*	530, 562, 711, 1273, 2444, 1713
501.6 ***2***	1805.1 *2*	1303.3 *2*	0.5 *1*	
530.2 ***1***	1241.4 *1*	711.3 *1*	10.5 *1*	482, 575, 614, 626, 711, 806
				867, 933, 1273, 1713, 1091
562.5 ***3***	1241.4 *1*	679.0 *3*	2.2 *2*	482, 575, 1273, 1713
575.0 ***2***	1816.3 *2*	1241.4 *1*	2.4 *2*	530, 711
613.8 ***3***	1855.3 *2*	1241.4 *1*	0.6 *2*	
626.5 ***2***	2175.0 *2*	1548.6 *1*	0.2 *1*	
643.9[b] ***6***	2367.6 *7*	1723.7 *2*	0.7 *2*	216, 828
698.8 ***1***	1410.1 *1*	711.3 *1*	4.4 *3*	711, 728, 1874
711.3 ***1***	711.25 *4*	0.0	44.9 *1.8*	482, 530, 575, 614, 699
				728, 876, 933, 963, 1002
				1020, 1091, 1105, 1144, 1273
				1713, 1779, 1796, 1853, 1874
				1951, 2042, 2283, 2379, 2726

Continued on next page

Table 5.1 – *Continued*

E_γ(keV)	$E_{in.level}$ (keV)	$E_{fin.level}$ (keV)	I_γ (%)[a]	γ-γ
				2772, 2792, 2954, 3061
728.0 *6*	2138.3 *1*	1410.1 *2*	0.4 *1*	699, 711
730.9 *2*	2563.5 *3*	1832.1 *4*	1.0 *2*	216, 936
776.1 *2*	3772.7 *1*	2996.5 *2*	2.3 *2*	216, 828, 1164, 1273
805.5 *2*	2529.1 *2*	1723.7 *2*	1.0 *1*	
828.2 *1*	1723.7 *2*	895.4 *4*	54.4 *20*	212, 216, 358, 644, 776
				806, 1273, 1406, 1713, 1779
				2049, 2095, 2444
864.5[b] *3*	1759.9 *5*	895.4 *4*	1.4 *2*	711
866.8[b] *4*	2108.3 *4*	1241.4 *1*	0.7 *3*	351
875.9[b] *2*	1587.2 *2*	711.3 *1*	0.6 *2*	711
920.4 *3*	1816.3 *2*	895.4 *4*	0.4 *1*	
933.1 *4*	2175.0 *2*	1241.4 *1*	0.23 *7*	
936.7 *1*	1832.1 *4*	895.4 *4*	22.4 *13*	216, 731, 1164, 1189, 1605
				1941, 2181, 2336
962.8 *5*	2693.5 *4*	1730.9 *2*	0.5 *2*	
991.3 *3*	4012.9 *2*	3021.3 *3*	0.5 *3*	216
1002.4[b] *4*	1713.7 *4*	711.3 *1*	1.0 *3*	711
1016.7 *5*	4012.9 *2*	2996.5 *2*	1.4 *4*	216, 828, 1273
1019.7 *2*	1730.9 *2*	711.3 *1*	5.9 *4*	711, 963, 2042, 2283
1045.1[b] *2*	1723.7 *2*	679.0 *3*	1.8 *2*	
1083.8 *4*	3503.2 *1*	2420.0 *3*	2.3 *11*	1117, 1303
1090.9[b] *5*	2332.4 *5*	1241.4 *1*	0.5 *1*	530
1105.3 *6*	1816.3 *2*	711.3 *1*	1.4 *3*	711
1116.7 *4*	2420.0 *3*	1303.3 *2*	3.1 *3*	1084, 1303, 1353
1137.2 *3*	1816.3 *2*	679.0 *3*	2.2 *2*	1956
1143.8 *3*	1855.3 *2*	711.3 *1*	1.8 *4*	711
1164.4 *2*	2996.5 *2*	1832.1 *4*	3.1 *3*	216, 776, 936
1176.7[b] *4*	1855.3 *2*	679.0 *3*	1.0 *2*	
1189.2 *2*	3021.3 *3*	1832.1 *4*	1.5 *2*	
1272.8 *4*	2996.5 *2*	1723.7 *2*	15.5 *9*	216, 482, 530, 776, 828
				1017, 1045
1286.4 *1*	1286.4 *1*	0.0	15.6 *10*	262, 1710, 2379

Continued on next page

Table 5.1 – *Continued*

E_γ(keV)	$E_{in.level}$ (keV)	$E_{fin.level}$ (keV)	I_γ (%)[a]	γ-γ
1303.3 *2*	1303.3 *2*	0.0	4.6 *4*	502, 1117, 1353
1352.8 *3*	3772.7 *1*	2420.0 *3*	2.9 *3*	1117, 1303
1405.7 *2*	3129.4 *2*	1723.7 *2*	1.8 *5*	216, 828
1548.6 *1*	1548.6 *1*	0.0	11.6 *7*	257, 626, 1956, 2273, 2464
1605.1 *4*	3437.1 *2*	1832.1 *4*	2.1 *3*	216, 936
1615.1[b] *5*	2510.5 *6*	895.4 *4*	0.5 *1*	
1633.5 *3*	2529.1 *2*	895.4 *4*	1.2 *2*	216
1668.1 *3*	2563.5 *3*	895.4 *4*	1.9 *3*	
1672.2 *3*	3503.2 *1*	1832.1 *4*	0.4 *1*	
1687.0[b] *5*	3503.2 *1*	1816.3 *2*	0.4 *1*	574, 711
1710.0 *2*	2996.5 *2*	1286.4 *1*	2.7 *5*	1286
1713.2 *2*	3437.1 *2*	1723.7 *2*	8.5 *6*	216, 482, 530, 562, 711, 828
1730.9 *5*	1730.9 *2*	0.0	1.3 *2*	
1779.3 *2*	3503.2 *1*	1723.7 *2*	3.4 *3*	216, 530, 711, 828
1796.1[b] *9*	2507.3 *9*	711.3 *1*	0.3 *1*	711
1805.0 *4*	1805.1 *2*	0.0	2.1 *2*	
1853.2 *6*	2563.5 *3*	711.3 *1*	0.7 *2*	
1874.3 *3*	4012.9 *2*	2138.3 *3*	2.7 *3*	
1941.0 *7*	3772.7 *1*	1832.1 *4*	1.0 *5*	216, 936
1950.6[b] *5*	2661.9 *4*	711.3 *1*	0.8 *2*	711
1955.6 *5*	3503.2 *1*	1548.6 *1*	1.4 *5*	1549
1955.6 *5*	3772.7 *1*	1816.3 *2*	0.9 *4*	
1982.0 *5*	2693.5 *4*	351.1 *1*	0.9 *2*	
2041.6 *4*	3772.7 *1*	1730.9 *2*	1.9 *3*	
2048.9 *5*	3772.7 *1*	1723.7 *2*	1.7 *7*	
2095.2 *5*	3819.5 *5*	1723.7 *2*	1.6 *2*	
2116.3 *7*	3665.3 *2*	1548.6 *1*	1.5 *3*	
2125.8 *3*	3021.3 *3*	895.4 *4*	3.1 *3*	
2138.4 *4*	2138.3 *1*	0.0	2.1 *3*	
2180.7 *2*	4012.9 *2*	1832.1 *4*	4.9 *4*	216, 936
2216.4 *3*	3503.2 *1*	1286.4 *1*	1.1 *2*	
2272.3 *8*	3819.5 *5*	1548.6 *1*	2.0 *3*	
2282.8 *4*	4012.9 *2*	1730.9 *2*	1.0 *4*	

Continued on next page

Table 5.1 – *Continued*

E_γ(keV)	$E_{in.level}$ (keV)	$E_{fin.level}$ (keV)	I_γ (%)[a]	γ-γ
2289.8 *5*	4012.9 *2*	1723.7 *2*	0.8 *2*	
2311.8 *10*	4035.0 *4*	1723.7 *2*	1.7 *3*	
2336.3 *4*	4167.9 *2*	1832.1 *4*	1.5 *2*	
2378.9 *3*	3665.3 *2*	1286.4 *1*	4.6 *21*	1286
2420.0 *4*	2420.0 *3*	0.0 *1*	2.7 *3*	
2444.1 *2*	4167.9 *2*	1723.7 *2*	12.7 *8*	216, 482, 711, 828
2464.1 *5*	4012.9 *2*	1548.6 *1*	2.8 *3*	
2542.0 *4*	3437.1 *2*	895.4 *4*	4.2 *4*	
2549.6 *4*	2549.6 *4*	0.0	2.7 *3*	
2553.6 *7*	4277.3 *7*	1723.7 *2*	1.4 *3*	
2725.9 *4*	3437.1 *2*	711.3 *1*	4.0 *4*	
2772.1 *4*	4012.9 *2*	1241.4 *1*	0.8 *2*	
2791.9 *4*	3503.2 *1*	679.0 *3*	2.3 *8*	
2881.3 *5*	4167.9 *2*	1286.4 *1*	1.3 *2*	
2926.1 *4*	4167.9 *2*	1241.4 *1*	0.6 *2*	
2954.3 *4*	3665.3 *2*	711.3 *1*	3.5 *3*	711
2986.1 *5*	3697.4 *3*	711.3 *1*	1.2 *3*	711
3061.2[b] *7*	3772.7 *1*	711.3 *1*	1.0 *2*	711
3272.6 *4*	4167.9 *2*	895.4 *4*	2.1 *3*	
3489.6 *7*	4167.9 *2*	679.0 *3*	1.8 *4*	
3503.0 *3*	3503.2 *1*	0.0	9.6 *10*	
3665.2 *3*	3665.3 *2*	0.0	5.3 *9*	
3697.4 *5*	3697.4 *3*	0.0	2.6 *4*	
3773.4 *5*	3772.7 *1*	0.0	2.2 *4*	
4034.9 *4*	4035.0 *4*	0.0	6.4 *8*	
4470.4 *12*	4470.4 *12*	0.0	2.7 *4*	

Table 5.1: All γ transitions from ^{81}Ge observed in coincidence with their relative intensities. The second and the third columns shows the initial and the final energy level. The last column contains the γ transitions seen in coincidences with the initial one.

[a] For absolute intensity per 100 decays, multiply by 0.352(30) (see text for details)).

[b] New γ transitions not observed in [Hof81].

The construction of the level scheme was based on the Fig. 9 from [Hof81]. All

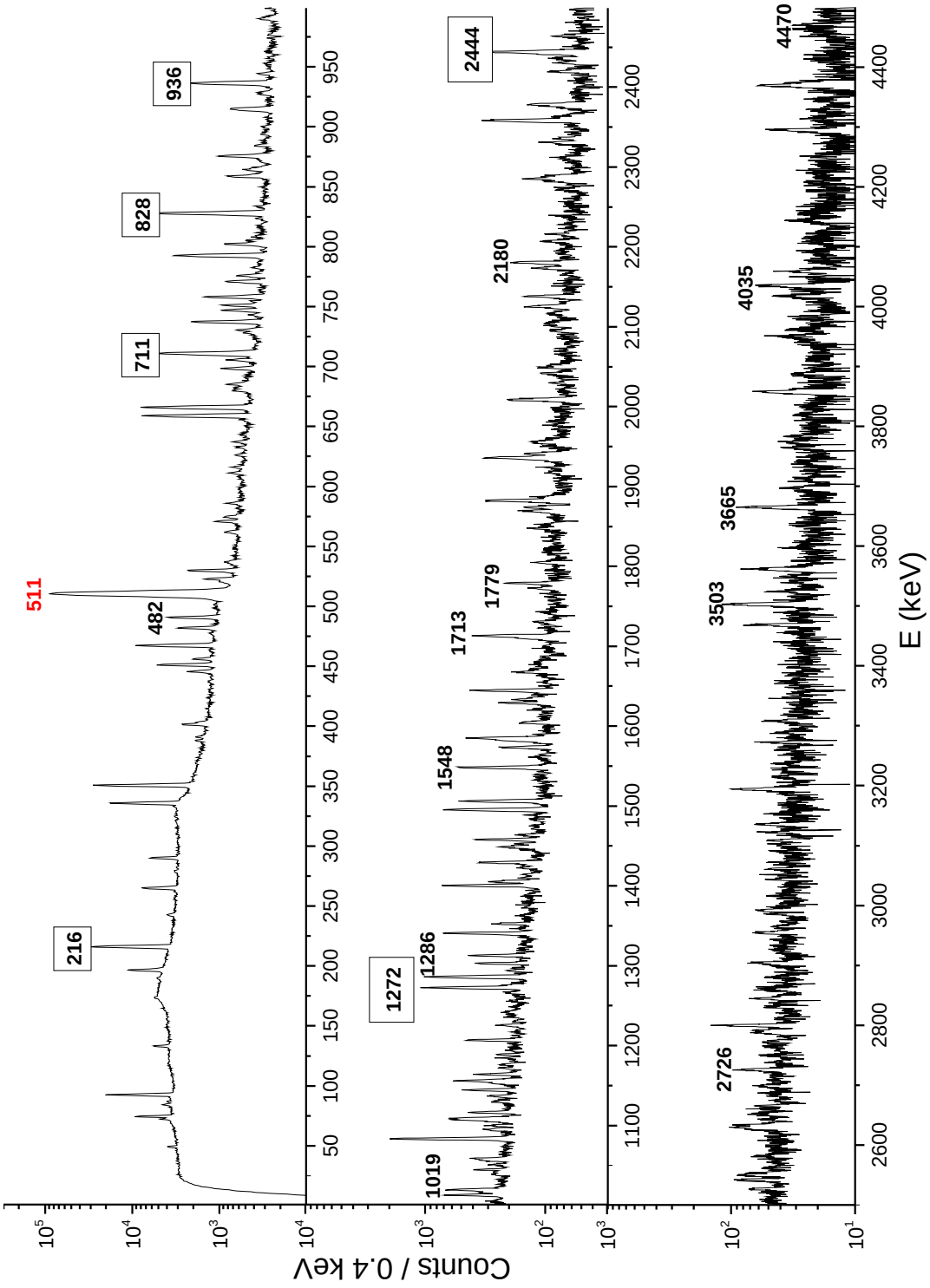

Figure 5.2: β-gated γ spectrum of the decay chain of ^{81}Zn. The most intense peaks from the decay of ^{81}Ga to ^{81}Ge are shown.

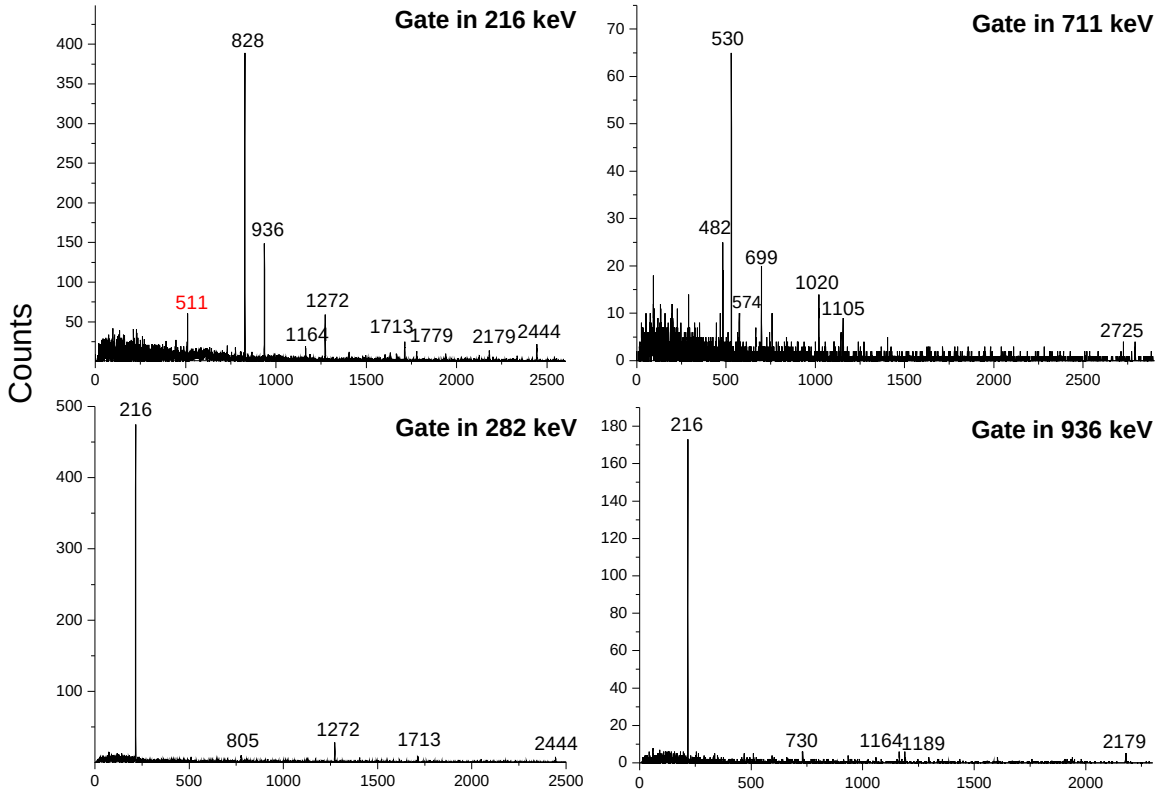

Figure 5.3: Energy spectrum of γ lines seen in $\gamma\gamma$ coincidences with the strongest transitions of 216, 711, 828 and 936 keV.

previously observed γ transitions were confirmed with our $\gamma\gamma$ coincidences. For this analysis a 3-parameter data set was sorted out containing the energies from HPGe detectors and time since last proton impinged on the target. The coincidence window between events from the germanium detectors was set to 8 μs. Fig. 5.3 contains the $\gamma\gamma$ coincident spectra. The energy gates were set on four of the most intense transitions (216, 711, 828 and 936 keV) in one HPGe and projected into another.

Once the $\gamma\gamma$ analysis was finished we placed all the γ lines into the decay scheme which was split in two parts. The low-energy part is plotted in Fig. 5.4. It collects the low-lying levels up to 1.8 MeV. The strongest γ-rays were placed de-exciting the states of the same energy. The level scheme from Fig. 5.5 contains the rest of energy levels with their de-exciting gammas. The highest level was found at 4.5 MeV, close to the 4828-MeV neutron separation energy [Aud12b]. Most of the transitions were already discovered by P. Hoff and Fogelberg [Hof81]. However, some new γ-rays were observed for the first time. Almost all of them were seen in coincidence with the strongest 216-, 711- and 828-keV lines and are marked in red. In the case of the 1045-, 1177-, 1687- and 3061-keV γ-rays the de-excited level was already measured and they were simply added to the scheme. The situation with the rest of new gammas is different as they do not de-excite any previously measured state and we have placed them tentatively depopulating a new energy level. In total, 15 new γ transitions and 11 new energy levels were added to the extended level scheme.

The population of levels in ^{81}Ge occurs directly from the ground state of ^{81}Ga whose spin-parity value was experimentally determined to be $5/2^-$ [Che10]. Even though it has

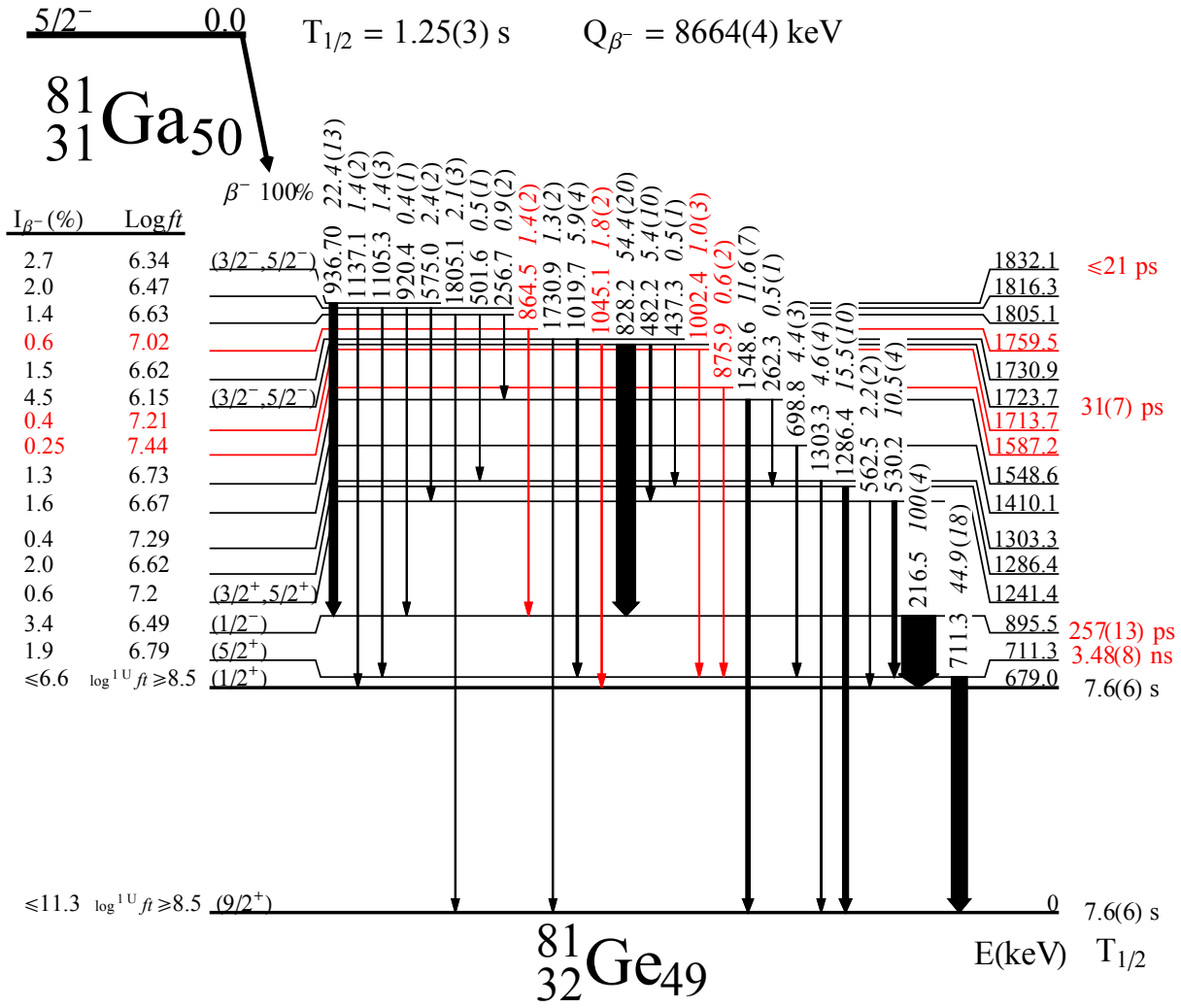

Figure 5.4: Low-energy level scheme of ^{81}Ge populated in the β-decay of ^{81}Ge. All previously known results were plotted in black, while the new γ transitions and energy levels appear in red. The half-life values are from our work.

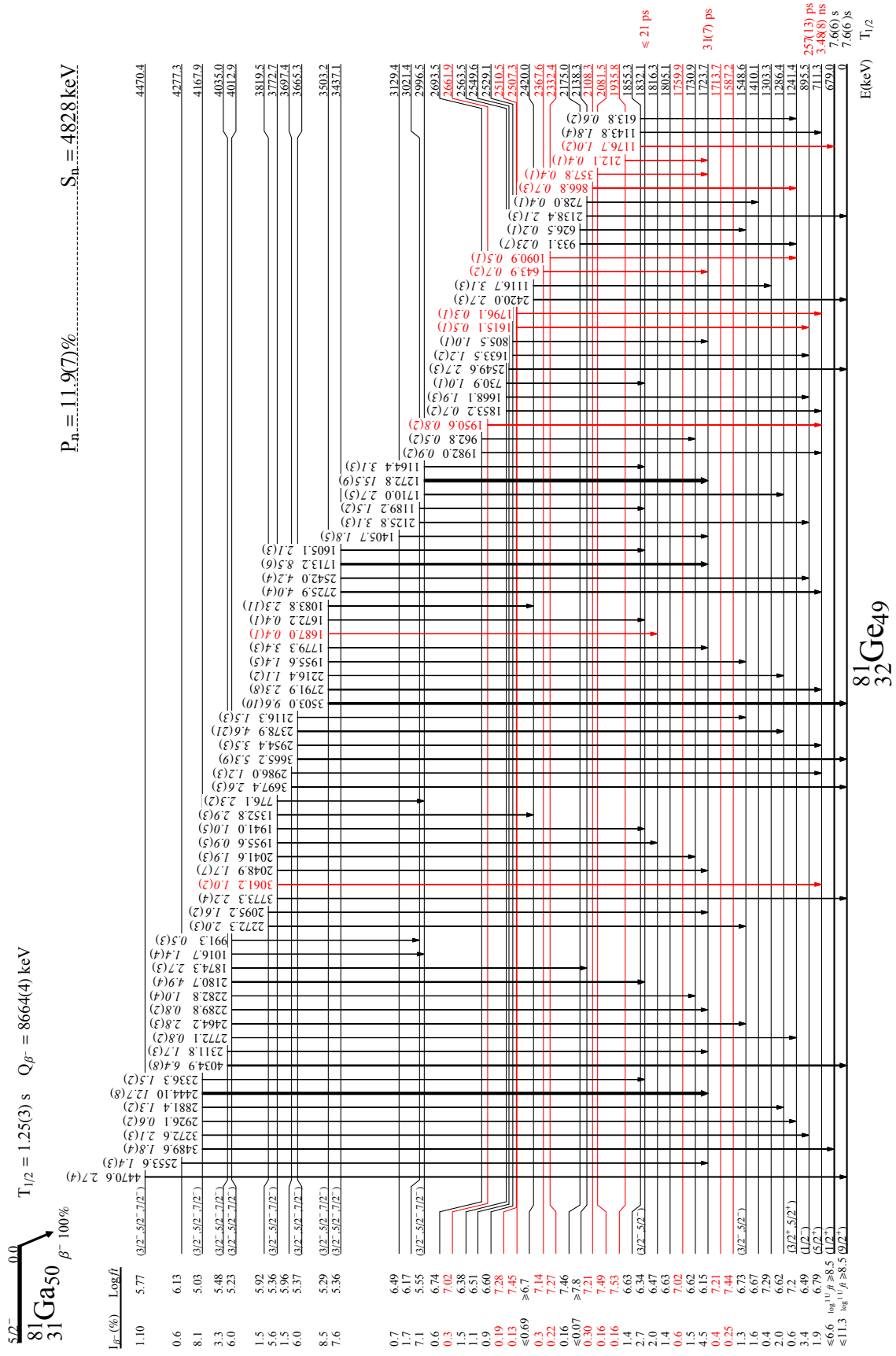

Figure 5.5: High-energy level scheme of ^{81}Ge populated in the β-decay of ^{81}Ge. All previously known results were plotted in black, while the new γ transitions and energy levels appear in red. Note that states up to the 1832-keV one are not drawn to scale.

not been directly measured, the most likely assignment for the ground state of ^{81}Ge is $9/2^+$. This is well supported by systematics and shell-model calculations. This state is characterized by a hole in the $1g_{9/2}$ orbit in the spherical shell-model picture. Thus, the β transition that connects both ground states should be the unique first forbidden and it is reasonable to establish a lower limit of $\log^{1U}ft$ of 8.5. This is in agreement with the latest review of logft values from many β-decays [Sin98]. This $\log^{1U}ft = 8.5$ corresponds to an upper limit of 11.3% for the β feeding of ^{81}Ge ground state. In case of the 679-keV isomer feeding the situation is more difficult, since the parity of the state is not clear at all. In any case, whether it is $1/2^+$ or $1/2^-$, so it implies the first forbidden unique or second forbidden β transition from the ground state of ^{81}Ga, the assumption of the 8.5 lower limit for $\log^{1U}ft$ is also acceptable here. This yields an upper limit of 6.6% for the β feeding upper limit of the isomer.

The relative intensities of γ transitions were computed by correcting the area of the peak with the efficiency as was explained in Eq. 3.4. The final values presented in the level scheme were obtained by normalizing all the intensity to the strongest 216-keV transition. The β feeding of each level was computed by subtracting the total γ intensity (in relative units) that feeds the level to the total γ intensity that depopulates it. For the absolute β intensity calculation we made use of the limits of the ground state and 679-keV isomer explained above. The absolute γ intensity was determined with the following normalization equation:

$$I_{\gamma}^{Ge}{}_{gs} + I_{\gamma}^{Ge}{}_{679} = 100 - I_{\beta n}^{Ga}(\%) - I_{\beta,gs}^{Ge}(\%) - I_{\beta,679}^{Ge}(\%), \tag{5.1}$$

which describes the balance between the relative γ intensity that feeds the ground state of ^{81}Ge and its 679-keV isomer and the β intensity distributed between the rest of the states. Considering 100 decays from the parent ^{81}Ga, the total β intensity should be shared between feeding the states in ^{81}Ge and feeding the states in ^{80}Ge via β-delayed neutron emission, whose probability of 11.9(7)% was also measured by P. Hoff and B. Fogelberg in the same experiment at OSIRIS. Adopting absolute intensities $I_{\beta,gs}^{Ge} = 5.7(56)\%$ and $I_{\beta,679}^{Ge}(\%) = 3.3(33)$ the normalization equation converts into:

$$I_{\gamma}^{Ge}{}_{gs} + I_{\gamma}^{Ge}{}_{679} = 79.2(65)\%. \tag{5.2}$$

The total relative γ intensity (given in arbitrary units normalized to the 216-keV line) that feeds the ground state and the 679-keV isomer measured in our experiment is 225(5). Therefore, the normalization factor to convert the arbitrary units into the absolute ones is 0.352(30), in good agreement with the 0.367(24) value adopted in Nuclear Data Sheets for $A = 81$ [Bag08].

Once the absolute β intensity is determined, the computation of logft values for each state can be performed. The $Q_\beta = 8664(4)$ keV needed for this purpose was taken from the latest Atomic Mass Evaluation [Aud12a]. The calculations were done with Logft stand-alone package from National Nuclear Data Center of Brookhaven National Laboratory [1]. The obtained values together with β feeding percentages were placed in the left hand side of the level schemes in Fig 5.4 and Fig 5.5. A very interesting group of states of low logft values is observed beyond 3 MeV (see Fig. 5.5). According to the

[1] www.nndc.bnl.gov/logft/

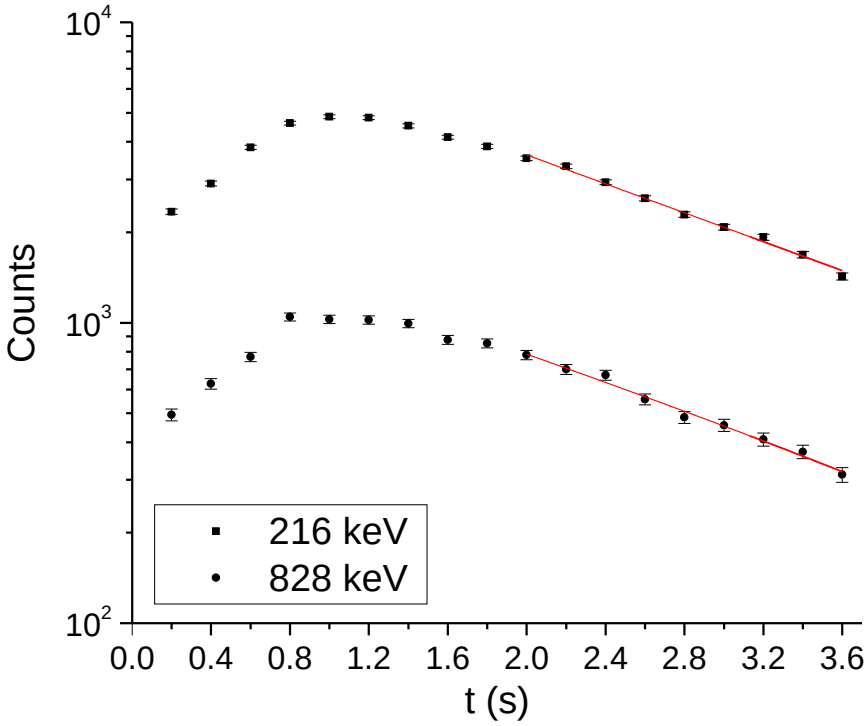

Figure 5.6: Determination of the half-life of ^{81}Ga from the fitting to the time spectra obtained by gating in 216- and 828-keV γ-ray.

β-decay selection rules these levels can be populated by allowed transitions giving possible spin-parity assignments of $3/2^-$, $5/2^-$ and $7/2^-$.

5.2.1 Half-life of ^{81}Ga

The two-parameter data set employed in the β-gated analysis was also used for the measurement of the β-decay half-life of ^{81}Ga. In this case we used the proton pattern parameter for the data sorting in order to exclude the consecutive pulses and those separated by 2.4 s. The energy gates in HPGe were set in 216- and 828-keV γ transitions and projected into the time elapsed since the last proton pulse impinged on the target. In order to increase statistics the time spectra from both HPGe detectors were added. As already mentioned, the beam gate was closed 600 ms after proton impact on target and the produced isotopes of ^{81}Zn were freely left to decay. After ^{81}Zn has decayed the decay of ^{81}Ga to ^{81}Ge was dominating. A fit to a single exponential decay plus a constant was performed in order to obtain the half-life of ^{81}Ga. Figure 5.6 shows the resulting fitted curves in logarithmic scale. As can be seen, the starting point of the fitting was established at 2.0 seconds, 1.4 seconds after the beam gated was closed and after ~ 7 half-lives of ^{81}Zn, which has practically disappeared. The weighted average value extracted from the 216-keV and 828-keV projections leads to $T_{1/2} = 1.25(3)$ s half-life of ^{81}Ga, which is consistent with adopted half-life of 1.217(5) s from [Bag08].

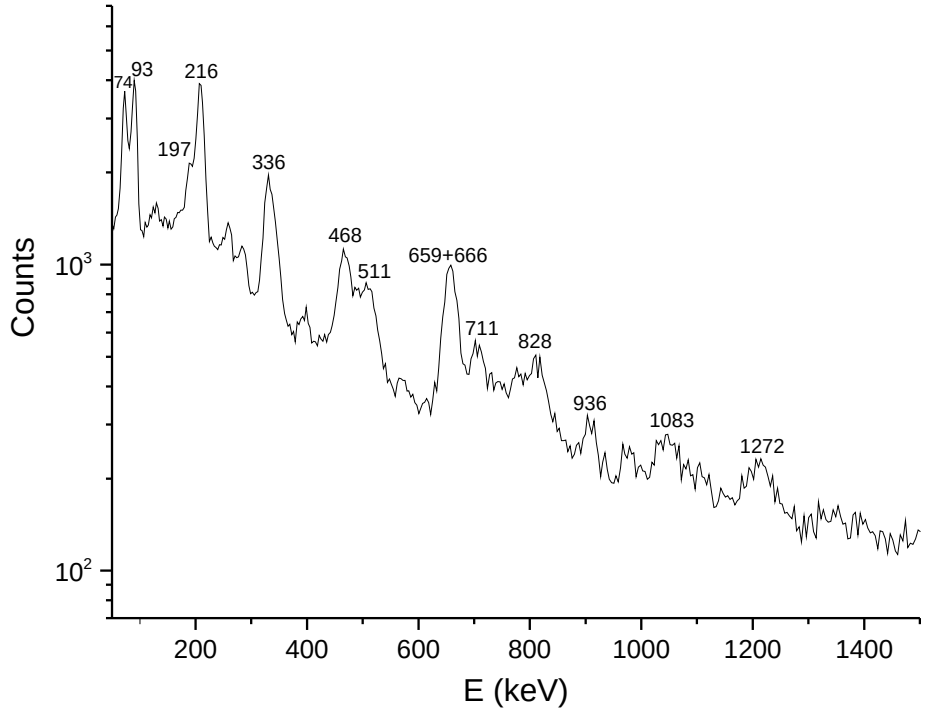

Figure 5.7: Energy spectrum of $LaBr_3$(Ce) in coincidence with β and FTAC. The first 1200 ms in the time since last proton were excluded in the sorting in order to avoid peaks from short-lived activity.

5.3 Fast Timing measurements

The recommended upper limit of 0.5 ns for the 896-keV state half-life [Bag08] opens the way to perform a deeper investigation in order to determine a more precise value with the ATD $\beta\gamma\gamma$ method [Mac89, Mos89]. In particular, the deconvolution method explained in Chapter 2 can be used. The 3.9(2)-ns half-life value of 711-keV energy level can be also examined. Finally, the high intensity of the 828- and 936-keV transitions makes measurable the apparently shorter half-lives of 1724- and 1832-keV states that are populated by the sufficiently strong γ-rays of 1273, 1713, 2444 and 1164 keV.

For half-live measurements the multi-parameter data set was presorted out. The data set includes 9 parameters: time since last proton impact, proton pattern, β energy, HPGe energy, $LaBr_3$(Ce) energy, time distribution from the FTAC, time difference between events from $LaBr_3$(Ce) and FTAC (within the same card of DAQ), time difference between events from β detector and $LaBr_3$ (Ce) and time difference between $LaBr_3$(Ce) and HPGe. The last three ones were employed for random subtraction.

The 216- and 711-keV γ transitions de-excite levels with half-lives long enough to be measured with the Convolution Technique explained in Chapter 3. Due to the $LaBr_3$(Ce) energy resolution both transitions can be selected directly from the energy spectrum of the $LaBr_3$(Ce), it is not necessary to include the HPGe parameter during the presorting process. This allows to have more statistics in the spectrum and reduce the error bar of the half-life during the fitting. However, the time response of the background ground must be checked carefully in this case. Fig. 5.7 shows the $\beta\gamma$(t) energy spectrum of $LaBr_3$(Ce) obtained from the multi-parameter data set where the HPGe was not included. In order to eliminate the short-lived activity from ^{81}Ga and ^{80}Ga lines the data accumulated during

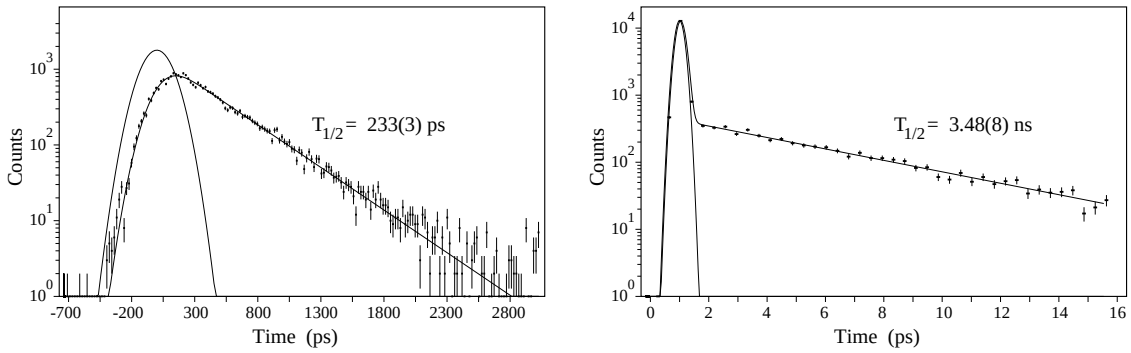

(a) (b)

Figure 5.8: Half-life measuring of 896- and 711-keV states in ^{81}Ge using Convolution Technique in the $\beta\gamma$ time-delayed spectra.

the first 1200 ms was were excluded in the sorting step. As can be seen from the plot, both peaks are well separated and can be selected as energy gates to do projections into the FTAC.

Once the gates in 216- and 711-keV are selected and projected into the FTAC we perform the fit to the convoluted function of the exponential decay and the prompt time distribution approximated by a Gaussian (see section 2.4.1). Figure 5.8 depicts two time spectra in which the fitted curves are plotted. In the plot (b) the time spectrum obtained by projecting 711-keV gate into the FTAC can be found. The fit yields to $T_{1/2} = 3.45(9)$ ns in $LaBr_3$(Ce)-1 and $T_{1/2} = 3.52(7)$ ns in $LaBr_3$(Ce)-2 leading to the final mean value of $T_{1/2} = 3.48(8)$ ns.

Plot (a) shows the fit used to obtain the half-life of the 896-keV state. The spectrum shows only one half-life composed by a slope in the time-delayed part. Increasing the binning the half-life value becomes stable giving $T_{1/2} = 227(3)$ ps in $LaBr_3$(Ce) labeled with 1 and $T_{1/2} = 239(3)$ in the crystal labelled as 2. The average value leads to $T_{1/2} = 233(6)$ ps, where the error bar was incremented in order to include the value from each detector. However, this half-life is influenced by Compton background on which the 216-keV peak is seating (see Fig. 5.7). Setting an equivalent energy gate on the right hand side of the peak and projecting it into FTAC we can check whether counts from Compton process provide an additional half-life in the time spectra. Fig. 5.9 shows the results where two lifetimes can be seen after fitting. Thus, the half-life of 896-keV state of ^{81}Ge obtained with 216-keV in $\beta\gamma$(t) coincidences is not totally correct.

In order to minimize the Compton background we extended the multiparameter data set by adding HPGe detector in the analysis for the selection of γ lines. In this way triple coincidences $\beta\gamma\gamma$(t) were used. Selecting the strong 828- and 936-keV transitions in HPGe the 216-keV transition will be seen in coincidence in $LaBr_3$(Ce). Our fast timing measurements of 1723- and 1832-keV states (see below) shows that their half-lives are below the timing resolution of our $LaBr_3$(Ce) crystals the half-live of 896-keV level. The obtained 216-keV peak looked sufficiently strong to be projected in the FTAC and perform the fitting to the convolution of the decay function and the prompt time distribution. Figure 5.10 shows β-$LaBr_3$(Ce) energy spectrum of 216-keV transition (left panel) projected into FTAC (right panel). The final value of $T_{1/2} = 257(13)$ ps was

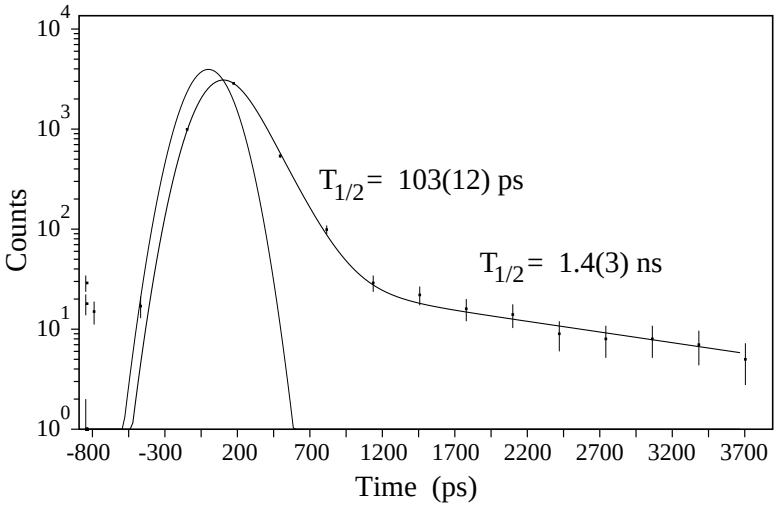

Figure 5.9: Time response of Compton background near 216-keV energy peak.

obtained after performing the weighted mean between $T_{1/2} = 256(23)$ from FTAC-1 and $T_{1/2} = 257(15)$ from FTAC-2.

If we set the energy gate in 216-keV line in HPGe and project into the $LaBr_3$(Ce) detector the 828- and 936-keV transitions can be observed with enough statistics to be analysed for determination of 1723- and 1832-keV level half-lives. However, we do not see any slope in the time-delayed part when projected separately these γ-rays into FTAC. Therefore, the Centroid Shift technique was applied to investigate whether the lifetimes are in the range below 60 ps.

The 1723-keV state is populated by two strong γ lines of 1272 and 2444 keV. These transitions de-excite high energy levels characterized by short half-lives expected in the femptosecond range. Projecting the 1272-keV transition selected in HPGe into $LaBr_3$(Ce) we see two strong peaks in coincidence: the 216- and 828-keV one. Setting now the 828-keV energy gate in $LaBr_3$(Ce) and projecting in the FTAC we obtain the centroid position due the 828-keV γ line. If we set the 828-keV gate in HPGe and project onto the $LaBr_3$(Ce) energy spectrum we will see again the 216-keV line and in this case the 1272-keV line. Setting the gate in latter one and projecting into the FTAC the centroid position due to the 1272-keV transition is obtained. The rest of the parameters from the sorted data file were optimized for this specific analysis. The subtraction of random events was performed with the time difference parameter from PIXIE internal clock, that is the difference between times of events from β and $LaBr_3$(Ce) detectors.

According to Eq. 2.19 the difference between these centroids provides the half-life of the 1723-keV level. Fig 5.11 shows the centroid positions of 828- and 1272-keV lines in the time spectrum from FTAC-1 and FTAC-2. As the timing response of $LaBr_3$(Ce) is not constant with the energy of prompt γ transitions the difference between centroid positions must be corrected by $\Delta\tau_0$, which represent the difference between the prompt time response of the lines which depopulate a given state and the lines which feeds it from the higher states. In our case $\Delta\tau_0^i = \tau_0^i(828) - \tau_0^i(1272)$ and its value can be computed from the Prompt Response Curve built in section 3.5.3 for each $LaBr_3$(Ce) detector labeled by i. After all, $\Delta\tau_0^1 = 164(4)$ ps while $\Delta\tau_0^2 = 146(4)$ ps. Due to non-negligible Compton background near 828-keV peak its centroid position must be also corrected by peak to

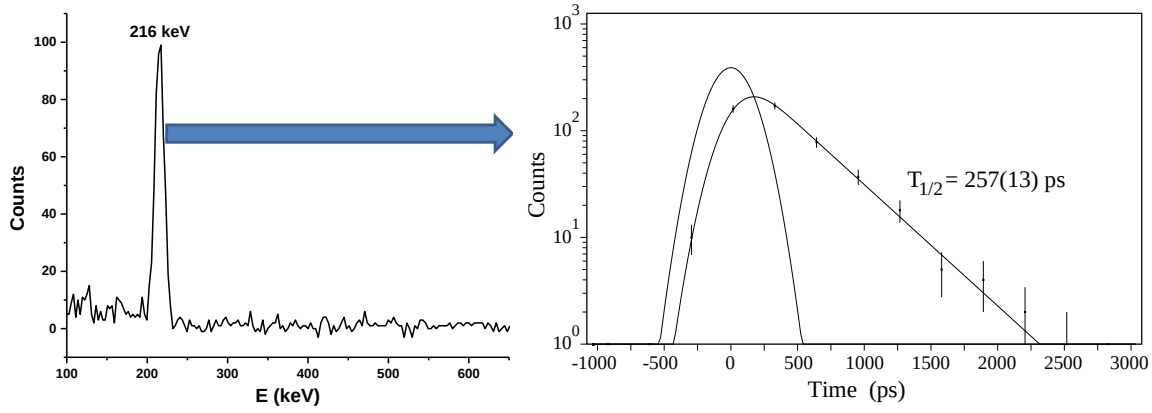

(a) (b)

Figure 5.10: Energy spectrum from one of the $LaBr_3$(Ce) detectors gated by 828- and 936-keV transitions in HPGe. The half-life of the 896-keV state of ^{81}Ge was obtained by projecting the energy gate of 216-keV peak into the FTAC and then employing the Convolution technique in triple $\beta\gamma\gamma$(t) coincidences to perform the fitting.

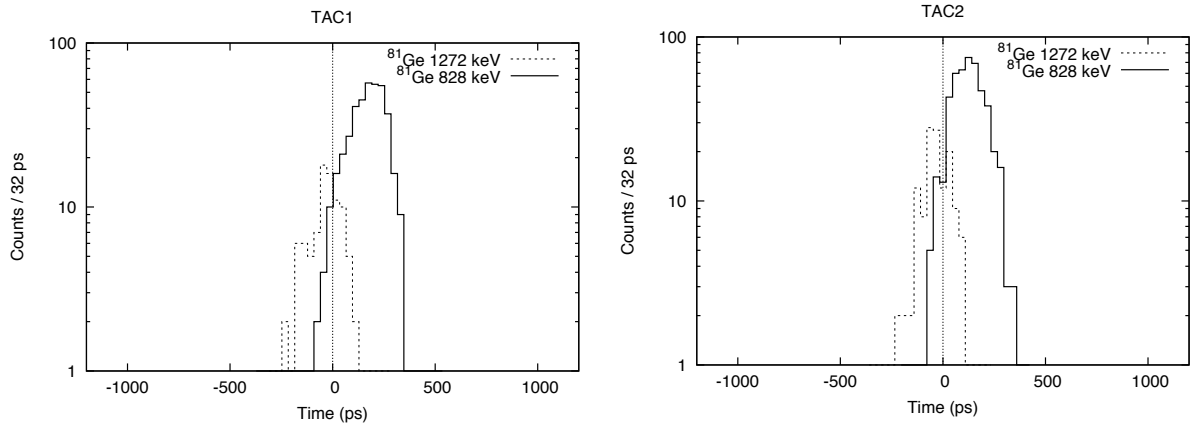

Figure 5.11: Centroid positions of 828- and 1272-keV transitions determined in FTAC-1 and FTAC-2. The plot is not yet corrected for the walk-correction or Compton-background contributions (see text for more details).

Compton ratio using the Compton Response curve as was explained in Sec. 3.5.3 with Eq. 3.5. Finally, the calculated mean life value with FTAC-1 is $\tau = 43(11)$ ps while the result from FTAC-2 yields $\tau = 46(9)$ ps. Averaging and multiplying by $ln2$ leads to obtain a final half-life value of 1723-keV state of $T_{1/2} = 31(7)$ ps.

A very similar procedure was applied for the half-life measurement of the 1832-keV state. Here we used the 936-keV transition which de-excites the level and 731-, 1164- and 1189-keV transitions which populate it. The difference between centroids in FTAC-1 gives $\tau = 13(13)$ ps while in FTAC-2 $\tau = 7(9)$ ps. These results do not allow to establish a mean value for the mean life of 1832-leV state and only an upper limit can be given. Taking into account the $ln2$ the final half-life is given by $T_{1/2} \leq 21$ ps.

5.4 Discussion of the results

As can be observed in the level scheme of ^{81}Ge in Fig. 5.5 several high-lying states receive considerable β feeding from the $5/2^-$ ground state of ^{81}Ga. The relatively low $\log ft$ values permit to state that the β transitions that connects them are most likely allowed and, thus, these sates will be of negative parity. The selection rules tell us that the spin can be 3/2, 5/2 or 7/2. According to the shell-model picture these states should arise from core excitations of neutrons from the pf shell.

With the calculated lifetimes and branching ratios from our level scheme we can compute the reduced transition probabilities and extract useful information to compute the spin-parity of the low-lying states. Tab. 5.2 summarize all the calculations that were performed using the expressions from Eq. (1.30) in Sec. 1.2.2. With these results, some tentative spin-parity could be assigned to low-lying levels.

The 679-keV isomer and 896-keV level

The 216-keV is a key transition for spin-parity assignment of the 679-keV isomer because it connects it with the 896-keV state whose half-life has been precisely determined in this work. The transition rates calculated in Tab.5.2 indicate that 216-keV can be either $E1$ or $M1$, both in agreement with the systematics of transition strengths in the region near $A = 81$ [End79]. However, the $E1$ is the most probable, and it was also measured by Hoff and Fogeleberg [Hof81] providing a 92% confidence limit. The systematics of the odd-mass $N = 49$ isotones shown in Fig. 5.1 strongly suggests the $1/2^-$ spin for the 679-keV isomer and $1/2^+$ for 896-keV level. Nevertheless, the $1/2^+$ spin-parity was recently measured via the transfer reaction at HRIBF [Ahn13], and a $1/2^+$ isomer was discovered at 1.10 MeV in ^{79}Zn [Orl15]. This breaks the systematics predictions. In this way, the 896-keV level is $1/2^-$, characterized by de-excitation of $g_{9/2}$ hole to $p_{1/2}$ state. The $1/2^+$ of 679-keV isomer comes from 1p-2h $\left|s_{1/2}0^+\right\rangle$ configuration given by the $3s_{1/2}$ neutron and 2 holes at $g_{9/2}$ coupled to 0^+.

The 711-keV level

A half-life of 3.48(8) ns has been measured for this state with increased precision compared to the 3.9(2) ns value from [Hof81] . As shown in Fig. 5.1, the $N = 49$ isotones

Level (keV)	$T_{1/2}$ (ps)	E_γ (keV)	τ^γ (ps)	Multipolarity	$B(X\lambda)$ (W.u.)
895.5	257(13)	216.5	373(19)	E1	$1.37(7)\times10^{-4}$
				M1	$8.39(4)\times10^{-3}$
711.3	3.48(8) ns	711.3	5.02(12) ns	E2	$4.28(10)\times10^{-2}$
				M1	$1.76(4)\times10^{-5}$
1723.7	31(7)	828.2	51(12)	E1	$1.8(4)\times10^{-5}$
				E2	2.0(4)
				M1	$1.1(3)\times10^{-3}$
1832.2	≤ 21	936.7	≤ 30	E1	$\geq 2.1\times10^{-5}$
				E2	≥ 1.8
				M1	$\geq 1.3\times10^{-3}$

Table 5.2: Calculated $B(X\lambda)$ from the half-lives values determined in previous section for ^{81}Ge. The calculation was done using the partial mean lives given by Eq. (1.27).

from ^{87}Sr to ^{79}Zn present a $5/2^+$ intruder state based on 1p-2h $\left|d_{5/2}0^+\right\rangle$ configuration. It seems that the $Z = 40$ subshell closure blocks protons from $Z = 28$ to $Z = 50$ and thus the intruder states ($5/2^+$ and also $1/2^+$) are expected to lie at higher energies in nuclei close to $Z = 40$ than in nuclei close to $Z = 28$. Precisely this was observed in ^{87}Sr and ^{85}Kr. The reduced transition probabilities for the $E2$ ($5/2^+\rightarrow9/2^+$) transitions in these nuclei were measured to be 0.13^{5}_{13} for 1770 keV, 7.5(23) W.u. for 1228 keV and 3.8^{15}_{21} W.u. for 1141 keV respectively [Sin14, Joh15]. The neighbouring ^{83}Se has the $5/2^+$ at 582 keV and its half-life was measured to be very similar to that from our work. The 582-keV transition that connects the intruder with the $9/2^+$ ground state was measured to be slow, with $B(E2) = 0.11(2)$ W.u. [Lie84]. The recent measurements in ^{79}Zn [Orl15] using the ^{78}Zn(d,p)^{79}Zn transfer reaction discovered the $5/2^+$ state at 983 keV and their results indicate a slow E2 ($0.005 < B(E2) < 0.2$ W.u.) between this level and the $9/2^+$ ground state. Moreover, state-of-the-art shell-model calculations made by Sieja and Nowacki [Sie12] predicted 0.2 W.u. for the transition connecting the $5/2^+$ and the $9/2^+$ states in ^{79}Zn. In this way, the E2 assignment for 711-keV line in ^{81}Ge fits properly within the systematics and the small reduced probability $B(E2) = 0.043(1)$ W.u. calculated with our measured half-life of the corresponding de-excited level is in good agreement with the structure of close neighbours ^{79}Zn and ^{83}Se.

The 1241-, 1723- and 1823-keV levels

The low β feeding of the 1241-keV state and the similar localization of the 1424-keV state in ^{79}Zn, 963-keV state in ^{83}Se and 1342-keV state in ^{85}Rb leads to state that the spin-parity is most likely $3/2^+$ or $5/2^+$. Due to the relatively low intensity of the 530-keV transition for fast-timing measurements it was not possible to determine its half-life.

The measured transition rates of the 1723- and 1832-keV states do not shed much light for the multipolarity determination of the 828- and 936-keV transitions because the $B(X\lambda)$ is compatible with $E1$, $M1$ and $E2$, as shown in Tab. 5.2. However, taking again

into account the structure of the odd-mass $N = 49$ isotones from Fig. 5.1 we observe a doublet of states strongly decaying to the $1/2^-$ level with $3/2^-$ and $5/2^-$ spins. On the other hand, many of the odd-mass nuclei with similar structure to ^{81}Ge ($^{79-75}$Ge, $^{79-75}$Zn, $^{83-79}$Se and $^{79-75}$Kr) have such pairs of states strongly populating the $1/2^-$ level by an $E2$ γ transition. This fact allows to suggest that the spins of 1723- and 1823-keV states are probably $3/2^-$ or $5/2^-$. Moreover, a doublet of states in ^{79}Zn with two strong lines populating the 1336-keV level connected by the 236-keV line with the 1/2+ isomer (similarly to the 896-keV level connected with the 679-keV isomer by the 216-keV transition) support this proposition.

5.5 Summary of the chapter

The β-decay scheme of ^{81}Ga to ^{81}Ge has benn extended with 15 new γ transitions and 11 new energy levels, giving a total of 111 transitions depopulating 47 energy levels. The previously known structure has been confirmed. The absolute γ transition intensities from our work are in good agreement with the previously reported ones [Hof81], yielding 35.2(30)% for the most intense 216-keV γ-ray compared to 36.7(24)%. The 1.25(3)-s half-life of ^{81}Ga was measured to be consistent with the adopted value from [Bag08].

Our fast-timing measurements allowed to obtain three half-lives of 711-, 896- and 1723-keV states. An upper limit of the 1832-keV level half-life could be established. Transfer reactions study of ^{81}Ge [Ahn13] and also of ^{79}Zn [Orl15] together with systematics considerations and $E1$ multipolarity of 216-keV line permit to firmly stablish the pair of intruder sattes of $1/2^+$ and $5/2^+$ at 679 and 711 keV respectively. Additionally, the low $B(E2)$ value of the 711-keV γ-ray obtained from the 3.48(8)-ns half-life of the 711-keV state indicates weak collectivity and, thus, confirms the single-particle configuration of $5/2^+$ intruder. Finally, two short half-lives in the picosecond range were measured for the first time for the states at 1723 and 1832 keV which are depopulated by the strong 828- and 936-keV transitions. The systematic behaviour of such pair of states in nuclei similar to ^{81}Ge permit to make a tentative assumption about their spins, that is $3/2^-$ or $5/2^-$. The weak β population of the 1241-keV level and analogous levels in the neighbouring nuclei strongly suggests $3/2^+$ or $5/2^+$ spin assignment. The situation at high energies includes nine states between 3.0 and 4.5 MeV with strong β feeding and, therefore, connected with the ground state of ^{81}Ga by allowed transitions. According to selection rules their spins can be $3/2^-$, $5/2^-$ or $7/2^-$, arising from the neutron core excitations.

Chapter 6

Nuclear structure of ^{81}As

The fourth nucleus in the decay chain of ^{81}Zn is the odd-mass $N = 48$, $Z = 33$ ^{81}As. Its location, almost in the middle of the $Z = 28 - 40$ shell can hlep understand the interplay of proton and neutron configurations and the role of collectivity. ^{81}As was populated from the β-decay of ^{81}Ge from both 679-keV isomeric $1/2^+$ state and $9/2^+$ ground state. Thus, we expect to have two decay level schemes that can differ one from due to the ΔJ spin difference of the populating levels in ^{81}Ge. However, it is very difficult to assign all the β transitions to a particular decay level of ^{81}Ge because both states have similar half-live of $T_{1/2} = 7.6(6)$ s. In any case, all the assignments will have a tentative character strongly supported by considerations of systematics of the region. Due to high production rate of ^{81}Zn in our experiment we expect to observe new features in structure of ^{81}As, specially at high energies. Moreover, half-life measurements of low-lying excited states can shed light on spin-parity assignments.

6.1 Previous studies of ^{81}As

The first and the most complete study of ^{81}As was done by P. Hoff and B. Fogelberg in 1981 [Hof81] at the OSIRIS fission product mass separator following the β-decay of Ga isotopes. This separator produced isotopes up to ^{82}Ga with significant yield. Due to the complex structure of ^{81}Ge discussed in the previous section two independent level schemes of ^{81}As corresponding to the decay of $1/2^+$ and $9/2^+$ isomers were built.

According to the level systematics of odd-mass As isotopes shown in Fig. 6.1 the low-lying states are dominated by $1/2^-$, $3/2^-$ and $5/2^-$ spins. As can be seen, the ground state of these isotopes originates from the proton $p_{3/2}$ configuration. The assignment of $3/2^-$ for the ground sate of ^{81}As was also based on the strong direct β feeding of the $1/2^-$ ground state of ^{81}Se [Kra75]. From the level systematics the most probable spins of 93- and 290-keV levels are $1/2^-$ and $3/2^-$. However, the authors of [Bag08] could not state which of the levels was $1/2^-$ and which was $3/2^-$. The 336-keV state was considered as a $5/2^-$. The level systematics also support this assignment. On the basis of ^{83}Se, where both isomers possess very different half-lives, the $9/2^+$ ground state does not populate strongly the levels below 1 MeV. This weak population was discovered for the first time in 1973 by P. Fettweis and S. Sadasivan [Fet73] and recently confirmed with more accuracy by K. S. Krane [Kra15]. In analogy with this situation no β feeding was assumed by P. Hoff and B. Fogelberg for the low lying states of ^{81}As populated from the $9/2^+$ ground sate decay of ^{81}Ge. Similarly to ^{83}Se, the strongly populated levels at 2.6-3.0 MeV were also

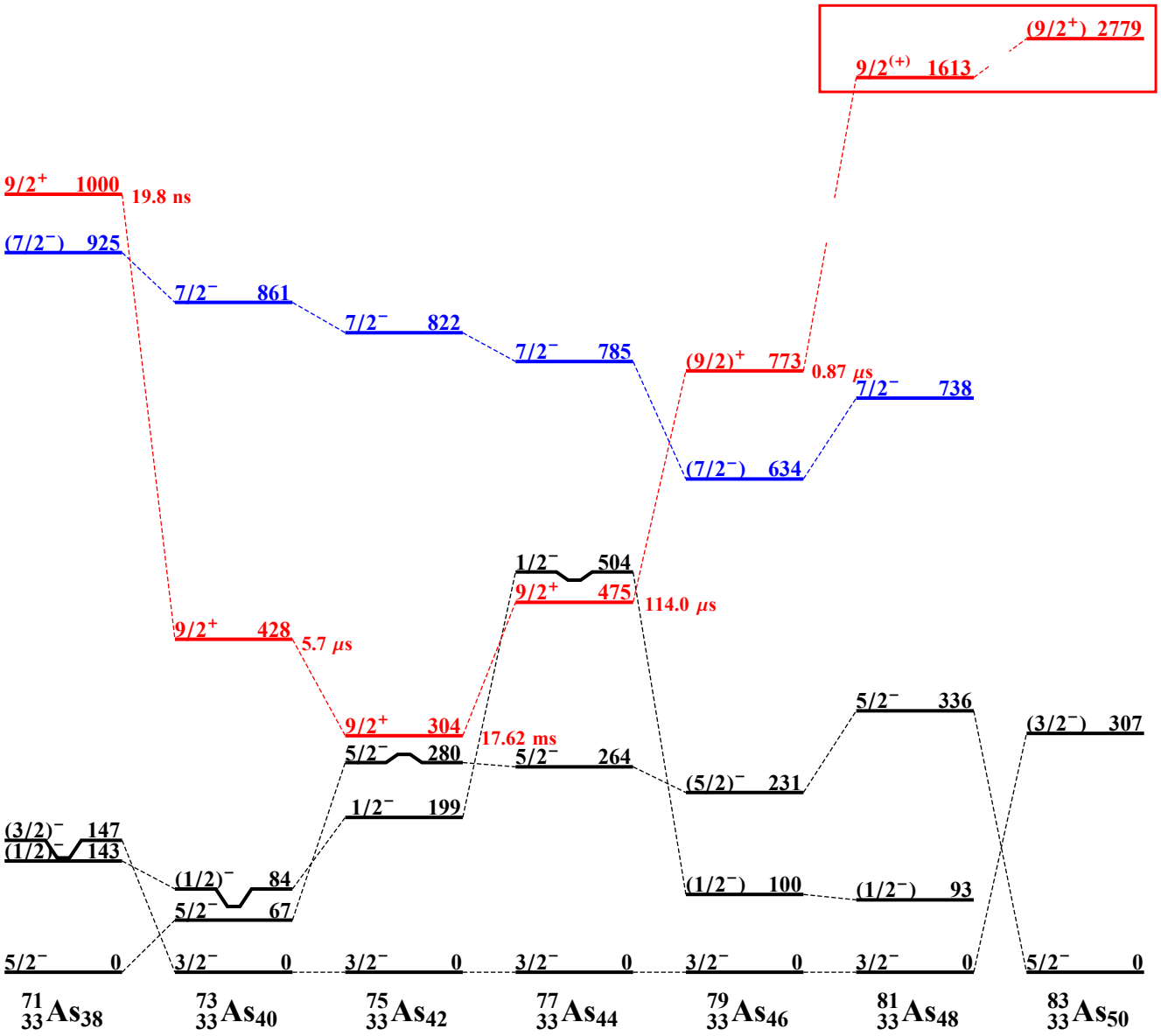

Figure 6.1: Level systematics for the odd-mass As isotopes. The low-lying $7/2^-$ states are marked with blue colour while the $9/2^+$ are shown in red [Abu11, Sin04, Neg13, Sin12, SIN02, Bag08, McC15].

placed in the decay scheme of $9/2^+$ ground state. The allowed β transitions to these states make it possible to assign a spin of $7/2^+$, $9/2^+$ or $11/2^+$. The rest of levels were placed very tentatively so that the $1/2^+$ isomer accounts for about 40% of the total intensity.

Due to the very difficult situation in the β-decay of ^{81}Ge to ^{81}As it was not so easy to allocate strong β transitions to a specific isomeric state of ^{81}Ge. Another study in which states of ^{81}As were populated was done by Porquet *et al.* and the results were published in 2011 [Por11]. The isotopes of ^{81}As were produced as fission fragments in the fusion reaction ^{18}O+^{208}Pb at 85 MeV bombarding energy. The gamma radiation was studied with the Euroball array. A total of 26 transitions depopulating 18 energy levels were assigned to ^{81}As including the strongest 336-, 737- and 793-keV γ-rays. Many of these transitions had already been observed by P. Hoff and B. Fogelberg in 1981. However, some new results were obtained, specially in the high energy region. The strongly populated 2758-keV level seen in β-decay has been also measured in this experiment, where it is populated by a cascade of three new low-energy γ lines of 216, 152 and 164 keV forming an yrast band at $17/2^+$ 3291-keV state. A new yrast band starting at $21/2^-$ 3669-keV level and finishing at the $3/2^-$ ground state has been reported. Another high energy level, which may lead to another yrast band, was observed at 3422 keV (see Fig. 4 from [Por11]).

After performing $\gamma\gamma$ correlation analysis, Porquet and collaborators proposed spin values of $5/2^-$, $7/2^-$ and $9/2^-$ for the states of 336, 738 and 1129 keV respectively. The other three levels of 2359, 3292 and 3669 keV that are part of the yrast configuration have $13/2^-$, $17/2^-$ and $21/2^-$ spins, calculated by increasing by one unit the spin of 1129-keV level. The 336-keV transition was proposed to be of strongly mixed $M1$+$E2$ character, while both 793- and 1230-keV lines should be of quadrupole character. On the other hand, the measured multipolarity of 638- and 738-keV was quadrupole whereas the multipolarity of 876-keV transition was a dipole one. In view of these results, 738-keV state cannot be populated in β-decay from the low-spin isomer of ^{81}Ge and must be placed in the decay of the $9/2^+$ ground state, as well as 2912- and 3368-keV levels connected to it. The 1613-keV state is considered to be $9/2^+$ because of dipole character of 876-keV line that links it with the 738-keV one and based on the results from Se(d,^{3}He) reaction [Rot83]. The other two levels of 2251 and 3422 keV that apparently form the yrast band with the 1613-keV state will have $13/2^+$ and $17/2^+$ spin-parity assignments. The strongly fed levels at 2624- and 2758-keV in the β-decay of ^{81}Ge were considered to be populated from the $9/2^+$ ground state via allowed β transition. Therefore, they have $7/2^+$, $9/2^+$ or $11/2^+$ spin. As they were considered to form the yrast band, the 2758-keV state is most likely $11/2^+$ while the 2624-keV level is $9/2^+$. The levels above the 2758-keV one will have respectively $13/2^+$, $15/2^+$ and $17/2^+$ spins.

6.2 Level scheme of ^{81}As

The main purpose of ^{81}As study is the determination of half-lives of low-lying states. The identification of γ transitions that belong to ^{81}As was mainly based on the $\gamma\gamma$ coincidences. As many of these transitions were already known, our task was to confirm their existence and explore the possibility to find new lines in coincidence with the known ones. The procedure followed for identification of γ transitions and its placement in the decay scheme is very similar to the one used in the previous section for ^{81}Ge. The presorted multi-parameter data file obtained for ^{81}Ge was used for the study of ^{81}As. It

includes the energy of events from the HPGe, the energy of events from the β detector, the time elapsed between the events and the last proton pulse, proton pattern and the time difference between events from HPGe and β detector. The identification of known peaks from the decay of ^{81}Ge to ^{81}As and the determination of their areas were done in the γ spectrum of HPGe gated by the β detector. In order to minimize the contribution of γ radiation coming from the short-lived decay of ^{81}Zn and 1.2-s decay of ^{81}Ga we performed an addition data sorting in which more specific gates were set. In this way, we excluded the first 3.6 seconds in the parameter which characterizes the time since last proton impinged the target. Many of previously known γ transitions were observed in our measurements with sufficiently high intensity.

Fig. 6.2 shows the whole β-gated spectrum in the energy range up to 4 MeV that contains the most intense peaks attributed in [Hof81] to the β-decay of ^{81}Ge to ^{81}As. Since the short-lived activity was eliminated with the gate on time, only peaks corresponding to the long-lived activity appear in the the plot. The most intense transitions from the decay of ^{81}Ga to ^{81}Ge and ^{81}Ge to ^{81}As are marked. The β-delayed neutron emission of ^{81}Zn and ^{81}Ga opened the channel of the $A = 80$ decay chain starting with ^{80}Ga. Therefore, some strong peaks from ^{80}Ge, ^{80}As and ^{80}Se can be also appreciated in Fig. 6.2. In this way, most of the previously known transitions from ^{81}As were directly identified from the β-gated energy spectrum and the area of each peak was computed in order to determine the relative intensities. This values were referred to the strongest 336-keV line. As shown in the figure, some peaks are mixed and it was not possible to determine their area directly from the β-gated singles spectrum and we had to turn to the $\gamma\gamma$ analysis as was explained in Sec. 3.5.2.

Once the most intense transitions were clearly identified we placed them into the level scheme. For that purpose, the $\gamma\gamma$ coincidences were performed between both HPGe detectors. The presorted files contained five parameters: the time since last proton impinged the target, the proton pattern, the energy of HPGe-1, the energy of HPGe-2 and the time difference between events of each HPGe. The coincidence window was established at 8 μs. This last parameter, as was explained in Sec. 3.4 (see Fig. 3.15), was used for subtraction of random events. After the multi-parameter data file for $\gamma\gamma$ coincidences was presorted a set of gates in the most intense peaks from the decay of ^{81}Ge to ^{81}As was set ifor each HPGe detector and projected into the other. After gainfshift corrections, they were added together to study coincidence events.

Figure 6.3 and Fig. 6.4 contain four plots each one representing the coincidence spectra of eight strong γ-rays of 93, 197, 336, 665, 737, 793, 1496 and 1883 keV detected in ^{81}As. The histograms involve summed contributions from HPGe-1 and HPGe-2. A very interesting situation was found for the 666- and 793-keV lines because each of them is doublet of transitions depopulating two different states. The first one connects the low-lying 758- and 93-keV levels and the high-lying 3290- and 2625-keV states. As can be seen in the fourth plot of Fig. 6.3 the 666-keV line has strong coincidence with the 1496-, 793-, and 336-keV lines, which allocate this transition de-exciting the 3291-keV level. On the other hand, a very intense 93-keV line is also observed in coincidence with the 666-keV line. This strong coincidence cannot be observed via the channel started from the 3291-keV state because of the weak intensity of the 243-keV γ-ray that populates the 93-keV level. This demonstrates that there exists another 666-keV transition feeding directly the 93-keV state and it was placed de-exciting the 758-keV state. A similar situation occurs with the 793-keV line. According to the second plot from Fig. 6.4 it has strong coincidence

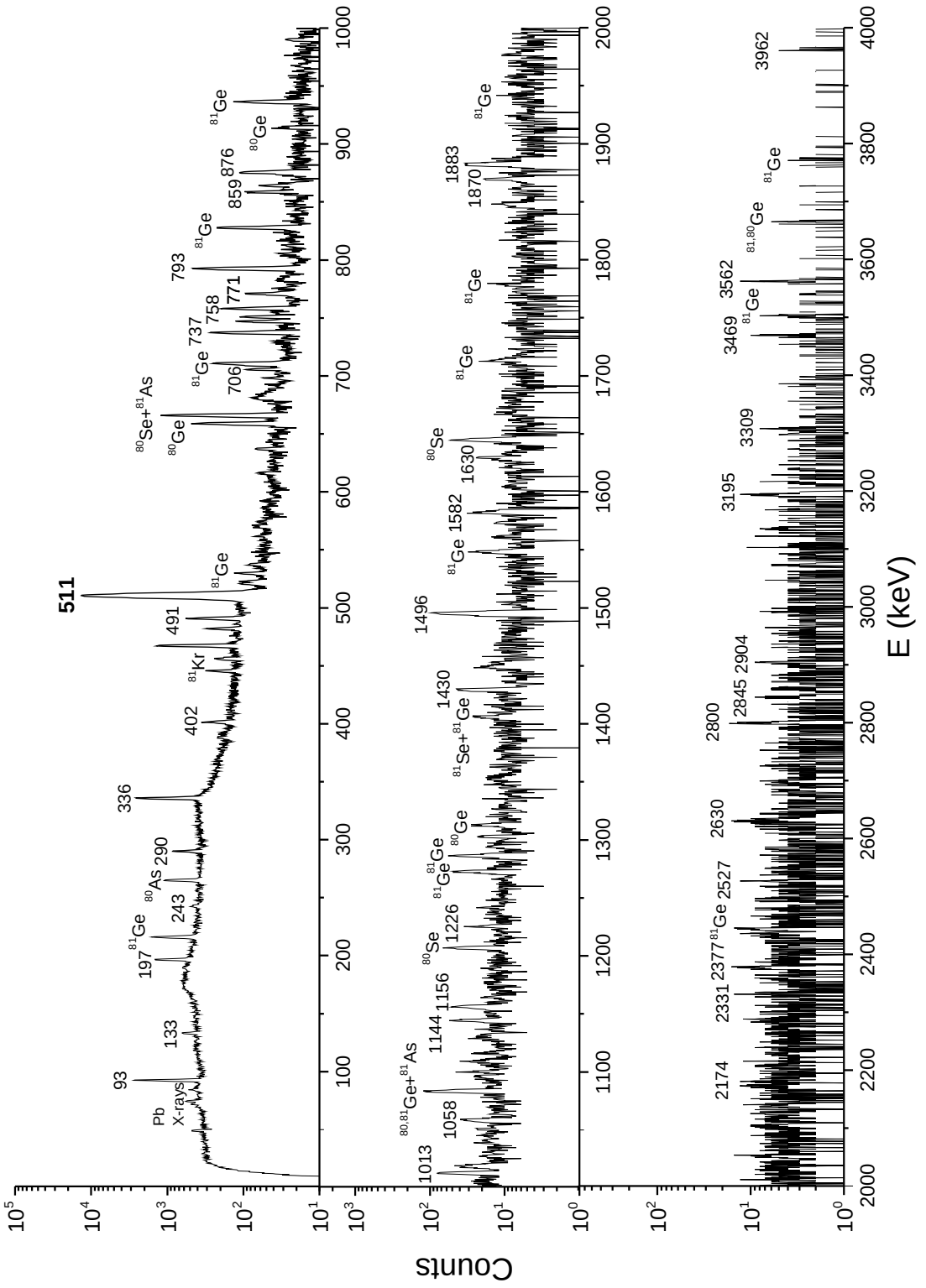

Figure 6.2: Energy spectrum of both HPGe detectors added and in coincidence with βs. The first 3.6 seconds of the decay had been excluded during the sorting process and only peaks from the long lived activity can be seen. The most intense peaks from the decay of ^{81}Ge to ^{81}As are shown. Some of the strongest γ-rays corresponding to ^{81}Ge, ^{81}Se, ^{80}Ge, ^{80}As and ^{80}Se are also indicated.

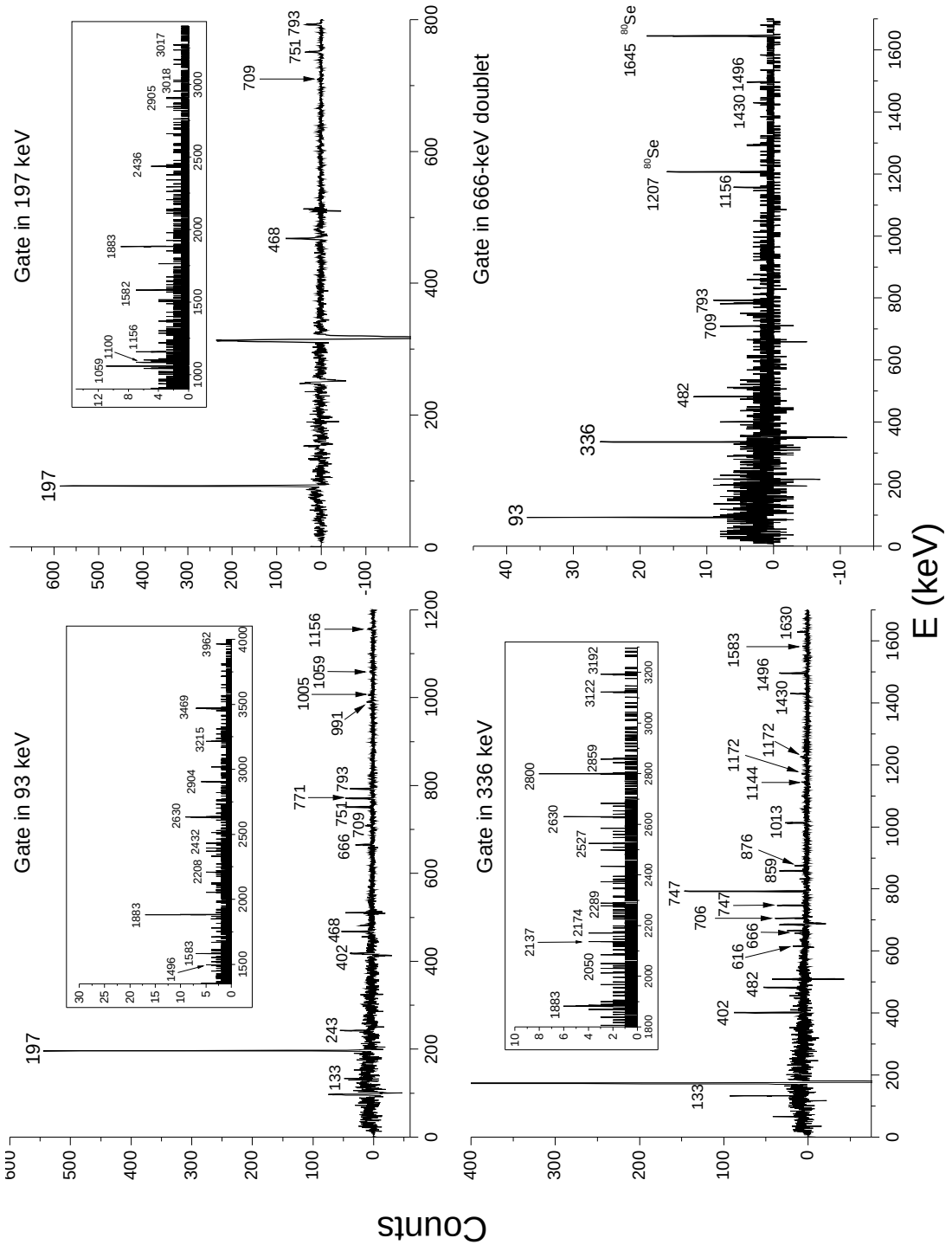

Figure 6.3: Energy spectrum of γ lines seen in $\gamma\gamma$ coincidences with the 93-, 197-, 336- and 666-keV transition.

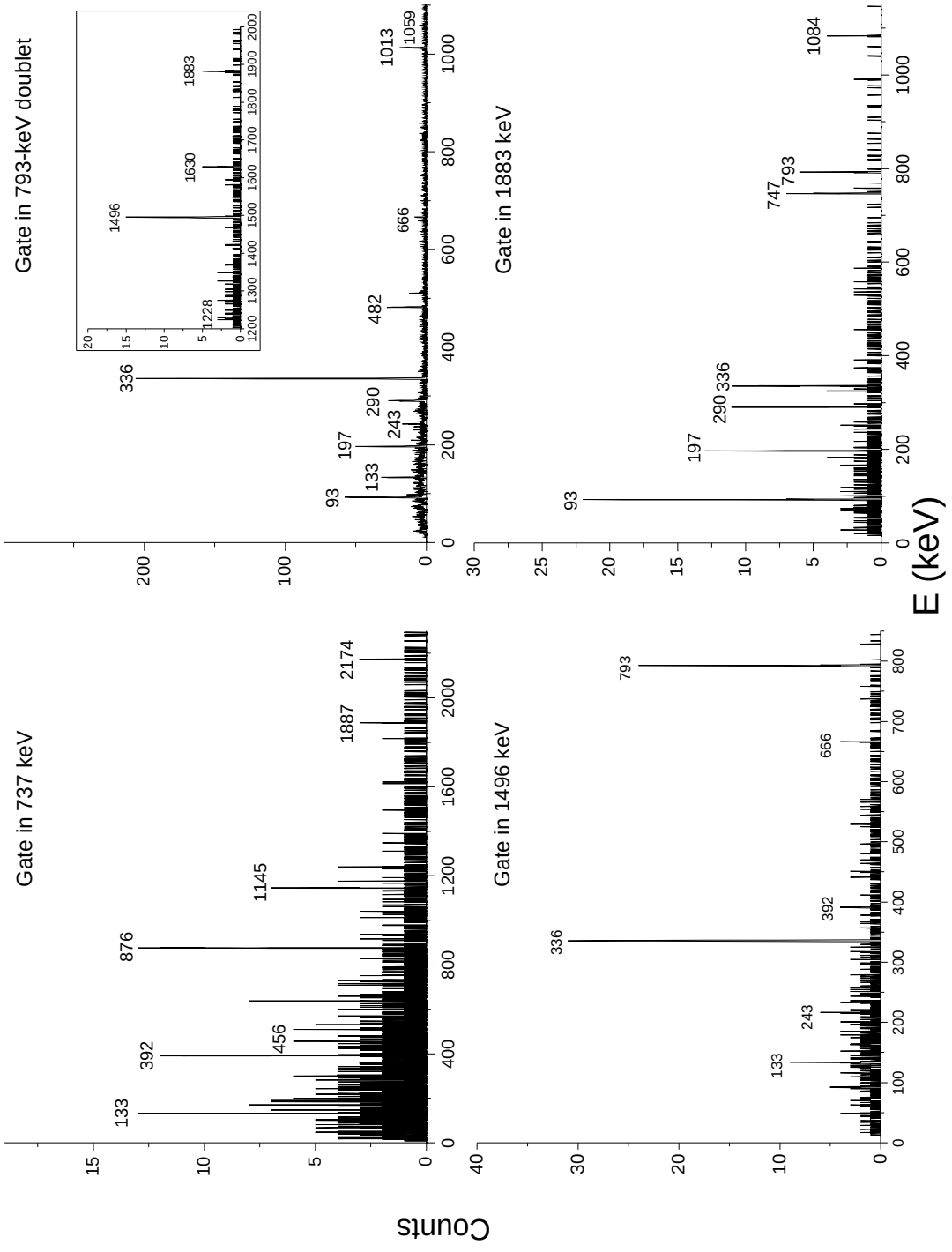

Figure 6.4: Energy spectrum of γ lines seen in $\gamma\gamma$ coincidences with the 737-, 793-, 1496- and 1883-keV transition.

with 93-, 197-, 336-, 482-, 1013-, 1496-, 1630- and 1883-keV. This permits to allocate the strong 793-keV line depopulating the 1129-keV state while the weak 793-keV transition was allocated to connect 1083- and 290-keV states. The intensity and energy values of 666- and 793-keV lines were computed during $\gamma\gamma$ analysis.

Due to the presence of two β-decaying long-lived isomers in ^{81}Ge we will treat their decay schemes separately. However, some common features can be presented in advance. The first argument that we used to allocate transitions in the level schemes is the spin-parity assignments from [Por11]. The key point that allows to assign the levels to either decay is their large spin difference. Another strong argument is the analogue decay of $^{83}_{34}Se_{49}$ to $^{83}_{35}Br_{48}$, which is expected to have a very similar decay pattern than $^{81}_{32}Ge_{49}$ with two $9/2^+$ and $1/2^-$ isomers [McC15]. In this way, the first six excited states of ^{81}As can be considered to be in both level schemes either β or γ fed. However, the measured $7/2^-$ spin of 737-keV state leads to place it only in the decay of $9/2^+$ isomer. The information about the β-decay of $^{79}_{30}Zn_{49}$ to $^{79}_{31}Ga_{48}$ can also contribute to our analysis. The latest publication of this decay was done in 1986 by Ekström *et al.* [Eks86]. The authors affirm the existence of low-spin isomer spin, but it was not observed in their experiment. Recent measurements [Orl15] position this isomer at 1.1 MeV attributing an $1/2^+$ spin-parity assignment to it. Thus, only the β-decay of the $9/2^+$ ground state feeds levels of ^{79}Ga in the experiment of Ekström *et al.*. In this way, their level scheme of ^{79}Ga can help to identify levels in ^{81}As populated from the decay of the $9/2^+$ ground state of ^{81}Ge.

6.2.1 Decay scheme of the $9/2^+$ ground state of ^{81}Ge

In order to construct the ^{81}As level scheme we assume that the 5 lowest lying states are β-populated only in the decay of $9/2^+$ state of ^{81}Ge. Based on the decay scheme of the $1/2^+$ state of ^{83}Se [McC15] and assuming that the low-spin assignments of g.s., 93- and 290-keV states this seems reasonable. We assign no β feeding of the 336-keV state in this decay scheme as occurs in the $9/2^+$ decay of ^{79}Zn [Eks86]. As already mentioned, due to large change of spin, the 737-keV $7/2^-$ level can only be fed in the decay of $9/2^+$ isomer and the levels at 2911 and 3368 keV connected to it were also placed in the same level scheme. The adopted $(7/2^-)$ spin for the 1041-keV state [Bag08] also favours the placement of this level in the decay scheme populated from the $9/2^+$ isomer. An additional fact that supports this idea is the weak 1870-keV transition that falls down to the 1041-keV level from the high-lying 2912-keV state. The 1083-keV level is depopulated by two relatively weak γ transitions, similarly to the 1030-keV state in ^{83}Br and the 1129-keV state has the same behaviour that the 1582-keV level in the decay ^{79}Zn to ^{79}Ga. Moreover, the 1041-keV does not receive any γ feeding from higher levels in the decay of $1/2^+$ isomer. The measured $9/2^-$ spin of 1129-keV level also indicates that we must place it into the decay scheme of $9/2^+$ isomer as the probability to have a third-forbidden β transition from the $1/2^+$ state is very low and γ feeding comes from higher spin states. The 1195-keV level is connected with the 336-keV one by 859-keV transition which is in coincidence with 1430-keV one. This latter de-excites the 2625-keV state, already allocated in the decay scheme of $9/2^+$ state. The strongly populated high-lying states in a 2.6-3.0 keV range, in analogy with ^{83}Br and ^{79}Zn, were also considered as fed in the $9/2^+$ decay, as well as the other levels beyond 3 MeV.

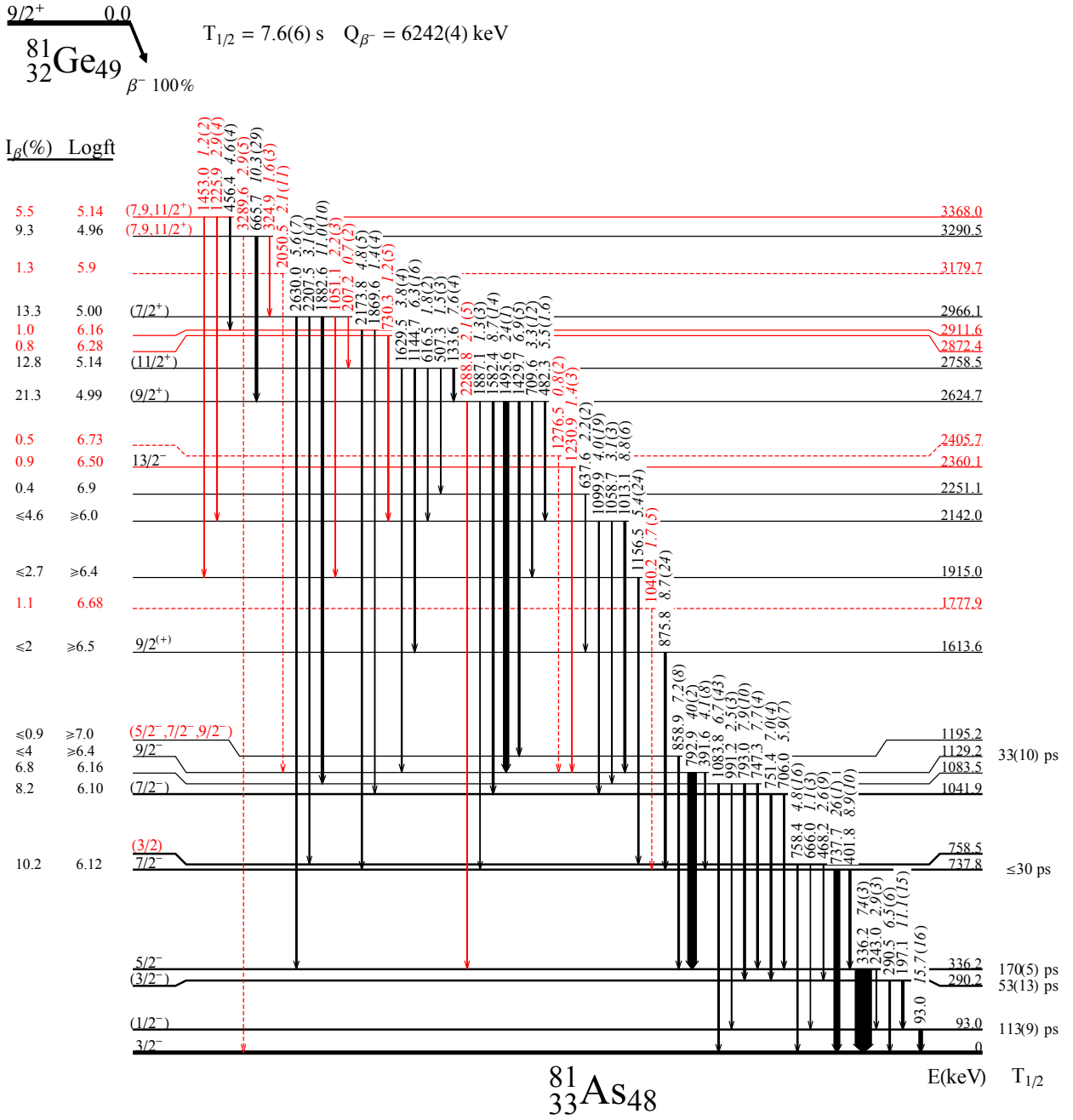

Figure 6.5: Level scheme of ^{81}As populated in the β-decay of $9/2^+$ of ^{81}Ge. The previously known results were plotted in black, while the new γ transitions and energy levels appear in red. The spin-parity assignments were based on results from [Por11], logft values and level systematics of As isotopes presented in Fig. 6.1 (see text for details). There are few γ-rays that could not be placed in the scheme but observed in coincidence with the strongest lines.

E_γ(keV)	E_i^{level} (keV) → E_f^{level} (keV)	I_γ (%)[a]	γ-γ
93.0 *1*	93→g.s.	15.7 *16*	134, 197, 243, 390, 402 456, 468, 482, 666, 709 751, 793, 991, 1059 1100, 1156, 1496, 1582 1870, 1883, 1978[c], 2208 2395[c], 2430[c], 2630 2965[c], 3451[c] 3538[c], 3567[c]
133.6 *1*	2758→2625	7.6 *4*	197, 336, 482, 710, 737 751, 758, 793, 858, 1013 1156, 1430, 1496, 1582
197.1 *1*	290→93	11.1 *15*	93, 468, 482, 710 751, 1059, 1100, 1156 1250, 1582, 1883, 2430[c]
207.2 *4*	2966→2758	0.7 *2*	
243.0 *4*	336→93	2.9 *3*	93, 402, 706, 747 793, 1013, 1496
290.5 *2*	290→g.s	6.5 *6*	468, 666, 710, 751 793, 1059, 1100, 1156 1496, 1583, 1883, 2430[c]
324.9 *2*	3290→2966	1.6 *3*	
336.2 *1*	336→g.s.	74 *3*	134, 402, 456, 482, 616 666, 706, 747, 793, 859 876, 1013, 1059, 1100, 1144 1226, 1231, 1430, 1496, 1583 1630, 1870, 1883, 1887 2050, 2174, 2289, 2630
391.6 *2*	1129→738	4.1 *8*[b]	402, 737, 1496
401.8 *2*	738→336	8.9 *10*[b]	392, 336, 876, 1145, 2174
456.4 *3*	3268→2912	4.6 *4*[b]	737, 2174
468.2 *2*	758→290	2.6 *9*[b]	93, 197, 290, 710, 1156, 2208
482.3 *2*	2625→2142	5.5 *1.6*[b]	93, 134, 336, 666 706, 737, 706, 747 751, 793, 1013, 1059

Continued on next page

Table 6.1 – *Continued*

E_γ(keV)	E_i^{level} (keV) → E_f^{level} (keV)	I_γ (%)[a]	γ-γ
507.3 *5*	2758→2251	1.5 *3*	
616.5 *2*	2758→2142	1.8 *2*	93, 336, 737, 793, 1013
637.6 *2*	2251→1614	2.2 *2*	336, 401, 507, 737, 876
665.7 *2*	3290→2625	10.3 *29*[b]	336, 482, 793
			1430, 1496, 1583
666.0 *2*	758→93	1.1 *3*[b]	93, 710, 1156
706.0 *1*	1042→336	5.9 *7*[b]	336, 482, 1583
709.6 *2*	2625→1915	3.3 *12*[b]	93, 134, 197, 290
			468, 666, 758, 793
			1059, 1144, 1156
730.3 *5*	2872→2142	1.2 *5*[b]	336, 793, 1013
737.7 *1*	738→g.s.	26 *1*	134, 391, 456, 482, 637
			876, 1040, 1145, 1887, 2174
747.3 *1*	1083→336	7.7 *4*	243, 336, 482, 1059, 1883
751.4 *1*	1042→290	7.0 *5*	93, 134, 197, 290, 482
			616, 666, 1100, 1583, 1870
758.4 *1*	758→g.s.	4.8 *1.6*	710, 1156, 2208
792.9 *1*	1129→336	40 *2*[b]	93, 197, 290, 1059, 1883
793.0 *2*	1083→290	7.9 *10*[b]	93, 134, 243, 336, 482
			616, 666, 1013, 1231, 1276
			1496, 2051, 1630, 1883
858.9 *2*	1195→336	7.2 *9*[b]	93, 134, 336, 666, 1430
875.8 *3*	1614→738	8.7 *24*[b]	336, 391, 402, 507
			637, 737, 1145
991.2 *4*	1083→93	2.4 *3*[b]	93
1013.1 *1*	2142→1129	8.8 *6*	134, 336, 391, 402, 482
			616, 666, 730, 793, 1226
1040.2 *5*	1778→738	1.7 *5*[b]	93, 737
1051.1 *4*	2966→1915	2.2 *3*	1156
1058.7 *4*	2142→1083	3.1 *3*	93, 134, 197, 336, 482
			747, 793, 1083, 1226
1083.8 *4*	1083→g.s.	6.7 *43*[b]	1083
1099.9 *5*	2142→1042	4.0 *19*[b]	92, 197, 290, 336

Continued on next page

Table 6.1 – *Continued*

E_γ(keV)	E_i^{level} (keV) → E_f^{level} (keV)	I_γ (%)[a]	γ-γ
			666, 751
1144.7 *3*	2758→1614	6.3 *16*[b]	207, 336, 402, 737, 876
1156.5 *4*	1915→758	5.4 *24*	93, 197, 290, 468, 666
			710, 758, 1051, 1453
1172.4[c] *3*		1.6 *3*	336
1225.9 *3*	3368→2142	2.9 *4*	336, 1013
1230.9 *4*	2360→1129	1.4 *3*	336, 793
1276.5 *5*	2406→1129	0.8 *2*	336, 793
1429.7 *2*	2625→1195	6.9 *6*[b]	134, 336, 468, 858
1453.0 *4*	3368→1915	1.2 *2*	758, 1156
1495.6 *1*	2625→1129	24 *1*	93, 134, 243, 336
			391, 666, 737, 793
1582.4 *4*	2625→1042	8.7 *14*[b]	93, 134, 197, 290
			336, 666, 706, 751
1629.5 *2*	2758→1129	3.8 *4*	93, 336, 737, 793
1817.8[c] *4*		1.5 *3*	336
1869.6 *3*	2912→1042	1.4 *4*[b]	336, 793
1882.6 *2*	2966→1083	11.0 *8*[b]	93, 197, 290, 325, 336
			747, 793, 1084
1887.1 *6*	2625→738	1.3 *3*	
1977.6[c] *7*		1.6 *3*	93
2050.5 *4*	3180→1129	2.1 *11*[b]	
2137.4[c] *3*		0.5 *2*[b]	336
2173.8 *3*	2912→738	4.8 *5*	402, 456, 737
2207.5 *3*	2966→758	3.1 *4*	
2288.8 *5*	2625→336	2.1 *5*	93, 134, 336
2394.7[c] *6*		0.6 *2*	93
2430.4[c] *5*		2.0 *4*	93, 197, 290
2630.0 *4*	2966→336	5.6 *7*	93, 336
2965.2[c] *7*		2.6 *4*	93
3229.3[c] *5*		2.0 *4*	93
3289.6 *4*	3291→g.s.	2.9 *5*	
3450.5[c] *6*		1.2 *2*	93

Continued on next page

Table 6.1 – *Continued*

E_γ(keV)	E_i^{level} (keV) → E_f^{level} (keV)	I_γ (%)[a]	γ-γ
3538.4[c] ***12***		1.4 *3*	93
3566.9[c] ***7***		1.0 *2*	93

Table 6.1: All γ transitions from the decay of the $9/2^+$ state of ^{81}Ge to ^{81}As observed in coincidence with their relative intensities normalized to the total intensity of 336-keV line measured in both decays of ^{81}Ge isomers. Intensities obtained from $\gamma\gamma$ coincidences have a significant larger uncertainty.

[a] Relative intensity. For absolute intensity per 100 decays, multiply by 0.71(3) *2*

[b] Calculated from $\gamma\gamma$ spectrum.

[c] Not placed in the level scheme.

The $\gamma\gamma$ coincidence analysis permitted to discover transitions that were not previously observed in β-decay. Such is the case of the 1231-keV γ-ray. It was seen in coincidence with 793- and 336-keV transitions and we placed it depopulating the 2360-keV state, which was already measured by Porquet *et al.* in 2011. Similar situation happened to 1276- and 2051-keV transitions, but the coincidences were weaker and we tentatively placed them de-exciting the new 2406- and 2180-keV states respectively. The 730-keV γ-ray had enough counts in coincidence with the 1013- and 793-keV lines to be placed de-exciting a new level at 2872 keV. From $\gamma\gamma$ spectrum of 1156- and 1144-keV transitions two new lines of 207 and 1051 keV were added to the 2966-keV state. It is interesting to note that we do not observe 1353- and 2228-keV transition measured in [Hof81]. The 325-keV transition was observed in coincidence with the high energy 1883-keV line and was added to the already allocated 3290-keV state. Finally, another two transitions of 1225 and 1453 keV were placed de-exciting the 3368-keV level, which was considered by P. Hoff and B. Fogelberg in the decay scheme of the $1/2^+$ isomer [Hof81]. We see the 1225-keV line with enough statistics in coincidence with 336-, 793- and 1013-keV transitions. The 1453-keV line was observed in coincidence with 1156-keV γ-rays. This is an additional argument that support the assumption to place the 3368-keV level in the decay of $9/2^+$ isomer. All the information about the energy, the relative intensity, the de-excited levels and the coincident transitions was compiled in Tab. 6.1 and the level scheme is presented in Fig. 6.5.

Significant modifications can be noted in comparison to the scheme from [Hof81]. First, the 2912- and 3368-keV states, previously assigned to the decay of $1/2^+$ isomer, belongs to the decay of the $9/2^+$ ground state of ^{81}Ge. New transitions of 1225 and 1453 keV that de-excites the 3368-keV level were also observed in coincidences with gammas that de-excites the already confirmed levels at 1915 and 2142 keV of this level scheme. Second, 12 new γ transitions and 7 new energy states, mostly located beyond 2 MeV have been included. Some γ transitions were only seen in coincidence with the strongest 93-, 197, 290- and 326-keV lines which appears in both decay scheme. There is no easy way to assign them to any of the decays of ^{81}Ge and we decided not to place them in the level scheme. However, they can be taken into account in the intensity computation.

As will be seen in Sec. 6.3 the half-life of 336-keV state was precisely measured in our experiment improving the previous upper limit of 0.7 ns. The half-lives of 93-, 290-, 738- and 1129-keV levels have been measured for the first time.

Most of the spins shown in Fig. 6.5 are taken from the previous works [Bag08] and [Por11]. The calculation of relative and absolute intensities is presented in Sec. 6.2.3. As can be seen in Tab. 6.1 our values are similar to those obtained in [Hof81]. In some cases, however, the error bar of intensities is much higher because some of γ lines were strongly mixed and their intensities were extracted using $\gamma\gamma$ coincidences, which increases considerably their uncertainty. In view of our results the two high-lying states of 3290 and 3368 keV are strongly populated in β-decay and the calculated $\log ft$ values suggest allowed β transition from the $9/2^+$ state of ^{81}Ge and thus $7/2^+$, $9/2^+$ or $11/2^+$ spins.

6.2.2 Decay scheme of the $1/2^+$ isomeric state of ^{81}Ge

The key to obtain the level scheme of ^{81}As populated from the β-decay of the $1/2^+$ isomer is the allocation of strongly populated high-lying states de-excited directly to the low-spin levels of 93, 290 and 336 keV or the ground state. This strong population gives low $\log ft$ values and thus the β transitions that connect the high energy states with the $1/2^+$ isomer from ^{81}Ge will be allowed. Selection rules of the β-decay suggest $1/2^+$ and $3/2^+$ spin-parity assignments. As the γ transitions that connect these high energy states to the low-spin excited states below 336 keV have normally low multipolarity we can conclude that the levels with high β feeding belong to the decay of $1/2^+$. Therefore, $\gamma\gamma$ coincidences permit to establish six states beyond 3 MeV. Three of them are presented for the first time in our work. The 3272-keV line was added to the previously know 3562-keV level. The 2863- and 864-keV states were placed in the decay of $1/2^+$ similarly to the 2810- and 867-keV levels populated in the β of $1/2^-$ isomer in ^{83}Se. The other two levels of 1870 and 1960 keV are in coincidence with 864-keV state de-excited by 771-keV γ-ray and thus also appear in the decay scheme of ^{81}As populated in $1/2^+$ decay.

The main difference with the scheme obtained by P. Hoff and B. Fogelberg in 1981 [Hof81] are the three new high energy states with strong β population and the 737- and 1041-keV levels which were removed due to the measured spins from [Por11]. Finally, the 2912- and 3368-keV levels were also transferred to the decay of $9/2^+$. We have obtained the β feeding value for the ground state based on the decay of ^{81}As to ^{81}Se (see next subsection). The 758-keV state appears in both decays of ^{81}Ge. In the case of the $9/2^+$ ground state decay it does not receive any direct β feeding while in the decay of $1/2^+$ isomer the $\log ft$ value point to the first forbidden or allowed decay, giving two possible spin values 1/2 and 3/2. Three γ-rays de-excite this level to $1/2^-$ and $3/2^-$ excited states and it is populated by the 2207-keV transition from the 2966-keV level, which has tentatively assigned $7/2^+$. This discards probably the 1/2 value for the spin and allows to keep $3/2^\pm$ spin-parity. The 1195-keV level has probably $5/2^-$, $7/2^-$ or $9/2^-$ due to the $\log ft$ value and the 859-keV transition which connects it to the $5/2^-$ 336-keV level. The lower limit of the $\log ft$ value of the 864-keV state points to a first forbidden β transition from the $1/2^+$ isomer an thus the spins are probably $1/2^-$, $3/2^-$ or $5/2^-$, in agreement with the de-excited 771-keV line which is probably $M1$ or $E2$. However, this state can be also $7/2^-$ in analogy to the 867-keV level of ^{83}Br. The rest of levels can be connected with the $1/2^+$ isomer of ^{81}Ge by an allowed or first forbidden β transitions that leads to assign 1/2 or 3/2 spins to them. All the results are collected in Tab. 6.2 and the level

scheme is plotted in Fig. 6.6.

E_γ(keV)	E_i^{level} (keV) → E_f^{level} (keV)	I_γ (%)[a]	γ-γ
93.0 *1*	93→g.s.	53 *5*	197, 243, 468, 666, 771 1006, 1978[c], 2331, 2377 2395[c], 2430[c], 2436, 2904 2965[c], 3017, 3215, 3237 3272, 3451[c], 3469 3538[c], 3567[c]
197.1 *1*	290→93	22.6 *20*	93, 468, 2430[c], 2436 2844, 2904, 3018, 3237
243.0 *4*	336→93	1.0 *2*	93
290.5 *2*	290→g.s	13.2 *9*	2904, 2430[c]
336.2 *1*	336→g.s.	26 *4*	1172[c], 1818[c], 2137[c] 2527 2800, 2859, 3122 3192, 3538[c], 3567[c]
468.2 *2*	758→290	6.5 *16*[b]	468, 2904
666.0 *2*	758→93	2.7 *4*[b]	93
758.4 *1*	758→g.s.	11.9 *25*	2104, 2377, 2436
771.3 *1*	864→93	6.7 *11*[b]	93, 1006, 1095
1006.0 *4*	1870→864.	0.8 *4*[b]	
1095.3 *3*	1960→864	1.9 *3*	93, 771
1172.4[c] *3*		1.6 *3*	336
1817.8[c] *4*		1.5 *3*	336
1869.6 *3*	1870→g.s.	2.1 *4*	
1977.6[c] *7*		1.6 *3*	93
2104.2 *6*	2863→758	1.2 *3*	
2137.4[c] *3*		0.5 *2*[b]	336
2331.0 *3*	3195→864	4.3 *4*	93, 771
2376.7 *4*	3136→758	4.4 *18*[b]	93, 197, 758
2394.7[c] *6*		0.6 *2*	93
2430.4[c] *5*		2.0 *4*	93, 197, 290
2436.2 *5*	3195→758	1.3 *4*[b]	
2526.9 *4*	2863→336	3.1 *4*	
2800.1 *3*	3136→336	7.9 *7*	336
2844.6 *4*	3136→290	4.1 *5*	93, 197

Continued on next page

Table 6.2 – *Continued*

E_γ(keV)	E_i^{level} (keV) → E_f^{level} (keV)	I_γ (%)[a]	γ-γ
2859.0 *4*	3195→336	2.4 *4*	
2862.0 *6*	2863→g.s	0.9 *3*	
2904.5 *5*	3195→290	4.2 *5*	93, 197, 290
2965.2[c] *7*		2.6 *4*	93
3017.4 *6*	3308→290	1.9 *4*	93, 197
3122.3 *4*	3458→336	3.1 *5*	93, 243, 336
3136.1 *4*	3136→g.s.	4.6 *6*	
3192.5 *8*	3528→336	2.4 *6*	336
3194.5 *4*	3195→g.s.	5.6 *9*[b]	
3215.2 *9*	3308→93	5.6 *6*	93
3229.3[c] *5*		2.0 *4*	93
3237.2 *5*	3528→290	2.6 *4*	93, 197
3271.7 *5*	3562→290	2.4 *7*	93, 197, 290
3308.5 *5*	3308→g.s.	3.7 *5*	
3450.5[c] *6*		1.2 *2*	93
3456.7 *8*	3458→g.s.	2.4 *4*	
3468.9 *4*	3562→93	4.9 *6*	93
3538.4[c] *12*		1.4 *3*	93
3562.1 *6*	3562→g.s.	6.3 *9*	
3566.9[c] *7*		1.0 *2*	93
3961.6 *5*	4055→93	4.5 *7*	93
4054.0 *8*	4055→g.s	1.5 *4*	

Table 6.2: All γ transitions of ^{81}As populated from the β-decay of the $1/2^+$ of ^{81}Ge observed in coincidence with their relative intensities normalized to the total intensity of 336-keV line obtained from both isomeric decays. Intensities obtained from $\gamma\gamma$ coincidences have a significantly larger uncertainty.

[a] Relative intensity. For absolute intensity per 100 decays, multiply by 0.62(7)

[b] Calculated from $\gamma\gamma$ spectrum.

[c] Not placed in the level scheme.

6.2.3 Absolute and relative intensities

The relative intensities of γ transitions were calculated with the use of Eq. 3.4. The peak areas were extracted directly from the β-gated HPGe energy spectra and the efficiency

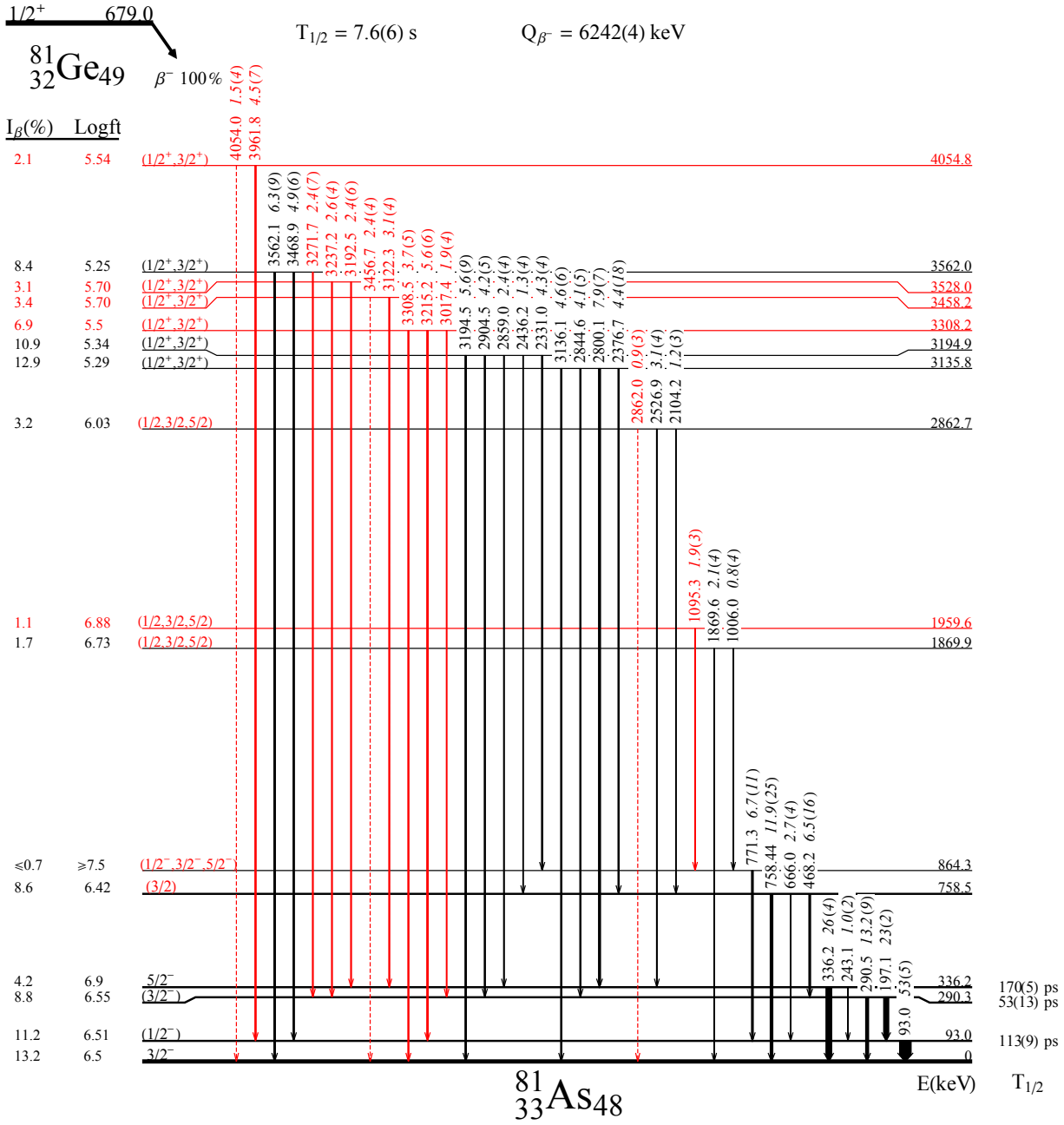

Figure 6.6: Level scheme of ^{81}As populated in the β-decay of $1/2^+$ isomer of ^{81}Ge. The previously known results were plotted in black, while the new γ transitions and energy levels appear in red. The spin-parity assignments are based on results from [Por11], logft values and level systematics of As isotopes presented in Fig. 6.1 (see text for details). There are few γ-rays that are not placed in the scheme but observed in coincidence with the strongest lines.

curves were obtained in Sec. 3.5.2. The final values presented in the level schemes and data tables from the previous section were normalized to the intensity of the strongest 336-keV transition. As this line belongs to both decays of ^{81}Ge a suitable division of intensity must be done first. The same happens to other mutual transitions, such as of 93, 197, 243, 290, 468, 666 and 758 keV.

In the case of the decay of the $9/2^+$ ground state of ^{81}Ge the β feeding of the low-spin states of 93 and 290 keV was considered zero as well as the β feeding to the $3/2^-$ ground state due to large change of spin ($\Delta J = 3, 4$). In analogy to the decay schemes of $9/2^+$ states of ^{79}Zn and ^{83}Se the low-lying $5/2^-$ level barely receives any direct β feeding. The 758-keV state, which appears in both level schemes, was also considered with no β feeding similarly to the decay of ^{83}Se. With these assumptions we can compute the fraction of intensity that corresponds to the shared transitions.

- **758-keV state**

As explained above, the 758-keV state does not receive any β feeding in the decay of $9/2^+$ state of ^{81}Ge and thus all γ feeding from the higher energy levels is transformed into three de-excited transitions of 468, 666 and 758 keV. The following equations describe the intensity balance of the incoming and de-exciting γ transitions in each level scheme:

$$\left(I_{758} + I_{666} + I_{468}\right)^{9/2^+} = \left(I_{1156} + I_{2207}\right)^{9/2^+}, \tag{6.1}$$

$$\left(I_{758} + I_{666} + I_{468}\right)^{1/2^+} = \left(I_{2104} + I_{2377} + I_{2476}\right)^{1/2^+} + I_{\beta}^{758,1/2+}, \tag{6.2}$$

$$\left(I_{468,666,758}\right)^{9/2^+} + \left(I_{468,666,758}\right)^{1/2^+} = \left(I_{468,666,758}\right), \tag{6.3}$$

where the incoming intensity can be calculated directly from the spectra. Equation 6.3 includes actually 3 equations for each energy. The ratio between intensities within the same level must be constant, that is:

$$\frac{I_{758}}{I_{666}}^{9/2^+} = \frac{I_{758}}{I_{666}}^{1/2^+} = \frac{I_{758}}{I_{666}}, \tag{6.4}$$

$$\frac{I_{758}}{I_{468}}^{9/2^+} = \frac{I_{758}}{I_{468}}^{1/2^+} = \frac{I_{758}}{I_{468}}, \tag{6.5}$$

$$\frac{I_{468}}{I_{666}}^{9/2^+} = \frac{I_{468}}{I_{666}}^{1/2^+} = \frac{I_{468}}{I_{666}}. \tag{6.6}$$

The right hand side terms without super index indicate the total relative intensity calculated with the peak area and relative efficiency. Taking into account the equations above we can extract the relative intensities of 468-, 666- and 758-keV γ lines from the decay of $1/2^+$ and $9/2^+$ isomers of ^{81}Ge. The results were directly collected in Tab. 6.1 and Tab. 6.2.

- **336-keV state**

In analogy to 758-keV state the intensity of γ transitions that de-excite the 336-keV level was calculated in the same way. In the case of the $9/2^+$ decay scheme all the γ intensity that populates the 336-keV state is transformed into the intensity of 243- and 336-keV lines:

$$\underset{to\ 336\ keV}{I_{\gamma}^{9/2^+}} = (I_{243} + I_{336})^{9/2^+}, \tag{6.7}$$

where the right hand side term is obtained by summing directly the intensities that feed the level. In order to extract the intensities of 243- and 336-keV lines the intensity conservation equation was employed:

$$\frac{I_{336}}{I_{243}}^{9/2^+} = \frac{I_{336}}{I_{243}}^{1/2^+} = \frac{I_{336}}{I_{243}} \quad . \tag{6.8}$$

On the other hand, the intensities of 243- and 336-keV transitions from the $1/2^+$ decay scheme can be computed by subtracting the values from the decay scheme of $9/2^+$ state to the total relative intensity calculated with the area and relative efficiency, similarly to Eq. 6.3:

$$(I_{243,336})^{1/2^+} = (I_{243,336}) - (I_{243,336})^{9/2^+}. \tag{6.9}$$

- **93- and 290-keV states**

The way to obtain the relative intensities of 197- and 290-keV is the same that in the cases of 243- and 336-keV lines. Finally, the relative intensity of 93-keV transition in the $9/2^+$ decay scheme is determined by summing directly the intensity of the four populating lines while in case of the $1/2^+$ decay scheme it was computed by subtracting the intensity from $9/2^+$ decay to the total relative intensity of 93-keV line.

Once all the relative intensities in arbitrary units for all γ transitions were computed in both level schemes they were normalized to the total relative intensity of 336-keV line, i.e.:

$$I_{336}^{1/2^+} + I_{336}^{9/2^+} = 100\% \tag{6.10}$$

Absolute intensity per 100 parent decays

Because the β feeding of the ground state of ^{81}As in the decay of $9/2^+$ state of ^{81}Ge was assumed to be zero, the normalization equation allows to transform the relative intensity units into the absolute units per 100 decays of the $9/2^+$ isomer of ^{81}Ge, was determined with the following expression:

$$\underset{to\ gs\ from\ 9/2^+}{I_{rel}^{\gamma+ce}} = 100\%. \tag{6.11}$$

The conversion coefficients $\alpha_{93} = 0.16(3)$, $\alpha_{197} = 0.01(5)$ and $\alpha_{336} = 0.007(3)$ were taken from the Nuclear Data Sheets for $A = 81$ [Bag08]. Adding all the relative intensities of transition that go directly to the ground states we obtain the normalization factor $f_{9/2^+} = 0.71(3)$.

$\mathbf{E_\gamma}$**(keV)**	$\mathbf{I_\gamma^{rel}}$**(%)**
388.4 *2*	3.5 *3*
467.7 *6*	100 *4*
491.2 *1*	43.4 *17*
520.8 *3*	1.4 *4*
1405.8 *3*	5.2 *8*
2029.9 *4*	3.7 *5*
2571.3 *6*	0.8 *3*
2831.4 *2*	0.9 *4*

Table 6.3: The strongest transitions observed in the decay of ^{81}As to ^{81}Se. For absolute intensity multiply by 0.440(14).

The situation in the decay of the $1/2^+$ isomer is more complicated because we do not know the direct β feeding of the ground state of ^{81}As. However, it can be estimated from the information of the decay of ^{81}As to ^{81}Se via the following expression:

$$I_{\beta,gs}^{1/2^+} = \left[\sum_{^{81}Se\ isomer+gs} I_{\gamma+ce} + I_{\beta,gs}^{^{81}Se} + I_{\beta,isomer}^{^{81}Se} \right] - \left[\sum_{^{81}As\ gs} I_{\gamma+ce}^{9/2^+} + \sum_{^{81}As\ gs} I_{\gamma+ce}^{1/2^+} \right], \quad (6.12)$$

which describes the balance between the relative γ intensity that feeds the long-lived 103-keV isomer and the ground state of ^{81}Se, the β feeding of this isomer and the ground state and the sum of γ and β intensities that feed the ground state of ^{81}As from the decays of ^{81}Ge. The β feeding of the 103-keV isomer and the ground state of ^{81}Se was taken from the latest evaluation [Bag08], while the γ intensity that directly feeds these levels was calculated from our spectrum by measuring the areas of the peaks of transitions that go directly to the isomer and the ground state according to the level scheme from the same reference. In this way, we have obtained the absolute intensities of the strongest γ lines observed in ^{81}Se. Tab.6.3 collects the energies of these transitions and their relative intensities. In order to get the absolute values per 100 decays of ^{81}As one should multiply by 0.440(14).

Once all ingredients from Eq. 6.12 are calculated the β feeding of the ground state of ^{81}As populated in the decay of $1/2^+$ isomer of ^{81}Ge was computed. The β feeding of the rest of levels was calculated by making the balance between the outgoing and incoming intensity and at the end all the intensities were normalized to 100% (see Fig. 6.5 and Fig. 6.6). Finally, in order to convert the relative normalized intensity into the absolute units per 100 decays of the $1/2^+$ isomer we use the following equation:

$$100\% = \sum_{to\ gs\ from\ 1/2^+} I_{rel}^{\gamma+ce} + I_{\beta,gs}^{1/2^+}. \quad (6.13)$$

The normalization factor that is extracted from this formula is $f_{1/2^+} = 0.62(7)$, which is in agreement and more precise that the value published in [Bag08]. Table 6.4 summarizes

the energy of the levels, β feeding and logft values obtained in the decay of the ground state and $1/2^+$ isomer of ^{81}Ge.

E(keV)	J^π	Decay of $9/2^+$		Decay of $1/2^+$	
		I^β_{abs}(%)	logft	I^β_{abs}(%)	logft
0.0	$3/2^-$			13 *8*	6.5 *3*
93.0^b ***1***	$(1/2^-)$			11 *4*	6.51 *17*
290.3^b ***1***	$(3/2^-)$			9 *2*	6.62 *12*
336.2^b ***1***	$5/2^-$			4 *3*	6.9 *4*
737.8 ***1***	$7/2^-$	10.2 *2*	6.12 *10*		
758.5^b ***1***	$(3/2)$			9 *2*	6.42 *13*
864.3 ***2***	$(1/2^-,3/2^-,5/2^-)$			≤ 0.7	≥ 7.5
1041.9 ***1***	$(7/2^-)$	8.2 *7*	6.10 *5*		
1083.5 ***1***		7 *3*	6.16 *19*		
1129.2 ***1***	$9/2^-$	2.2 *18*	≥ 6.4		
1195.2 ***2***	$(5/2^-,7/2^-,9/2^-)$	0.2 *7*	≥ 7.0		
1613.6 ***3***	$9/2^{(+)}$	0.1 *18*	≥ 6.5		
1777.9 ***5***		1.1 *3*	6.68 *13*		
1869.9 ***2***	$(1/2,3/2,5/2)$			1.7 *4*	6.73 *11*
1915.0 ***4***		1.1 *16*	≥ 6.4		
1959.6 ***4***	$(1/2,3/2,5/2)$			1.1 *2*	6.88 *9*
2142.0 ***3***		2.9 *17*	≥ 6.0		
2251.1 ***3***		0.4 *2*	6.9 *2*		
2360.1 ***5***	$13/2^-$	0.9 *2*	6.50 *11*		
2405.7 ***5***		0.5 *2*	6.73 *18*		
2624.7 ***1***	$(9/2^+)$	21 *3*	4.99 *7*		
2758.5 ***1***	$(11/2^+)$	12.8 *13*	5.14 *6*		
2862.7 ***3***	$(1/2,3/2,5/2)$			3.2 *5*	6.04 *8*
2872.4 ***6***		0.8 *3*	6.28 *17*		
2911.6 ***2***		1.0 *5*	6.16 *22*		
2966.1 ***1***	$(7/2^+)$	13.3 *11*	5.00 *5*		
3135.8 ***2***	$(1/2^+,3/2^+)$			12.9 *19*	5.30 *8*
3179.7 ***4***		1.3 *7*	5.9 *2*		
3194.9 ***2***	$(1/2^+,3/2^+)$			10.9 *14*	5.34 *7*
3290.5 ***2***	$(7/2^+,9/2^+,11/2^+)$	9 *2*	4.96 *10*		

Continued on next page

Table 6.4 – *Continued*

E(keV)	J^π	**Decay of $9/2^+$**		**Decay of $1/2^+$**	
		I^β_{abs}(%)	logft	I^β_{abs}(%)	logft
3308.2 *3*	$(1/2^+,3/2^+)$			7 *4*	5.5 *3*
3368.0 *2*	$(7/2^+,9/2^+,11/2^+)$	5.5 *5*	5.14 *6*		
3458.2 *4*	$(1/2^+,3/2^+)$			3.4 *0.5*	5.74 *8*
3528.0 *4*	$(1/2^+,3/2^+)$			3.1 *6*	5.70 *9*
3562.0 *3*	$(1/2^+,3/2^+)$			8.4 *12*	5.26 *8*
4054.5 *4*	$(1/2^+,3/2^+)$			3.7 *6*	5.31 *8*

Table 6.4: Energy, absolute β feeding and logft values of levels populated in the β-decay of $1/2^+$ and $9/2^+$ isomers of ^{81}Ge.

[a] logft values were computed from https://nndc.bnl.gov/logft.

[b] Levels found in both isomeric decays of ^{81}Ge.

As can be observed in Tab. 6.1 and Tab. 6.2 some transitions were not placed in any of the decay schemes. All of them populate the low-lying levels and may belong to the decay of the $1/2^+$ isomer or $9/2^+$ ground state of ^{81}Ge. They were definitely observed in coincidence with 93-, 197-, 290- and 336-keV lines and probably de-excite the corresponding level obtained by summing its energy and the populated level. However, there is no easy way to make any strong decision about their allocation. Nevertheless, we can estimate the possible loss of intensity that feeds a certain level. In case of 93-keV state six γ-rays of 1978, 2395, 2965, 3451, 3538 and 3567 keV can be placed populating it directly. This corresponds to 8.4(5)% of relative intensity that must be taken into account for the β-feeding calculations. If all of this transitions belong to the decay of $1/2^+$ isomer the β feeding of 93-keV level should be reduced to 6.4(38)% in absolute units. The rest of states suffer smaller modifications in their β feeding and can be included in the error bar and do not seriously affect the logft values. Considering the rest of lines of 1172, 1818 and 2138 keV that populate the 336-keV level and the 2430-keV line that populates the 290 state, the β feeding of each state will be reduced to 2.0(29)% and 7.8(21)%) respectively. In the case of the 336-keV level the lower limit of logft will be 6.8, in good agreement with a first unique β transition from $1/2^+$ to $5/2^-$.

If all the unallocated transitions belong to the decay of $9/2^+$ state of ^{81}Ge the relative intensity of 93-keV transition in this decay will be increased from 15.7(18)% to 24.1(18)% and the relative intensity of 336-keV will be modified from 74.4(46)% to 78.0(46)%. The change of intensity in 197- and 290-keV lines will be much smaller, as the intensity of 2430-keV transition that would populate the 290-keV level is only 2.0(4)%. All these modification will reduce the relative intensities of 93-, 197, 290- and 336-keV in the decay of $1/2^+$ and thus the β feeding to the states de-excited by these lines. Anyhow, the logft will not suffer any significant changes.

6.3 Lifetime measurements

The measured upper limit of 0.7 ns for the 336-keV state provides an opportunity to compute the value by measurements with ATD $\beta\gamma\gamma$(t) method. Our data show enough statistics for half-life measurements of the 93- and 290-keV, states which seem to lie also in the subnanosecond range. Finally, the strong intensity of 737- and 793-keV gammas open the possibility to determine the lifetime of the 738- and 1129-keV levels employing the Centroid Shift technique.

In order to perform the fast-timing measurements a specific multi-parameter data set was presorted out as discussed in Chapter 3. Coincidences between the three different cards of PIXIE-4 DAQ were done. The first card (labeled with 0) contains the information about the proton pulses and energies from both HPGe detectors. The card labelled with 1 and 2 carries the signals of the $LaBr_3$(Ce) energy and corresponding FTAC while the card number 3 contains the input signal of the β energy. The presorting was done for different combinations of $LaBr_3$(Ce) detectors and HPGe. In total, four multi-parameter files were presorted containing the four possible combinations between these detectors. The data analysis was done with each file separately and summing at the end the contribution of both HPGe. The data set includes 9 parameters: time since last proton, proton pattern, β energy, HPGe energy, $LaBr_3$(Ce) energy, time distribution from the FTAC, time difference between events from $LaBr_3$(Ce) and FTAC (within the same card), time difference between events from β detector and $LaBr_3$(Ce) and time difference between $LaBr_3$(Ce) and HPGe. The last three ones were employed for random subtraction.

- **Half-life of the 1129-keV state**

The strong 793-keV transition must be of $E2$ character because it connects the $9/2^-$ and $5/2^-$ states. According to the compilation of transition strengths made by P. M. Endt in 1979 [End79] the $B(E2)$ should not exceed 40 W.u. and is higher than 1 W.u. in nuclei in the intermediate neighbourhood of ^{81}As. These values transformed to the partial lifetime of 793-keV transition leads to 3-125 ps, within the sensitivity of our fast-timing techniques.

Unfortunately, the low efficiency of $LaBr_3$(Ce) at energies beyond 1 MeV does not allow us to use directly the 793- and 1496-keV sequential transitions since the latter can be barely selected in the energy spectrum. However, the energy gate in 336-keV peak in HPGe detector can be set to see both mentioned lines in coincidence with the scintillator detector. Doing that the Centroid Shift technique is employed to obtain the lifetime making use of the following expression:

$$T_{1/2}\,(1129\text{ keV}) = ln2\,[\Delta t - (\tau_0(793) - \tau_0(1496))]\,. \tag{6.14}$$

Due to the very low Compton background, its correction was considered negligible in this case. The prompt position τ_0 at these energies is determined with the Prompt Response Curve from Fig. 3.26. A $\tau = 47(11)$ ps mean-life is obtained with $LaBr_3$(Ce)-1 while the $LaBr_3$(Ce)-2 gives a less precise value of $\tau = 49(17)$ ps. The mean value multiplied by $ln2$ leads to $T_{1/2} = 33(10)$ ps. It is well within the range expected from the systematics. The difference between the centroids of 793 and 1496 time response in FTAC-1 and FTAC-2 is plotted in Fig. 6.7. Note that around 250 ps of difference does not include the correction by Prompt Response Curve $\Delta\tau_0$ which considerably reduces this value.

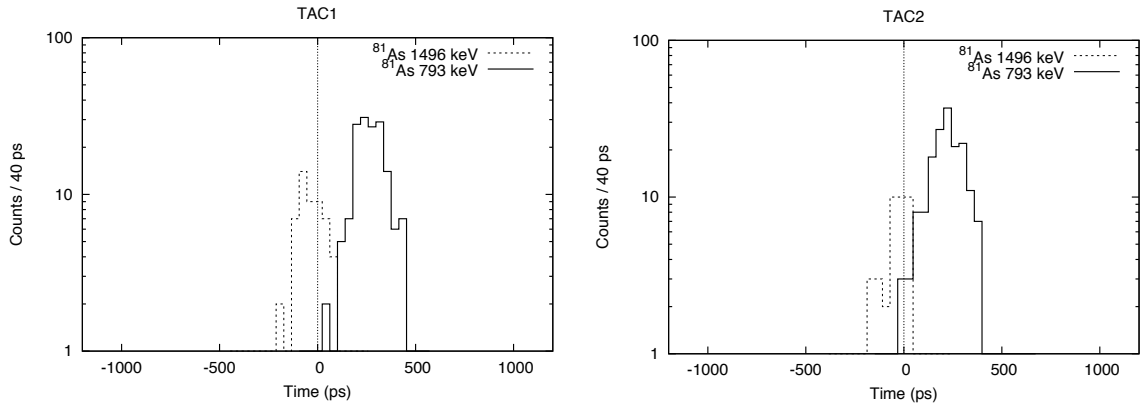

Figure 6.7: Centroid positions of 793- and 1496-keV transitions determined in FTAC-1 and FTAC-2. The plot is not yet corrected for the walk-correction or Compton-background contributions (see text for more details).

This half-life is just on the limit of application of the Convolution technique. Being in direct coincidence with the strong 336-keV line the 793-keV transition can be projected into FTAC and fitted to the deconvolution function. The result is limited by statistics but it is consistent with a slope of the order of 30 ps (see Fig. 6.8). However, as the final result the value obtained from Centroid Shift technique is considered.

- **Half-life of the 738-keV state**

In this case, the 738-keV transition is unfortunately not in coincidence with any strong line to be used with enough statistics in fast timing measurements. On the other hand, it is not strong enough to be selected directly in $LaBr_3$(Ce) energy spectrum from $\beta\gamma$(t) analysis. The only way to estimate the half-life of the 738-keV is using the Centroid Shift technique with the use of 876-keV transition populating this state. The poor statistics will increase considerably the error bar. Similarly to the situation with 793- and 1496-keV transitions, no Compton correction was included in determination of centroids in the time spectrum for 738- and 876-keV lines. We followed the Eq. 6.14 using $\tau_0(738)$ and $\tau_0(876)$. The scintillator detector labelled with 1 provides $\tau = 36(18)$ ps and the other one labelled with 2 gives $\tau = 10(20)$ ps leading to establish an upper limit of 30 ps for the half-life. This result is in good agreement with the estimation of the partial half-life of 738-keV transition obtained assuming that $B(E2)$, similarly to 793-keV line, can vary between 1 and 40 W.u. In this case, the range of the partial half-life of 738-keV line is 4-180 ps and our measured half-life of 1129-keV level falls inside this interval.

- **Half-life of 336-keV state**

The 336-keV state is strongly de-excited by a γ-ray of the same energy. P. Hoff and B. Fogelberg measured an upper limit of 0.7 ns for the half-life of this level using the $\gamma\gamma$(t) technique with Ge detectors [Hof81]. As the half-life apparently lies in the subnanosecond range it is reasonable to employ the Convolution Technique for its measurement. In the first instance we use $\beta\gamma$(t) coincidences. The data were presorted in multi-parameter file including the time since last proton impacted on target, the β energy, the energy of $LaBr_3$(Ce), the TAC and time differences between the β-$LaBr_3$(Ce) and $LaBr_3$(Ce)-TAC.

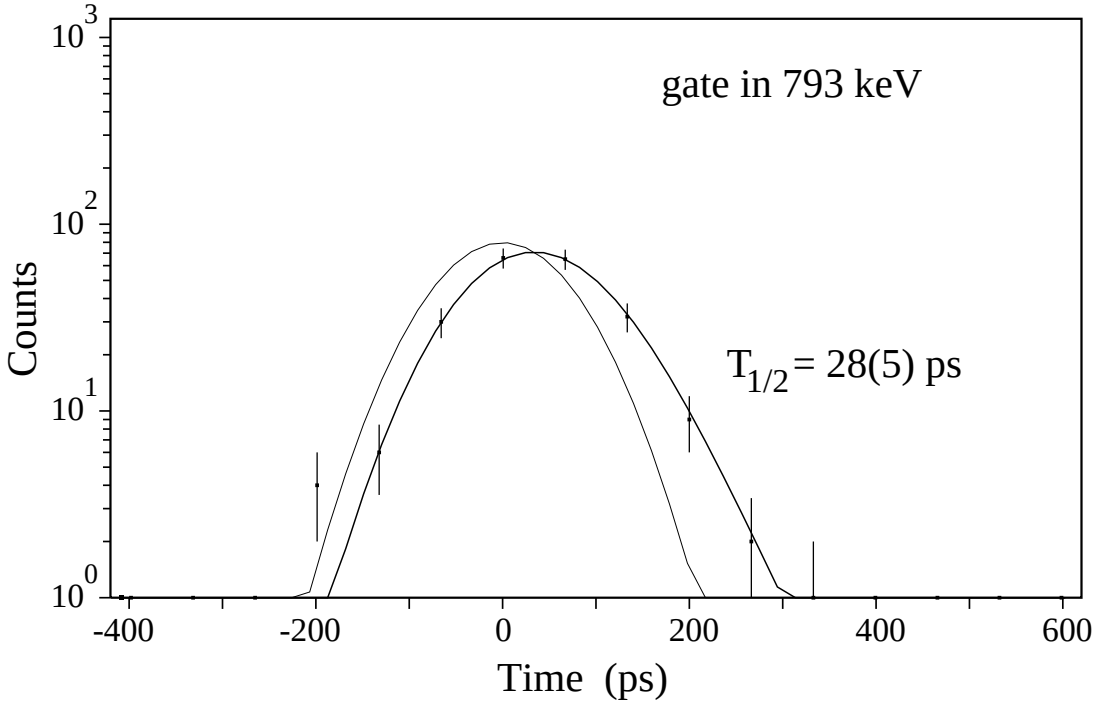

Figure 6.8: Half-life of the 1129-keV state obtained with the energy gate set in 793-keV transition in $LaBr_3$(Ce) projected into FTAC.

During the sorting we excluded the first 2.4 s since proton impact in order to minimize the contribution of short-lived activity and clean the 336-keV peak strongly mixed with the intense 351-keV line from ^{81}Ga. A suitable energy range, which permit to minimize the contribution of 511-keV peak, was set in β spectrum, excluding the low energy portion. Fig. 6.9 shows the obtained energy spectrum from the $LaBr_3$(Ce) detector. The gate set in 336-keV peak was projected into FTAC and the points in time spectrum were fitted to deconvolution function as was explained in Sec. 2.4.1. The mean value between two detectors gives $T_{1/2}$ = 159(4) ps half-life for 336-keV state. However, from the figure we can see that the 336-keV peak is seating on the non-negligible Compton background (peak to Compton ratio is ∼6) which may also cary a lifetime. Setting an energy gate on the right hand side of the full energy peak as shown in Fig. 6.9 and projecting again into FTAC we see that this lifetime reaches 59(4) ps.

Because Compton events provide a half-life it must be eliminated from the fit. One way to do it is subtracting directly a portion of counts on the right hand side of 336-keV peak during the sorting process and projecting directly into FTAC and correcting for the Compton curve. Doing this for both detectors and compressing systematically the time spectrum until reach a stable value we get $T_{1/2}$ = 169(5) ps in the detector 1 and $T_{1/2}$ = 172(4) ps in the detector 2. The mean value permit to announce the final $T_{1/2}$ = 170(5) ps value of 336-keV state half-life. The fitted time spectrum is shown in Fig. 6.10.

- **Half-life of the 290-keV state**

As it can be seen in Fig. 6.9 the 197-keV transition can be selected directly in the $LaBr_3$(Ce) energy spectrum and projected to the FTAC. However, the 216-keV transition

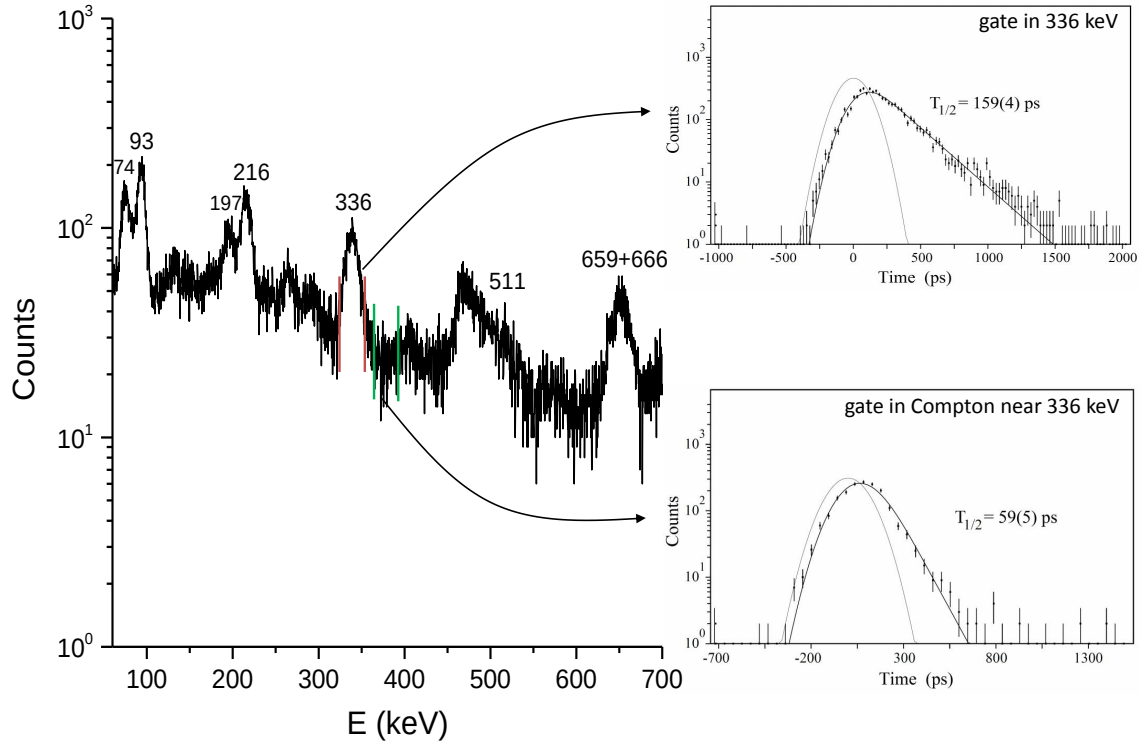

Figure 6.9: Energy spectrum of $LaBr_3$(Ce). The first 2.4 s were excluded during the sorting and no short-lived activity can be observed. The full energy peak of 336 keV and Compton background were projected into the FTAC. The contribution of 511-keV peak was considerably reduced thanks to gating in the β spectrum.

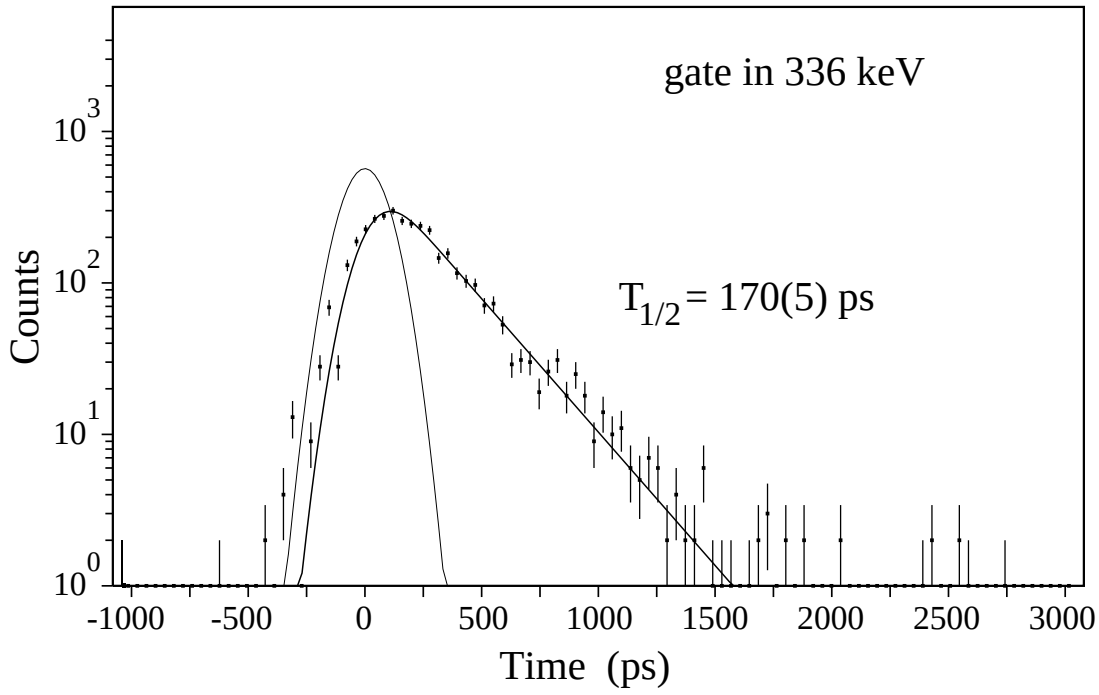

Figure 6.10: Half-life of the 336-keV state obtained with Compton suppression in $LaBr_3$(Ce) projected into FTAC.

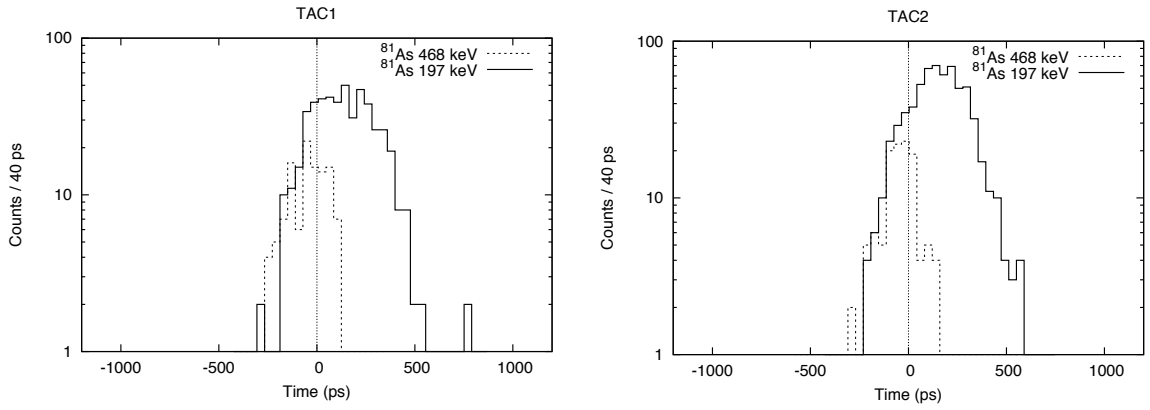

Figure 6.11: Centroid positions of 197- and 468-keV transitions determined in FTAC-1 and FTAC-2. The plot is not yet corrected for the walk-correction or Compton-background contributions (see text for more details).

from ^{81}Ge, whose lifetime was precisely determined in previous chapter, is strongly mixed with the 197-keV one and its relatively long half-life will dominate the time delayed spectrum. Even a very strict gate in time, excluding the first 4.8 s, can not completely eliminate the 216-keV contribution from $LaBr_3$(Ce) energy spectrum. Moreover, as we have already seen with 336-keV line, the Compton background also provides non-negligible half-life and can complicate the analysis. Anyhow, choosing the energy gate involving both 197- and 216-keV lines and projecting into FTAC two decay components are observed. One definitely represents the long lifetime of the 896-keV state of ^{81}Ge de-excited by the 216-keV γ-ray. Another one, of about 50 ps, may come from the 197-keV transition. This short half-life has a big error ($\approx 20 - 30$ ps) and should not be taken as the final value. For this reason, we decided to employ the Centroid Shift technique.

The 468-keV line that de-excites the 758-keV state and feeds the 290-keV one was chosen in coincidence with 197-keV transition to use triple $\beta\gamma\gamma$(t) coincidences with the Centroid Shift technique. Selecting 93-keV in the HPGe detector, both mentioned transitions will be observed in the $LaBr_3$(Ce) energy spectrum. The difference between their centroids obtained after projecting into the FTAC will render the half-life of 290-keV state. The following equation summarizes it:

$$T_{1/2}^{290} = ln2\left[\Delta t - (\tau_0(197) - \tau_0(468))\right], \tag{6.15}$$

Where Δt indicates the difference between the centroid positions due to 197- and 468-keV transitions in the time spectrum and τ_0 was taken from the Prompt Response Curve shown in Fig. 3.26 for each energy. However, as the full energy peaks sit on the Compton background, the centroid positions calculated from the time spectrum in FTAC must be corrected according to the Eq. (2.2). Once this is done, applying the Eq. (6.15) we obtain $\tau = 80(18)$ ps with the detector 1 and $\tau = 74(20)$ ps with the detector 2. Averaging this values we get the final $\tau = 77(19)$ ps or $T_{1/2} = 53(13)$ ps half-life for 290-keV state.

In the determination of this half-live we assumed that the lifetimes of 1042-, 1083-keV and 1915-keV levels, that contain transitions connecting them with the 290-keV state, are smaller than 10 ps, which is the order of magnitude of our precision.

- **Half-life of the 93-keV state**

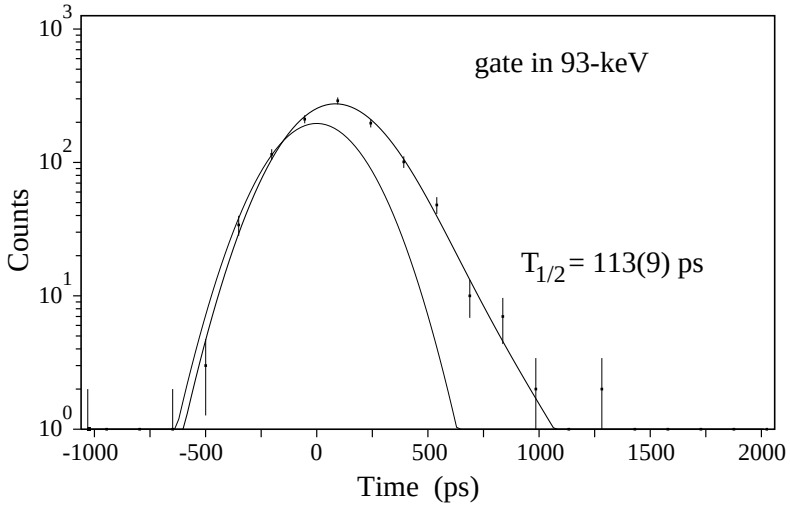

Figure 6.12: Half-life of the 93-keV state obtained by fitting in the time delayed spectrum obtained in triple coincidences. The 93-keV peak was produced in $LaBr_3$(Ce) by setting an energy gate in 197-keV transition in HPGe. The data fit included two decay functions corresponding to the half-lives of 290- and 93-keV states. The previously determined $T_{1/2} = 53(13)$ ps half-life of the first one was fixed during the fit.

In order to minimize the huge amount of Compton background in the 93-keV peak we make use of triple coincidences between HPGe, $LaBr_3$(Ce) and β detectors. The 197-keV transition was selected in germanium detector. The coincident 93-keV peak chosen in $LaBr_3$(Ce) was projected in to FTAC. As the result, the time distribution will be composed by a prompt semi-Gaussian function and exponential decays of 93- and 290-keV levels and thus apparently two slopes. The mean life of the 290-keV state has been already measured and will be used as fixed parameter. Therefore, the half-life of 93-keV level is obtained directly from the fitted slope and leads to $T_{1/2} = 113(9)$ ps (see Fig. 6.12)

In order to verify this value the Centroid Shift technique was used with the sequential 93- and 197-keV transitions. As in case of 290-keV half-life determination the centroids in time delayed spectrum were corrected by the Compton curve. The expression which describes the half-life of 93-keV level is:

$$T_{1/2}^{93} = ln2\,[\Delta t - (\tau_0(93) - \tau_0(197))]\,. \tag{6.16}$$

Unfortunately, the prompt response for 93 keV could not be determined directly from the Prompt Response Curve because it starts at 138-keV point which corresponds to a γ-ray from ^{138}Ba. Thus, linear extrapolation was necessary to be used to calculate $\tau_0(93)$. As can be seen from Fig. 3.26 the behaviour of curves towards low energies is not clear. Thus, we cannot state the goodness of our approximation. After all, the half-life obtained from the first $LaBr_3$(Ce) detector is $T_{1/2} = 105(11)$ ps while the $LaBr_3$(Ce)-2 gives $T_{1/2} = 123(9)$ ps. This leads to the average value of $T_{1/2} = 114(20)$ ps. The uncertainty was intentionally increased by a factor of 2 in order to take in account linear extrapolation error. In any case, the half-life obtained with the Centroid Shift technique is in good agreement with the result from using the Convolution technique. As final value we take the result from the de-convolution, $T_{1/2} = 113(9)$ ps

6.4 Discussion of the results

With the measured lifetimes, the reduced transition probabilities were computed and useful information for spin-parity assignments was extracted. Tab. 6.5 summarizes the results. In view of the results, some conclusions can be extracted.

If the $B(M1)$ and $B(E2)$ values for 93-keV γ-ray, that connects the first excited state and the $3/2^-$ ground state, are calculated directly from the measured mean-life value of 93-keV state slightly modified by a conversion coefficient of 0.16(3) adopted in [Bag08], the $M1$ multipolarity is the most probable because the $B(E2)$ results two orders of magnitude higher (see Tab. 6.5) than indicates the RUL [End79]. However, P. Hoff and B. Fogelberg pointed in 1981 that the 93-keV transition has a mixed $M1+E2$ character with 6.4(26)% of $E2$ [Hof81]. Using this result we can recalculate the reduced transition probabilities of 93-keV transition for $M1$ and $E2$ component. Our measured half-life of 113(9) ps must be corrected also by the branching ratio coefficient:

$$br^i_{93} = \frac{I^i_{93}}{I^{M1}_{93}(1+\alpha^{M1}_T) + I^{E2}_{93}(1+\alpha^{E2}_T)}, \tag{6.17}$$

where the index i can be $M1$ or $E2$ and partial intensities of $M1$ and $E1$ are equal to 93.6(26)% and 6.4(26)% respectively. For computation of total conversion coefficients α^i_T we used internal conversion coefficient database (BrIcc)[1] which provides $\alpha^{M1}_T = 0.1097(16)$ and $\alpha^{E2}_T = 1.035(15)$ for 93-keV transition of ^{81}As. Introducing these values into Eq. 6.17 we get $br^{M1}_{93} = 0.80(5)$ and $br^{E2}_{93} = 0.6(2)$, and thus $\tau^{M1} = 204(20)$ ps and $\tau^{M1} = 3.0(1.2)$ ns partial mean-lives. In this way, the reduced transition probabilities, as shown in Tab. 6.5, leads to $B(M1) = 0.19(2)$ W.u. and $B(E2) = 1.9(8) \times 10^3$ W.u. This results indicates that 6.4(26)% for $E2$ measured in [Hof81] is not compatible with the half-life measured in our work and should be significantly lower. An estimation of 1% mixing for $E2$ component would give $B(E2) \sim 300$ W.u. while 0.1% of mixing leads to $B(E2) \sim 30$ W.u., which is in good agreement with the systematic prediction in $A = 81$ region. In conclusion, according the measured 93-keV state half-life, the 93-keV transition is of almost pure $M1$ character. This result strongly suggests that the 93-keV state has $1/2^-$ spin-parity.

The reduced transition probability of the 197-keV transition is also much higher than the recommended upper limit (RUL) [End79]. The $E1$ possibility is very unlikely because it is difficult to have positive low-spin states at low energies in ^{81}As. However, we cannot definitely exclude this possibility, since the reduced transition probability is compatible with the systematics from [End79]. Thus, the 197-keV lines is most likely of $M1$ character and the 290-keV state takes $3/2^-$ spin-parity assignment. This assumption is also in good agreement with multipolarity of the 290-keV transition that de-excites the same level. According to Tab. 6.5 it can be of $E2$, $M1$ or mixed character.

The measured $5/2^-$ spin of 336-keV state [Por11] shows that the strong 336-keV line can have $M1$ or $E2$ multipolarity. Our measurements are in good agreement with this, but we cannot definitely claim whether it is mixed or is of pure $M1$ or $E2$ multipolarity. The other transition that de-excites the 336-keV level, the 243-keV one, is probably an $E2$.

Our assumptions about 738- and 793-keV E2 transitions were confirmed with the half-life measurements of 738- and 1129-keV states. The reduced transition probability of the

[1] http://bricc.anu.edu.au/index.php

Level (keV)	$T_{1/2}$ **(ps)**	E_γ **(keV)**	τ^γ **(ps)**	**Multipolarity**	$B(X\lambda)$ **(W.u.)**
93.0	113(9)	93.0	189(16)	E1	$3.4(3)\times10^{-3}$
				E2	$3.0(3)\times10^{4}$
				M1	0.21(2)
			3.0(12) ns	E2 6.4%	$1.9(8)\times10^{3}$
			204(20)	M1 93.6%	0.19(2)
290.3	53(13)	197.1	122(22)	E1	$5.6(10)\times10^{-4}$
				E2	$1.1(2)\times10^{3}$
				M1	$3.4(6)\times10^{-2}$
		290.5	212(39)	E1	$10(2)\times10^{-5}$
				E2	89(16)
				M1	$6.1(11)\times10^{-3}$
336.2	170(5)	243.0	6.7(8) ns	E1	$5.4(6)\times10^{-6}$
				E2	6.8(8)
				M1	$3.3(4)\times10^{-4}$
		336.2	256(20)	E1	$5.3(4)\times10^{-5}$
				E2	35(3)
				M1	$3.3(2)\times10^{-3}$
737.8	≤ 30	401.8	≤ 170	E1	$\geq 1.5\times10^{-5}$
				E2	≥ 22
				M1	$\geq 2.9\times10^{-3}$
		737.7	≤ 58	E1	$\geq 2.2\times10^{-5}$
				E2	≥ 3.1
				M1	$\geq 1.4\times10^{-3}$
1129.2	33(10)	391.6	0.51(16) ns	E1	$1.7(5)\times10^{-5}$
				E2	8(3)
				M1	$1.0(3)\times10^{-3}$
		792.9	52(16)	E1	$2.0(6)\times10^{-5}$
				E2	2.8(7)
				M1	$1.2(4)\times10^{-3}$

Table 6.5: Calculated $B(X\lambda)$ from the half-lives values determined in previous section for ^{81}As. In the cases of 290- and 336-keV states, which are de-excited by more than one γ transition, the computation was done using the partial mean-lives given by Eq. (1.27) and shown in the fourth column. In the case of 93-keV the reduced transition probabilities were computed first without taking into account the $M1 + E2$ mixing. The obtained values can be compared to $B(M1)$ and $B(E2)$ computed with the use of measured mixing factor of 6.4(26)% for $E2$ component.

738-keV γ-ray has a big error bar and the value is slightly enhanced comparing to the systematics of the $A = 81$ region. In view of our results we can confirm the $5/2^-$ and $9/2^-$ spin parity assignments of 336-, 738- and 1129-keV states measured in [Por11].

The $9/2^+$ spin-parity assignment was done for two states at 1614 and 2625 keV in the mentioned reference. We do observe them in our work. However, since no de-exciting transition to any $5/2^-$ level was detected, we cannot shed light in $\pi g_{9/2} \rightarrow \pi f_{5/2}$ proton excitation energy investigation.

As was already mentioned in the text, the six high-lying states beyond 3 MeV populated in the β-decay of $1/2^+$ isomer of ^{81}Ge were assigned to have $1/2^+$ or $3/2^+$ due to relatively high β feeding, which indicates allowed β transitions. The $\log ft$ values of the rest of levels, except the first three excited states, point to the first forbidden β transitions and thus $1/2^-$ or $3/2^-$ spin-parity assignments. A similar situation occurs in the decay of $9/2^+$ state of ^{81}Ge where the $\log ft$ value of 1195-keV level suggests the first forbidden decay with $\Delta J = 0, 1, 2$ and thus $5/2^-$, $7/2^-$ or $9/2^-$ spins for this level. The two high energy states at 3291 and 3368 keV are most likely populated via β allowed transitions and their spins can be $7/2^+$, $9/2^+$ or $11/2^+$.

6.5 Conclusions of the chapter

The β-decay of ^{81}Ge to ^{81}As was simultaneously produced via the β-decay of the long-lived $1/2^+$ isomer and the second one is the $9/2^+$ ground state. As it was not possible to distinguish the half-lives of this states the tentative allocation of γ transitions was done based on the large difference of spins and the previously known information.

The level scheme obtained from the decay of $1/2^+$ is shown in Fig. 6.6. It contains five new energy levels at 1960, 3308, 3458, 3528 and 4055 keV with respect to the latest publication of the β-decay of ^{81}Ge [Hof81]. We do not confirm the 3531-keV state in our work because the 3195-keV transition was not seen in coincidence with 336-keV. The 3368- and 2911-keV states were placed in the decay scheme of $9/2^+$ state. The 1042- and 738-keV levels were also removed from this decay due to the high change of spin from $1/2^+$. Ten not previously observed γ transitions were placed de-exciting already confirmed states and five new levels. New spin-parity assignments were done for the levels beyond 3 MeV. The absolute intensity was determined for the all γ lines and the new absolute and intensities were calculated with more precision than in previous works [Bag08].

The decay scheme of $9/2^+$ state includes all previously known structure and seven new levels, as was plotted in Fig. 6.5. New spin-parity assignments were already discussed in Sec. 6.4. Many of them were taken from transfer reaction experiment [Por11] and some of them were proposed based on the level scheme from this work. Twelve new γ transitions were found. Four of them were added to the already measured levels. The absolute intensities were determined with the use of decay of ^{81}As to ^{81}Se. With this information we also could calculate the absolute intensities of transitions in this decay.

We have measured five new half-lives of 93-, 290-, 336-, 738- and 1129-keV states (see Tab. 6.5). Our results confirms the $9/2^-$ spin of 1129-keV level, the $7/2^-$ spin of 738-keV level and the $5/2^-$ spin of 336-keV level. Half-lives of 93- and 290-keV states gives strong arguments to state that their spins are $1/2^-$ and $3/2^-$, respectively. We confirm the $E2$ character for 793- and 738-keV lines, mixed $M1 + E2$ nature for 336- and 197-keV transitions and an almost pure $M1$ component for 93-keV line.

Conclusions and Outlook

The modification of the ordering of single-particle levels in nuclei with large neutron to proton ratio with respect to stable nuclei, provides rich information on the structure of exotic nuclei and are crucial for the development of nuclear models that can be applied at the limits of the nuclear chart. The regions around radioactive doubly-magic nuclei such as ^{78}Ni, ^{100}Sn and ^{132}Sn are especially interesting. This PhD thesis is aimed at the study of nuclei in the region around the doubly-magic nucleus ^{78}Ni, with $Z = 28$ and $N = 50$. Although ^{78}Ni itself is, up to now, very difficult to reach, some of the neighbouring nuclei can be investigated with different experimental tools at large scale facilities such as ISOLDE at CERN (Switzerland), RIBF at RIKEN Nishina Center (Japan) or GANIL in Caen (France) or the NSCL at MSU (USA). In addition, properties of nuclei in this region have a role in the astrophysical rapid neutron capture process.

Starting from the β-decay of ^{81}Zn, the structure of four very exotic nuclei of ^{81,80}Ga, ^{81}Ge and ^{81}As have been explored in this thesis. The experimental campaign had been performed at the ISOLDE Radioactive Beam Facility situated at the accelerating complex of CERN (Geneva, Switzerland), within experiment IS441. Several improvements in the beam production, aimed at reducing the otherwise high Rb contamination, allowed to produce an almost pure beam of Zn isotopes. The high purity and intensity of Zn beams delivered by the ISOLDE facility at CERN have made it possible to obtain about ten-fold higher statistics than previous attempts [Pad10].

The experimental set-up was optimized for the measurement of lifetimes of the excited nuclear states and included five detectors: two with excellent energy resolution for γ detection (HPGe), two scintillator crystals with very good timing properties ($LaBr_3$(Ce)) and a thin plastic scintillator for the detection of β particles. The combinations HPGe-HPGe and β-HPGe were employed to deduce the nuclear decay schemes and the use of β-$LaBr_3$-FTAC and β-$LaBr_3$-HPGe-FTAC was applied for lifetime measurements in the range of nanoseconds and tens of picoseconds. The Advanced Time Delayed (ATD) $\beta\gamma\gamma$(t) method (fast-timing) [Mac89, Mos89] was used for lifetime measurements of the excited states. Together with the decay branching ratios, they provided reduced transition probabilities for several transitions, which help clarify the low-lying structure of the nuclei under study.

The main contributions of this thesis are summarized below. They concern both high-resolution gamma spectroscopy and fast-timing measurements from the beta-decay of ^{81}Zn, ^{81}Ga and ^{81}Ge. New information on β-decay schemes, γ-ray absolute intensities, β feeding of the populated states, and ground state half-lives is provided. Beta-delayed neutron emission probabilities have been also measured when possible.

Several level lifetimes have been measured for the first time, and several half-life limits are provided as well. The half-life measurements of the excited states were performed

using either the convolution technique or the centroid shift technique. The first one was employed for longer half-lives (from 60 ps to 5 ns) while with the second one we measured half-lives down to 10 ps. Timing calibrations were done with ^{138}Cs and ^{140}Ba sources. During the analysis we could determine two long-lived half-lives of the 1899- and 2083-keV levels from the ^{138}Cs and ^{140}Ba decays, respectively. Our results are in good agreement with the previous measurements [Mac95a].

The reduced transition probabilities have been obtained, and possible spin-parity assignments based on the experimental information and the systematics of the region have been discussed for each of the nuclei under study. The results are compared with large-scale model calculations, when possible. The new structure of ^{81}Ga (and ^{80}Ga) populated in the β-decay of ^{81}Zn is summarized in an article submitted to *Physical Review C* while the results on ^{81}Ge and ^{81}As are in preparation.

Results on the β-decay of ^{81}Zn and structure of ^{81}Ga

The level scheme of the $N = 50$ nucleus ^{81}Ga has been significantly expanded with 47 new levels and 70 transitions in the energy range up to 6.5 MeV, very close to the neutron separation energy. The 290(4)-ms half-life of ^{81}Zn measured in this work is in good agreement with the previous works [Pad10, Xu14]. The direct β feeding to the ^{81}Ga ground state measured in our experiment is compatible with zero, and much lower than proposed previously by Padgett *et al.* [Pad10], thus compatible with both $5/2^+$ and $1/2^+$ assignments for the ^{81}Zn ground state. We do not observe β nor γ population to the $9/2^+$ state seen in other $N = 50$ isotones and also predicted by our shell-model calculations at around 3 MeV. Both observations are compatible with a ^{81}Zn ground state of $1/2^+$ nature, which then will point towards a crossing of the neutron $\nu(s_{1/2})$ and $\nu(d_{5/2})$ single-particle orbitals for the $N = 51$ ^{81}Zn.

Negative-parity levels are densely packed in the region from 1 to 2 MeV of the level scheme of ^{81}Ga. This is consistent with $\pi(p_{3/2})$ and $\pi(f_{5/2})$ single-particle states coupled to the 2^+ core in ^{80}Zn, and it is well reproduced by our shell-model calculations. These states should be populated by first-forbidden β transitions. The level scheme of the $N = 50$ isotone ^{83}As [Win88b] also shows similar high density around 1400 keV and it is much alike. Moreover, a similar structure is found in the ^{85}Br nucleus with $N = 50$ and $Z = 35$, populated by the β-decay of ^{85}Se [Sin14]. The situation changes beyond 5 MeV where we observe several states with sizeable apparent β-feeding, which should arise from allowed transitions from the ^{81}Zn positive-parity ground state. These levels of positive parity are confirmed by our theoretical calculations made with the $JUN45$ and $jj44b$ effective interactions. They can be interpreted as neutron particle-hole excitations from the ^{78}Ni core, and their high energy gives evidence for a strong neutron shell closure, contrary to statements made in [Por09]. The β feeding to high-lying ^{81}Ga states is of strong interest, but can probably only be fully understood by performing a total absorption spectroscopy experiment.

The level scheme of ^{80}Ga populated in the β-delayed neutron emission from ^{81}Zn was built for the first time. It is in agreement with the scheme presented in [Lic14] from the β-decay of ^{80}Ga, including the low-lying 22-keV isomer. The new level scheme contains 11 γ transitions that de-excite 9 levels. The β-delayed neutron emission probability of ^{81}Zn was measured to be 23(4)%. This result is more precise than the value of 30(13) %

measured in [Hos10] and consistent with the lower limit of 10 % proposed in [Kös05]. The apparent half-life of ^{80}Ga, in which both the 22-keV isomer and the g.s. are involved, was measured to be $T_{1/2}$ = 1.70(3) s, which is in good agreement with the adopted value of 1.676(14) s form [Sin05] and with the average half-life of 1.71(2) calculated by Verney *et al.* [Ver13].

For the first time we have measured the half-life of the first excited state in ^{81}Ga to be $T_{1/2}$ = 60(10) ps, which indicates a l-forbidden $M1$ transition of 351 keV between $\pi p_{3/2}$ to the $\pi f_{5/2}$ configuration. This is supported by our shell-model calculations, where the dominant occupations for the ground and first-excited states are found. The occupation probability and our experimental results strongly suggests the $\pi(f_{5/2})^2 \otimes \pi(p_{3/2})^1$ configuration for the first excited state of ^{81}Ga. The calculated transition rate supports this assignment too. From the shell-model calculations its value can be estimated as 3 W.u. leading to 97% of branching ratio for $M1$. For the second excited state a half-life of 23(16) ps is found. This allows to propose a $\pi(f_{5/2})^3$ *cluster* configuration built on the ^{78}Ni core, and a $3/2^-$ spin-parity assignment for this state. Our measurements also confirm the long 18.3(13)-ns half-life of 708-keV isomer from ^{80}Ga.

A comparison to the neighbouring Ga isotopes with $N = 40$ to $N = 50$ supports this description of the low-lying states, where the $5/2^-$ single-particle configuration becomes the ground state for ^{81}Ga, and the $3/2^-$ evolves to higher energies. The $N = 50$ systematics reveals a consistent picture for odd-A nucleus with $Z = 31$ to $Z = 37$, that is, ^{81}Ga, ^{83}As, ^{85}Br, and ^{87}Rb, with the $3/2^-$ $\pi(p_{3/2})^1$ configuration becoming the ground state for ^{85}Br, once the $\pi f_{5/2}$ is filled. A half-life of $T_{1/2}$ = 80(5) ps for the first-excited state in very similar ^{87}Rb had been reported, in excellent agreement with our finding for the first excited state in ^{81}Ga.

Results on the structure of ^{81}Ge

The β-decay of ^{81}Ga to ^{81}Ge had already been thoroughly studied in [Hof81] at the OSIRIS fission separator. In this work we have extended the ^{81}Ge level scheme by including 15 new γ transitions and 11 new energy levels, giving in total 111 transitions depopulating 47 energy levels. The previously known structure has been confirmed. The measured absolute gamma intensities are in very good agreement with the previous value [Hof81]. A 1.25(3)-s half-life of ^{81}Ga has been measured, in agreement with the adopted value of 1.217(5) s from [Bag08]. The situation at high energies includes nine states between 3.0 and 4.5 MeV with strong β feeding and, therefore, connected with the ground state of ^{81}Ga by allowed transitions. According to selection rules their spins may be $3/2^-$, $5/2^-$ or $7/2^-$, arising from excitations of the core.

Fast-timing measurements have allowed to measure three precise half-lives of the 711-, 896- and 1723-keV states in ^{80}Ge. We were able to establish an upper limit of the half-life of the 1832-keV level as well. The values obtained can be examined in the light of existing information for the same states, specially the transfer reaction study of ^{81}Ge [Bag08] (complemented by the ^{79}Zn investigation [Orl15] with the same technique) and the systematics of the region. This, combined with the $E1$ multipolarity of 216-keV transition makes confirms the assignment of the pair of intruders of $1/2^+$ and $5/2^+$ at 679 and 711 keV respectively. Additionally, the low $B(E2)$ value of 711-keV γ-ray determined with 3.48(8)-ns half-life of 711-keV state indicates weak collectivity and, thus, confirms

the single-particle configuration of $5/2^+$ intruder. Finally, the two short half-lives in picosecond range were measured for the first time for strongly depopulated states at 1723 and 1832 keV. Systematic behaviour of such pair of states in nuclei similar to ^{81}Ge makes it possible to forecast a tentative assignment of their spins, namely $3/2^-$ or $5/2^-$.

The comparison of the systematics of the neutron intruder $1/2^+$, $3/2^+$ and $5/2^+$ states with respect to the $9/2^+$ ground states in the $N = 49$ isotones with Z below 40 reveals a very consistent picture, including the recently available data for ^{79}Zn [Orl15]. The minimum energy of these intruder configurations occurs for ^{83}Se, and it is already increasing in ^{81}Ge. The energy gap between the single-particle $1/2^+$ and $3/2^+$ states remains practically constant at around 550 keV in the isotonic chain. The lifetime measurements of excited states in ^{81}Ge from our work provide compelling indication of the robustness of this description.

Results on the structure of ^{81}As

The excited structure of ^{81}As was simultaneously populated in the decay of the both β-decaying long-lived $1/2^+$ isomer and the $9/2^+$ ground state of ^{81}Ge. Since there was no option to select their decay due to the undistinguishable β-decay half-lives a tentative allocation of γ transitions to either state has been done basing on large difference of spins and the existing information in the literature.

The level scheme obtained from the decay of $1/2^+$ state of ^{81}Ge contains five new levels at 1960, 3308, 3458, 3528 and 4054 keV, compared to the latest publication of the β-decay spectroscopy of ^{81}Ge [Hof81]. We cannot confirm the 3531-keV state in our work because of the lack of coincidences of the 3195-keV transition with the 336-keV γ-ray. The 3368- and 2911-keV states were chosen to belong to the decay scheme of $9/2^+$ state, whereas the 1042- and 738-keV levels were removed from the decay of the $1/2^+$ ^{81}Ge isomer due to the large spin difference of the populating radiation. Ten not previously observed γ transitions were placed de-exciting already confirmed states and also a few tentative new levels. New spin-parity assignments were proposed for the levels beyond 3 MeV. The absolute intensity was determined for all γ lines with better precision than previously available [Bag08]. The decay scheme of $9/2^+$ ground state of ^{81}Ge includes all the previously known levels and seven new states. Twelve new γ transitions were found. Four of them were added to de-excite already measured levels. The absolute intensities were determined with the help of the decay of ^{81}As to ^{81}Se. With this information we also could calculate the absolute intensities of transitions in this decay.

For the first time, we have measured five new half-lives of the low-lying 93-, 290-, 336-, 738- and 1129-keV states in ^{81}As. Our results are consistent with the $9/2^-$ spin of 1129-keV level, the $7/2^-$ spin of 738-keV level and the $5/2^-$ spin of 336-keV level. The new half-lives of the 93- and 290-keV states provide strong arguments for spin-parity assignments of $1/2^-$ and $3/2^-$. We confirm the $E2$ behaviour for 793- and 738-keV line, and the mixed $M1+E2$ nature for 336- and 197-keV transitions. From our measurements a pure or almost pure $M1$ character of the 93-keV transition connecting the first-excited state to the ground state is deduced. This points towards a dominating single-proton configuration for the 93-keV state. The low-lying structure of ^{81}As is in agreement with the trend observed in the odd-A As isotopes.

Outlook

In spite of the impact of spectroscopic properties of neutron-rich nuclei far from the stability line, they have not been thoroughly studied yet due to technical limitations. The region around the doubly-magic ^{78}Ni is of the highest interest. Our comprehensive measurement of the ^{81}Zn β-decay to ^{81}Ga, providing detailed spectroscopy results, is the closest approach to date to the spectroscopy of the β-decay of ^{79}Ni to ^{79}Cu, a nucleus with a valence neutron to a nucleus with a valence proton above the ^{78}Ni core. Such study will be of the highest interest to elucidate the single-particle configurations and excitation energies in ^{79}Cu, but also to probe the solidity of the ^{78}Ni shell closure, and should be possible at the RIBF facility in the RIKEN Nishina center in Japan. Complementary approaches will also be desirable to understand the β-feeding pattern, such as the total absorption measurement mentioned above, and to understand the physics underlying forbidden β transitions. Mass measurements in the region, including Zn and Cu isotopes up to ^{79}Cu are feasible at ISOLDE, and have already been performed or are under preparation.

The low-lying structure is of $N = 49$, $N = 50$ and $N = 51$ nuclei in the vicinity of ^{78}Ni needs to be experimentally studied to understand the nuclear structure in this region. It can also be relevant for the r-process neutron capture rates that produce the elemental abundances. Complementary techniques, such as β-decay, fast-timing methods, β-delayed neutron spectroscopy, and transfer reactions provide a wider view on the region. A recent experimental study employs the ^{78}Zn(d,p) transfer reaction at REX-ISOLDE to populate ^{79}Zn single-particle neutron states [Orl15] and concludes the the lowest-lying excited states originate from neutron orbits across the $N = 50$ shell gap. Transfer reactions of this kind illustrate the complementarity of experimental techniques that can be employed to investigate this corner of the nuclide chart.

The data subject of analysis in this Thesis are part of a systematic high-resolution spectroscopy and fast timing investigation of exotic nuclei around ^{78}Ni populated in the β-decay of Zn at the ISOLDE-CERN facility (experiment IS441). Data analysis is ongoing for several decay chains, including the ^{82}Ga structure obtained from the β-decay of ^{82}Zn, and the study of the $A = 80$ isobars.

Finally, it is worth mentioning that large-scale radioactive ion beam facilities are being constructed or upgraded around the world. They will be able to produce beams of the radioactive nuclei subject of this Thesis with unprecedented intensities, which will pave the way for high sensitivity studies. These facilities include the RIKEN Radioactive Ion Beam Factory (RIBF), already delivering the highest-intensity fragmentation beams, the High Intensity and Energy ISOLDE upgrade (HIE-ISOLDE project) at CERN and the future Facility for Rare Isotope Beams (FRIB) based in the Michigan NSCL, USA. In order to profit from such facilities, developments in instrumentations needs to match the advancement in production of rare species. Experimental groups around the world are working on constructing highly-developed setups for the detection of gamma-rays, neutrons and charge particles. A FAst TIMing Array (FATIMA) based on state-of-the-art scintillators is under commissioning for the [Fra15].

Publications and conference presentations

The list of articles and conference presentations done by the candidate during the thesis is included below.

Articles

1. *Fast timing study of ^{81}Ga from the β decay of ^{81}Zn.* **V. Paziy**, H. Mach, L. M. Fraile, A. Aprahamian, C. Bernards, J. A. Briz, B. Bucher, C. J. Chiara, Z. Dlouhý, I. Gheorghe, D. Ghiţa, P. Hoff, J. Jolie, U. Köster, W. Kurcewicz, R. Lica, N. Marginean, R. Marginean, B. Olaizola, J.-M. Régis, M. Rudigier, T. Sava, G. S. Simpson, M. Stanoiu, L. Stroe, J. M. Udías, W. B. Walters. Submitted to Physical Review C.

2. *Ground state doublet in ^{73}Ga.* V. Vedia, L. M. Fraile, **V. Paziy**, H. Mach, , A. Aprahamian, C. Bernards, J. A. Briz, B. Bucher, C. J. Chiara, Z. Dlouhý, I. Gheorghe, D. Ghiţa, P. Hoff, J. Jolie, U. Köster, W. Kurcewicz, R. Lica, N. Marginean, R. Marginean, B. Olaizola, J.-M. Régis, M. Rudigier, T. Sava, G. S. Simpson, M. Stanoiu, L. Stroe, J. M. Udías, W. B. Walters. In preparation.

3. *Fast-timing study of the l-forbidden $1/2^+ \to 3/2^+$ $M1$ transition in ^{129}Sn.* R. Lica, H. Mach, L. M. Fraile, A. Gargano, M. J. G. Borge, N. Marginean, C. O. Sotty, V. Vedia, A. N. Andreyev, G. Benzoni, P. Bomans, R. Borcea, L. Coraggio, C. Costache, H. De Witte, F. Flavigny, H. Fynbo, L. P. Gaffney, P. T. Greenlees, L. J. Harkness-Brennan, M. Huyse, P. Ibánez, D. S. Judson, J. Konki, A. Korgul, T. Kröll, J. Kurcewicz, S. Lalkovski, I. Lazarus, M. V. Lund, M. Madurga, R. Marginean, I. Marroquín, C. Mihai, R. E. Mihai, A. I. Morales, E. Nacher, A. Negret, R. D. Page, J. Pakarinen, S. Pascu, **V. Paziy**, A. Perea, M. Perez-Liva, E. Picado, V. Pucknell, E. Rapisarda, P. Rahkila, F. Rotaru, J. A. Swartz, O. Tengblad, P. Van Duppen, M. Vidal, R. Wadsworth, W. B. Walters and N. Warr. Phys. Rev. C 93, 044303 (2016).

4. *The mutable nature of particle-core excitations with spin in the one-valence-proton nucleus ^{133}Sb.* G. Bocchi, S. Leoni, B. Fornal, G. Colo, P.F. Bortignon, S. Bottoni, A. Bracco, C. Michelagnoli, D. Bazzacco, A. Blanc, G. De France, M. Jentschel, U. Koster, P. Mutti, J.-M. Regis, G. Simpson, T. Soldner, C.A. Ur, W. Urban, L.M. Fraile, R. Lozeva, B. Belvito, G. Benzoni, A. Bruce, R. Carroll, N. Cieplicka-Orynczak, F.C.L. Crespi, F. Didierjean, J. Jolie, W. Korten, T. Kröll, S. Lalkovski, H. Mach, N. Marginean, B. Melon, D. Mengoni, B. Million, A. Nannini, D. Napoli,

B. Olaizola, **V. Paziy**, Zs. Podolyakn, P.H. Regann, N. Saed-Samii, B. Szpak, V. Vedia. arXiv:1603.08056 (2016).

5. *Measurement of picosecond lifetimes in neutron-rich Xe isotopes.* S. Ilievaa, Th. Kröll, J.-M. Régis, N. Saed-Samii, A. Blanc, A.M. Bruce, L.M. Fraile, G. de France, A.-L. Hartig, C. Henrich, A. Ignatov, M. Jentschel, J. Jolie, W. Korten, U. Köster, S. Lalkovski, H. Mach, N. Marginean, P. Mutti, **V. Paziy**, P.H. Regan, G.S. Simpson, T. Soldner, M. Thürauf, C.A. Ur, W. Urban. In preparation.

6. *Fast-Timing Study in the ^{78}Ni Region: β-Decay of ^{81}Zn.* **V. Paziy**, H. Mach, L. M. Fraile, A. Aprahamian, C. Bernards, J. A. Briz, B. Bucher, C. J. Chiara, Z. Dlouhý, I. Gheorghe, D. Ghiţa, P. Hoff, J. Jolie, U. Köster, W. Kurcewicz, R. Lica, N. Marginean, R. Marginean, B. Olaizola, J.-M. Régis, M. Rudigier, T. Sava, G. S. Simpson, M. Stănoiu, L. Stroe, J. M. Udías, W. B. Walters. JPS Conf. Proc. 6, 030009 (2015).

7. *Lifetime Measurements in Neutron-Rich Xe Isotopes – Evolution of Quadrupole Collectivity Beyond ^{132}Sn.* S. Ilieva, S. Bönig, A.-L. Hartig, C. Henrich, A. Ignatov, Th. Kröll, M. Thürauf, J. Jolie, J.-M. Régis, N. Saed-Samii, A. Blanc, G. de France, M. Jentschel, U. Köster, P. Mutti, G. S. Simpson, T. Soldner, W. Urban, N. Marginean, C. A. Ur, H. Mach, L. M. Fraile, **V. Paziy**, P. H. Regan, A. M. Bruce, S. Lalkovski, W. Korten. JPS Conf. Proc. 6, 020011 (2015).

8. *The Generalized Centroid Difference method for lifetime measurements via γ-γ coincidences using large fast-timing arrays.* J.-M. Régis, J. Jolie, H. Mach, G.S. Simpson, A. Blazhev, G. Pascovici, M. Pfeiffer, M. Rudigier, N. Saed-Samii, N. Warr, A. Blanc, G. de France, M. Jentschel, U. Köster, P. Mutti, T. Soldner, C.A. Ur, W. Urban, A.M. Bruce, F. Drouet, L.M. Fraile, S. Ilieva, W. Korten, T. Kröll, S. Lalkovski, S. Marginean, **V. Paziy**, Zs. Podolyák, P.H. Regan, O. Stezowski and A. Vancraeyenest. EPJ Web of Conferences 93, 01013 (2015).

9. *The (n, γ) campaigns at EXILL.* J. Jolie, J.-M. Régis, D. Wilmsen, S. Ahmed, M. Pfeiffer, N. Saed-Samii, N. Warr, A. Blanc, M. Jentschel, U. Köster, P. Mutti, T. Soldner, G. Simpson, G. De France, W. Urban, F. Drouet, A. Vancraeyenest, P. Baczyk, M. Czerwinski, A. Korgul, C. Mazzocchi, T. Rzaca-Urban, A. Bruce, O.J. Roberts, L.M. Fraile, H. Mach, **V. Paziy**, A. Ignatov, S. Ilieva, Th. Kröll, M. Scheck, M. Thürauf, D. Ivanova, S. Kisyov, S. Lalkovski, Zs. Podolyák, P.H. Regan, W. Korten, M. Zielinska, M.D. Salsac, D. Habs, P.G. Thirolf, C. A. Ur, C. Bernards, R.F. Casten, N. Cooper, V. Werner, R.B. Cakirli, S. Leoni, G. Benzoni, G. Bocchi, S. Bottoni, F.C.L. Crespi, B. Fornal, N. Cieplicka, B. Szpak, C.M. Petrache, R. Leguillon, R. John, C. Lorenz, R. Massarczyk, R. Schwengner, D. Curien, R. Lozeva, L. Sengele, N. Marginean and R. Lica. EPJ Web of Conferences 93, 01014 (2015).

10. *Test of the SO(6) selection rule in ^{196}Pt using cold-neutron capture.* J. Jolie, J.-M. Régis, D. Wilmsen, N. Saed-Samii, M. Pfeiffer, N. Warr, A. Blanc, M. Jentschel, U. Köster, P. Mutti, T. Soldner, G. S. Simpson, G. De France, W. Urban, F. Drouet, A. Vancraeyenest, A. M. Bruce, O. J. Roberts, L. M. Fraile, **V. Paziy**, A. Ignatov, Th. Kröll, D. Ivanova, S. Kisyov, S. Lalkovski, Zs. Podolyák, P. H. Regan, E.

Wilson, W. Korten, C. A. Ur, R. Lica, N. Marginean. Nuclear Physics A 934 (2015) 1-7.

11. *B(E2;$2_1^+ \rightarrow 0_1^+$) value in ^{90}Kr.* J.-M. Régis, J. Jolie, N. Saed-Samii, N. Warr, M. Pfeiffer, A. Blanc, M. Jentschel, U. Köster, P. Mutti, T. Soldner, G. S. Simpson, F. Drouet, A. Vancraeyenest, G. de France, E. Clément, O. Stezowski, C. A. Ur, W. Urban, P. H. Regan, Zs. Podolyák, C. Larijani, C. Townsley, R. Carroll, E. Wilson, L. M. Fraile, H. Mach, **V. Paziy**, B. Olaizola, V. Vedia, A. M. Bruce, O. J. Roberts, J. F. Smith, T. Kröll, A.-L. Hartig, A. Ignatov, S. Ilieva, M. Thürauf, S. Lalkovski, D. Ivanova, S. Kisyov, W. Korten, M.-D. Salsac, M. Zielińska, N. Marginean, D. G. Ghita, R. Lica, C. M. Petrache, A. Astier, and R. Leguillon. Phys. Rev. C 90, 067301 (2014).

12. *Germanium-gated γ-γ fast timing of excited states in fission fragments using the EXILL&FATIMA spectrometer.* J.-M. Régis, G.S. Simpson, A. Blanc, G. de France, M. Jentschel, U. Köster, P. Mutti, **V. Paziy**, N. Saed-Samii, T. Soldner, C.A. Ur, W. Urban, A.M. Bruce, F. Drouet, L.M. Fraile, S. Ilieva, J. Jolie, W. Korten, T. Kröll, S. Lalkovski, H. Mach, N. Marginean, G. Pascovici, Zs. Podolyák, P.H. Regan, O.J. Roberts, J.F. Smith, C. Townsley, A. Vancraeyenest, N. Warr. Nuclear Instruments and Methods in Physics Research A 763 (2014) 210-220.

13. *Low-lying isomeric states in ^{80}Ga from the β-decay of ^{80}Zn.* R. Lica, N. Marginean, D. Ghiţa, H. Mach, L.M. Fraile, G. Simpson, A. Aprahamian, C. Bernards, J. A. Briz, B. Bucher, C. J. Chiara, Z. Dlouhý, I. Gheorghe, P. Hoff, J. Jolie, U. Köster, W. Kurcewicz,, R. Marginean, B. Olaizola, **V. Paziy**, J.-M. Régis, M. Rudigier, T. Sava, M. Stanoiu, L. Stroe, and W. B. Walters. Phys. Rev. C 90, 0143320 (2014).

14. *Fast Timing Study of a $CeBr_3$ crystal: time resolution below 120 ps at ^{60}Co energies.* L. M. Fraile, H. Mach, V. Vedia, B. Olaizola, **V. Paziy**, E. Picado, J. M. Udías, Nuclear Instruments and Methods in Physics Research A 701 (2013) 235–242.

15. *Structure of ^{81}Ga populated from the β-decay of ^{81}Zn.* **V. Paziy**, H. Mach, L.M. Fraile, A. Aprahamian, C. Bernards, J. A. Briz, B. Bucher, C. J. Chiara, Z. Dlouhý, I. Gheorghe, D. Ghiţa, P. Hoff, U. Köster, W. Kurcewicz, R. Lica, N. Marginean, R. Marginean, B. Olaizola, J. M. Régis, M. Rudigier, T. Sava, G. Simpson, M. Stanoiu, L. Stroe, J. M. Udías, and W. B. Walters. AIP Conf. Proc. 1541, 185-186 (2013).

16. *Assessment of New Photosensors for Fast Timing Applications with Large Scintillator Detectors.* L. M. Fraile, H. Mach, B. Olaizola, **V. Paziy**, E. Picado, J. J. Sanchez, J. M. Udías, J. J. Vaquero, V. Vedia, Nuclear Science Symposium and Medical Imaging Conference (NSS/MIC), IEEE Conference Records ISSN 1082-3654, 72-74 (2011).

Conference presentations

1. 3rd European Nuclear Physics Conference, Groningen, The Netherlands. September, 1-4, 2015. Talk: *Half-life measurements of the excited states of ^{81}Ge.*

2. 2nd Conference on Advances in Radioactive Isotope Science (ARIS2014), Tokyo, Japan. September, 1-4, 2015. Talk: *Half-life measurements of the excited states of* ^{81}Ge.

3. XXXIV Bienal Meeting of RSEF, Valencia, Spain. July, 15-19, 2013. Talk: *Fast-timing study in* ^{78}Ni *region: structure of* ^{81}Ga.

List of Figures

List of Tables

Bibliography

[Aas96] A.J. Aas, H. Mach, M.J.G. Borge, B. Fogelberg, I.S. Grant, K. Gulda, E. Hagebo, W. Kurcewicz, J. Kvasil, A. Lindroth, T. Martínez, D. Nosek, B. Rubio, J.F. Smith, K. Steffensen, J.L. Tań, O. Tengblad, and T.F. Thorsteinsen, *Enhanced and quenched B(E1) transition rates between parity doublet bands in* ^{227}Ra, Nuclear Physics A **611**, no. 2-3, 281 - 314 (1996).

[Aas99] A.J. Aas, H. Mach, J. Kvasil, M.J.G. Borge, B. Fogelberg, I.S. Grant, K. Gulda, E. Hagebø, P. Hoff, W. Kurcewicz, A. Lindroth, G. Lovhoiden, A. Mackova, T. Martínez, B. Rubio, M. Sánchez-Vega, J.F. Smith, J.L. Tań, R.B.E. Taylor, O. Tengblad, and T.F. Thorsteinsen, *Quenched E1 transition rates in* ^{231}Th, Nuclear Physics A **654**, no. 3-4, 499 - 522 (1999).

[Abu11] Khalifeh Abusaleem and Balraj Singh, *Nuclear Data Sheets for A=71*, Nuclear Data Sheets **112**, no. 1, 133 - 273 (2011).

[Ada82] I. N. Adam, V. B. Antoneva, Brudanin, M. Budzynski, Ts. Vylov, V. A. Dzhashi, A. Zhumamuratov, A. I. Ivanov, V. G. Kalinnikov, A. Kugler, V. V. Kuznetsov, Li Zon Sik, T. M. Muminov, A. F. Novgorodov, Yu. N. Podkopaev, Z. D. Shavgulidze, and V. L. Chikhladze, *Study of the radioactive decay of isobars with mass A = 140*, Izvestiya Akademii Nauk SSSR, Seriya Fizicheskaya **46**, 133-137 (1982).

[Ahn13] Sunghoon Ahn, *The study of nuclear structure of neutron-rich* ^{81}Ge *and its contribution in the r-process via the neutron transfer reaction* ^{80}Ge*(d,p)*, Ph.D. thesis, University of Tennessee, Knoxville, (2013).

[Aud12a] G. Audi, M. Wang, A.H. Wapstra, F.G. Kondev, M. MacCormick, X. Xu, and B. Pfeiffer, *The ame2012 atomic mass evaluation*, Chinese Physics C **36**, no. 12, 1287 (2012).

[Aud12b] G. Audi, M. Wang, A.H. Wapstra, F.G. Kondev, M. MacCormick, X. Xu, and B. Pfeiffer, *The Ame2012 atomic mass evaluation*, Chinese Physics C **36**, no. 12, 1287 (2012).

[Bac15] P. Baczyk, W. Urban, D. Złotowska, M. Czerwiński, T. Rzaca-Urban, A. Blanc, M. Jentschel, P. Mutti, U. Köster, T. Soldner, G. de France, G. Simpson, and C. A. Ur, *Near-yrast excitations in nucleus* ^{83}As*: Tracing the* $\pi g_{9/2}$ *orbital in the* ^{78}Ni *region*, Phys. Rev. C **91**, 047302 (2015).

[Bag08] Coral M. Baglin, *Nuclear Data Sheets for A = 81*, Nuclear Data Sheets **109**, no. 10, 2257 - 2437 (2008).

[Bet71] R. R. Betts, D. J. Pullen, W. Scholz, and B. Rosner, *Positive-parity states in odd-even as isotopes*, Phys. Rev. Lett. **26**, 1576–1578 (1971).

[Bev92] P. R. Bevington and D. K. Robinson, *Data reduction and error analysis for the physical sciences*, New York: McGraw-Hill, (1992).

[Bha79] P. Bhattacharyya, R.K. Chattopadhyay, B. Sethi, A. De, J.M. Chatterjeedas, and S.K. Mukherjee, Nuovo Cim. **51A**.

[Boh75] A. Bohr and B. Mottelsen, *Nuclear Structure*, Benjamin, New York, (1975).

[Bor05] I. N. Borzov, *β-delayed neutron emission in the ^{78}Ni region*, Phys. Rev. C **71**, 065801 (2005).

[Bou07] E. Bouquerel, R. Catherall, M. Eller, J. Lettry, S. Marzari, T. Stora, and ISOLDE Collaboration, *Purification of a Zn radioactive ion beam by alkali suppression in a quartz line target prototype*, The European Physical Journal Special Topics **150**, no. 1, 277-280 (2007) (English).

[Bro86] E. Browne, *Calculated uncertainties of absolute γ-ray intensities and decay branching ratios derived from decay schemes*, Nuclear Instruments and Methods in Physics Research Section A: Accelerators, Spectrometers, Detectors and Associated Equipment **249**, no. 2-3, 461 - 467 (1986).

[Bro14a] P. A. Bromiley, *Products and Convolutions of Gaussian Probability Density Functions*, Tech. report, Imaging Sciences Research Group, Institute of Population Health, School of Medicine, University of Manchester, 2014.

[Bro14b] B.A. Brown and W.D.M. Rae, *The shell-model code NuShellX@MSU*, Nuclear Data Sheets **120**, 115 - 118 (2014).

[Bur57] E. Margaret Burbidge, G. R. Burbidge, William A. Fowler, and F. Hoyle, *Synthesis of the elements in stars*, Rev. Mod. Phys. **29**, 547–650 (1957).

[Car74] G. H. Carlson, W. L. Talbert, and J. R. McConnell, *Decays of mass-separated ^{138}Xe and ^{138}Cs*, Phys. Rev. C **9**, 283–298 (1974).

[Cau05a] E. Caurier, G. Martínez-Pinedo, F. Nowacki, A. Poves, and A. P. Zuker, *The shell model as a unified view of nuclear structure*, Rev. Mod. Phys. **77**, 427–488 (2005).

[Cau05b] E. Caurier, G. Martínez-Pinedo, F. Nowacki, A. Poves, and A. P. Zuker, *The shell model as a unified view of nuclear structure*, Rev. Mod. Phys. **77**, 427–488 (2005).

[Che10] B. Cheal, E. Mané, J. Billowes, M. L. Bissell, K. Blaum, B. A. Brown, F. C. Charlwood, K. T. Flanagan, D. H. Forest, C. Geppert, M. Honma, A. Jokinen, M. Kowalska, A. Krieger, J. Krämer, I. D. Moore, R. Neugart, G. Neyens, W. Nörtershäuser, M. Schug, H. H. Stroke, P. Vingerhoets, D. T. Yordanov, and M. Žáková, *Nuclear spins and moments of ga isotopes reveal sudden structural changes between $N = 40$ and $N = 50$*, Phys. Rev. Lett. **104**, 252502 (2010).

[Dau10] J. M. Daugas, T. Faul, H. Grawe, M. Pfützner, R. Grzywacz, M. Lewitowicz, N. L. Achouri, J. C. Angélique, D. Baiborodin, R. Bentida, R. Béraud, C. Borcea, C. R. Bingham, W. N. Catford, A. Emsallem, G. de France, K. L. Grzywacz, R. C. Lemmon, M. J. Lopez Jimenez, F. de Oliveira Santos, P. H. Regan, K. Rykaczewski, J. E. Sauvestre, M. Sawicka, M. Stanoiu, K. Sieja, and F. Nowacki, *Low-lying isomeric levels in* ^{75}Cu, Phys. Rev. C **81**, 034304 (2010).

[Dir10a] J. Diriken, I. Stefanescu, D. Balabanski, N. Blasi, A. Blazhev, N. Bree, J. Cederkäll, T. E. Cocolios, T. Davinson, J. Eberth, A. Ekström, D. V. Fedorov, V. N. Fedosseev, L. M. Fraile, S. Franchoo, G. Georgiev, K. Gladnishki, M. Huyse, O. V. Ivanov, V. S. Ivanov, J. Iwanicki, J. Jolie, T. Konstantinopoulos, Th. Kröll, R. Krücken, U. Köster, A. Lagoyannis, G. Lo Bianco, P. Maierbeck, B. A. Marsh, P. Napiorkowski, N. Patronis, D. Pauwels, P. Reiter, M. Seliverstov, G. Sletten, J. Van de Walle, P. Van Duppen, D. Voulot, W. B. Walters, N. Warr, F. Wenander, and K. Wrzosek, *Coulomb excitation of* ^{73}Ga, Phys. Rev. C **82**, 064309 (2010).

[Dir10b] J. Diriken, I. Stefanescu, D. Balabanski, N. Blasi, A. Blazhev, N. Bree, J. Cederkäll, T. E. Cocolios, T. Davinson, J. Eberth, A. Ekström, D. V. Fedorov, V. N. Fedosseev, L. M. Fraile, S. Franchoo, G. Georgiev, K. Gladnishki, M. Huyse, O. V. Ivanov, V. S. Ivanov, J. Iwanicki, J. Jolie, T. Konstantinopoulos, Th. Kröll, R. Krücken, U. Köster, A. Lagoyannis, G. Lo Bianco, P. Maierbeck, B. A. Marsh, P. Napiorkowski, N. Patronis, D. Pauwels, P. Reiter, M. Seliverstov, G. Sletten, J. Van de Walle, P. Van Duppen, D. Voulot, W. B. Walters, N. Warr, F. Wenander, and K. Wrzosek, *Coulomb excitation of* ^{73}Ga, Phys. Rev. C **82**, 064309 (2010).

[Eks86] B Ekström, B Fogelberg, P Hoff, E Lund, and A Sangariyavanish, *Decay properties of* $^{75-80}$Zn *and* Q_β *values of neutron-rich Zn and Ga isotopes*, Physica Scripta **34**, no. 6A, 614 (1986).

[End79] P.M. Endt, *Strengths of gamma-ray transitions in A = 45-90 nuclei*, Atomic Data and Nuclear Data Tables **23**, no. 6, 547 - 585 (1979).

[Fet73] P. Fettweis and S. Sadasivan, *The decay of* ^{83g}Se *and* ^{83m}Se, Zeitschrift für Physik **263**, no. 2, 99–120 (1973).

[Fla09] K. T. Flanagan, P. Vingerhoets, M. Avgoulea, J. Billowes, M. L. Bissell, K. Blaum, B. Cheal, M. De Rydt, V. N. Fedosseev, D. H. Forest, Ch. Geppert, U. Köster, M. Kowalska, J. Krämer, K. L. Kratz, A. Krieger, E. Mané, B. A. Marsh, T. Materna, L. Mathieu, P. L. Molkanov, R. Neugart, G. Neyens, W. Nörtershäuser, M. D. Seliverstov, O. Serot, M. Schug, M. A. Sjoedin, J. R. Stone, N. J. Stone, H. H. Stroke, G. Tungate, D. T. Yordanov, and Yu. M. Volkov, *Nuclear spins and magnetic moments of* ^{71,73,75}Cu*: Inversion of* $\pi 2p_{3/2}$ *and* $\pi 1f_{5/2}$ *levels in* ^{75}Cu, Phys. Rev. Lett. **103**, 142501 (2009).

[For76] K. Forssten and M. Brenner, *On the decay of* ^{73}*Ga to levels in* ^{73}*Ge*, Zeitschrift für Physik A Atoms and Nuclei **278**, no. 1, 27-33 (1976).

[Fra99] L.M. Fraile, A.J. Aas, M.J.G. Borge, B. Fogelberg, L.M. Garcá-Raffi, I.S. Grant, K. Gulda, E. Hagebø, W. Kurcewicz, J. Kvasil, G. Løvhøiden, H. Mach, A. Mackova, T. Martńez, B. Rubio, J.L. Tań, A.G. Teijeiro, O. Tengblad, and T.F. Thorsteinsen, *Octupole correlations in* ^{229}Ra, Nuclear Physics A **657**, no. 4, 355 - 390 (1999).

[Fra01a] L.M. Fraile, M.J.G. Borge, H. Mach, R. Boutami, A.J. Aas, B. Fogelberg, L.M. García-Raffi, I.S. Grant, K. Gulda, E. Hagebo, W. Kurcewicz, J. Kvasil, M.J. López, G. Lovhiden, T. Martínez, B. Rubio, J.L. Taín, and O. Tengblad, *Persistence of octupole correlations in* ^{231}Ra, Nuclear Physics A **686**, no. 1-4, 71 - 108 (2001).

[Fra01b] S. Franchoo, M. Huyse, K. Kruglov, Y. Kudryavtsev, W. F. Mueller, R. Raabe, I. Reusen, P. Van Duppen, J. Van Roosbroeck, L. Vermeeren, A. Wöhr, H. Grawe, K.-L. Kratz, B. Pfeiffer, and W. B. Walters, *Monopole migration in* ^{69,71,73}Cu *observed from* β *decay of laser-ionized* $^{68-74}$Ni, Phys. Rev. C **64**, 054308 (2001).

[Fra15] L. M. Fraile, *Technical Report for the Design, Construction and Commissioning of FATIMA, the FAst TIMing Array*, Tech. report, FAIR ECE, 2015.

[GM55] M. Goeppert Mayer and J. H. D. Jensen, *Elementary theory of nuclear shell structure*, John Wiley, (1955).

[Got14] A. Gottberg, T.M. Mendonca, R. Luis, J.P. Ramos, C. Seiffert, S. Cimmino, S. Marzari, B. Crepieux, V. Manea, R.N. Wolf, F. Wienholtz, S. Kreim, V.N. Fedosseev, B.A. Marsh, S. Rothe, P. Vaz, J.G. Marques, and T. Stora, *Experimental tests of an advanced proton-to-neutron converter at ISOLDE-CERN*, Nuclear Instruments and Methods in Physics Research Section B: Beam Interactions with Materials and Atoms **336**, 143 - 148 (2014).

[Gra74] B. Grapengiesser, E. Lund, and G. Rudstam, *Survey of short-lived fission products obtained using the isotope-separator-on-line facility at Studsvik*, Journal of Inorganic and Nuclear Chemistry **36**, no. 11, 2409 - 2431 (1974).

[Gra85] P.W. Gray and A. Ahmad, *Linear classes of Ge(Li) detector efficiency functions*, Nuclear Instruments and Methods in Physics Research Section A: Accelerators, Spectrometers, Detectors and Associated Equipment **237**, no. 3, 577 - 589 (1985).

[Gul02] K. Gulda, W. Kurcewicz, A.J. Aas, M.J.G. Borge, D.G. Burke, B. Fogelberg, I.S. Grant, E. Hagebo, N. Kaffrell, J. Kvasil, G. Lovhoiden, H. Mach, A. Mackova, T. Martínez, G. Nyman, B. Rubio, J.L. Taín, O. Tengblad, and T.F. Thorsteinsen, *The nuclear structure of* ^{229}Th, Nuclear Physics A **703**, no. 1-2, 45 - 69 (2002).

[Hak08] J. Hakala, S. Rahaman, V.-V. Elomaa, T. Eronen, U. Hager, A. Jokinen, A. Kankainen, I. D. Moore, H. Penttilä, S. Rinta-Antila, J. Rissanen, A. Saastamoinen, T. Sonoda, C. Weber, and J. Äystö, *Evolution of the* $n = 50$ *shell gap energy towards* ^{78}Ni, Phys. Rev. Lett. **101**, 052502 (2008).

[Ham75] W. D. Hamilton and editor, *The electromagnetic interaction in nuclear spectroscopy*, North Holland Publishing Company, Amsterdam, (1975).

[Har77] J.C. Hardy, L.C. Carraz, B. Jonson, and P.G. Hansen, *The essential decay of pandemonium: A demonstration of errors in complex beta-decay schemes*, Physics Letters B **71**, no. 2, 307 - 310 (1977).

[Hax49] Otto Haxel, J. Hans D. Jensen, and Hans E. Suess, *On the "magic numbers" in nuclear structure*, Phys. Rev. **75**, 1766–1766 (1949).

[Hof81] P. Hoff and B. Fogelberg, *Properties of strongly neutron-rich isotopes of germanium and arsenic*, Nuclear Physics A **368**, no. 2, 210 - 236 (1981).

[Hon09] M. Honma, T. Otsuka, T. Mizusaki, and M. Hjorth-Jensen, *New effective interaction for f_5pg_9-shell nuclei*, Phys. Rev. C **80**, 064323 (2009).

[Hos10] P. Hosmer, H. Schatz, A. Aprahamian, O. Arndt, R. R. C. Clement, A. Estrade, K. Farouqi, K.-L. Kratz, S. N. Liddick, A. F. Lisetskiy, P. F. Mantica, P. Möller, W. F. Mueller, F. Montes, A. C. Morton, M. Ouellette, E. Pellegrini, J. Pereira, B. Pfeiffer, P. Reeder, P. Santi, M. Steiner, A. Stolz, B. E. Tomlin, W. B. Walters, and A. Wöhr, *Half-lives and branchings for β-delayed neutron emission for neutron-rich Co–Cu isotopes in the r-process*, Phys. Rev. C **82**, 025806 (2010).

[Hur75] M.H. Hurdus and L. Tomlinson, *Gamma-ray emission from* $^{84-87}$Se *and* $^{85-88}$Br *isotopes*, Journal of Inorganic and Nuclear Chemistry **37**, no. 1, 1 - 9 (1975).

[Jäc87] B. Jäckel, W. Westmeier, and P. Patzelt, *On the photopeak efficiency of germanium gamma-ray detectors*, Nuclear Instruments and Methods in Physics Research Section A: Accelerators, Spectrometers, Detectors and Associated Equipment **261**, no. 3, 543 - 548 (1987).

[Jia11] H. Jiang, G. J. Fu, Y. M. Zhao, and A. Arima, *Low-lying structure of neutron-rich Zn and Ga isotopes*, Phys. Rev. C **84**, 034302 (2011).

[Joh15] T.D. Johnson and W.D. Kulp, *Nuclear data sheets for A=87*, Nuclear Data Sheets **129**, 1 - 190 (2015).

[Kaw90] K. Kawade, H. Yamamoto, A. Yamada, Katoh A., T. Katoh, T. Iida, and A. Takahashi, *Measurement of formation cross sections of short-lived nuclei by 14 mev neutrons - Mg, Si, S, Cl, Cr, Zn, Ga, Y, In* -, Tech. report, 1990.

[Kaw92] K. Kawade, H. Yamamoto, A. Tanaka, A. Hosoya, T. Katoh, T. Iida, and A. Takahashi, *Measurement of beta-decay half-lives of short-lived nuclei*, JAERI-M–92-027, 364–368 (1992).

[Kay09a] B. P. Kay, C. J. Chiara, J. P. Schiffer, F. G. Kondev, S. Zhu, M. P. Carpenter, R. V. F. Janssens, T. Lauritsen, C. J. Lister, E. A. McCutchan, D. Seweryniak, and I. Stefanescu, *Properties of excited states in* ^{77}Ge, Phys. Rev. C **80**, 01701 (2009).

[Kay09b] B. P. Kay, J. P. Schiffer, S. J. Freeman, T. Adachi, J. A. Clark, C. M. Deibel, H. Fujita, Y. Fujita, P. Grabmayr, K. Hatanaka, D. Ishikawa, H. Matsubara, Y. Meada, H. Okamura, K. E. Rehm, Y. Sakemi, Y. Shimizu, H. Shimoda, K. Suda, Y. Tameshige, A. Tamii, and C. Wrede, *Nuclear structure relevant*

to neutrinoless double β decay: The valence protons in ^{76}Ge *and* ^{76}Se, Phys. Rev. C **79**, 021301 (2009).

[Kha11] Yu. Khazov, A. Rodionov, and F.G. Kondev, *Nuclear Data Sheets for A = 133*, Nuclear Data Sheets **112**, no. 4, 855 - 1113 (2011).

[Kib08] T. Kibédi, T.W. Burrows, M.B. Trzhaskovskaya, P.M. Davidson, and C.W. Nestor Jr., *Evaluation of theoretical conversion coefficients using bricc*, Nuclear Instruments and Methods in Physics Research Section A: Accelerators, Spectrometers, Detectors and Associated Equipment **589**, no. 2, 202 - 229 (2008).

[Kös01] U. Köster, *How to produce intense and pure {ISOL} beams*, Progress in Particle and Nuclear Physics **46**, no. 1, 411 - 412 (2001).

[Kös02] U. Köster, *Intense radioactive-ion beams produced with the isol method*, Eur. Phys. J. A **15**, no. 1, 255-263 (2002).

[Kös05] U. Köster, T. Behrens, C. Clausen, P. Delahaye, V. N. Fedoseyev, L. M. Fraile, R. Gernhäuser, T. J. Giles, A. Ionan, T. Kröll, H. Mach, B. Marsh, M. Seliverstov, T. Sieber, E. Siesling, E. Tengborn, F. Wenander, and J. Van de Walle, *Isolde beams of neutron-rich zinc isotopes: yields, release, decay spectroscopy*, AIP Conference Proceedings **798**, no. 1, 315-326 (2005).

[Kös08] U. Köster, O. Arndt, E. Bouquerel, V.N. Fedoseyev, H. Frånberg, A. Joinet, C. Jost, I.S.K. Kerkines, and R. Kirchner, *Progress in ISOL target-ion source systems*, Nuclear Instruments and Methods in Physics Research Section B: Beam Interactions with Materials and Atoms **266**, no. 19-20, 4229 - 4239 (2008).

[Kra75] J.V. Kratz, H. Franz, N. Kaffrel, and G. Herrmann, *Gamma-ray emission from* $^{80-86}$As *isotopes*, Nuclear Physics A **250**, no. 1, 13 - 37 (1975).

[Kra87] K. S. Krane, *Introductory nuclear physics*, Wiley, (1987).

[Kra91a] K.-L. Kratz, H. Gabelmann, P. Möller, B. Pfeiffer, H.L. Ravn, and A. Wöhr, *Neutron-rich isotopes around the r-process "waiting-point" nuclei* $^{79}_{29}Cu_{30}$ *and* $^{80}_{30}Zn_{50}$, Zeitschrift für Physik A Hadrons and Nuclei **340**, no. 4, 419-420 (1991).

[Kra91b] K.-L. Kratz, H. Gabelmann, P. Möller, B. Pfeiffer, H.L. Ravn, and A. Wöhr, *Neutron-rich isotopes around the r-process waiting-point nuclei* $^{79}_{29}$Cu$_{50}$ *and* $^{80}_{30}$Zn$_{50}$, Zeitschrift für Physik A Hadrons and Nuclei **340**, no. 4, 419-420 (1991).

[Kra93] K.-L. Kratz, J.-P. Bitouzet, F.-K. Thielemann, P. Moeller, and B. Pfeiffer, *Isotopic r-process abundances and nuclear structure far from stability - Implications for the r-process mechanism*, The Astrophysical Journal **403**, 216-238 (1993).

[Kra15] K.S. Krane, *Gamma-ray spectroscopy in the decay of* ^{83}Se *to levels of* ^{83}Br, Applied Radiation and Isotopes **97**, 12 - 20 (2015).

[Kug00] Erich Kugler, *The isolde facility*, Hyperfine Interactions **129**, no. 1-4, 23-42 (2000).

[Lan76] J. C. Lange, J. Bron, A. Poelgeest, H. Verheul, and W. B. Ewbank, *The decay of* ^{93g}Ru, ^{93m}Ru, ^{91g}Mo, ^{91m}Mo, ^{91c}Tc *and* ^{91m}Tc, Zeitschrift für Physik A Atoms and Nuclei **279**, no. 1, 79–91 (1976).

[Lei91] M. Leino, P. P. Jauho, J. Äystö, P. Decrock, P. Dendooven, K. Eskola, M. Huyse, A. Jokinen, J. M. Parmonen, H. Penttilä, G. Reusen, P. Taskinen, P. Van Duppen, and J. Wauters, *Independent and cumulative yields of very neutron-rich nuclei in 20 mev p - and 18–41 mev d -induced fission of* ^{238}U, Phys. Rev. C **44**, 336–344 (1991).

[Let97] J. Lettry, R. Catherall, P. Drumm, P. Van Duppen, A.H.M. Evensen, G.J. Focker, A. Jokinen, O.C. Jonsson, E. Kugler, and H. Ravn, *Pulse shape of the {ISOLDE} radioactive ion beams*, Nuclear Instruments and Methods in Physics Research Section B: Beam Interactions with Materials and Atoms **126**, no. 1-4, 130 - 134 (1997), International Conference on Electromagnetic Isotope Separators and Techniques Related to Their Applications.

[Lic14] R. Lică, N. Mărginean, D. G. Ghiţă, H. Mach, L. M. Fraile, G. S. Simpson, A. Aprahamian, C. Bernards, J. A. Briz, B. Bucher, C. J. Chiara, Z. Dlouhý, I. Gheorghe, P. Hoff, J. Jolie, U. Köster, W. Kurcewicz, R. Mărginean, B. Olaizola, V. Paziy, J. M. Régis, M. Rudigier, T. Sava, M. Stanoiu, L. Stroe, and W. B. Walters, *Low-lying isomeric states in* ^{80}Ga *from the* β^- *decay of* ^{80}Zn, Phys. Rev. C **90**, 014320 (2014).

[Lie84] O. G. Lien, *A fully automated radiochemical preparation system for gamma-spectroscopy on fission products and the study of the intruder and vibrational levels in* ^{83}Se, Dissertation Abstract international B **45**, 2550 (1984).

[Lis04] A. F. Lisetskiy, B. A. Brown, M. Horoi, and H. Grawe, *New* $T = 1$ *effective interactions fot the* $f_{5/2}p_{3/2}p_{1/2}g_{9/2}$ *model space: Implications for valence-mirror symmetry and seniority isomers*, Phys. Rev. C **70**, 044314 (2004).

[LLC13] XIA LLC, *Xia instruments that advance the art.*, Tech. report, 2013.

[Mac86] H. Mach, *A method of nuclear half-life measurements in the picosecond range form neutron-rich nuclei*, Bull. Am. Phys. Soc. **31**, no. 1235.

[Mac89] H. Mach, R.L. Gill, and M. Moszyński, *A method for picosecond lifetime measurements for neutron-rich nuclei: (1) outline of the method*, Nuclear Instruments and Methods in Physics Research Section A: Accelerators, Spectrometers, Detectors and Associated Equipment **280**, no. 1, 49 - 72 (1989).

[Mac91] H. Mach, F.K. Wohn, G. Molnár, K. Sistemich, John C. Hill, M. Moszyński, R.L. Gill, W. Krips, and D.S. Brenner, *Retardation of B(E2;* $0_1^+ -> 2_1^+$*) rates in* $^{90-96}$Sr *and strong subshell closure effects in the A∼100 region*, Nuclear Physics A **523**, no. 2, 197 - 227 (1991).

[Mac92] H. Mach, M. Hellström, B. Fogelberg, D. Jerrestam, and L. Spanier, *Nature of the* 0_3^+ *state in* ^{152}Sm *from picosecond-lifetime measurement: "correspondence" interpretation of the* 0^+ *bands in heavy Sm and Gd*, Phys. Rev. C **46**, 1849–1862 (1992).

[Mac95a] H Mach and B Fogelberg, *Fast timing studies of the neutron-rich singly-magic $N = 82$ nuclei*, Physica Scripta **1995**, no. T56, 270 (1995).

[Mac95b] H. Mach, D. Jerrestam, B. Fogelberg, M. Hellström, J. P. Omtvedt, K. I. Erokhina, and V. I. Isakov, *Structure of the p-h nucleus* ^{132}Sb, Phys. Rev. C **51**, 500–508 (1995).

[Mam13] Bruno Olaizola Mampaso, *Ultra-fast timing study of exotic neutron-rich Fe isotopes*, Ph.D. thesis, Universidad Complutense de Madrid, (2013).

[Mar13] M.J. Martin, *Nuclear Data Sheets for $A = 152$*, Nuclear Data Sheets **114**, no. 11, 1497 - 1847 (2013).

[Mat85] G. J. Mathews and R. A. Ward, *Neutron capture process in astrophysics*, Reports on Progress in Physics **48**, no. 10, 1371 (1985).

[May49] Maria Goeppert Mayer, *On closed shells in nuclei. II*, Phys. Rev. **75**, 1969–1970 (1949).

[McC75] Graham J. McCallum and Graeme E. Coote, *Systematic errors in transition intensities of* ^{56}Co *and* ^{66}Ga, Nuclear Instruments and Methods **124**, no. 1, 309 - 311 (1975).

[McC15] E.A. McCutchan, *Nuclear Data Sheets for $A = 83$*, Nuclear Data Sheets **125**, 201 - 394 (2015).

[Mcm71] D.K. Mcmillan and B.D. Pate, *The decay of* ^{80}As, Nuclear Physics A **174**, no. 3, 593 - 603 (1971).

[Mei12] G. Meierhofer, P. Grabmayr, L. Canella, P. Kudejova, J. Jolie, and N. Warr, *Prompt γ-rays in* ^{77}Ge *and* ^{75}Ge *after thermal neutron capture*, The European Physical Journal A **48**, no. 2 (English).

[Mey82] R. A. Meyer, O. G. Lien, and E. A. Henry, *Coexisting intruder bands in* ^{83}Se *and evidence for the role of proton subshell closure in inhibiting formation of odd-neutron intruder bands*, Phys. Rev. C **25**, 682–685 (1982).

[Mih07] L.C. Mihailescu, C. Borcea, and A.J.M. Plompen, *Data acquisition with a fast digitizer for large volume HPGe detectors*, Nuclear Instruments and Methods in Physics Research Section A: Accelerators, Spectrometers, Detectors and Associated Equipment **578**, no. 1, 298 - 305 (2007).

[Mis93] V.I. Mishin, V.N. Fedoseyev, H.-J. Kluge, V.S. Letokhov, H.L. Ravn, F. Scheerer, Y. Shirakabe, S. Sundell, and O. Tengblad, *Chemically selective laser ion-source for the cern-isolde on-line mass separator facility*, Nuclear Instruments and Methods in Physics Research Section B: Beam Interactions with Materials and Atoms **73**, no. 4, 550 - 560 (1993).

[Mor82] S. Mordechai, S. Lafrance, and H. T. Fortune, *Excitation of* ^{81}As *by the* ^{82}Se*(t,α) reaction*, Phys. Rev. C **25**, 1276–1282 (1982).

[Mor04] David J. Morrissey and Brad M. Sherrill, *In-flight separation of projectile fragments*, The Euroschool Lectures on Physics with Exotic Beams, Vol. I (Jim Al-Khalili and Ernst Roeckl, eds.), Lecture Notes in Physics, vol. 651, Springer Berlin Heidelberg, 2004, pp. 113–135 (English).

[Mos89] M. Moszyński and H. Mach, *A method for picosecond lifetime measurements for neutron-rich nuclei: (2) timing study with scintillation counters*, Nuclear Instruments and Methods in Physics Research Section A: Accelerators, Spectrometers, Detectors and Associated Equipment **277**, no. 2-3, 407 - 417 (1989).

[Mum16] M.R. Mumpower, R. Surman, G.C. McLaughlin, and A. Aprahamian, *The impact of individual nuclear properties on r-process nucleosynthesis*, Progress in Particle and Nuclear Physics **86**, 86 - 126 (2016).

[Nak10] K Nakamura and Particle Data Group, *Review of particle physics*, Journal of Physics G: Nuclear and Particle Physics **37**, no. 7A, 075021 (2010).

[Neg13] Alexandru Negret and Balraj Singh, *Nuclear Data Sheets for A = 75*, Nuclear Data Sheets **114**, no. 8-9, 841 - 1040 (2013).

[Ng68] Anne Ng, R. E. Wood, J. M. Palms, P. Venugopala Rao, and R. W. Fink, *Gamma rays from the decay of* ^{75}Ge *and* ^{77}Ge, Phys. Rev. **176**, 1329–1338 (1968).

[Nic07] N. Nica, *Nuclear Data Sheets for A = 140*, Nuclear Data Sheets **108**, no. 7, 1287 - 1470 (2007).

[Nii14] M. Niikura, et al., and for the EURICA collaboration, *Study on neutron-rich Zn isotopes via β-γ spectroscopy*, book of abstracts from the 2nd Conference in Advances in Radioactive Isotope Science, 110-111 (2014).

[nuc] *Scintillator for the Physical Sciences, brochure No.126P*, Tech. report, Nuclear Enterprises, Unc., San Carlos, CA 94070, USA.

[Ola13] B. Olaizola, L. M. Fraile, H. Mach, A. Aprahamian, J. A. Briz, J. Cal-González, D. Ghiţa, U. Köster, W. Kurcewicz, S. R. Lesher, D. Pauwels, E. Picado, A. Poves, D. Radulov, G. S. Simpson, and J. M. Udías, β^- *decay of* ^{65}Mn *to* ^{65}Fe, Phys. Rev. C **88**, 044306 (2013).

[Orl09] R. Orlandi, G. de Angelis, P. G. Bizzeti, S. Lunardi, A. Gadea, A. M. Bizzeti-Sona, A. Bracco, F. Brandolini, M. P. Carpenter, C. J. Chiara, F. Della Vedova, E. Farnea, J. P. Greene, S. M. Lenzi, S. Leoni, C. J. Lister, N. Mărginean, D. Mengoni, D. R. Napoli, B. S. Nara Singh, O. L. Pechenaya, F. Recchia, W. Reviol, E. Sahin, D. G. Sarantites, D. Seweryniak, D. Tonev, C. A. Ur, J. J. Valiente-Dobón, R. Wadsworth, K. T. Wiedemann, and S. Zhu, *Coherent contributions to isospin mixing in the mirror pair* ^{67}As *and* ^{67}Se, Phys. Rev. Lett. **103**, 052501 (2009).

[Orl15] R. Orlandi, D. Mücher, R. Raabe, A. Jungclaus, S.D. Pain, V. Bildstein, R. Chapman, G. de Angelis, J.G. Johansen, P. Van Duppen, A.N. Andreyev, S. Bottoni, T.E. Cocolios, H. De Witte, J. Diriken, J. Elseviers, F. Flavigny, L.P. Gaffney, R. Gernhäuser, A. Gottardo, M. Huyse, A. Illana, J. Konki,

T. Kröll, R. Krücken, J.F.W. Lane, V. Liberati, B. Marsh, K. Nowak, F. Nowacki, J. Pakarinen, E. Rapisarda, F. Recchia, P. Reiter, T. Roger, E. Sahin, M. Seidlitz, K. Sieja, J.F. Smith, J.J. Valiente Dobón, M. von Schmid, D. Voulot, N. Warr, F.K. Wenander, and K. Wimmer, *Single-neutron orbits near* ^{78}Ni*: Spectroscopy of the isotope* ^{79}Zn, Physics Letters B **740**, 298 - 302 (2015).

[Ots05] Takaharu Otsuka, Toshio Suzuki, Rintaro Fujimoto, Hubert Grawe, and Yoshinori Akaishi, *Evolution of nuclear shells due to the tensor force*, Phys. Rev. Lett. **95**, 232502 (2005).

[Owe07] Alan Owens, A.J.J. Bos, S. Brandenburg, E.-J. Buis, C. Dathy, P. Dorenbos, C.W.E. van Eijk, S. Kraft, R.W. Ostendorf, V. Ouspenski, and F. Quarati, *Assessment of the radiation tolerance of labr3:ce scintillators to solar proton events*, Nuclear Instruments and Methods in Physics Research Section A: Accelerators, Spectrometers, Detectors and Associated Equipment **572**, no. 2, 785 - 793 (2007).

[Pad10] S. Padgett, M. Madurga, R. Grzywacz, I. G. Darby, S. N. Liddick, S. V. Paulauskas, L. Cartegni, C. R. Bingham, C. J. Gross, K. Rykaczewski, D. Shapira, D. W. Stracener, A. J. Mendez, J. A. Winger, S. V. Ilyushkin, A. Korgul, W. Królas, E. Zganjar, C. Mazzocchi, S. Liu, J. H. Hamilton, J. C. Batchelder, and M. M. Rajabali, *β decay of* ^{81}Zn *and migrations of states observed near the* $N = 50$ *closed shell*, Phys. Rev. C **82**, 064314 (2010).

[Por09] M. G. Porquet, A. Astier, Ts. Venkova, A. Prévost, I. Deloncle, F. Azaiez, A. Buta, D. Curien, O. Dorvaux, G. Duchêne, B. J. P. Gall, F. Khalfallah, I. Piqueras, M. Rousseau, M. Meyer, N. Redon, O. Stézowski, R. Lucas, and A. Bogachev, *High-spin excitations of* ^{81,82,83,85}Se *: Competing single-particle and collective structures around* $n = 50$, The European Physical Journal A **39**, no. 3, 295–306 (2009).

[Por11] M.-G. Porquet, A. Astier, D. Verney, Ts. Venkova, I. Deloncle, F. Azaiez, A. Buta, D. Curien, O. Dorvaux, G. Duchêne, B. J. P. Gall, F. Khalfallah, I. Piqueras, M. Rousseau, M. Meyer, N. Redon, O. Stézowski, and A. Bogachev, *Medium-spin states in neutron-rich* ^{83}As *and* ^{81}As, Phys. Rev. C **84**, 054305 (2011).

[Ram00] S. Raman, C. Yonezawa, H. Matsue, H. Iimura, and N. Shinohara, *Efficiency calibration of a Ge detector in the 0.1-11.0 MeV region*, Nuclear Instruments and Methods in Physics Research Section A: Accelerators, Spectrometers, Detectors and Associated Equipment **454**, no. 2-3, 389 - 402 (2000).

[Rég13] J.-M. Régis, H. Mach, G.S. Simpson, J. Jolie, G. Pascovici, N. Saed-Samii, N. Warr, A. Bruce, J. Degenkolb, L.M. Fraile, C. Fransen, D.G. Ghita, S. Kisyov, U. Koester, A. Korgul, S. Lalkovski, N. Mărginean, P. Mutti, B. Olaizola, Z. Podolyak, P.H. Regan, O.J. Roberts, M. Rudigier, L. Stroe, W. Urban, and D. Wilmsen, *The generalized centroid difference method for picosecond sensitive determination of lifetimes of nuclear excited states using large fast-timing arrays*, Nuclear Instruments and Methods in Physics Research Section A: Accelerators, Spectrometers, Detectors and Associated Equipment **726**, 191 - 202 (2013).

[Rég14] J.-M. Régis, G.S. Simpson, A. Blanc, G. de France, M. Jentschel, U. Koester, P. Mutti, V. Paziy, N. Saed-Samii, T. Soldner, C.A. Ur, W. Urban, A.M. Bruce, F. Drouet, L.M. Fraile, S. Ilieva, J. Jolie, W. Korten, T. Kroll, S. Lalkovski, H. Mach, N. Mărginean, G. Pascovici, Zs. Podolyak, P.H. Regan, O.J. Roberts, J.F. Smith, C. Townsley, A. Vancraeyenest, and N. Warr, *Germanium-gated γ-γ fast timing of excited states in fission fragments using the exill-fatima spectrometer*, Nuclear Instruments and Methods in Physics Research Section A: Accelerators, Spectrometers, Detectors and Associated Equipment **763**, 210 - 220 (2014).

[Ros57] M.E. Rose, *Elementary Theory of Angular Momentum*, John Wiley & Sons, Inc., New York, (1957).

[Rot80] G. Rotbard, M. Vergnes, G. Berrier-Ronsin, and J. Vernotte, *Neutron rich* ^{73}Ga *and* ^{79}As *isotopes via the (α,p) reaction*, Phys. Rev. C **21**, 2293–2302 (1980).

[Rot83] G. Rotbard, M. Vergnes, J. Vernotte, G. Berrier-Ronsin, J. Kalifa, and R. Tamisier, *Proton occupancies in the even Se ground states via the (d,* ^{3}He*) reaction*, Nuclear Physics A **401**, no. 1, 41 - 58 (1983).

[Rud76] G. Rudstam and E. Lund, *Delayed-neutron activities produced in fission: Mass range 79-98*, Phys. Rev. C **13**, 321–330 (1976).

[Run83] E. Runte, W.-D. Schmidt-Ott, P. Tidemand-Petersson, R. Kirchner, O. Klepper, W. Kurcewicz, E. Roeckl, N. Kaffrell, P. Peuser, K. Rykaczewski, M. Bernas, P. Dessagne, and M. Langevin, *Decay studies of neutron-rich products from* ^{76}Ge *induced multinucleon transfer reactions including the new isotopes* ^{62}Mn, ^{63}Fe *and* ^{71,72,73}Cu, Nuclear Physics A **399**, no. 1, 163 - 180 (1983).

[Sch92] Th. Schaefer, E. Lohmann, and R. Vianden, *The quadrupole moment of the 66 kev,* $5/2^-$ *state of* ^{73}*As*, Zeitschrift für Physik A Hadrons and Nuclei **343**, no. 3, 279-281 (1992).

[Sie12] K. Sieja and F. Nowacki, *Three-body forces and persistence of spin-orbit shell gaps in medium-mass nuclei: Toward the doubly magic* ^{78}*ni*, Phys. Rev. C **85**, 051301 (2012).

[Sim07] G. S. Simpson, J. C. Angelique, J. Genevey, J. A. Pinston, A. Covello, A. Gargano, U. Köster, R. Orlandi, and A. Scherillo, *New information on excited states below the μs isomer in* ^{136}Sb, Phys. Rev. C **76**, 041303 (2007).

[Sin98] B. Singh, J.L. Rodríguez, S.S.M. Wong, and J.K. Tuli, *Review of logft values in β decay*, Nuclear Data Sheets **84**, no. 3, 487 - 563 (1998).

[SIN02] BALRAJ SINGH, *Nuclear Data Sheets for A = 79*, Nuclear Data Sheets **96**, no. 1, 1 - 176 (2002).

[Sin04] Balraj Singh, *Nuclear Data Sheets for A = 73*, Nuclear Data Sheets **101**, no. 2, 193 - 323 (2004).

[Sin05] Balraj Singh, *Nuclear Data Sheets for A = 80*, Nuclear Data Sheets **105**, no. 2, 223 - 418 (2005).

[Sin12] Balraj Singh and Ninel Nica, *Nuclear Data Sheets for A = 77*, Nuclear Data Sheets **113**, no. 5, 1115 - 1314 (2012).

[Sin14] Balraj Singh and Jun Chen, *Nuclear Data Sheets for A = 85*, Nuclear Data Sheets **116**, 1 - 162 (2014).

[Smi04] N. A. Smirnova, A. De Maesschalck, A. Van Dyck, and K. Heyde, *Shell-model description of monopole shift in neutron-rich Cu*, Phys. Rev. C **69**, 044306 (2004).

[Son03] A.A. Sonzogni, *Nuclear Data Sheets for A = 138*, Nuclear Data Sheets **98**, no. 3, 515 - 664 (2003).

[Sri12] P. C. Srivastava, *Structure of* $^{71-78}$Ga *isotopes in the* $f_{5/2}pg_{9/2}$ *and* $fpg_{9/2}$ *spaces*, Journal of Physics G: Nuclear and Particle Physics **39**, no. 1, 015102 (2012).

[Ste08] I. Stefanescu, G. Georgiev, D. L. Balabanski, N. Blasi, A. Blazhev, N. Bree, J. Cederkäll, T. E. Cocolios, T. Davinson, J. Diriken, J. Eberth, A. Ekström, D. Fedorov, V. N. Fedosseev, L. M. Fraile, S. Franchoo, K. Gladnishki, M. Huyse, O. Ivanov, V. Ivanov, J. Iwanicki, J. Jolie, T. Konstantinopoulos, Th. Kröll, R. Krücken, U. Köster, A. Lagoyannis, G. Lo Bianco, P. Maierbeck, B. A. Marsh, P. Napiorkowski, N. Patronis, D. Pauwels, G. Rainovski, P. Reiter, K. Riisager, M. Seliverstov, G. Sletten, J. Van de Walle, P. Van Duppen, D. Voulot, N. Warr, F. Wenander, and K. Wrzosek, *Interplay between single-particle and collective effects in the odd-A Cu isotopes beyond* $N = 40$, Phys. Rev. Lett. **100**, 112502 (2008).

[Ste09] I. Stefanescu, W. B. Walters, R. V. F. Janssens, S. Zhu, R. Broda, M. P. Carpenter, C. J. Chiara, B. Fornal, B. P. Kay, F. G. Kondev, W. Krolas, T. Lauritsen, C. J. Lister, E. A. McCutchan, T. Pawlat, D. Seweryniak, J. R. Stone, N. J. Stone, and J. Wrzesinski, *Identification of the* $g_{9/2}$*-proton bands in the neutron-rich* ^{71,73,75,77}Ga *nuclei*, Phys. Rev. C **79**, 064302 (2009).

[Sue56] Hans E. Suess and Harold C. Urey, *Abundances of the elements*, Rev. Mod. Phys. **28**, 53–74 (1956).

[Suh07] J. Suhonen, *From nucleons to nucleus: Concepts of microscopic nuclear theory*, Springer, (2007), ISBN 978-3-540-48859-0.

[Sur13] R. Surman, M. Mumpower, G. C. McLaughlin, R. Sinclair, W. R. Hix, and K. L. Jones, *Neutron capture rates and r-process nucleosynthesis*, 2013.

[Tak96] Nobuo Takaoka, Yoshinobu Motomura, and Keisuke Nagao, *Half-life of* ^{130}Te *double-*β *decay measured with geologically qualified samples*, Phys. Rev. C **53**, 1557–1561 (1996).

[Til02] D.R. Tilley, C.M. Cheves, J.L. Godwin, G.M. Hale, H.M. Hofmann, J.H. Kelley, C.G. Sheu, and H.R. Weller, *Energy levels of light nuclei A=5, 6, 7*, Nuclear Physics A **708**, no. 1-2, 3 - 163 (2002).

[Tri75] Virginia Trimble, *The origin and abundances of the chemical elements*, Rev. Mod. Phys. **47**, 877–976 (1975).

[Tro13] Yu.A. Trofimov, E.E. Lupar, and V.N. Yurov, *Linearity of the energy scale of a detector based on a labr3(ce) scintillator*, Instruments and Experimental Techniques **56**, no. 2, 151-155 (2013) (English).

[VD06] P. Van Duppen, *Isotope separation on line and post acceleration*, The Euroschool Lectures on Physics with Exotic Beams, Vol. II (Jim Al-Khalili and Ernst Roeckl, eds.), Lecture Notes in Physics, vol. 700, Springer Berlin Heidelberg, 2006, pp. 37–77 (English).

[Ved15] V. Vedia, H. Mach, L.M. Fraile, J.M. Udás, and S. Lalkovski, *Enhanced time response of 1-in. $LaBr_3(Ce)$ crystals by leading edge and constant fraction techniques*, Nuclear Instruments and Methods in Physics Research Section A: Accelerators, Spectrometers, Detectors and Associated Equipment **795**, 144 - 150 (2015).

[Ved16] V. Vedia, L. M. Fraile, V. Paziy, H. Mach, A. Aprahamian, C. Bernards, J. A. Briz, B. Bucher, C. J. Chiara, Z. Dlouhý, I. Gheorghe, D. G. Ghiţă, P. Hoff, J. Jolie, U. Köster, W. Kurcewicz, N. Mărginean, R. Mărginean, B. Olaizola, J. M. Régis, M. Rudigier, T. Sava, G. S. Simpson, M. Stanoiu, L. Stroe, and W. B. Walters, *Ground state doublet in* ^{73}Ga, In preparation.

[Ver79] M. N. Vergnes, G. Rotbard, E. R. Flynn, D. L. Hanson, S. D. Orbesen, F. Guilbaut, D. Ardouin, and C. Lebrun, ^{71}Ga *and* ^{73}Ga *levels as observed in the (t,p) reaction*, Phys. Rev. C **19**, 1276–1287 (1979).

[Ver07] D. Verney, F. Ibrahim, C. Bourgeois, S. Essabaa, S. Galès, L. Gaudefroy, D. Guillemaud-Mueller, F. Hammache, C. Lau, F. Le Blanc, A. C. Mueller, O. Perru, F. Pougheon, B. Roussière, J. Sauvage, and O. Sorlin, *Low-energy states of* $^{81}_{31}Ga_{50}$*: Proton structure of the nuclei close to* ^{78}Ni, Phys. Rev. C **76**, 054312 (2007).

[Ver12] Preeti Verma, Chetan Sharma, Suram Singh, Arun Bharti, and S.K. Khosa, *Microscopic insight into the structure of gallium isotopes*, Nuclear Physics A **884-885**, 1-20 (2012).

[Ver13] D. Verney, B. Tastet, K. Kolos, F. Le Blanc, F. Ibrahim, M. Cheikh Mhamed, E. Cottereau, P. V. Cuong, F. Didierjean, G. Duchêne, S. Essabaa, M. Ferraton, S. Franchoo, L. H. Khiem, C. Lau, J.-F. Le Du, I. Matea, B. Mouginot, M. Niikura, B. Roussière, I. Stefan, D. Testov, and J.-C. Thomas, *Structure of* ^{80}Ge *revealed by the β decay of isomeric states in* ^{80}Ga*: Triaxiality in the vicinity of* ^{78}Ni, Phys. Rev. C **87**, 054307 (2013).

[Wei51] V. F. Weisskopf, *Radiative transition probabilities in nuclei*, Phys. Rev. **83**, 1073–1073 (1951).

[Win88a] J. A. Winger, John C. Hill, F. K. Wohn, R. L. Gill, X. Ji, and B. H. Wildenthal, *Test of the singly magic character of the N=50 isotone* ^{83}As *populated in* ^{83}Ge *decay*, Phys. Rev. C **38**, 285–294 (1988).

[Win88b] J. A. Winger, John C. Hill, F. K. Wohn, R. L. Gill, X. Ji, and B. H. Wildenthal, *Test of the singly magic character of the N=50 isotone* ^{83}As *populated in* ^{83}Ge *decay*, Phys. Rev. C **38**, 285–294 (1988).

[Woh73] F. K. Wohn, J. K. Halbig, W. L. Talbert, and J. R. McConnell, *Beta spectrum of* ^{87}Kr, Phys. Rev. C **7**, 160–165 (1973).

[Woo54] Roger D. Woods and David S. Saxon, *Diffuse surface optical model for nucleon-nuclei scattering*, Phys. Rev. **95**, 577–578 (1954).

[Xu14] Z. Y. Xu, S. Nishimura, G. Lorusso, F. Browne, P. Doornenbal, G. Gey, H.-S. Jung, Z. Li, M. Niikura, P.-A. Söderström, T. Sumikama, J. Taprogge, Zs. Vajta, H. Watanabe, J. Wu, A. Yagi, K. Yoshinaga, H. Baba, S. Franchoo, T. Isobe, P. R. John, I. Kojouharov, S. Kubono, N. Kurz, I. Matea, K. Matsui, D. Mengoni, P. Morfouace, D. R. Napoli, F. Naqvi, H. Nishibata, A. Odahara, E. Şahin, H. Sakurai, H. Schaffner, I. G. Stefan, D. Suzuki, R. Taniuchi, and V. Werner, *β-decay half-lives of* ^{76,77}Co, ^{79,80}Ni, *and* ^{81}Cu*: Experimental indication of a doubly magic* ^{78}Ni, Phys. Rev. Lett. **113**, 032505 (2014).

[Yoh76] W.A. Yoh, S.E. Darden, and S. Sen, *A study of the* ^{70,72,74,76}Ge*(d, p)*^{71,73,75,77}Ge *reactions using polarized deuterons*, Nuclear Physics A **263**, no. 3, 419 - 444 (1976).

[Zen80] M. Zendel, N. Trautmann, and G. Herrmann, *Decay of* $^{85-88}$Se *to levels in* $^{85-88}$Br, Journal of Inorganic and Nuclear Chemistry **42**, no. 10, 1387 - 1395 (1980).

[Zol70] W.H. Zoller, W.B. Walters, and G.E. Gordon, *Decay of 2.4 min* ^{71g}Zn *and 3.9 h* ^{71m}Zn *to levels of* ^{71}Ga, Nuclear Physics A **142**, no. 1, 177 - 203 (1970).